

Kinetics and Catalyst Overheating in the  
Gas Phase Polymerization of Propylene

## Dissertation

zur Erlangung des  
Doktorgrades der Ingenieurwissenschaften (Dr.-Ing.)

der

Naturwissenschaftlichen Fakultät II  
Chemie, Physik und Mathematik

der Martin-Luther-Universität  
Halle-Wittenberg

vorgelegt von

Herr Jorik Hill  
geb. am 15.02.1990 in Göttingen

Gutachter: Prof. Dr.-Ing. Michael Bartke  
Martin-Luther-Universität Halle-Wittenberg

Prof. Dr. Reinhard Schomäcker  
Technische Universität Berlin

Tag der Promotion: 27.05.2021

## **Abstract**

Scope of this PhD work is the kinetic study of four Ziegler-Natta catalysts in the gas phase polymerization of propylene under industrially relevant conditions. The focus is placed on the effect of catalyst overheating in lab-scale with particle heat transfer conditions that apply to those of industrial plants.

Modern, highly active Ziegler-Natta catalysts show high initial polymerization rates and thus face the challenge of overheating which causes a reduction in the overall catalyst activity and poor particle morphology. One method to overcome this issue is prepolymerization which is industrially realized by an additional reactor before the main reactors operated at low temperatures. However, this prepolymerization reactor adds costs and complexity to the process. This lab-scale study therefore seeks to analyze the effect of overheating on the polymerization kinetics.

First, the effect of a seed bed is analyzed for two catalysts in detail. Experiments are performed in a 5 L horizontal stirred tank reactor under industrially relevant conditions. After establishment of the seed bed polymerization method, a kinetic study is conducted for three Ziegler-Natta catalysts with focus on the effect of hydrogen on the catalyst activity and melt flow rate. Moreover, the morphology of the produced polypropylene particles is investigated. The effect of overheating is studied by comparing two different methods: prepolymerization and direct injection at the main reaction temperature in presence of a seed bed.

The concentration of propylene in polypropylene is crucial for kinetic modeling since it is directly linked to the polymerization rate. As literature results differ widely, an experimental solubility study is conducted in a high pressure magnetic suspension balance. State-of-the-art thermodynamic models relevant for process modeling are tested in describing the propylene/polypropylene system.

The analysis of the polymerization kinetics is extended by developing a phenomenological kinetic model which is combined with an experimentally validated thermodynamic equation of state. The catalyst specific kinetic parameters are estimated and the kinetic model is validated.

## Abstract

Zielsetzung dieser Doktorarbeit ist die kinetische Untersuchung von vier Ziegler-Natta-Katalysatoren in der Gasphasenpolymerisation von Propen unter industriell relevanten Bedingungen. Der Schwerpunkt liegt auf der Untersuchung der Katalysatorüberhitzung im Labormaßstab, wobei die Partikelwärmeübertragungsbedingungen industrieller Anlagen nachgeahmt werden.

Moderne, hochaktive Ziegler-Natta-Katalysatoren weisen hohe Anfangsreaktionsraten auf und neigen daher zur Überhitzung, was zu einer Verringerung der Gesamtkatalysatoraktivität und einer schlechten Partikelmorphologie führt. Eine Methode zur Überwindung dieses Problems ist die Präpolymerisation, welche industriell durch einen zusätzlichen, bei niedriger Temperatur betriebenen Reaktor vor den Hauptreaktoren realisiert wird. Dieser Reaktor erhöht jedoch die Kosten und die Komplexität des Prozesses, sodass in dieser Studie die Auswirkungen der Überhitzung auf die Polymerisationskinetik genauer analysiert werden sollen.

Zunächst wird die Wirkung eines Saatbetts für zwei Katalysatoren im Detail analysiert. Die Experimente werden in einem horizontalen 5 L Rührkesselreaktor unter industriell relevanten Bedingungen durchgeführt. Nach Etablierung der Saatbettpolymerisationsmethode wird eine kinetische Studie für drei Ziegler-Natta-Katalysatoren durchgeführt, wobei der Schwerpunkt auf der Wirkung von Wasserstoff auf die Katalysatoraktivität und den Schmelzflussindex liegt. Darüber hinaus wird die Morphologie der erzeugten Polypropylenpartikel untersucht. Die Auswirkung der Überhitzung wird durch den Vergleich zweier verschiedener Methoden untersucht, nämlich durch Präpolymerisation und Direkteinschuss bei Hauptreaktionsbedingungen in Gegenwart eines Saatbetts.

Die Propenkonzentration in Polypropylen ist für die kinetische Modellierung entscheidend, da sie direkt mit der Polymerisationsrate verknüpft ist. Da Literaturergebnisse diesbezüglich sehr unterschiedlich sind, wird eine experimentelle Löslichkeitsstudie in einer Hochdruckmagnetschwebewaage durchgeführt. Zur Beschreibung des Propen/Polypropylen-Systems werden moderne thermodynamische Modelle verwendet, die für die Prozessmodellierung relevant sind.

Die Analyse der Polymerisationskinetik wird durch die Entwicklung eines phänomenologischen kinetischen Modells erweitert, welches mit einer experimentell validierten thermodynamischen Zustandsgleichung kombiniert wird. Darin werden die katalysatorspezifischen kinetischen Parameter bestimmt und das kinetische Modell validiert.

## Danksagung

An dieser Stelle bedanke ich mich vor allem bei meinem Doktorvater Prof. Dr. Michael Bartke für die großartige Betreuung während meiner Zeit an der Martin-Luther-Universität Halle-Wittenberg. Das Thema mit seiner Nähe zur Industrie war für mich besonders spannend. Bei der Arbeit im Polymerisationslabor hatte ich die Möglichkeit, viel praktische Erfahrung zu sammeln und mir nicht nur im Arbeitskreis selbst, sondern auch auf internationalen Konferenzen ein breites Wissen in der Polymerisationstechnik anzueignen.

Bei der Lummus Novolen Technology GmbH bedanke ich mich vorweg für die finanzielle Unterstützung, ohne welche diese Arbeit nicht möglich gewesen wäre. Ich schätzte vor allem die äußerst angenehme Zusammenarbeit und die zahlreichen konstruktiven Diskussionen. Ganz besonders zu erwähnen sind hier die stets hilfreichen sowie anregenden Gespräche mit Dr. Thomas Kröner und Dr. Sebastian Fries. Mein Dank gilt ebenfalls Dr. Thorsten Sell, Dr. Oliver Ruhl, Dr. Stefan Bangerth, Dr. Oliver Schuster, Dr. Martin Dietrich und Dr. Johannes Günther.

Vielen Dank darüber hinaus an meine ehemaligen Kollegen Dr. Joana Kettner, Dr. Miguel Plata, Arkom Drawpateep, Sina Valaei und Dr. Janine Anders für die gute Zusammenarbeit, gegenseitige Unterstützung und das nette Arbeitsklima. Ebenfalls danke ich Jana Klabunde für ihren großen Beitrag zu den Löslichkeitsmessungen.

Prof. Dr. Schomäcker danke ich für die Erstellung des Gutachtens. Bei Prof. Dr. Hahn und Jenny Bienias-Dragon bedanke ich mich für die vielen Dichte- und Porositätsmessungen sowie bei Prof. Dr. Thurn-Albrecht und Katrin Herfurt für die zahlreichen DSC-Messungen. Frank Syrowatka danke ich für die REM-Aufnahmen und Prof. Dr. Moritz und Marcus Jilge für die Lichtmikroskopiebilder, ferner Prof. Dr. Beiner, Dr. Gaurav Gupta und Dr. Varun Danke für die WAXS-Messungen und die Hilfe bei der Datenauswertung. Maximilian Münzner danke ich für die Möglichkeit, Partikelgrößenverteilungen messen zu können.

Dr. Benedikt Heinrich, Dr. Janine Anders und Jana Klabunde danke ich für die Durchsicht dieser Arbeit.

Abschließend bedanke ich mich von ganzem Herzen bei meiner Familie für den permanenten Rückhalt und die unentwegte Unterstützung.

# Table of Contents

<b>1</b>	<b>Introduction</b>	<b>1</b>
1.1	Polypropylene market and applications	1
1.2	Polypropylene: Microstructure, properties and resin types	2
1.3	Industrial processes for the production of polypropylene	4
1.3.1	Bulk (liquid propylene) processes	5
1.3.2	Gas phase processes	6
<b>2</b>	<b>Theory and Literature Review</b>	<b>9</b>
2.1	Catalysts for the polymerization of propylene	9
2.2	Experimental methods and polymerization kinetics	11
2.2.1	Measurement of gas phase polymerization kinetics	11
2.2.2	The effect of hydrogen	12
2.2.3	Prepolymerization	13
2.2.4	Seed bed polymerization and heat transfer	16
2.3	Solubility and diffusion of propylene in polypropylene	17
2.3.1	Equilibrium solubility	17
2.3.2	Diffusion	19
2.4	Modeling of coordinative olefin polymerization	20
2.4.1	Multi-scale modeling	20
2.4.2	Kinetic modeling	21
2.4.3	Single particle models	24
2.4.4	Thermodynamic modeling	25
<b>3</b>	<b>Research Objectives and Thesis Outline</b>	<b>27</b>
<b>4</b>	<b>Experimental Setup and Polymer Characterization</b>	<b>28</b>
4.1	Setup for the polymerization experiments	28
4.1.1	Raw material supply and purification	28
4.1.2	Lab-scale polymerization reactor	30
4.1.3	Measurement of reaction kinetics and control units	31
4.1.4	Data acquisition	31
4.2	Chemicals and catalyst preparation	32
4.3	Polymerization procedure	33
4.3.1	Reactor inertization	33
4.3.2	Polymerization with a prepolymerization step	34

4.3.3	Polymerization without a prepolymerization step .....	34
4.3.4	Seed bed polymerization experiments.....	36
4.4	Experimental plan .....	36
4.5	Polymer characterization .....	36
4.5.1	Melt flow rate and molecular weight .....	37
4.5.2	Crystallinity.....	38
4.5.2.1	Differential scanning calorimetry .....	39
4.5.2.2	Wide angle X-ray scattering .....	40
4.5.2.3	Helium pycnometry .....	41
4.5.3	Particle morphology .....	41
4.5.3.1	Light and scanning electron microscopy.....	42
4.5.3.2	Bulk density.....	42
4.5.3.3	Mercury porosimetry .....	43
4.5.3.4	Particle size distribution.....	43
<b>5</b>	<b>Experimental Study of the Gas Phase Polymerization of Propylene.....</b>	<b>45</b>
5.1	Results of the gas phase polymerization experiments .....	45
5.1.1	Reaction condition profiles and catalyst activity.....	45
5.1.2	Reproducibility of catalyst activity .....	48
5.1.3	Influence of the initial temperature.....	49
5.1.4	Establishment of the seed bed polymerization method.....	50
5.1.5	Hydrogen variation .....	58
5.2	Crystallinity and particle morphology .....	69
5.2.1	Crystallinity by DSC .....	69
5.2.2	Particle morphology .....	70
<b>6</b>	<b>Solubility and Diffusion of Propylene in Polypropylene.....</b>	<b>79</b>
6.1	Comparison of literature solubility data.....	79
6.2	Experimental method .....	80
6.2.1	Magnetic suspension balance and operational procedure .....	80
6.2.2	Buoyancy force correction and polymer swelling .....	81
6.2.3	Experimental plan .....	84
6.3	Equilibrium solubility results .....	85
6.3.1	Solubility.....	85
6.3.2	Comparison of solubility results with literature data .....	87

6.3.3	Effective propylene concentration .....	91
6.4	Thermodynamic modeling .....	92
6.4.1	Sanchez-Lacombe and PC-SAFT equations of state.....	92
6.4.2	Pure component parameters and density calculations.....	94
6.4.3	Simulation of amorphous solubility and concentration .....	96
6.5	Diffusion results.....	103
6.5.1	Sorption curves .....	103
6.5.2	Effective diffusion coefficients and test for mass transfer limitations.....	106
<b>7</b>	<b>Kinetic Model.....</b>	<b>112</b>
7.1	Derivation of the kinetic model .....	112
7.1.1	Model assumptions .....	112
7.1.2	Kinetic scheme.....	114
7.1.3	Mass balances .....	116
7.1.4	Method of moments and molecular weight averages.....	118
7.1.5	Catalyst site, monomer and hydrogen concentration .....	120
7.2	Model implementation and parameter estimation .....	122
7.3	Comparison of experiment and simulation.....	129
<b>8</b>	<b>Summary.....</b>	<b>134</b>
<b>9</b>	<b>Appendix.....</b>	<b>138</b>
9.1	Data of the gas phase polymerization experiments .....	138
9.2	Experimental solubility data.....	142
9.3	Recalculation of literature solubility data.....	144
9.4	Density of amorphous and crystalline PP .....	145
<b>10</b>	<b>Nomenclature .....</b>	<b>147</b>
<b>11</b>	<b>References.....</b>	<b>153</b>



# 1 Introduction

## 1.1 Polypropylene market and applications

Polymers are one of the most important materials nowadays and have largely influenced the modern world. They are found in a vast variety of applications and have become indispensable. The global production of plastics reached almost 360 million tons in 2018. The European plastic demand amounted up to 62 million tons in the same year with polypropylene (PP) having the second largest market share of 19 % next to polyethylene (PE) with about 30 % (Figure 1.1). [1] Global installed capacities of PP approached 70 million tons in 2015 [2] and average annual growth rates are expected to maintain at about 5 % in the next years [3].

The high PP demand can be explained by its superior cost/performance balance. PP is produced at relatively low costs in comparison to other polymers. Nevertheless, PP products can be produced with versatile properties suitable for various application areas. It is one of the plastics that is relatively equally applied over a range of segments such as packaging (largest segment), building and construction, automotives, electronics, agriculture and household and sport items. PP products range from films, hinged caps and containers for food packaging over pipes, fibers and industrial tanks to interior parts for cars, capacitors or bank notes. [1–3]

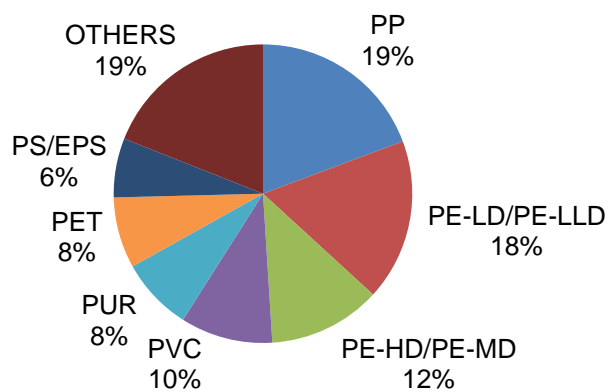


Figure 1.1: European plastic demand by resin type. [1]

## 1.2 Polypropylene: Microstructure, properties and resin types

Polypropylene is a semi-crystalline polymer. The crystallinity is essentially determined by the polymer microstructure. In case of polypropylene, this is particularly the orientation of the methyl groups of the propylene repeating units along the polymer backbone. Depending on how these methyl groups are arranged in relation to each other, a different tacticity results (Figure 1.2). The three most common polypropylene configurations are:

- a) *Isotactic*: The methyl groups are all on the same side of the polymer backbone.
- b) *Syndiotactic*: The methyl groups alternate sides on the polymer backbone.
- c) *Atactic*: The methyl groups are randomly distributed along the polymer chain.

The isotactic type dominates the polypropylene market as it is readily produced with modern heterogeneous Ziegler-Natta or metallocene catalysts. It is highly crystalline and shows a melting temperature of about 165 °C. Syndiotactic polypropylene is also semi-crystalline, but generally shows a slightly lower melting temperature than isotactic PP. It is only produced by some metallocene catalysts and has yet little commercial relevance. Due to the random distribution of the methyl groups, the atactic type does not (or barely) crystallize. It shows a much lower melting temperature of about 128 °C and has marginal commercial value. [4, 5]

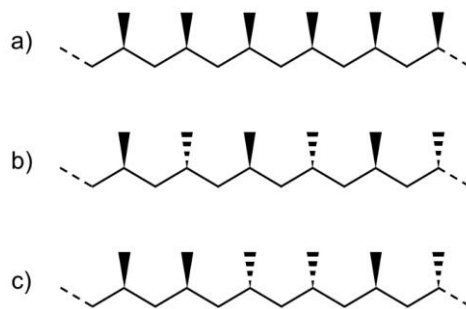


**Figure 1.2:** The three main polypropylene configurations: a) isotactic, b) syndiotactic and c) atactic. [4]

The majority of polypropylene is produced by heterogeneous Ziegler-Natta catalysts. State-of-the-art catalysts create products with high isotactic content and a very small fraction of atactic material. Non-specific catalyst sites are considered to be responsible for the formation of atactic byproducts. Minimization of the number of these sites was achieved over decades by improvement in catalyst design (section 2.1). Besides high stereo-regularity, polymer chains produced with modern catalysts show a low number of regio-errors. Head-to-tail enchainment (1,2-insertion) is favored resulting in highly regio-regular polymers. Defects such as a 2,1-insertion (Figure 1.3) lead to irregularities (head-to-head and tail-to-tail addition) which decreases the crystallinity and melting temperature of the polymer. [4]

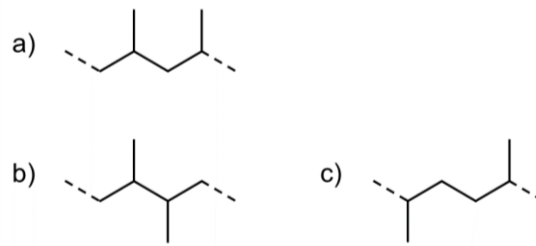


**Figure 1.3:** Regio-regularity in polypropylene: a) head-to-tail, b) head-to-head and c) tail-to-tail. [4]

The properties of polypropylene are governed by various factors. They depend to a large extent on the molecular weight, molecular weight distribution and polymer microstructure, all which are defined by the used catalyst system and polymerization conditions. Furthermore, thermal processing and the use of additives influence the crystalline structure which in return affects the mechanical properties. [5] As a thermoplastic, polypropylene is readily processed in conventional equipment for this type of plastic. With 40 to 50 %, injection molding is the largest method for processing of PP. Extrusion of fibers and films, especially processed by the use of orientation to develop enhanced properties, accounts for the remaining processes. [6, 7] Commercial PP grades typically have weight average molecular weights between 200 and 600 kg/mol [5]. The molecular weight distribution is rather broad with polydispersity indices of 3 up to 20 [2] (for the mainly used heterogeneous Ziegler-Natta catalysts). PP is a lightweight material (lighter than PE) and shows a narrow density range of about 900 to 920 kg/m<sup>3</sup> [5]. The Young's modulus is in the range of 1300 to 1800 MPa [8], the melting temperature 162 to 168 °C [5] and the glass transition temperature relatively high with about 0 °C [5]. Improvement in the performance of PP at low temperatures is achieved by copolymerization (see below). Generally, PP comes with various useful end-use properties. It is a rigid and tough material, has a high upper working temperature of about 100 to 120 °C (20 °C higher than PE) and it shows strong resistance to a wide range of chemicals except for powerful oxidizing agents and highly aromatic or chlorinated solvents. [6]

The property range of polypropylene is further broadened by the use of comonomers in the polymerization process. Beyond homopolymers, two other PP-modifications are commercially relevant and therefore, PP resins are generally categorized into three different product classes:

- a) Homopolymers
- b) Random copolymers
- c) High impact copolymers

Random copolymers contain up to about 6 wt% ethylene or other comonomers (e.g. 1-butene) which are randomly distributed along the polymer chain. This leads to a lower crystallinity and melting temperature. These products come along with improved clarity and lower modulus. [7] Heterophasic high impact copolymers consist of a polypropylene or random copolymer matrix and an amorphous ethylene-propylene rubber phase. These resins are produced in at least two reactors in series. In the first reactor, the rigid polypropylene matrix is generated. The second reactor is a gas phase reactor in which the rubber phase is produced and dispersed in the PP matrix, although these two compounds are immiscible. The rubber phase largely increases impact strength of the final product, especially at low temperatures, overcoming some disadvantages of the pure homopolymer. [4, 7, 9]

### **1.3 Industrial processes for the production of polypropylene**

The industrial development of Ziegler-Natta catalysts (section 2.1) for the polymerization of propylene went hand in hand with the evolution of PP production processes. During the last 60 years, commercial plants record major improvements in efficiency and throughput while decreasing capital investment costs. Single line production capacities have increased from a few kilo tons to above 500 kt per year [10]. The plants from the 1970s typically included a series of up to seven stirred tank reactors using low activity catalysts. The polymerization was conducted in slurry using diluents ranging from C<sub>6</sub> to C<sub>12</sub> hydrocarbons. Due to the attained low yield products, catalyst removal (deashing) was required. Furthermore, another energy intensive step was necessary: The removal of atactic PP to achieve better product properties. Nowadays, slurry (inert diluent) processes have become rare and produce specialty products for niche markets. They cannot compete in efficiency with modern bulk (liquid propylene) or gas phase processes. As the polymerization is conducted in liquid or gaseous monomer, much higher reaction rates are achieved due to the higher propylene concentration. Additionally, polymer and monomer are separated by flashing and an extensive diluent recovery unit is avoided. Modern plants run with advanced catalyst systems (section 2.1) which give high polymerization rates, good polymer microstructural control and controlled particle morphology. Neither deashing nor atactic PP removal is required anymore. A variety of different processes exist each offering their own advantages such as low capital investment costs, high productivity or a broad range of products with diverse application properties. [2, 4]

### 1.3.1 Bulk (liquid propylene) processes

In bulk processes, the polymerization takes place in liquid propylene. Sometimes these processes are also referred to as mixed phase processes because after one or two liquid phase reactors, often gas phase reactors are used for the production of heterophasic copolymers. Advantages are the enhanced polymerization rates due to the higher monomer concentration and better heat removal than in gas phase processes. Examples of such processes are the Borstar (*Borealis*), the Hypol (*Mitsui*) and the Spheripol process (*LyondellBasell*) with the latter one being briefly described in the following. [2]

The Spheripol process of *LyondellBasell* is the dominant process for the production of PP by which about one third of the world's polypropylene is produced [4]. A typical process configuration consists of a small loop for prepolymerization, two main loops for bimodal homopolymer synthesis and a fluidized bed reactor (FBR) for high impact PP production (Figure 1.4). The prepolymerizer guarantees morphology control and ensures high catalyst activity. The main loop reactors are operated at 75 to 80 °C and 40 to 45 barg. A pump circulates the liquid propylene and solid PP particles with up to 55 wt% with high velocities enabling turbulent flow. Thus solids settlement is avoided and heat transfer is improved. The polymerization heat is removed by jacket cooling. The residence time distribution (RTD) is close to a continuous stirred tank reactor (CSTR) because of the high recirculation rates and the residence time of one loop is in the order of 1 h. Parts of the bulk mixture are withdrawn from the second loop and the solid PP particles are separated from liquid propylene by a high-temperature flash before entering the FBR for high impact copolymer production. This reactor is operated at 70 to 80 °C and 10 to 14 barg and cooling is achieved by a gas recirculation loop. The final solid products are separated from monomer and unreacted gases are recycled. [2, 4, 10]

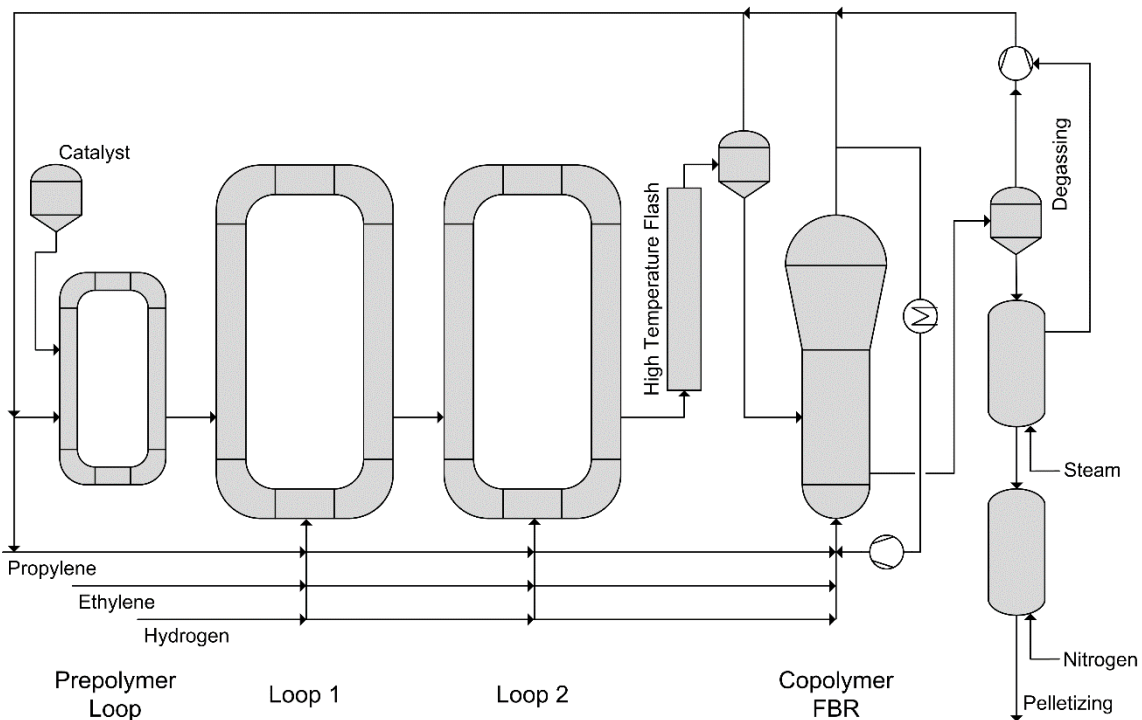


**Figure 1.4:** Schematic flowsheet of the Spheripol process. [4, 10]

### 1.3.2 Gas phase processes

The gas phase polymerization of propylene comes with the disadvantages of lower reaction rates (lower monomer concentration than in liquid propylene) and more difficulties in heat removal because of the lower thermal conductivity of gases compared to liquids. On the other hand, an advantage is the lower energy requirement for the flash separation of gaseous monomer and polymer leading to cost reductions. Besides, as there is no solubility limit for hydrogen or ethylene, a broader product range (higher melt flow rates and comonomer contents) is possible. Various commercial technologies exist such as the Unipol (*Grace*), the Innovene (*INEOS*), the Novolen (*Lummus Technology*), or the Spherizone process (*LyondellBasell*). Each one uses a different reactor technology, specifically a FBR, a horizontal stirred bed reactor, a vertical stirred bed reactor and a multizone circulating reactor, respectively. The two latter gas phase processes are shortly explained as examples. [2, 4]

Developed by *BASF* in the 1960s and now licensed by *Lummus Technology*, the Novolen process dates back to the first PP technologies and was one of the first gas phase processes for the production of PP. In principle, the reactor is a stirred autoclave with a bottom-mounted helical stirrer (Figure 1.5). The polymerization heat is removed by condensed mode cooling. Monomer is recycled through an external heat exchanger and part of the monomer is

condensed and re-enters the reactor as liquid, whereas the other part is returned as cooled gas. The process typically consists of two such vertical stirred bed reactors which can be operated in series or parallel for the production of high impact copolymer or homopolymer (and random copolymer), respectively. The advantage of the process is its simple design and operation resulting in low capital and operating costs. The catalyst system, monomers and hydrogen are fed to the reactors in series or parallel (depending on operational mode) and the produced polymer particles are separated from the gases in a discharge vessel close to atmospheric pressure. Residual propylene is removed by nitrogen in a purge silo and the polymer powder is formed to pellets in an extruder. Unreacted gases are recovered and recycled into the reactors. [4, 11]

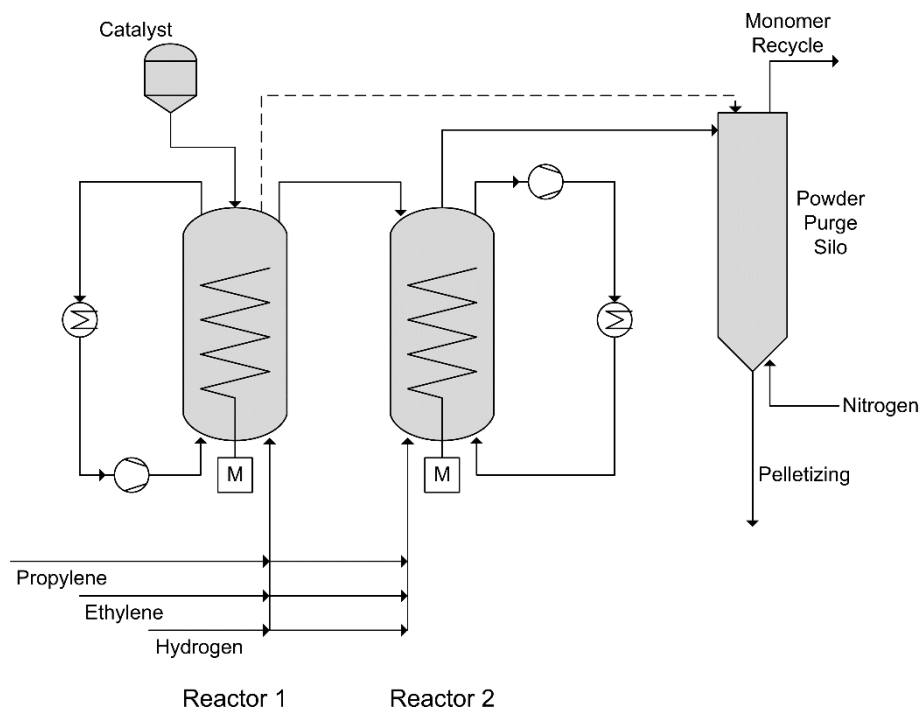


**Figure 1.5:** Schematic flowsheet of the Novolen process. [11]

The latest PP process technology development was introduced in the early 2000s by *LyondellBasell* in form of the Spherizone process. The major breakthrough is the new multi-zone circulating reactor (MZCR) which allows the production of a homogeneous two-phase polypropylene in one reactor (Figure 1.6). The reactor is basically a loop reactor that consists of two reaction zones with different polymerization conditions. Growing polymer granules circulate multiple times between the two zones leading to enhanced polymer phase homogeneity and thus better product properties than in two reactors which are operated in series. In the MZCR, catalyst particles first enter the “riser” zone, which behaves like an expanded FBR, operated above the critical fluidization velocity. At the top, the formed PP particles are separated from the riser by a cyclone and pass into the “downer” zone which behaves like a moving packed bed. A barrier fluid is injected at the top of the “downer”. It has

a higher density than the “riser” gas phase in order to stop the entrainment of lighter gases, specifically hydrogen and/or ethylene, into the “downer” zone. Thus two distinct reaction zones can be achieved within one reactor. The particles of the “downer” move downwards by the force of gravity. Some of the PP particles are withdrawn at the bottom of the “downer”, but most re-enter the “riser” zone as the MZCR is operated with high recycle ratios. The overall process is very similar to the Spheripol process with the MZCR replacing the two main loop reactors, i.e. process units such as monomer recovery and a FBR for the production of high impact copolymer are adapted from the Spheripol technology. [2, 4, 12, 13]

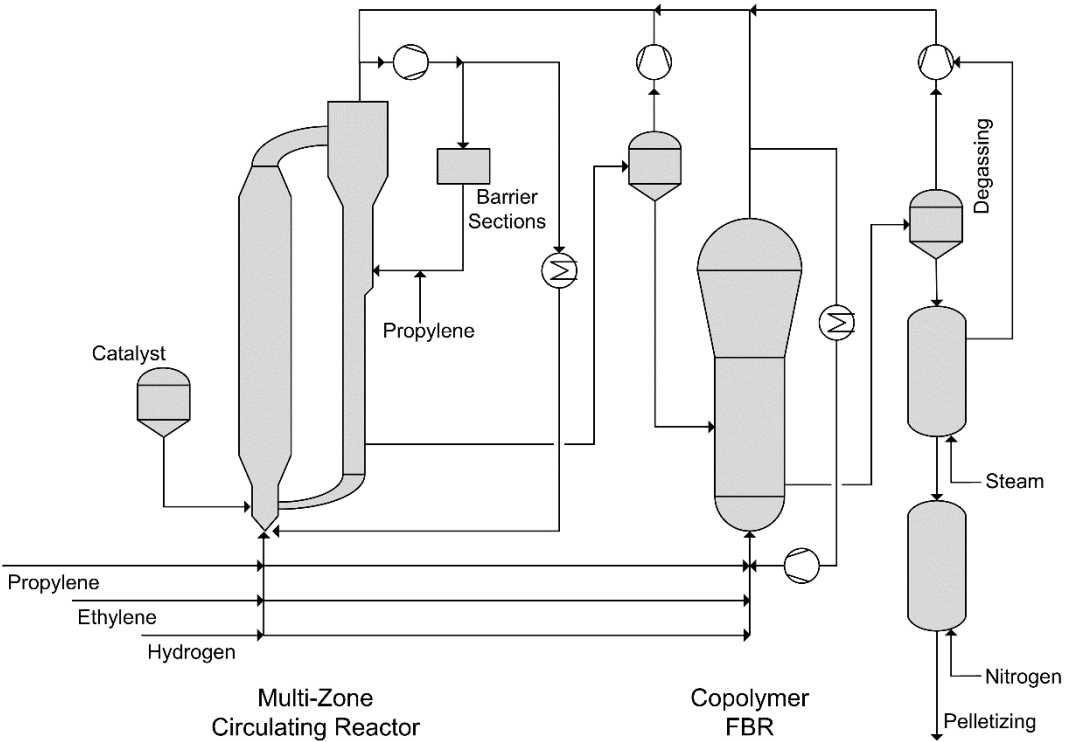


**Figure 1.6:** Schematic flowsheet of the Spherizone process. [2, 12]



## 2 Theory and Literature Review

### 2.1 Catalysts for the polymerization of propylene

All polyolefins, with the exception of low density polyethylene which is synthesized by radical polymerization under very high reaction pressures, are industrially produced by coordinative polymerization. The catalyst greatly determines the polymer microstructure and thus the product properties. The industrial aim for enhanced polymer properties and process performance has and will push the development of new catalysts.

The wide range of commercial polyolefin products with varying rheological and mechanical properties resides in the use of different types of catalysts. Polyolefin coordination catalysts can be grouped into four main families: Ziegler-Natta (ZN), Phillips, metallocene and late transition metal catalysts. Ziegler-Natta catalysts are the workhorse of the polypropylene industry and have a large share in the production of polyethylene. Phillips catalysts were discovered in the early 1950s and are based on chromium oxide supported on SiO<sub>2</sub>. They are of great importance in the production of high density polyethylene. Metallocene catalysts, in contrast to Ziegler-Natta and Phillips catalyst, offer the advantage of producing polymers with very narrow molecular weight distributions and unimodal and narrow chemical composition distributions. They can be used as homogeneous catalysts in solution polymerization, but need to be supported for the use in slurry or gas phase processes. Metallocenes have a niche market in the production of polypropylene, but are used to produce 20 to 25 % of the world's polyethylene. Late transition metal catalysts were discovered in the early 1990s by Brookhart and researchers from *DuPont*, however, a commercial breakthrough has not yet happened. [2, 4, 14]

Heterogeneous Ziegler-Natta catalysts are predominantly used in the production of polypropylene. State-of-the-art catalysts are spherical particles of 10 to 100 μm diameter consisting of titanium chloride as active compound supported on typically porous magnesium chloride or sometimes silica particles. A so called internal electron donor is added during catalyst synthesis to attain a high isotactic polymer content. Electron donors tend to coordinate to non-stereospecific catalyst sites. These sites are hereby poisoned or modified resulting in an increased isotacticity index of the produced PP. In addition to the supported catalyst, an organometallic cocatalyst is needed for the activation of the metal sites – most commonly used is triethylaluminum (TEA). Furthermore, an external electron donor is typically introduced to the polymerization reactor to guarantee high isotacticity since the alkyl aluminum cocatalyst generally causes the partial removal of the internal donor. [2, 4, 7] Supported ZN catalysts are considered to be multi-site catalysts. They have more than one

type of active site resulting in polymer products of broad molecular weight distributions with polydispersity indices between 3 and 10 or even up to 20. [2] Each site type can be considered to have its own individual kinetic response leading to a specific polymer chain population. Thus the produced PP can be seen as a blend of different polymers each one contributing with a different number and mass average molecular weight, stereo-regularity, regio-regularity and so on. [4]

Ziegler-Natta catalysts are commonly divided into different generations based on their historic development (Table 2.1). After the discovery of Ziegler in 1953 to polymerize ethylene at mild reaction conditions by the use of mixtures of  $\text{TiCl}_4$  and aluminum alkyls, Natta used the same catalyst system and succeeded in synthesizing polypropylene one year later. He then increased the isotactic contents up to 90 % by using crystalline  $\text{TiCl}_3$ . [7] Further research led to what now is considered the first generation of ZN catalysts: The combination of  $\text{TiCl}_3$  and aluminum chloride with  $\text{AlEt}_2\text{Cl}$  (DEAC). However, the thereby produced PP resins required energy intensive removal of atactic polymer and catalyst residues (deashing). Further improvements by Solvay in the 1970s led to the second generation. By the use of diisoamyl ether in the catalyst synthesis route, the polymerization activity was greatly increased along with enhanced stereo-selectivity. [2] The third generation was developed by supporting  $\text{TiCl}_4$  on porous  $\text{MgCl}_2$ . By the addition of an appropriate Lewis base during catalyst preparation (internal electron donor), typically ethyl benzoate, and another Lewis base to the polymerization reactor (external electron donor) such as methyl *p*-toluate or ethyl *p*-ethoxybenzoate, high activities were achieved. These catalysts were sufficiently active to avoid the need for catalyst deashing, i.e. the catalyst was not removed and remained in the final polymer product. [7] Further research on the combination of the electron donors led to the fourth generation of ZN catalysts. The application of phthalates as internal and alkoxysilanes as external donors once more enhanced the polymerization productivity. Additionally, isotacticity indices up to 99 % were achieved. [4] Furthermore, improvement in the morphology of the final PP particles was enabled by the use of spherical  $\text{MgCl}_2$  catalysts based on chemical activation of magnesium chloride. At present, the phthalate-based ZN catalysts are the most widely used system for the production of polypropylene since they cover the majority of product properties and applications. [2] A new group of internal donors, such as diethers or succinates, can be seen as the basis of the fifth generation of Ziegler-Natta catalysts. Diethers are not removed from the support upon contact with the alkyl aluminum cocatalyst enabling the production of highly isotactic polypropylene in the absence of any external donor. The diether-based catalysts give particularly high polymerization rates resulting in yields above 100  $\text{kg}_{\text{PP}}/\text{g}_{\text{Cat}}$ . [2]

**Table 2.1:** Overview of the development of heterogeneous Ziegler-Natta catalysts. [7]

Generation	Catalyst System	Yield	Isotacticity	Comment
		[kg <sub>PP</sub> /g <sub>Cat</sub> ]	[wt%]	
First	TiCl <sub>3</sub> /AlCl <sub>3</sub> + DEAC	0.8-1.2 <sup>a</sup>	90-94	Deashing + atactic PP removal
Second	TiCl <sub>3</sub> + DEAC	3-5 <sup>a</sup>	94-97	Deashing
Third	TiCl <sub>4</sub> /MgCl <sub>2</sub> /Ester + AlR <sub>3</sub> /Ester	15-30 <sup>b</sup>	90-95	Atactic PP removal
Fourth	TiCl <sub>4</sub> /MgCl <sub>2</sub> /Diester + TEA/Silane	30-60 <sup>b</sup>	95-99	No purification + morphology control
Fifth	TiCl <sub>4</sub> /MgCl <sub>2</sub> /Diether + TEA	70-120 <sup>b</sup>	95-99	No purification + morphology control

<sup>a</sup> Hexane slurry, 70 °C, 7 bar, 4 h, with H<sub>2</sub>

<sup>b</sup> Bulk (liquid) propylene, 70 °C, 2 h, with H<sub>2</sub>

## 2.2 Experimental methods and polymerization kinetics

### 2.2.1 Measurement of gas phase polymerization kinetics

The catalyst is often regarded as the heart of a chemical process. In coordinative polymerization, the catalyst defines, in dependence on the process conditions, the polymerization kinetics and the polymer properties. Industrial catalyst development is therefore crucial to optimize the polymerization process and design products with enhanced properties. Before a new catalyst can be used in an industrial plant, it is carefully tested in reactors of smaller sizes, e.g. at bench and pilot scale. In the laboratory, the catalyst's specific polymerization kinetics can be gathered in reactors operating under industrially relevant conditions, i.e. reaction pressures, temperatures and catalyst activities close to commercial plants. Stirred tank reactors of 0.1 to 5 L are typically used for gas phase polymerizations. A thermostat and a pressure controller ensure isothermal and isobaric conditions, respectively. Such reactors are operated in semi-batch mode in order to obtain the monomer conversion as a function of time. During the course of reaction, gaseous monomer is converted to solid polymer. In absence of a monomer feed into the reactor (batch mode), a pressure drop would result as a consequence of the much higher density of the polymer than of the monomer. This pressure drop is overcome in semi-batch mode by continuously feeding monomer via a mass flow controller within a pressure control loop. At constant pressure and temperature, the fed monomer mass rate equals the consumption of monomer by reaction which is proportional to the gross polymerization rate. By dividing the

monomer mass feed by the used catalyst amount, the catalyst activity can be calculated over the reaction time resulting in the catalyst specific activity-time profile.

When performing kinetic investigations of coordinative catalysts in the gas phase, the temperature and pressure have to be controlled in a narrow range to gather reliable data. Furthermore, external mass transfer limitations need to be avoided which can be achieved by assuring stirring rates that are high enough. [15] Kinetic investigations of the gas phase polymerization of propylene were conducted by a variety of researchers such as Choi and Ray [16], Han-Adebekun and Ray [17], Meier et al. [18, 19], van Putten [20], Patzlaff [21] and Kettner [22]. Kröner [23] studied the kinetics of the high impact copolymerization of propylene and ethylene in a 5 L horizontal stirred tank reactor operated in semi-batch mode. The gas composition was analyzed by a  $\mu$ -gas chromatograph. Thus the individual consumption rates could be obtained. In combination with experimentally determined mass transport properties of the polymer particles, a diffusion-reaction model was developed. Eventually, model-based analysis revealed a pronounced diffusion limitation of ethylene in the copolymerization stage.

### 2.2.2 The effect of hydrogen

Hydrogen is an effective chain transfer agent in the polymerization of olefins and thus used to control the molecular weight in industrial plants. The effect of hydrogen is not solely limited to chain transfer, but the catalyst activity is often observed to change upon variations in the hydrogen concentration. Contrary to the coordinative polymerization of ethylene, hydrogen generally leads to rate enhancement in the polymerization of propylene. [4]

The widely accepted explanation for the increase in polymerization rate is based on the so-called dormant site theory. During polymerization of propylene, the catalyst favors 1,2-insertion of the monomer into to the growing polymer chain, i.e. a head-to-tail addition is most likely (section 1.2). However, there is a small chance that regio-errors happen. A 2,1-misinsertion leads to a dormant chain which is assumed to be marginally reactive for further propagation (Figure 2.1). The active center of this polymer chain is sterically hindered because the methyl group is closer to the metal active center. Theoretically, this should lead to a lower propagation rate for this dormant site. Hydrogen, as a much smaller molecule in comparison to propylene, is still able to efficiently react with this dormant chain resulting in a dead polymer molecule and a yet active metal (hydride) center. This reactivated center is considered to now be available for further chain propagation reactions. Thus, based on the dormant site theory, an increase in hydrogen concentration leads to a higher rate of reactivation of dormant chains by hydrogen. This leads to a higher concentration of active centers resulting in an overall higher polymerization rate. [4]

The concept of dormant sites is supported by various experimental investigations. [16, 24–28] It was observed that the addition of hydrogen during a polymerization experiment led to an elevation in activity and that this new activity level agreed well with the one from an experiment which was already started at the same hydrogen concentration. Vice versa, removal of hydrogen during polymerization caused an activity drop to the level which was observed for an experiment conducted without hydrogen. [28] This reversibility agrees well with the dormant site theory. Furthermore, experimental chain-end analysis supports the formation of dormant chains. An increased number of *n*-butyl chain ends was found for high hydrogen concentrations which are formed by the reactivation step. [26]

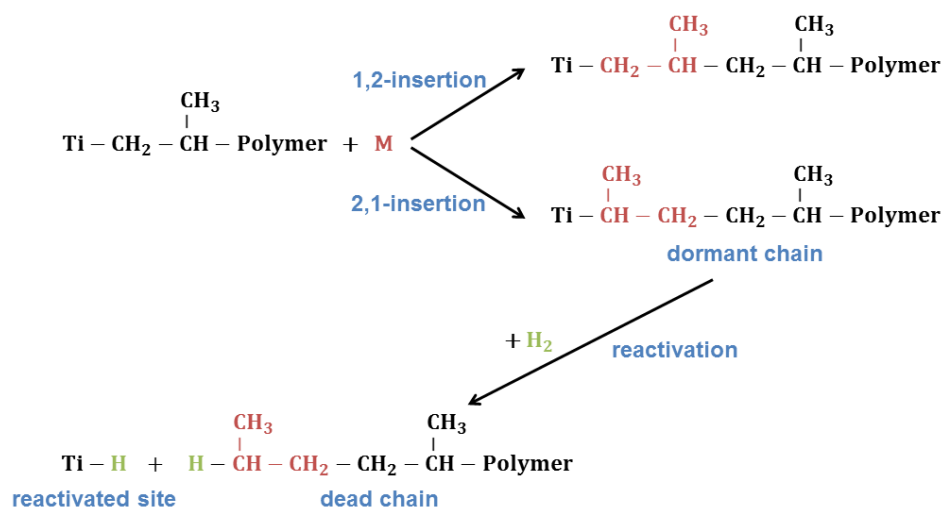


**Figure 2.1:** Hydrogen effect based on the dormant site theory: Regio-regular propagation by 1,2-insertion in comparison to regio-irregular propagation by 2,1-insertion leading to a dormant chain, and reactivation of the dormant site by hydrogen to a dead polymer chain and a reactivated metal center. [4]

### 2.2.3 Prepolymerization

The term prepolymerization refers to the method of starting the polymerization at mild conditions, i.e. much lower temperatures and/or monomer concentrations than in the main reaction, in order to enhance the catalyst activity and improve particle morphology. This method is covered in several patents [29–32] and commercially applied in technologies such as the Spheripol [4, 14] (section 1.3.1) or the Borstar process [2].

Modern, highly active Ziegler-Natta catalysts are associated with challenges regarding heat removal upon polymerization start, particularly from the catalyst particle to the surrounding and especially in the gas phase (due to much lower thermal conductivities of gases than liquids). These catalysts typically show a very fast activation period and a maximum activity

right at the polymerization start. Upon injection of the fresh catalyst into a reactor operated at high temperatures (60 to 80 °C) and pressures (close to or above the vapor pressure), the high initial polymerization rate is accompanied with a rapid generation of heat due to the exothermic nature of the reaction. When the heat is not sufficiently removed from the particle, the particle temperature rises which can cause thermal deactivation of the catalyst sites resulting in an overall lower activity level. Thus the full productivity potential of the catalyst is not exploited. In extreme cases, the temperature may rise close to the melting temperature of the polymer leading to softening or partial melting of the particles which causes the formation of agglomerates. In addition, the rapid initial polymerization rate can cause an uncontrolled catalyst fragmentation. Loss of the ideal spherical morphology and generation of fines are likely consequences. The presence of large amounts of fines in industrial continuous plants can cause severe operational problems such as fouling, plugging, clogging and/or intensification of electrostatic charging. [4]

To overcome these particular issues of highly active catalysts, a prepolymerization step can be employed. In commercial continuous plants, the prepolymerization stage is realized by an additional small reactor. This prepolymerization reactor is operated at low temperatures of about room temperature and after a certain residence time, the prepolymerized catalyst particles are transferred to the first main reactor. In the laboratory, prepolymerization is often realized by injecting the catalyst at much lower temperatures than applied for the main polymerization. After a certain prepolymerization time, the reactor is heated to the main reaction conditions and the polymerization is continued. This method is referred to as in-situ prepolymerization. Although the prepolymerization step comes along with clear benefits, the additional unit operation increases capital and operating costs and adds complexity to the process. This should be considered because the extent of the prepolymerization advantages are, as always in coordinative polymerization, catalyst specific; thus they vary from catalyst to catalyst.

The advantages of prepolymerization can be grouped into different aspects. The low rate conditions lead to a less pronounced heat release avoiding or at least reducing particle overheating. Therefore, as the applied conditions are also far away from critically high temperatures, the catalyst does not suffer from thermal deactivation. Furthermore, during the prepolymerization stage, the catalyst particles grow resulting in a larger particle surface area. This facilitates heat removal in the main stage polymerization. Thus overheating is avoided and higher polymerization rates can be achieved. Besides, the catalyst has more time for activation in the prepolymerization step, possibly increasing the number of active sites which in return should increase the overall activity. In addition to the benefits on the catalyst activity, morphology control is improved. The low rate conditions lead to a controlled catalyst

fragmentation by which just enough stress is generated to evenly fragment the particle, but to avoid particle disintegration. The spherical catalyst morphology is preserved and typically high bulk densities of the final polymer particles are observed allowing higher plant productivity. [4]

The effect of prepolymerization was studied by a number of researchers. [22, 33–38] Samson et al. studied the polymerization of propylene both in liquid [33] and in gaseous [34] monomer and found an increase in yield of up to 30 and 15 %, respectively, when applying a prepolymerization step. Pater et al. [35–38] investigated various aspects of prepolymerization. Using a prepolymerization step, high polymerization rates could be achieved even at high reaction temperatures of up to 80 °C. [37] This was explained by the prevention of thermal runaway on particle scale. During prepolymerization, the particle surface area was enlarged allowing for increased heat transfer in the main stage polymerization. Further studies revealed that a very short prepolymerization time was already sufficient to obtain high catalyst activities. [36] Instead of performing the prepolymerization for a certain time at a constant temperature, it was also possible to produce high yields by injecting the catalyst at a low temperature and then directly heating up the reactor to the main reaction temperature. This non-isothermal prepolymerization method additionally gave good particle morphology (high bulk density and good replication of the catalyst particle) since, as concluded, the initial polymerization rate was the main factor which determined the final particle morphology. [38] Kettner [22] analyzed the effect of prepolymerization on the lab-scale gas phase polymerization kinetics of two supported Ziegler-Natta catalysts. Without a prepolymerization step, catalyst activities decreased after exceeding a reaction temperature of 70 °C. Applying a prepolymerization step, the particle morphology could be improved and the polymerization rate was enhanced, especially at high reaction temperatures. The effect of prepolymerization on the activity was found to be catalyst specific with the more active catalyst showing higher activities upon prepolymerization. The normalized kinetic profiles with and without a prepolymerization were identical suggesting that the difference in the activity level could be explained by a different number of active sites. The harsh injection conditions in absence of a prepolymerization step likely resulted in a lower number of active sites due to particle overheating which caused thermal catalyst deactivation and/or uncontrolled catalyst fragmentation leading to reduced activation of titanium sites.

## 2.2.4 Seed bed polymerization and heat transfer

For lab-scale polymerization of olefins, a bed material is sometimes used to improve catalyst distribution throughout the reactor upon catalyst injection. The inert particles are added to prevent catalyst agglomeration and to ensure proper fluidization of the catalyst particles. This so-called seed bed is placed inside the reactor as part of the preparation of the polymerization experiment. Several bed materials ranging from polymers [39–42], salts [18, 19, 34, 43, 44] and silica [45, 46] were used in the literature. The selection of a certain support material depends on different factors. As an example, sodium chloride offers the advantage of easy separation from the polyolefin product after the experiment. Nevertheless, it has to be noted that by the addition of a bed material into the reactor a supplementary source for possible impurities is created and thus catalyst poisoning may occur. Therefore, certain pretreating steps are commonly applied, e.g. drying the bed material at high temperatures and vacuum, in order to remove residues of moisture and air. Eventually, a seed bed material has to be chosen for which no catalyst poisoning is observed since the two main criteria for bed selection are good experimental reproducibility and high activity.

Samson et al. [34] and Meier et al. [18, 19] used NaCl as seed bed, whereas Marx [41] and Piduhn [45] observed catalyst poisoning for this material and chose PP and silica instead, respectively. Although various studies on different bed materials can be found in the open literature, the effect of the seed bed on the polymerization reaction in terms of heat transfer and activity was not analyzed yet.

Heat transfer investigations on polymerization catalysts by means of computational fluid dynamics calculations of McKenna et al. [47–49] revealed that classical Nusselt correlations such as the commonly used Ranz-Marshall correlation [50, 51] are only valid for large particles. Here, convection is the dominant heat transfer mechanism. In contrast, for small particles of diameters below 100  $\mu\text{m}$ , i.e. catalyst particles, conduction by particle-particle contact also plays an important part in the evacuation of heat. Generally, catalysts will likely have a much higher temperature than their surrounding upon injection due to their high initial polymerization rates in combination with a low surface area for heat removal. Whereas grown polymer particles will have a temperature close to the reactor temperature due to lower reaction rates and a much larger surface area. Upon contact of these particles, heat is efficiently transferred from small, hot catalyst particles to much larger, relatively cool polymer particles. This particle-particle interaction is encountered in continuous, industrial gas phase plants where the fresh catalyst is fed to a reactor with high solid contents of polymer particles. Catalyst heat removal should therefore be facilitated in such systems. Since the heat transfer conditions of a lab-scale seed bed polymerization are similar to the continuous



process, the use of a bed material should also help to improve heat transfer and reduce catalyst overheating.

### 2.3 Solubility and diffusion of propylene in polypropylene

During the gas phase polymerization of propylene, monomer is consumed at the active catalyst centers which are distributed inside the growing polymer particle. These centers can be regarded as a monomer sink. Fresh monomer molecules originating from the gas phase are first transported through the particle boundary layer, then through the pore network of the particle and finally through the polymer phase to reach the catalyst centers. Here, they react and are converted to polypropylene. The effective concentration at the catalyst centers, i.e. the monomer concentration inside the polymer phase, is directly linked to the rate of polymerization. Therefore, this concentration, which can be calculated from the solubility, is essential for the determination of kinetic parameters and process simulation. Additionally, knowing the mass transport properties of the studied polymer particles, possible mass transfer limitations can be detected which adds valuable information about the catalyst system. Moreover, mass transport properties of the polymer particles might not only be important during the polymerization stage, but also during the degassing step in the downstream section of a polymerization plant.

#### 2.3.1 Equilibrium solubility

The solubility of propylene in polypropylene can be obtained by various experimental techniques such as chromatography [40, 52], pressure decay methods [53, 54] or gravimetric measurements [18, 55–61]. In the commonly employed gravimetric measurement, a magnetic suspension balance is typically used which can be operated at various temperatures and pressures, ideally at the same conditions as in the polymerization reactor. The polymer sample is placed in the sorption chamber and the mass uptake upon sorption of the monomer into the sample is measured by the magnetic balance. The solubility  $S$  is defined as the ratio of absorbed propylene mass  $m_{C3}$  and PP mass  $m_{PP}$ :

$$S = \frac{m_{C3}}{m_{PP}} \quad (2.1)$$

Since the monomer is only absorbed in the amorphous phase of the polymer [62, 63], the amorphous solubility  $S_{am}$  can be calculated knowing the crystalline mass fraction  $w_{cr}$  of the polymer:

$$S_{am} = \frac{m_{C3}}{m_{am}} = \frac{S}{1 - w_{cr}} \quad (2.2)$$

The crystallinity can be determined by different methods such as differential scanning calorimetry (DSC), polymer density measurements via for instance helium pycnometry or X-ray diffraction (XRD). The correct determination of the crystalline mass (or volume) fraction is crucial as it directly affects the calculation of the effective monomer concentration. However, different methods were reported to give different results [53, 54, 59] which should be considered when comparing solubility data. Eventually, the effective (amorphous) monomer concentration  $c_{am}$  that is proportional to the polymerization rate can be calculated by using the (swollen) amorphous polymer volume  $V_{am}$ :

$$c_{am} = \frac{n_{C3}}{V_{am}} = \frac{S_{am}\rho_{am}}{(S_{am} + 1)MW_{C3}} \quad (2.3)$$

At low gas pressures, the monomer concentration increases linearly with monomer pressure  $P_{C3}$  and can be expressed by Henry's law:

$$c_{am} = k_H P_{C3} \quad (2.4)$$

Stern et al. [64] analyzed the sorption behavior of several gases in semi-crystalline polyethylene and proposed a correlation for the calculation of the Henry constant  $k_H$  as a function of only temperature and critical temperature  $T_c$  of the gas. Hutchinson and Ray [65] used this correlation to fit various literature data on the gas solubility of hydrocarbons including propylene in PE. The best fit was obtained by the following Stern correlation:

$$\log k_H = -2.38 + 1.08 \left( \frac{T_c}{T} \right)^2 \quad (2.5)$$

A number of researchers found a good agreement between this correlation and their experimentally determined solubility of propylene in PP at low pressures. [52, 57] At higher pressures, the solubility becomes non-linear due to the plasticizing effect of the penetrant and Henry's law is not applicable any more. [65] Stern et al. [64] proposed a correlation to estimate at which pressures Henry's law solubility starts to deviate by 5 %. As an example for propylene, this deviation in solubility can be found at a pressure of 11.8 bar for a temperature of 80 °C. Above these pressures, other thermodynamic models should be applied.

Several researchers investigated the sorption of propylene in polypropylene at elevated pressures. However, some of the authors only analyzed a limited number of samples and conditions since their research was focused on additional gases and polymers. Sato et

al. [54] studied the solubility of propylene in PP in detail. Two PP samples with very different stereo-regularities and thus different crystalline mass fractions of 19 and 47 wt% (DSC) were analyzed at 50 and 75 °C up to the vapor pressure. With lower temperature, the solubility increased. The sample with the lower crystallinity showed a much higher solubility even when comparing the purely amorphous solubility. Swelling was experimentally analyzed by measuring the change in length of a thin PP film placed inside a high pressure view cell. A maximum swelling of about 15 vol% was observed. The solubility data could be well described with the Sanchez-Lacombe equation of state, whereas the swelling data was underestimated with average deviations of 20 % and linear additivity of the volumes of liquid propylene and polymer better described the swelling behavior. In a further study on different gases in PP homopolymer and high impact copolymer, Sato et al. [53] reported the solubility of propylene in PP at 50, 70 and 90 °C up to the vapor pressure for a sample with 66.9 wt% crystallinity (chromatography). Meier et al. [18] studied the propylene solubility between 41 and 73 °C up to a pressure of 25 bar for a PP sample with 44 wt% crystallinity (DSC) by applying a gravimetric method. They considered swelling by assuming that the volumes of PP and (liquid) propylene add linearly. Bobak et al. [56] analyzed the morphology characteristics of PP particles governing mass transport in a magnetic suspension balance. In their study, the propylene solubility isotherm was measured at 85 °C up to 30 bar for a sample with a crystallinity of 37 wt% (DSC). Swelling was experimentally determined via video-microscopy. Kröner and Bartke [58] studied the solubilities of ethylene and propylene in high impact copolymers, but also measured the solubility of propylene in PP (39 wt% crystallinity by XRD) at 70 °C. Cancelas et al. [59] analyzed the solubility of gas mixtures in a high impact copolymer. Solubility isotherms of propylene in PP (72 wt% by density method) were measured at 50, 70 and 85 °C up to 20 bar.

### 2.3.2 Diffusion

Mass transfer in polyolefin particles is strongly affected by the particle morphology. The distribution of pore and polymer space throughout the polymer particle is characteristic for a given catalyst system and will differ from catalyst to catalyst. In common mathematical models that combine polymerization kinetics and mass transfer such as the multi-grain model (section 2.4.3), three different levels of mass transport resistance are often considered: a) through the particle boundary layer, b) through the particle pores and c) through the polymer phase of small micro-grains. [56] Although the existence of these micro-grains of about 1  $\mu\text{m}$  was experimentally validated by electron microscopy techniques [66, 67], further imaging studies revealed the existence of larger compact zones of aggregated micro-grains [39, 68, 69]. In recent experimental investigations on diffusion in polyolefin particles, the main

resistance for mass transfer was found to be diffusion through the polymer phase of these large compact zones [55, 56, 58] or even of the entire particle [40, 52].

Sliepevich et al. [52] studied the diffusivity of olefins in PP particles by gas chromatography. They found that the rate determining step is the diffusion in the polymer and not in the macro-pores with a characteristic diffusive length close to the particle diameter suggesting that the particles consist of a pseudo-continuum polymer phase rather than a cluster of segregated micro-particles. Bartke et al. [55] analyzed the diffusion of propylene and ethylene in PP homopolymers and heterophasic copolymers in a magnetic suspension balance. By combined sorption studies with powder samples and compressed films, the effective length scale for diffusion could be determined which was not the particle diameter, but much smaller with about 125  $\mu\text{m}$  for all particles and independent of the particle size. They concluded that the effective length scale for diffusion was thus in between the micro- and macro-particle scale as used in classical particle modeling. Bobak et al. [56] performed gravimetric degassing experiments to estimate the morphology characteristics of porous PP particles. They found that a simple Fick's diffusion model could not be used to model the degassing behavior. By proposing a particle model including two sizes of compact polymer granules, i.e. depicting the particle morphology to consist of a certain number of small and large polymer sub-particles, the degassing curves could be described and the fractions of small and large compact zones were estimated. The large polymer granules could be well estimated to have a diameter of 240  $\mu\text{m}$  and the rate determining step was found to be the diffusion through the polymer phase of the compact granules. Kröner and Bartke [58] measured sorption rates of ethylene and propylene in PP homopolymers and high impact copolymers using a high pressure sorption balance. Non-porous films were first studied to obtain the material specific diffusion coefficients. Using these coefficients, the sorption curves of the powders were used to estimate the integral, effective diffusion length. This revealed that subdomains (micro-grain clusters) of 250 to 500  $\mu\text{m}$  were the rate determining length scale for mass transport. By correlating the size of these clusters with the yield of the different powder samples, conclusions about the morphology development during (co)polymerization could be drawn.

## **2.4 Modeling of coordinative olefin polymerization**

### **2.4.1 Multi-scale modeling**

In a polyolefin reactor, the various chemical and physical phenomena occur at different length scales. To account for these scales within a mathematical model, a model hierarchy

can be defined. According to the leading work of Ray [70, 71], the polymerization model can be classified into three different length scales:

- 1) Micro-scale (kinetic model)
- 2) Meso-scale (particle model)
- 3) Macro-scale (reactor model)

At the micro-scale, the (molecular) polymerization kinetics taking place at the catalyst sites are considered. The phenomena occurring at the particle scale such as particle growth, heat transfer and mass transfer are modelled at the meso-scale. The reactor dynamics including overall heat balances, reactor hydrodynamics, residence time distributions and so on are covered at the macro-scale.

The phenomena taking place at the different scales are of course coupled with each other. For instance, the polymerization rate at the active catalyst site (micro-scale) affects both the temperature and heat transfer of the polymer particle (meso-scale) as well as the integral reactor heat balance (macro-scale). When considering all processes occurring at the three different length scales, polymerization models can become very complex. Depending on the modeling objective, a specific length scale is sometimes focused on (e.g. the meso-scale to analyze particle mass transfer limitations) while the other scales are strongly simplified or even neglected.

#### 2.4.2 Kinetic modeling

At the micro-scale, the polymer chain reactions take place that determine the chain microstructure which in return is linked to the final polymer properties. [72] To model the molecular processes of this length scale, a kinetic model is used. In this model, the polymerization is expressed in terms of kinetic rate constants and concentrations of reactants in order to describe the temporal course of the polymerization rates and molecular property distributions (e.g. molecular weight distributions). Since the kinetic constants needed for the model are catalyst specific, these need to be estimated using experimentally determined polymerization data, i.e. polymerization profiles for various conditions, in order to eventually simulate the polymerization behavior of the studied catalyst.

The elementary reaction steps occurring during the coordinative polymerization of olefins are very complex and not fully understood. To reduce the complexity but still being able to model the kinetic behavior of common industrial Ziegler-Natta catalysts, the kinetic mechanism is

described by a set of standard reaction steps. [14, 72–74] Depending on the modeling objective and the experimental data available to estimate the numerous kinetic rate constants, a set of reaction steps is chosen which best describes the experimental observations. The general kinetic scheme (Table 2.2) for the polymerization of olefins via organometallic catalysts consists of the following basic reaction steps:

- 1) Catalyst activation
- 2) Chain initiation
- 3) Chain propagation
- 4) Chain transfer
- 5) Catalyst deactivation

The titanium sites of ZN catalysts are typically activated by a cocatalyst (e.g. triethylaluminum). Other activation paths such as the activation by hydrogen, by monomer, or spontaneously are also possible. By this activation step, the potential catalyst site is converted to a vacant active site. A new polymer chain is created by the initiation step, in which one monomer molecule is added to the vacant active center forming a living polymer chain with a chain length of one. This chain can now grow by chain propagation. Here, the monomer is attached to the active site of the living chain, increasing the chain length by one monomer unit in each propagation step. The chain growth continues until a transfer reaction occurs. In the chain transfer reaction, the living polymer chain reacts with a chain transfer species. The living chain is terminated and a dead polymer chain and a vacant active site are produced. In industry, hydrogen is used to control the molecular weight since it is an effective chain transfer agent. Additionally, the transfer step may occur by other species such as monomer, cocatalyst or spontaneously ( $\beta$ -hydride elimination). The typical activity loss of Ziegler-Natta catalysts observed over time during the polymerization of olefins is believed to occur because of catalyst site deactivation. Both the vacant sites as well as the living polymer chains can deactivate forming a dead catalyst site or a dead polymer chain and a dead site, respectively. The deactivation step may happen spontaneously or by monomer, cocatalyst, hydrogen, or other species.

To the general kinetic scheme presented in Table 2.2 further reaction steps may be added. Site transformation [73, 75–77] and the multi-site nature of ZN catalyst [78, 79] are often considered. For the latter case, the kinetic scheme is still valid, but would apply to each single catalyst site type. The multi-site approach is required in order to model the broad molecular weight distributions (MWD) of ZN catalysts. This can be achieved by MWD deconvolution techniques by which the number of site types is estimated. [4, 80]

**Table 2.2:** Overview of standard reaction steps for the kinetic modeling of coordinative polymerization. [14, 72] In this scheme,  $S_p$ ,  $CoCat$ ,  $S_a$ ,  $M$ ,  $H_2$ ,  $P_n$ ,  $D_n$  and  $S_d$  are symbols for the potential catalyst site, cocatalyst, active catalyst site, monomer, hydrogen, living polymer of length  $n$ , dead polymer of length  $n$  and dead catalyst site, respectively.

Reaction Step	Chemical Equation
Activation	
• by cocatalyst	$S_p + CoCat \xrightarrow{k_{aCo}} S_a$
• by monomer	$S_p + M \xrightarrow{k_{aM}} S_a$
• by hydrogen	$S_p + H_2 \xrightarrow{k_{aH}} S_a$
• spontaneous	$S_p \xrightarrow{k_{aSp}} S_a$
Initiation	$S_a + M \xrightarrow{k_i} P_1$
Propagation	$P_n + M \xrightarrow{k_p} P_{n+1}$
Transfer	
• by hydrogen	$P_n + H_2 \xrightarrow{k_{trH}} S_a + D_n$
• by monomer	$P_n + M \xrightarrow{k_{trM}} P_1 + D_n$
• by cocatalyst	$P_n + CoCat \xrightarrow{k_{trCo}} S_a + D_n$
• spontaneous	$P_n \xrightarrow{k_{trSp}} S_a + D_n$
Deactivation	
• spontaneous	$P_n \xrightarrow{k_{dSp}} S_d + D_n$
	$S_a \xrightarrow{k_{dSp}} S_d$
• by species X	$P_n + X \xrightarrow{k_{dX}} S_d + D_n$
(e.g. $H_2$ , $M$ , or $CoCat$ )	$S_a + X \xrightarrow{k_{dX}} S_d$

A further important kinetic phenomenon observed for the polymerization of propylene is the rate enhancement by hydrogen. This can be explained by the dormant site theory (section 2.2.2) which was implemented in kinetic models in different forms. [4, 27, 36, 73, 81] The kinetic scheme can be simplified to three reaction steps (Table 2.3). [81] The dormant chain is formed by the regio-irregular 2,1-insertion of a propylene molecule into a living polymer chain. This dormant species can now be reactivated in two different ways: via hydrogen or monomer. The dormant chain can react with hydrogen to form a dead polymer chain and a hydrogenated active site (equally treated as a vacant active site). The reactivation step with hydrogen models the polymerization rate enhancement observed upon increase of the hydrogen concentration. With this kinetic step, the concentration of active sites is effectively increased, whereas the concentration of dormant chains not contributing to the polymerization rate is decreased. In a third reaction step, the reactivation of dormant chains is modeled in absence of hydrogen. By the 1,2-insertion of monomer into the dormant chain,

a living polymer chain is formed. Without this second reactivation step, the polymerization would come to a standstill in absence of hydrogen.

**Table 2.3:** Kinetic scheme for the rate enhancement by hydrogen based on the dormant site theory. [81] In this scheme,  $P_n$ ,  $M$ ,  $P_n^{dorm}$ ,  $H_2$ ,  $S_a$  and  $D_n$  are symbols for the living polymer of length  $n$ , monomer, dormant polymer of length  $n$ , hydrogen, active catalyst site and dead polymer of length  $n$ , respectively.

Reaction Step	Chemical Equation
Dormant Chain Formation	$P_n + M \xrightarrow{k_{dorm}} P_{n+1}^{dorm}$
Reactivation	
• by hydrogen	$P_n^{dorm} + H_2 \xrightarrow{k_{reH}} S_a + D_n$
• by monomer	$P_n^{dorm} + M \xrightarrow{k_{reM}} P_{n+1}$

### 2.4.3 Single particle models

The polymerization of olefins via supported catalysts starts on the catalyst particle and proceeds within the growing polymer particle. Since the (spatial) conditions within the particle such as temperature and monomer concentration directly affect the polymerization rates and therefore also the polymer properties, a special interest lies in modeling the processes of this length scale. To account for the physical processes occurring at the meso-scale, single particle models are employed connecting the micro- and macro-scale. Here, phenomena such as heat and mass transfer through the particle boundary layer and within the particle, particle growth and catalyst fragmentation are considered. Various particle models and modifications of these exist which were reviewed by Dubé et al. [82] and McKenna and Soares [83]. The two most common ones, the multigrain model (MGM) and the polymeric flow model (PFM), are explained briefly in the following.

The multigrain model was first developed by Yermakov et al. [84], Crabtree et al. [85] and Nagel et al. [86] between 1970 and 1980. Two levels of mass and heat transfer resistances are considered. The particle (macro-particle or secondary particle) is assumed to consist of an agglomerate of micro-particles (primary particles) (Figure 2.2) resembling the heterogeneous morphology of real polyolefin particles as observed by researchers such as Hock [87], Kakugo et al. [66, 67] and Noristi et al. [88]. Each micro-particle consists of a catalyst fragment covered by a layer of dead and living polymer. Monomer from the bulk phase first diffuses through the pores of the macro-particle and then through the polymer layer of the micro-particles to reach the active sites at the surface of the catalyst fragments where the polymerization occurs. The newly formed polymer accumulates there which leads to micro-particle and thus macro-particle growth. The MGM was further developed by



researchers such as Floyd et al. [51, 89], who used it to study aspects of heat and mass transfer, and Hutchinson et al. [90, 91] who analyzed particle overheating, particle growth and development of particle morphology.

The polymeric flow model was developed by Schmeal and Street [92], Singh and Merrill [93] and Galvan and Tirrell [94, 95] in the 1970s and 1980s. The essential assumption is that polymer chains and catalyst fragments form a continuum. Heat and mass transfer take place through the pseudo-homogeneous polymer matrix. The PFM is less complex than the MGM both in terms of the number of required parameters (only one level of transport resistance) and the numerical solution, but still gives qualitatively similar predictions. [4] Bartke and Reichert [96] calculated the complete molecular weight distribution as a function of the radial position within a growing polymer particle using the PFM. Kittilsen et al. [97] extended the PFM to include convection effects which was further developed by Parasu Veera et al. [98, 99]. Yiagopoulos et al. [100] studied heat transfer phenomena at the early growth of catalyst particles following the PFM developments of Hoel et al. [101]. Kanellopoulos et al. [102] extended the PFM to include both convective effects and a dual diffusion mechanism accounting for the change in particle morphology leading to the “random-pore polymeric flow model”.

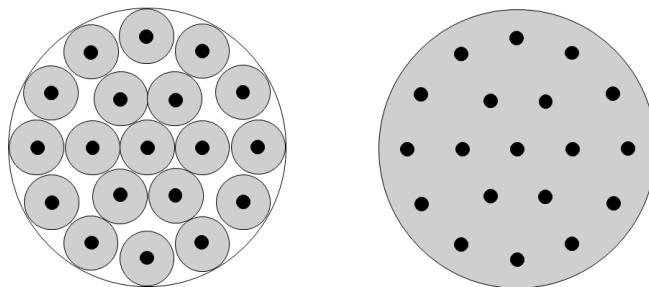


**Figure 2.2:** Schematic representation of the multigrain model (left) and of the polymeric flow model (right). [83]

#### 2.4.4 Thermodynamic modeling

Important variables of the described models, e.g. reactant concentrations in kinetic modeling, can be obtained via thermodynamic models. More general, physical properties relevant for process modeling are typically calculated based on thermodynamic models. For polyolefin systems, the Sanchez-Lacombe (SL) and Perturbed-Chain Statistical Association Fluid Theory (PC-SAFT) equations of state (EoS) are regarded as the two major state-of-the-art thermodynamic models. Both account for the size and shape of molecules and describe thermodynamic properties and phase behavior of polymer systems well. The SL EoS stands

out with its simplicity, whereas the PC-SAFT model, although more complex, shows superior predictive capabilities. [103, 104]

The SL EoS is based on lattice theory (Figure 2.3) and can be viewed as an extension of the classical Flory-Huggins theory. The basic model concept is that molecules consist of “mers” (parts) which are arranged within a lattice structure. Three macroscopic parameters are needed to describe a pure component: the characteristic temperature  $T^*$ , pressure  $P^*$  and closed-packed mass density  $\rho^*$ . Originally developed by Sanchez and Lacombe [105, 106], the SL model was applied to many different polyolefin systems [53, 54, 107–109].

The PC-SAFT EoS is a continuum model in which molecules are pictured to consist of spherical segments freely jointed and exhibiting repulsive and attractive forces among them. A pure component is characterized by three parameters: the number of segments per molecule  $m$ , the segment diameter  $\sigma$  and the energy related to the interaction of two segments  $\varepsilon$ . A detailed description of the PC-SAFT EoS is found in the original works of Gross and Sadowski [110, 111]. Applications of the PC-SAFT model to polyolefin systems are described in further literature [79, 112–114].

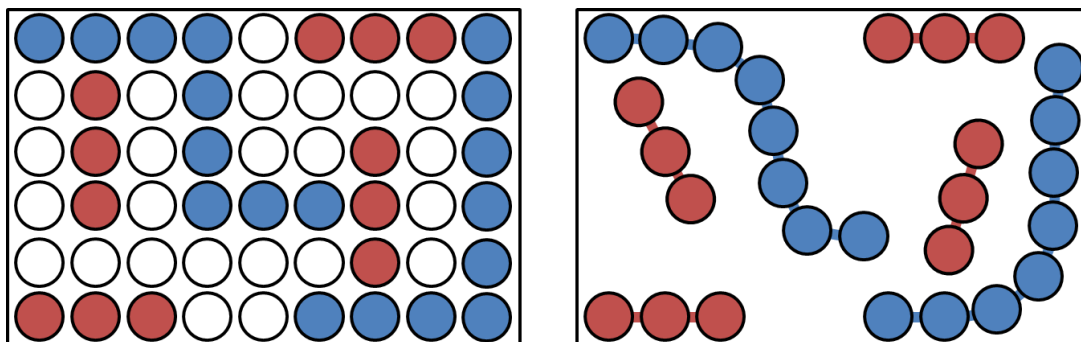


**Figure 2.3:** Schematic comparison of model concepts of the Sanchez-Lacombe (left) and PC-SAFT (right) equations of state. [103]

### 3 Research Objectives and Thesis Outline

Ziegler-Natta catalysts are considered as the workhorse of the polypropylene production industry. Since the catalyst greatly defines the process productivity as well as the product properties, process and product development is mainly driven in search of new catalysts with enhanced polymerization performance. One aspect in the development of these is lab-scale testing before pilot or commercial trials are tackled. However, the typical semi-batch reactor used for measuring gas phase polymerization kinetics is not directly comparable to an industrial continuous plant in which the catalyst is not fed to an empty reactor, but one with high solid contents of polymer particles. This mismatch may affect the information output of a lab-scale kinetic study.

Scope of this work is to study the kinetics of four modern Ziegler-Natta catalysts for the gas phase polymerization of propylene under lab-scale conditions that more resemble the situation in continuous industrial plants. A special emphasis is put on the effect of catalyst overheating which is a common challenge for highly active catalysts.

The thesis is grouped into three main sections. The first section deals with the kinetic study in which experiments were conducted in a 5 L horizontal stirred tank reactor under industrial relevant conditions. A seed bed polymerization method is established by analyzing the effect of a PP bed material on the kinetics of two catalysts. Subsequently, the polymerization kinetics are analyzed for three ZN catalysts with focus on the effect of catalyst overheating by comparing two different methods: prepolymerization and seed bed polymerization. The activity and MFR responses towards hydrogen as well as the particle morphology are investigated.

In the second section, the solubility of propylene in PP is measured in a high pressure magnetic suspension balance. State-of-the-art thermodynamic models relevant for process modeling are tested in describing the propylene/PP system.

In the third section, a phenomenological kinetic model is developed based on the results of the polymerization experiments and combined with an experimentally validated thermodynamic equation of state. The catalyst specific kinetic parameters are estimated and the kinetic model is validated.

## 4 Experimental Setup and Polymer Characterization

### 4.1 Setup for the polymerization experiments

Polymerization experiments were conducted in an existing laboratory setup (Figure 4.1). [22, 23, 41] The setup can be divided into four main parts: The raw material supply including the propylene purification unit, the polymerization reactor, the control units and the data acquisition system.

#### 4.1.1 Raw material supply and purification

The used Ziegler-Natta catalysts are sensitive to feed stream impurities such as water, oxygen and other polar compounds. In order to achieve high activities and good reproducibility, the raw materials were purified before entering the reactor. In particular, the monomer was purified by a multi-stage purification system.

Propylene (*Air Liquide*) was supplied in gas bottles with a purity of 99.5 mol%. A diaphragm pump (ORLITA MhS 18/5, *ProMinent*) guaranteed the monomer conveyance through the five stage purification system. In the first column, molecular sieve with a pore size of 4 Å was used to remove traces of water. In the second stage, an oxidized copper catalyst (PuriStar® R3-12, *BASF*) assured the removal of sulfur, arsine, H<sub>2</sub>S and COS compounds. In the third column, a 50:50 mixture of Selexsorb® CDL/COS (*BASF*) was used to adsorb a wide range of polar compounds. The fourth column contained PuriStar® R3-17 (*BASF*) in order to remove CO. The last stage consisted of two columns filled with Dynocel 680 which has a high capacity for polar organic and acid gas compounds. For improved removal of impurities, the liquid propylene was recycled several times through the purification system at a pressure of 40 bar.

Hydrogen (*Linde*) of purity 5.0 was supplied in gas bottles and applied as chain transfer agent. It was used as received without further purification.

In-house nitrogen (liquid storage tank, *Air Liquide*) of quality 5.0 was used for inertization of the reactor system. Further purification was performed by passing the gas over an Oxisorb® cartridge (*Linde*) in order to remove oxygen traces.

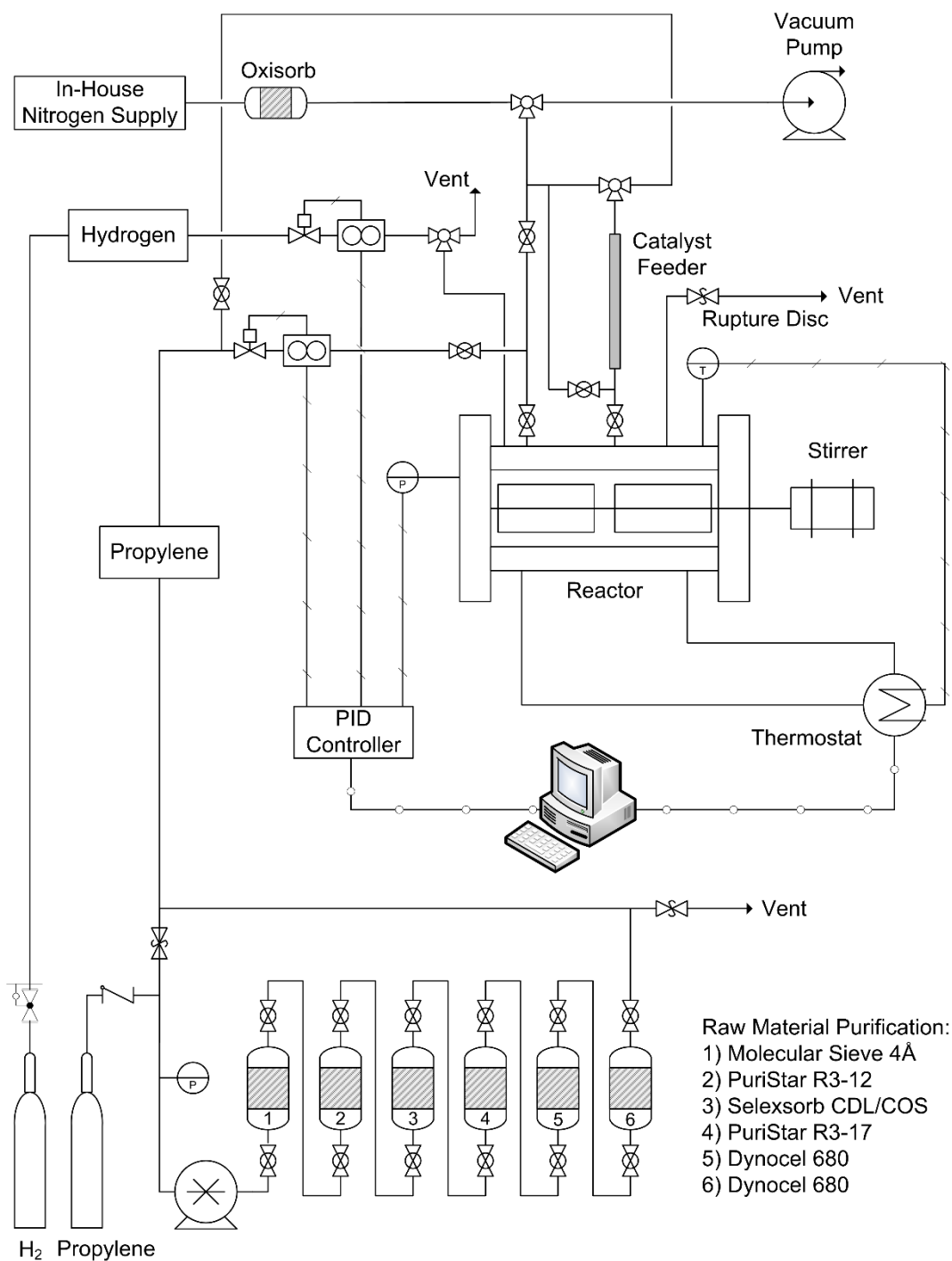


**Figure 4.1:** Experimental setup for the gas phase polymerization of propylene.

**Table 4.1:** Gas supply and quality.

Gas	Supplier	Purity
Propylene	<i>Air Liquide</i>	2.5
Hydrogen	<i>Linde</i>	5.0
Nitrogen	<i>Air Liquide</i>	5.0

#### 4.1.2 Lab-scale polymerization reactor

The gas phase polymerization experiments were performed in a 5 L horizontal stirred tank reactor under industrial relevant conditions (Figure 4.2). The reactor is designed for pressures up to 40 bar and temperatures up to 120 °C. The stainless steel reactor is cooled and heated via the jacket using a commercial thermostat (Proline RP 855, *Lauda*) with a maximum heating power of 3.5 kW and a maximum cooling power of 1.6 kW. A thermal oil (Therminol® ADX 10, *Frago*) was used as thermostating liquid. Since propylene is fed to the reactor in the liquid state, cooling is additionally caused by monomer evaporation. However, this only amounts up to a fraction of about 20 % as the specific heat of evaporation is 18.4 kJ/mol [115] and the specific reaction heat is 102 kJ/mol [116]. The temperature is measured in the center of the reactor with a Pt100. The pressure is measured with a digital pressure sensor (IUT-10, *WIKA*) within a range of 0 to 40 bar and a relative error of 0.15 %. The anchor-type stirrer is rotated via a magnetic coupling (bmd 300, *Büchi*) driven by a three phase variable gear motor (*Büchi*). Stirring speeds up to 800 rpm can be realized.

The gases and the catalyst system are inserted via the top of the reactor. Propylene is fed via a liquid phase mass flow controller (Flomega 5882, *Brooks*) and hydrogen via a gas phase mass flow controller (MF50S, *Brooks*). The catalyst system is injected directly with liquid propylene from the purification unit without passing the mass flow controller. The fast injection fluid flow is caused by the pressure difference of liquid propylene at 40 bar and the reactor pressure.

A slide vane rotary vacuum pump (P 6 Z, *Ilmvac*) and the in-house nitrogen are connected to the reactor for inertization.

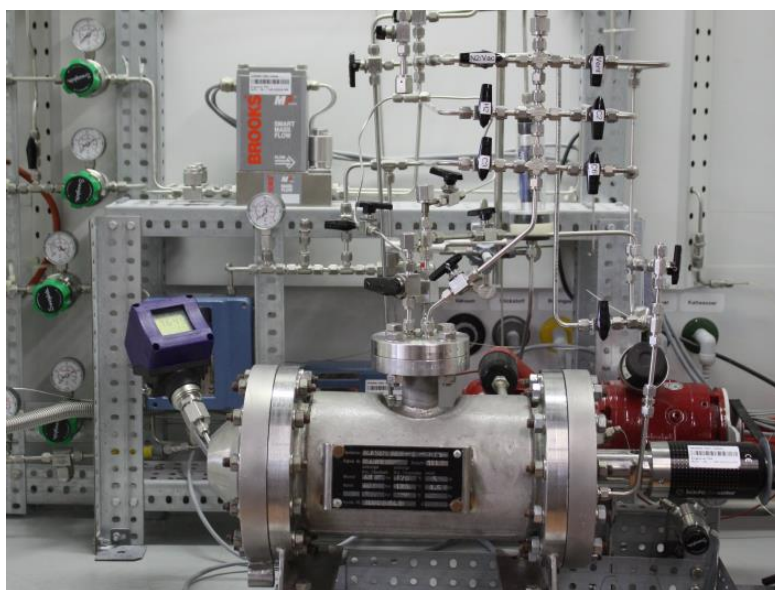


**Figure 4.2:** Horizontal gas phase polymerization reactor.

#### 4.1.3 Measurement of reaction kinetics and control units

The polymerization reactor is operated in semi-batch mode at isobaric and isothermal conditions. During the reaction, gaseous propylene is converted to solid polypropylene. The density of the solid is much higher than the density of the gas. The consequent pressure drop is compensated by constantly feeding monomer to the reactor. At constant pressure and temperature, the mass flow of propylene into the reactor is equal to the gross propylene consumption by reaction which is proportional to the polymerization rate or activity of the catalyst. Thus the reaction rate is accessible during the polymerization experiment.

In order to maintain isobaric conditions, monomer is fed to the reactor in a closed pressure control loop. The pressure value is transmitted from the *WIKA* pressure sensor to a PID controller (i16, Omega i-Series, *Newport*) via a voltage signal. Depending on the difference between the measured pressure value and the set point, the controller forwards a voltage signal to a control box (*Brooks Instrument*) which regulates the propylene flow via the mass flow controller.

Isothermal conditions are achieved by a cascade closed loop control which is available via the *Lauda* thermostat. The cascaded control consists of an outer and an inner PID controller. The outer PID controller compares the reactor temperature with the manually entered temperature set point and adjusts the inner thermostat bath temperature set point in order to maintain the target reactor temperature. The inner PID controller manipulates the heating power in order to achieve the set thermostat bath temperature.

#### 4.1.4 Data acquisition

The commercial software *DASYLab 9 (National Instruments)* was used for data acquisition. A snapshot of the interface during a typical polymerization experiment is shown in Figure 4.3. During an experiment, pressure, temperature and mass flows are collected, processed and displayed. The data of each experiment is recorded and stored in an ASCII-file. For safety reasons, the process inputs, i.e. the set temperature and pressure, could also be set manually directly at the corresponding controllers.

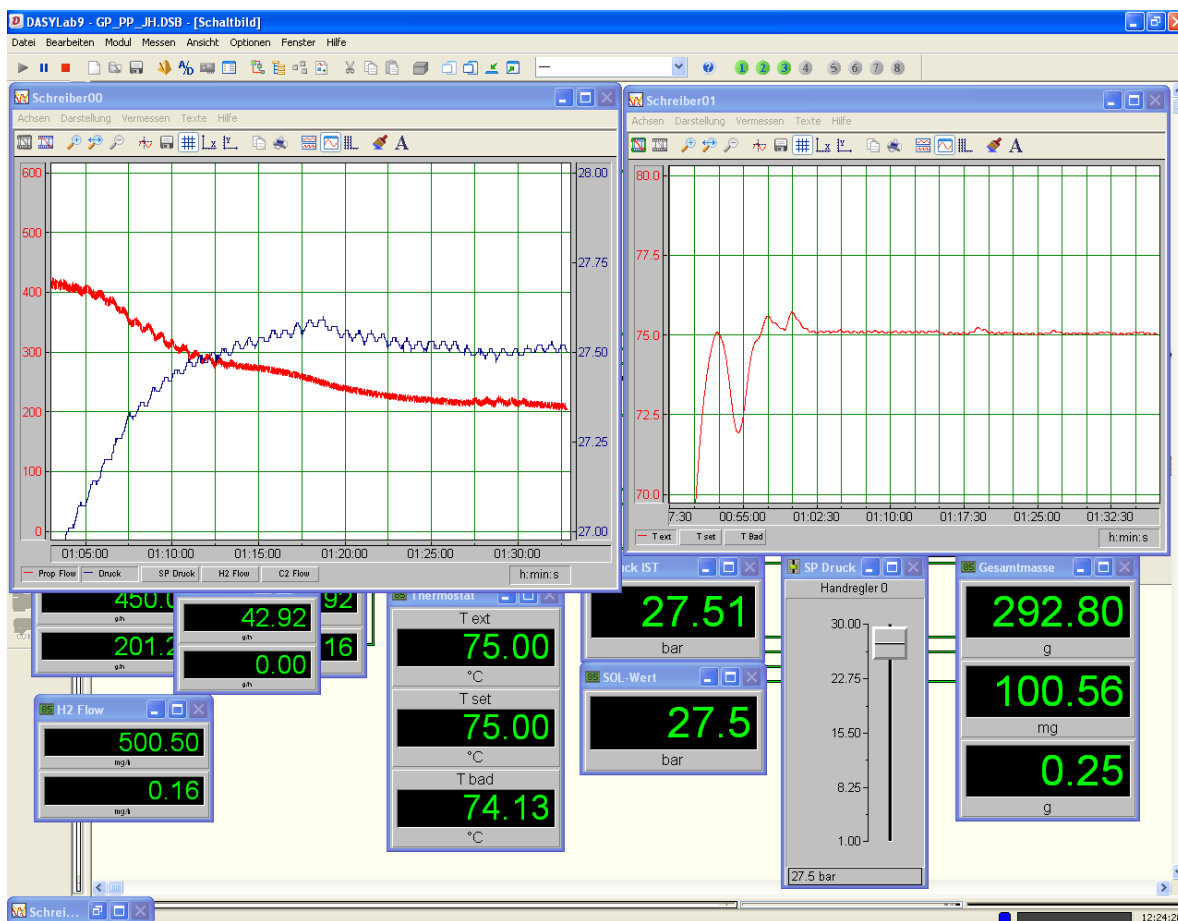


Figure 4.3: User interface of DASYLab 9 during a polymerization experiment.

## 4.2 Chemicals and catalyst preparation

Four different commercial Ziegler-Natta catalysts were studied in the gas phase polymerization of propylene. The catalysts were provided by the industrial partner and can be grouped into the 4<sup>th</sup> and 5<sup>th</sup> generation with catalyst A and B being phthalate-based and C and D diether-based. The active compound of all catalysts is titanium.

Triethylaluminum (TEA, 93 %, *Sigma Aldrich*) was used as cocatalyst. TEA does not only function as cocatalyst, but also as a scavenger reacting with impurities which might still be present in the reactor. A fixed TEA amount of 0.3 mL was used in all polymerization experiments. Isobutylisopropyldimethoxysilane (*abcr*) was used as external donor in form of a 0.5 M solution in *n*-heptane (*Sigma Aldrich*). The external donor was used in a fixed ratio with respect to the catalyst.

ZN catalysts are very sensitive to impurities such as water or air and contact with such media results in catalyst poisoning. Furthermore, the cocatalyst TEA is extremely reactive with air (and water) and exposure to air must be avoided. Therefore, catalyst preparation was carried



out under inert conditions in a glove-box (*Jacomex*). For catalyst preparation, 8 to 12 mg of the dry catalyst were weighed in a glass weighing boat and transferred to one chamber of a specially designed double-chambered steel injector (short: feeder, Figure 4.4). 0.6 mL of mineral oil (*Primol 352, ExxonMobil*) were added to the catalyst in order to remove possible electrostatic charges, mechanically protect the catalyst during injection and reduce overheating. The latter case is because upon catalyst injection, oil needs to be exchanged with monomer to start the polymerization and thus the initial polymerization rate is reduced. [117] The external donor and TEA were filled into the second chamber. Precontact of catalyst and cocatalyst is avoided by the separation of the two chambers by a ball valve. Once the feeder was filled with all needed components and the valves were closed, the feeder could be safely transferred to the reactor.

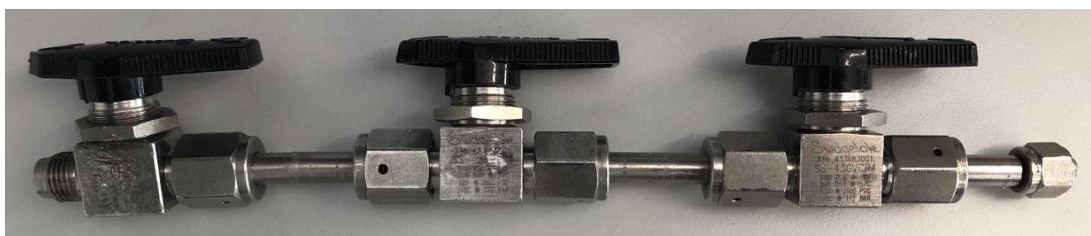


**Figure 4.4:** Double-chambered steel injector for catalyst/oil (left chamber) and external donor/cocatalyst (right chamber).

## 4.3 Polymerization procedure

### 4.3.1 Reactor inertization

Due to the high sensitivity of ZN catalysts to traces of oxygen or water, careful reactor inertization is needed prior to each polymerization experiment in order to obtain high activity and reproducibility. The reactor was therefore heated up to 100 °C to remove any moisture on the reactor walls. Vacuum was applied for about 30 min followed by pressurizing the reactor with nitrogen up to 10 bar for about 5 min. The vacuum-nitrogen cycle was repeated for at least six times. After these steps, the reactor was cooled down and pressurized with nitrogen.

When a seed bed polymerization was performed, a certain amount (standardly 100 g) of PP powder was placed inside the reactor prior to the inertization procedure. The reactor was prepared in the same way as described above with the seed bed being stirred at 10 rpm during the vacuum/nitrogen cycle.

### 4.3.2 Polymerization with a prepolymerization step

Polymerization experiments including a prepolymerization step, i.e. starting the polymerization at a relatively low temperature, were conducted as follows (Figure 4.5). After the reactor was rendered inert, vacuum was applied for about 15 min. Then, the reactor was filled with propylene and hydrogen and heated to the desired initial reaction temperature. Note that the standard prepolymerization temperature was 40 °C, but some variations were performed with respect to this temperature. The stirrer was turned on and the stirring speed set to 350 rpm. The initial pressure was controlled to be about 2 bar below the vapor pressure of propylene in order to avoid formation of liquid propylene. Prior to the polymerization start, the catalyst was prepared as described in section 4.2. The feeder was connected to the reactor under nitrogen flow with the catalyst chamber mounted closest to the reactor. The connections were rendered inert by alternating nitrogen and vacuum for at least 20 times. The polymerization was started by catalyst injection with liquid propylene. Here, the bottom valve of the feeder was opened first and directly afterwards simultaneously the middle and top valves resulting in flushing of catalyst, cocatalyst and external donor into the reactor. The valves were opened for a few seconds resulting in a pressure increase of 1 bar. It was assured that gas phase conditions were preserved. Upon catalyst injection, the reactor was directly heated to the desired main polymerization temperature. The feeder was flushed for a second time with liquid propylene to ensure complete injection of the catalyst system. Parallel to the reactor heat up, propylene was fed to the reactor via the mass flow controller with the maximum flowrate of about 1 kg/h while maintaining gas phase conditions inside the reactor. When the reaction temperature and pressure of 28.5 bar were reached, the monomer feed was changed to the controlled mode. Propylene was fed via the pressure control loop according to the set pressure. The reaction was carried out for one hour (with the polymerization starting upon catalyst injection). The experiment was stopped by releasing the pressure and cooling down the reactor. The remaining propylene in the produced PP was removed by nitrogen purging for 30 min. The full deactivation of the catalyst system was achieved by inserting air into the reactor before opening the reactor and collecting the produced polymer.

### 4.3.3 Polymerization without a prepolymerization step

Polymerization experiments without a prepolymerization step differed only slightly in the operational procedure: The initial temperature and pressure of the reactor were set to the main reaction conditions. Furthermore, no heat up was needed since the required reaction conditions were achieved right upon polymerization start.

The experimental procedure without a prepolymerization step is shown in Figure 4.6. The reactor was evacuated, filled with propylene and hydrogen, and heated up to reaction temperature. The initial pressure was adjusted to be 1 to 2 bar below the reaction pressure of 28.5 bar since the catalyst injection further increased the reactor pressure. The catalyst feeder was prepared and the catalyst system was injected with liquid propylene as described before. Propylene was fed via the pressure control loop and the reaction was carried out for one hour upon catalyst injection at a stirring rate of 350 rpm.

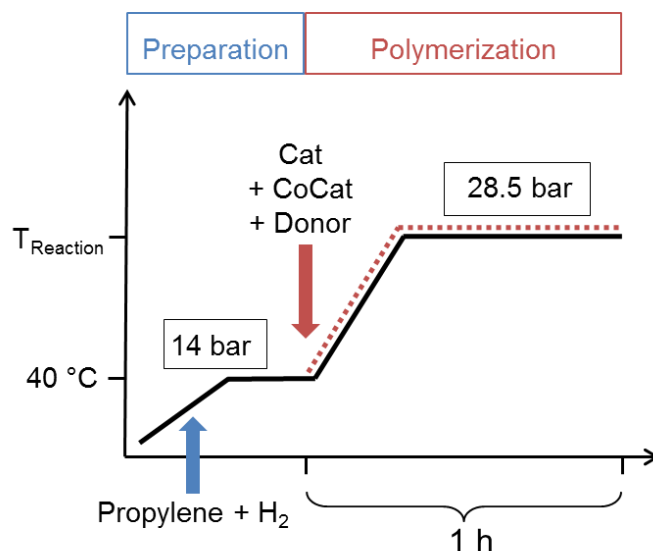


**Figure 4.5:** Experimental polymerization procedure with a prepolymerization step.

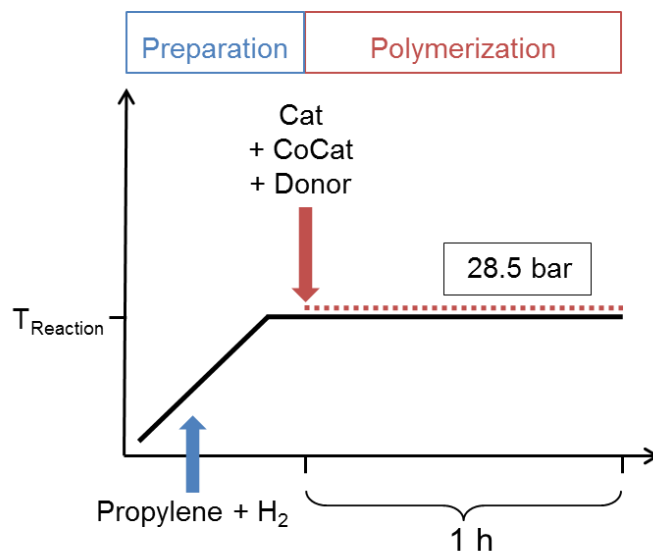


**Figure 4.6:** Experimental polymerization procedure without a prepolymerization step.

#### 4.3.4 Seed bed polymerization experiments

Seed bed polymerization experiments were carried out in the exact same ways as the procedures with and without a prepolymerization step. The only difference is the use of a seed bed. For that, prior to rendering the reactor inert, a defined amount of PP (standard: 100 g) from earlier polymerization runs was placed inside the empty reactor. The reactor was rendered inert and the polymerization was performed according to section 4.3.2 or 4.3.3.

#### 4.4 Experimental plan

The polymerization kinetics of four different ZN catalysts A to D were analyzed experimentally in the 5 L gas phase reactor. The main focus was to study the influence of the initial temperature, seed bed mass and hydrogen mass. The main reaction temperature and pressure were not varied. The following industrial relevant conditions were studied:

- Reaction temperature: 80 °C (Cat A&B) or 75 °C (Cat C&D)
- Reaction pressure: 28.5 bar
- Initial temperature: 40 to 80 °C
- Seed bed mass: 0 to 200 g
- Hydrogen mass: 0 to 400 mg

The experimental analysis can be separated into two objectives. First, the effect of the initial temperature and a seed bed was studied in detail for catalysts A and B at a fixed hydrogen mass of 100 mg. The influence of the seed bed mass was then extended to catalysts C and D. Having established a seed bed polymerization procedure, the second objective was to study the effect of hydrogen on the polymerization kinetics of catalysts A, C and D for the two different polymerization methods of prepolymerization (catalyst injection at 40 °C) and seed bed polymerization (catalyst injection at the main reaction temperature in presence of a seed bed).

#### 4.5 Polymer characterization

The PP products were characterized by their melt flow rate, weight average molecular weight and crystallinity. The morphology of the produced powders was qualitatively analyzed by light and scanning electron microscopy and quantitatively by bulk density, porosity and particle

size distribution measurements. Note that for the seed bed polymerization experiments the obtained samples are a mixture of the freshly produced PP powder and the seed bed particles and the characterization was performed for the mixture of particles.

#### 4.5.1 Melt flow rate and molecular weight

The melt flow rate (MFR) correlates with the melt viscosity and thus the molecular weight of a polymer sample. It is a standardized test which is very common for quality control at commercial polyolefin plants and one of the grade's property specifications for PP processors. The MFR is defined by the mass rate of molten polymer that flows through a standardized orifice at a given temperature under pressure of a standardized load. [4] The unit is g/10 min. This standard test method is defined by ASTM D 1238 [118] and ISO 1133 [119] with the specific test temperature of 230 °C and test load of 2.16 kg for PP.

For MFR measurements, a micro flow melt indexer (CSI-127MF, *Custom Scientific Instruments*) was used which allowed the estimation of the MFR for small quantities of polymer. The output of the measurement was the recorded time the molten sample needed to pass through a certain distance of a die. A calibration curve was therefore established to correlate the measured time with the actual MFR (Figure 4.7). Various samples with known, but different MFR (provided by the project partner) were measured with the micro flow melt indexer. The measurement time  $t$  [s] and MFR [g/10 min] could be correlated by:

$$MFR = 428.06 t^{-1.137} \quad (4.1)$$

To determine the MFR of a produced PP sample, at least five measurements were performed and the average recorded time was used to calculate the MFR.

Based on the obtained MFR, the weight average molecular weight  $M_w$  [kg/mol] was calculated by an empirical correlation provided by the industry partner:

$$M_w = 538.445 MFR^{-0.249} \quad (4.2)$$

The experimental error of the MFR measurement was estimated to be of 15 %. The reproducibility of the MFR measurements is shown in Figure 4.8. Note that each MFR was obtained from a separate PP powder produced in the gas phase reactor under the same conditions.

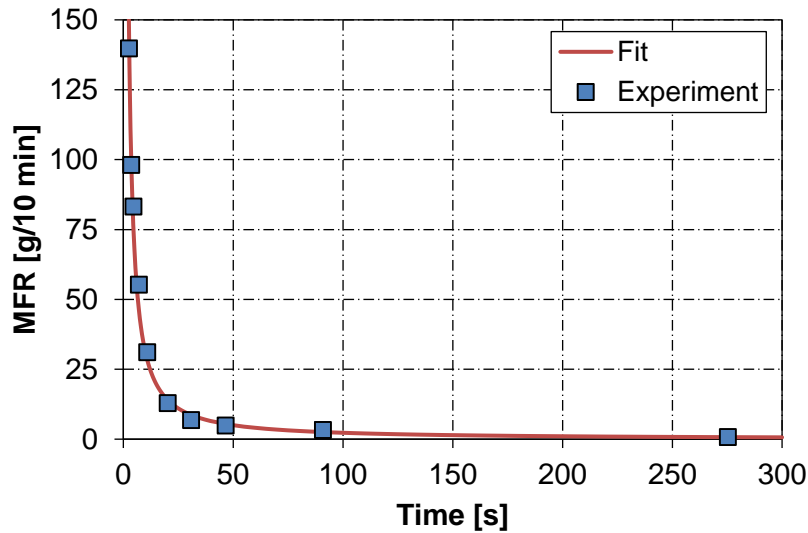


**Figure 4.7:** Calibration curve fit ( $R^2 = 0.993$ ) for MFR and measured time of the micro flow melt indexer.

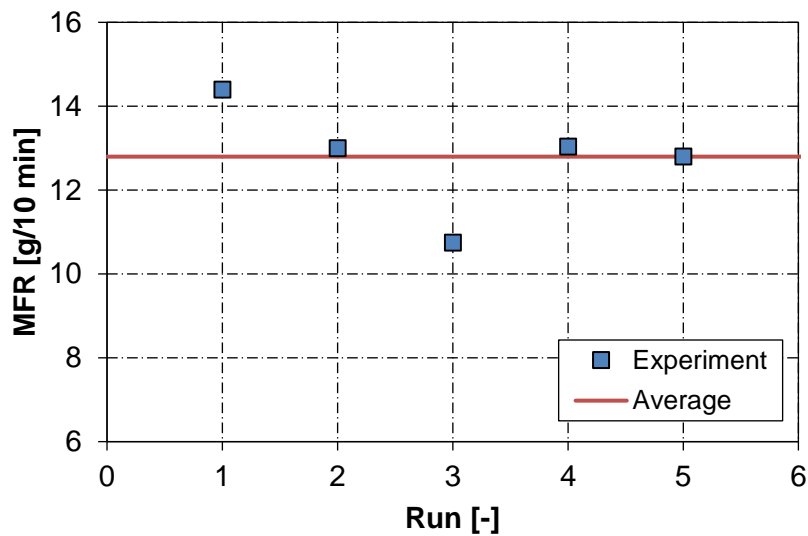


**Figure 4.8:** Reproducibility of MFR measurements. Each MFR value was obtained from a separate PP sample which was produced under identical polymerization conditions.

#### 4.5.2 Crystallinity

The crystallinity of polypropylene correlates with its mechanical properties. Depending on how the PP chains are able to align, few or many crystalline domains are present in a given PP powder. The alignment depends on the stereo- and regio-regularity of the polymer chains and crystallinity is highest for isotactic PP with a low number of stereo- and regio-defects. In case of the commercially relevant isotactic PP, the crystallinity varies only in a narrow range of about 40 to 70 % and is mainly determined by the catalyst system in use. [7]

The term crystallinity is actually not very precise and one should distinguish between the crystalline mass and volume fraction. In this thesis, crystallinity is used as a short term for the crystalline mass fraction  $w_{cr}$  which is defined as:

$$w_{cr} = \frac{m_{cr}}{m_{am} + m_{cr}} = \frac{m_{cr}}{m_{PP}} \quad (4.3)$$

The crystalline volume fraction  $v_{cr}$  is given by:

$$v_{cr} = \frac{V_{cr}}{V_{am} + V_{cr}} = \frac{V_{cr}}{V_{PP}} \quad (4.4)$$

As sorption only takes place in the amorphous fraction of the polymer, the determination of crystallinity is crucial in order to calculate the effective monomer concentration in the amorphous phase. Different analytical methods can be used to obtain the crystallinity of a given PP sample such as differential scanning calorimetry, X-ray diffraction or Helium pycnometry (via density).

#### 4.5.2.1 Differential scanning calorimetry

The crystalline mass fraction of PP can be determined by differential scanning calorimetry (DSC). By integration of the first melting peak, the specific enthalpy of fusion  $\Delta H_f$  of the sample can be obtained. By relating this specific enthalpy to the theoretical enthalpy of fusion of 100 % crystalline PP  $\Delta H_{f,100\%}$ , the crystalline mass fraction can be estimated:

$$w_{cr} = \frac{\Delta H_f}{\Delta H_{f,100\%}} \quad (4.5)$$

DSC measurements (UNIX DSC7, *Perkin Elmer*) were performed at the Experimental Polymer Physics Group of the Martin-Luther-University Halle-Wittenberg. 10 mg of a sample were used for each run. The sample was heated up from room temperature to 200 °C with a heating rate of 10 K/min. Only the first scan was used for crystallinity analysis to determine the nascent polymer powder properties. The integration was conducted from 60 to 180 °C and the theoretical enthalpy of fusion of 100 % crystalline PP was taken to be 209 J/g [116].

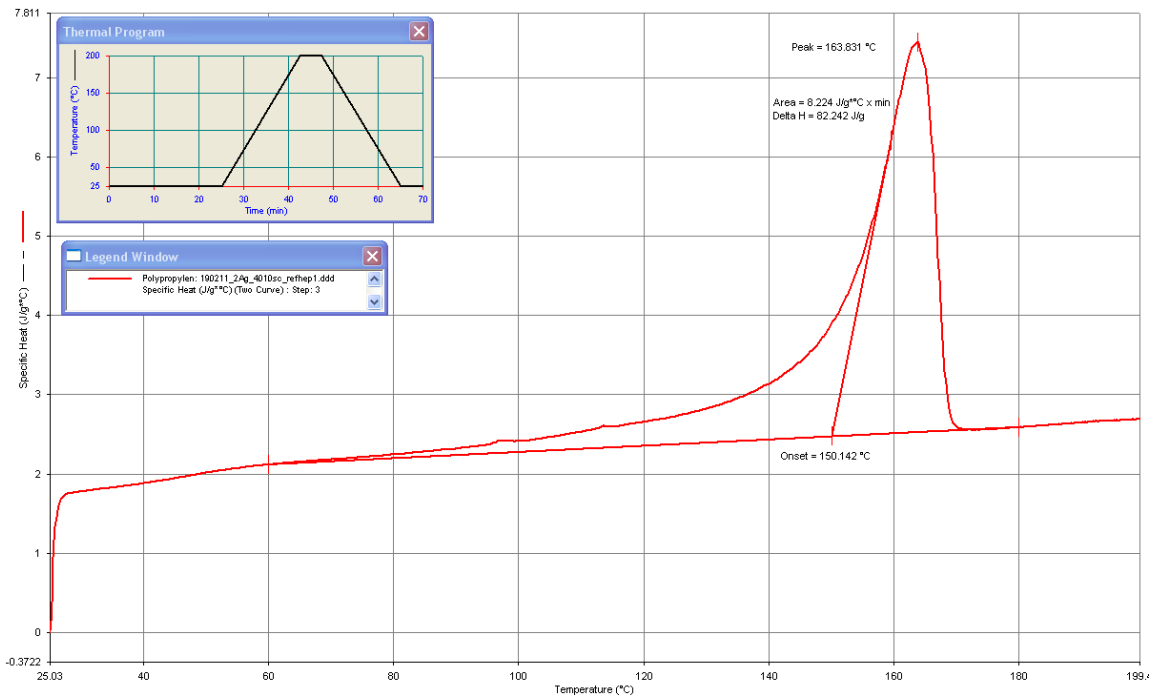


**Figure 4.9:** DSC curve of a PP sample.

#### 4.5.2.2 Wide angle X-ray scattering

Another method for crystallinity estimation is wide angle X-ray scattering (WAXS). Selected samples were analyzed at the Experimental Polymer Physics Group of the Martin-Luther-University Halle-Wittenberg. WAXS experiments were performed in transmission mode using a SAXSLAB laboratory setup (Retro-F) equipped with an AXO microfocus x-ray source and an AXO multilayer x-ray optic (*AXO Dresden GmbH*) used as monochromator for Cu-K $\alpha$  radiation ( $\lambda = 0.154$  nm). A two-dimensional (2D) detector (PILATUS3 R 300K, *DECTRIS*) was used to record the 2D scattering patterns. The samples were measured at room temperature and in the molten state at 180 °C to obtain the spectrum of the completely amorphous PP. The resulting spectra (Figure 4.10) were used to calculate the crystalline volume fraction. Here, the obtained intensity spectra needed to be integrated and the ratio of the integration areas of the completely amorphous (molten) sample  $A_{am}$  and the sample measured at room temperature  $A_{sample}$  was used to estimate the crystalline volume fraction:

$$v_{cr} = 1 - \frac{A_{am}}{A_{sample}} \quad (4.6)$$



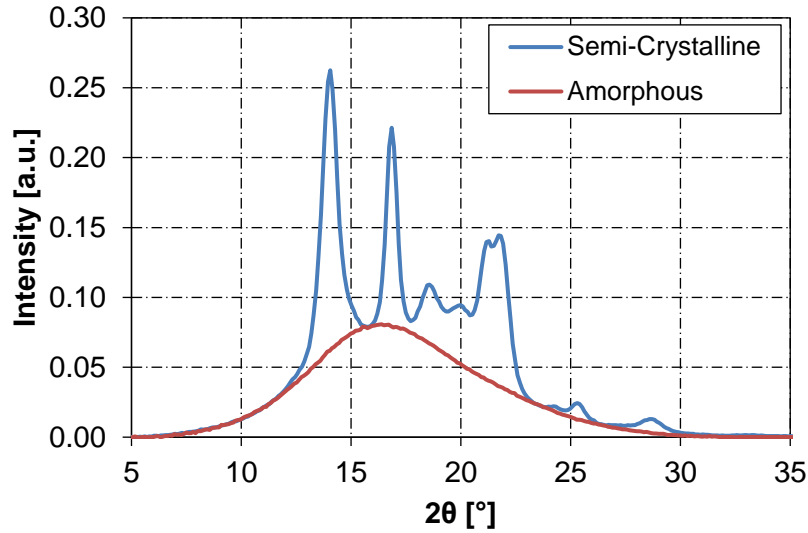


**Figure 4.10:** Example of the WAXS spectra of a PP powder sample obtained at room temperature (semi-crystalline) and at 180 °C in the molten state (amorphous). The sample was synthesized with catalyst A at 80 °C, 28.5 bar and 100 mg hydrogen with the method of prepolymerization.

#### 4.5.2.3 Helium pycnometry

The polymer density was measured at room temperature via Helium pycnometry (Pycnomatic ATC, *Porotec GmbH*) at the Department of Industrial Chemistry of the Martin-Luther-University Halle-Wittenberg. Helium pycnometry is a non-destructive method which is commonly applied in order to estimate the density of porous materials. The density of PP is directly correlated with its crystallinity. Once the polymer density  $\rho_{PP}$  of a given PP sample is known, the crystalline volume fraction can be calculated by using the theoretical density values for completely amorphous  $\rho_{am}$  and completely crystalline PP  $\rho_{cr}$ , which were taken to be 852 and 937 kg/m<sup>3</sup> [116], respectively [60, 65, 120]:

$$v_{cr} = \frac{\rho_{PP} - \rho_{am}}{\rho_{cr} - \rho_{am}} \quad (4.7)$$

The crystalline mass fraction is given by:

$$w_{cr} = \frac{\rho_{cr}}{\rho_{PP}} \frac{\rho_{PP} - \rho_{am}}{\rho_{cr} - \rho_{am}} = \frac{\rho_{cr}}{\rho_{PP}} v_{cr} \quad (4.8)$$

#### 4.5.3 Particle morphology

Selected powders were analyzed by different methods to receive an insight into the particle morphology. Light and scanning electron microscopy were used as a rather qualitative

description of the morphology, whereas measurements of the bulk density were used in an attempt to quantitatively capture the powder morphology. Furthermore, the porosity and particle size distribution measurements were conducted.

#### 4.5.3.1 Light and scanning electron microscopy

Selected samples were analyzed by light microscopy in order to capture the particles “outer morphology”, i.e. to identify rather spherical or non-spherical particles. Images were taken by a digital camera (EOS 600D, *Canon*) mounted onto a stereomicroscope (S8AP0, *Leica Biosystems*) at the Group of Developmental Biology of the Martin-Luther-University Halle-Wittenberg.

For further magnification, scanning electron microscopy (SEM) was used. Selected samples were analyzed at the Group of General Material Science of the Martin-Luther-University Halle-Wittenberg. The polymer samples were fixed on a SEM sample holder and sputtered with a conductive chromium layer. The prepared samples were analyzed under high vacuum ( $10^{-6}$  mbar) using the scanning electron microscope Philips ESEM XL 30 FEG with an acceleration voltage of 1 to 2 kV in the secondary electron mode.

#### 4.5.3.2 Bulk density

The bulk density can be used as an approximate, but quantitative evaluation of the morphology of the produced PP powders. To measure the bulk density, a graduated measuring cylinder with a diameter of 25 mm was filled with PP powder up to the 20 mL mark. During filling, the cylinder was tapped several times until the volume remained constant. Thus the results presented in this thesis refer to the so called tapped bulk density. The tapped density was chosen instead of the poured bulk density because a better reproducibility was found for the former case. The filled cylinder was weighted. This procedure was performed at least three times and the bulk density was calculated by dividing the average powder mass by the filled volume of 20 mL. An estimation of the reproducibility of the bulk density measurements is given in Figure 4.11.

Although the bulk density may be affected by many different factors such as the porosity of the powder, the shape of the particles, or the particle size distribution (small particles might fill void spaces and lead to an increase in bulk density), it allows a simple estimation of powder morphology. In combination with other analytical methods, a more detailed comparison of the produced powders is possible.

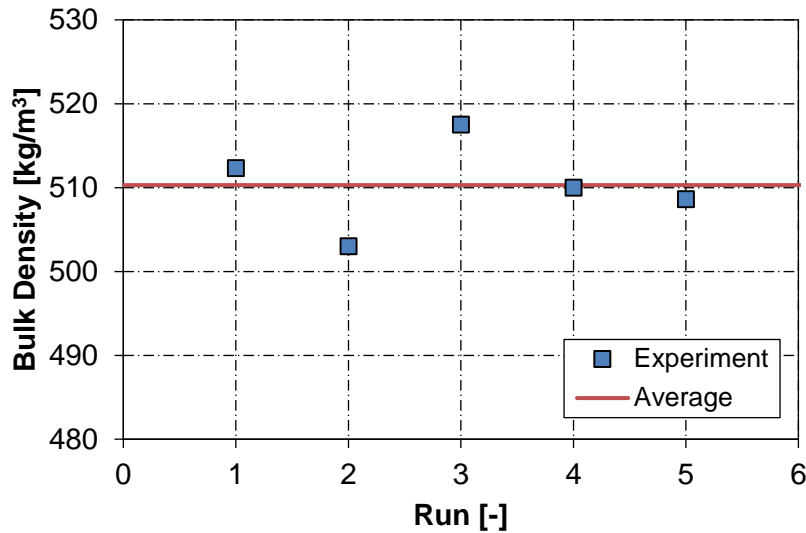


**Figure 4.11:** Reproducibility of bulk density measurements. Each bulk density value was obtained from a separate PP sample which was produced under identical polymerization conditions.

#### 4.5.3.3 Mercury porosimetry

The porosity of the polymer powders was measured via Mercury porosimetry. Both low and high pressure runs were performed on a Pascal 140 (up to 4 bar) and Pascal 440 (up to 4000 bar) porosimeter (both *Thermo Finnigan*), respectively, at the Department of Industrial Chemistry of the Martin-Luther-University Halle-Wittenberg. By combining both measurement results, the total porosity was evaluated.

#### 4.5.3.4 Particle size distribution

The particle size distribution (PSD) was measured by the method of laser diffraction using a Mastersizer 3000 (*Malvern Panalytical*). The entire PP sample was mixed thoroughly by moving the sample bag continuously changing its orientation in order to achieve a representative measurement. In order to avoid plugging inside the Mastersizer setup, a sieve was used to remove particles larger than about 4 mm. These particles were typically agglomerates or sheet like particles of a negligible fraction. About 10 g of the sample were used for one measurement run. Two to three runs were performed for each sample to check for reproducibility (Figure 4.12). Since the upper detection limit is 3.5 mm in diameter, particles larger than this size could not be detected. However, the amount of particles larger than 3.5 mm was found to be rather small.

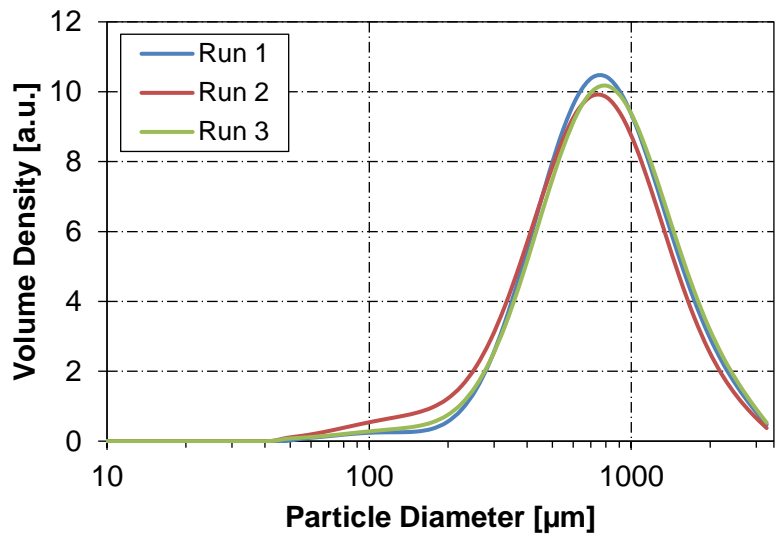


**Figure 4.12:** Reproducibility of particle size distribution measurements. Each PSD was obtained from a single measurement run from the same sample.

## 5 Experimental Study of the Gas Phase Polymerization of Propylene

This chapter is divided into two parts. In the first one, the polymerization kinetics are discussed based on mainly the results of catalyst activity and MFR. In the second part, the particle morphology aspects are elevated in detail.

### 5.1 Results of the gas phase polymerization experiments

In this section, the experimental kinetic results of the gas phase polymerization of propylene with the four different Ziegler-Natta catalysts A, B, C and D are presented. In the first part, the effect of the initial temperature and a seed bed on the polymerization kinetics of catalysts A and B are discussed and the effect of the seed bed mass is extended to catalysts C and D. After having established the prepolymerization and seed bed polymerization method, in the second part, the effect of hydrogen is presented for catalysts A, C and D for the two methods.

#### 5.1.1 Reaction condition profiles and catalyst activity

The obtained experimental data of a typical polymerization run for both direct injection and prepolymerization are presented in Figure 5.1 and Figure 5.2. When isothermal and isobaric conditions are reached, the mass flow of propylene into the reactor equals the gross consumption of propylene by reaction and the kinetic profile is accessible. This stage is typically reached after about 10 min for the case of direct injection (Figure 5.1). Upon polymerization start (catalyst injection), first the temperature needs to be stabilized by the temperature controller. The bath temperature has to be lowered by several degrees Celsius in order to remove the heat of polymerization. Additionally, the reaction pressure needs to be reached as well.

In case of the prepolymerization experiment (Figure 5.2), upon catalyst injection, first the temperature is raised to reaction conditions. Propylene is fed simultaneously (maintaining gas phase conditions) in order to obtain the desired reaction pressure. After the reaction conditions are reached, the system needs to stabilize and typically after about 20 min the kinetic profile is available.

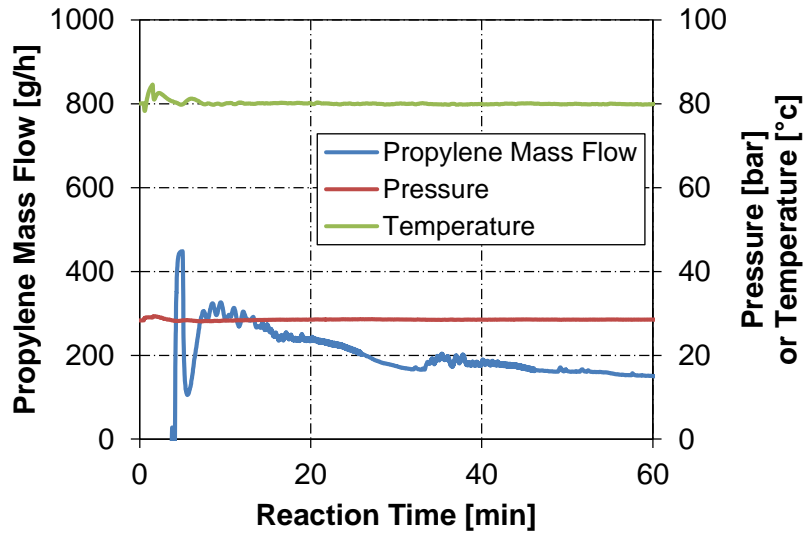


**Figure 5.1:** Propylene mass flow, pressure and temperature during a polymerization experiment for the seed bed polymerization method using catalyst A, i.e. without a prepolymerization step and in presence of a seed bed. Reaction conditions: 80 °C, 28.5 bar, 100 mg H<sub>2</sub>.

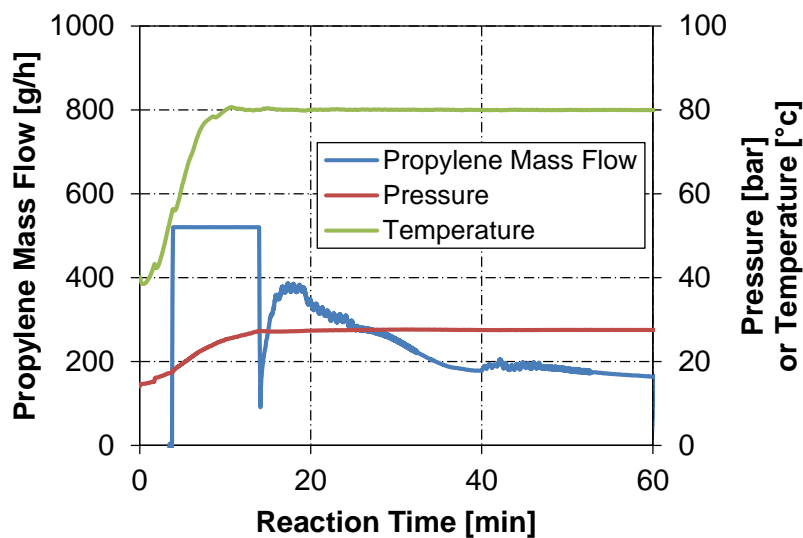


**Figure 5.2:** Propylene mass flow, pressure and temperature during a polymerization experiment including a prepolymerization step using catalyst A. Reaction conditions: 80 °C, 28.5 bar, 100 mg H<sub>2</sub>.

Once the reactor is under constant pressure and temperature, the mass flow of propylene can be used to calculate the time-dependent catalyst activity. The activity is defined as the mass of polypropylene that is produced per mass of catalyst and time. Since the mass feed of monomer into the reactor equals the mass production of PP by reaction, the activity  $A$  can be calculated by simply dividing the propylene mass flow  $\dot{m}_{C_3}$  by the used catalyst mass  $m_{Cat}$ :

$$A(t) = \frac{\dot{m}_{C3}(t)}{m_{Cat}} \quad (5.1)$$

The calculated activity profile is shown as an example in Figure 5.3 together with the pressure profile. Note that the fluctuations in the activity are not due to the actual polymerization reaction, but because of control oscillations caused by the pressure controller.

Besides the actual activity profile, the yield  $y$  of each polymerization experiment was obtained by relating the weighted final polymer mass to the used catalyst amount:

$$y = \frac{m_{PP}}{m_{Cat}} \quad (5.2)$$

When dividing the yield by the reaction time  $t_r$ , the average activity  $\bar{A}$  is received:

$$\bar{A} = \frac{y}{t_r} \quad (5.3)$$

In this work, the reaction time was always one hour. It was counted from the injection of the catalyst system to the end of the reaction which was defined by opening the valve to vent off the monomer. The average activity was used as a simple quantity to compare the influence of different conditions affecting the polymerization rate.

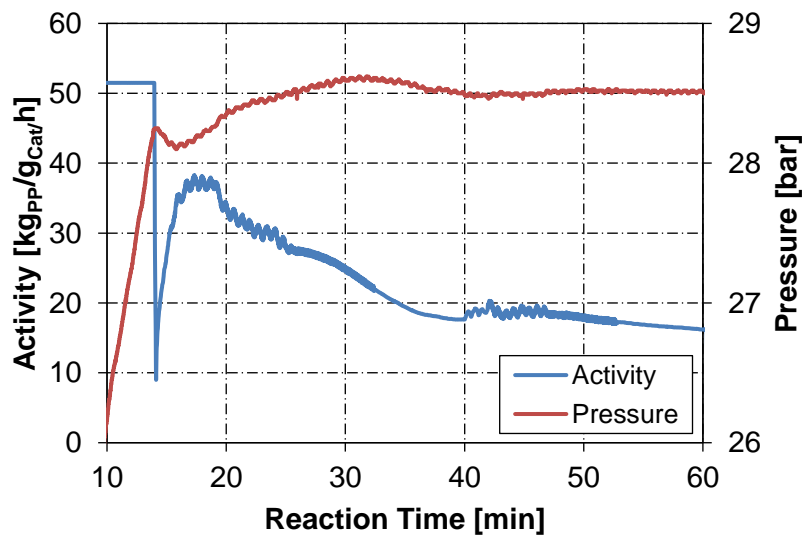


**Figure 5.3:** Activity and pressure profile during a polymerization experiment including a prepolymerization step using catalyst A. Reaction conditions: 80 °C, 28.5 bar, 100 mg H<sub>2</sub>.

### 5.1.2 Reproducibility of catalyst activity

Ziegler-Natta catalysts are sensitive to impurities and even minor traces of these may affect the activity by partial poisoning of the catalyst. Therefore, it is crucial to obtain reproducible results in order to discuss the experimental observations on a solid basis. To verify the reproducibility of the experiments, several polymerization runs were carried out under the exact same conditions. Three activity profiles of catalyst A including a prepolymerization step are compared in Figure 5.4 and show good agreement. Furthermore, the average activities of repeated experiments show minor deviations (Figure 5.5). Generally, an error of 10 % was assumed for the experimental determined average activities.

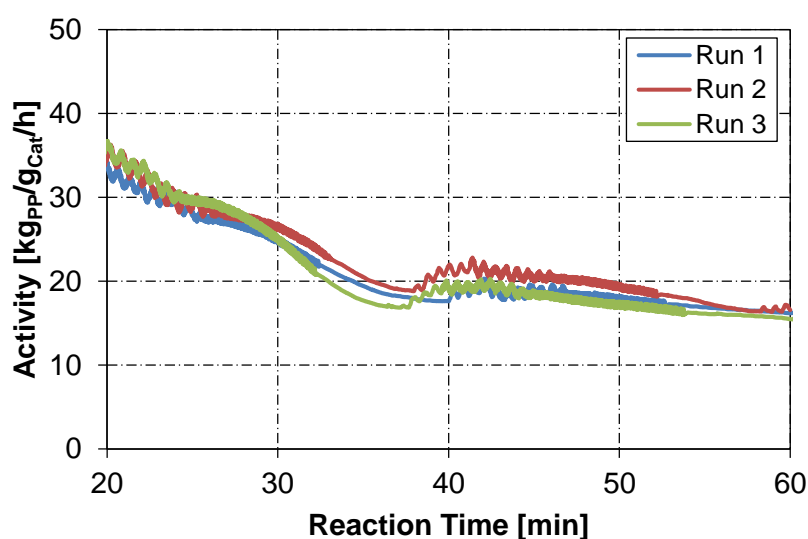


**Figure 5.4:** Reproducibility of activity profiles for three identical polymerization experiments of catalyst A including a prepolymerization step. Reaction conditions: 80 °C, 28.5 bar, 100 mg H<sub>2</sub>.

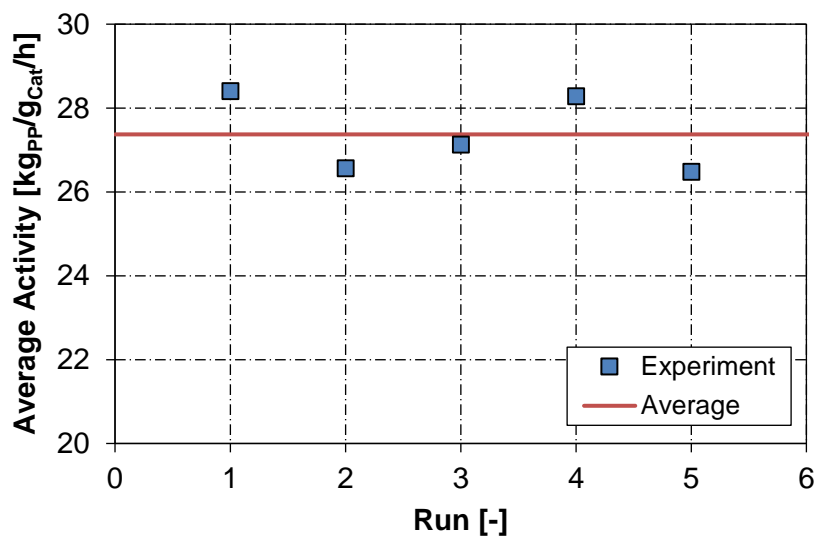


**Figure 5.5:** Reproducibility of the average activity for five identical polymerization experiments of catalyst A including a prepolymerization step. Reaction conditions: 80 °C, 28.5 bar, 100 mg H<sub>2</sub>.



### 5.1.3 Influence of the initial temperature

To analyze the prepolymerization effect, the initial temperature was varied from 40 °C up to the reaction temperature. The results -without seed bed- are presented for catalysts A and B in Figure 5.6. Both catalysts show the same trend of decreasing average activity with increasing initial temperature. For the initial temperature of 40 °C, the activity of both catalysts is about 28 kg<sub>PP</sub>/g<sub>Cat</sub>/h. For the injection at 60 °C, the activity decreases by about 32 % to 19 kg<sub>PP</sub>/g<sub>Cat</sub>/h. Whereas for direct injection (polymerization start at the main reaction temperature of 80 °C), the activity of about 11 kg<sub>PP</sub>/g<sub>Cat</sub>/h is only 39 % of the prepolymerization activity, i.e. the catalyst loses about two thirds of its potential. Thus starting the polymerization at a lower temperature than the reaction temperature, i.e. performing a prepolymerization step, generates a much higher productivity of the catalyst.

When comparing the two catalysts A and B, they show the very same trend and can be viewed identical in their activity response. Catalyst B shows a higher activity by 2 kg<sub>PP</sub>/g<sub>Cat</sub>/h at the injection temperature of 60 °C, whereas this is opposite for direct injection at 80 °C. All in all, the two catalyst show the same activity within the experimental deviations with respect to the variation of the initial temperature.

The explanation for the enhancement in activity with lower starting temperature was discussed in detailed in section 2.2.3. Highly active Ziegler-Natta catalysts tend to overheat upon polymerization start at high temperatures due to the fast initial polymerization rates. The heat of reaction may not be removed efficiently resulting in poor catalyst fragmentation and thermal deactivation of catalyst active sites. This can be prevented by a prepolymerization step, where the polymerization rate is largely reduced resulting in better catalyst fragmentation. Furthermore, the surface area is increased leading to improved heat transfer for the subsequent reaction stage of high polymerization rates.

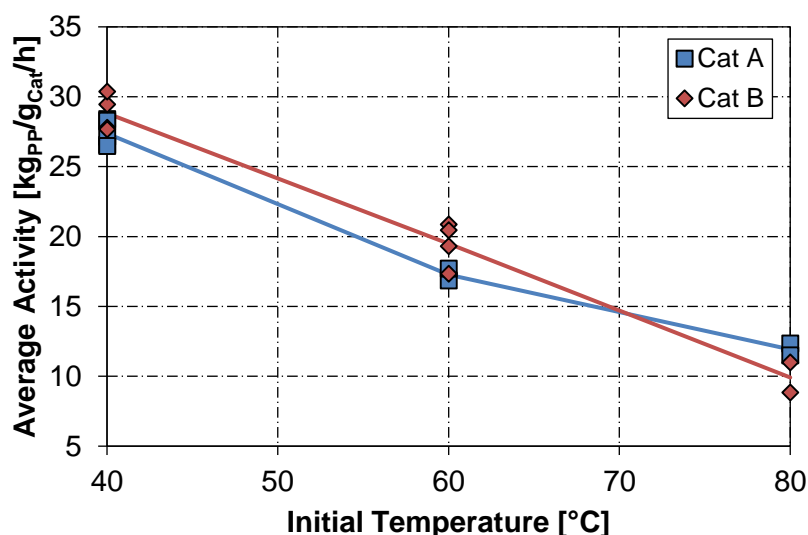


**Figure 5.6:** Effect of the initial reactor temperature on the average activity for catalyst A and B. Reaction conditions: 80 °C, 28.5 bar, 100 mg H<sub>2</sub>.

#### 5.1.4 Establishment of the seed bed polymerization method

In literature, lab-scale gas phase polymerization experiments of olefins were performed with various bed materials such as different polymers, sodium chloride or silica. [18, 19, 34, 39–46] The inert particles were used as a support bed to prevent catalyst agglomeration and to ensure proper fluidization of the catalyst particles. However, with the addition of a bed material to the reactor, a supplementary source for possible impurities is created that may lead to catalyst poisoning. Therefore, it is crucial to remove air and moisture from the support bed by certain pretreating steps.

When reviewing the results of the first polymerization experiments, it can be concluded that no bed material was necessary. At least for the experiments including a prepolymerization step, no agglomeration was observed suggesting proper distribution of the catalyst particles inside the reactor. For the experiments with direct injection, minor agglomeration was found, nevertheless good reproducibility was achieved. Therefore, it is assumed that poor fluidization can be neglected. However, the bed material may have an effect on the heat transfer of the catalyst particles [49] which in turn is crucial to prevent particle overheating. That is why a closer look of the effects of a support bed on the polymerization rate was taken.

In this study, polypropylene was used as a seed bed. The PP bed material was taken from previous gas phase polymerizations with a prepolymerization step in order to have spherical particles with relatively large particle size (high yield). The PP seed bed was chosen from

experiments that were performed under the exact same reaction conditions (catalyst type, temperature, pressure, hydrogen mass, etc.) as planned for the target seed bed polymerization conditions. For instance, a polymerization experiment with a prepolymerization step was performed for a given catalyst under certain conditions. Then a part of the obtained PP powder was taken as the seed bed for the following seed bed polymerization experiment which was conducted under the same reaction conditions except for the initial temperature. The disadvantage of choosing PP as the bed material is that the resulting product will be a mixture of the seed bed and the freshly produced polymer. Important product characteristics such as MFR, bulk density, crystallinity and so forth will be properties of the mixture and the true property of the newly synthesized PP may be hard or even impossible to obtain. However, for most of the studied properties, as will be shown in the following passages, a good agreement between the seed bed property and the one from the mixture was found. Whenever this is the case, the property from the freshly produced PP can be directly taken from the mixture property. For other characteristics, at least a qualitative comparison can be drawn. Although other bed materials such as sodium chloride salt can be easily removed from the polymer product, in this work PP was used as a seed bed as it gave reproducible results with relatively high activities suggesting simple and successful removal of support material impurities. Furthermore, when using PP powder as a seed bed, the particle-particle heat transfer will be very close to the situation in an industrial, continuous plant. Here, the fresh catalyst is fed to a reactor which has a high content of larger PP particles comparable to the seed bed polymerization conditions.

The first seed bed polymerization experiments were conducted with 100 g of PP bed material. In case of insufficient purification of the seed bed material, impurities are introduced into the reactor and the activity should decrease. Therefore, as a control test, the prepolymerization experiment of catalyst A was re-performed in presence of a seed bed. The average activity is identical to the one without a seed bed (blue squares, Figure 5.7). This means that the catalyst activity is not reduced by possible impurities and the bed material is inert. However, for the method of direct injection, the average activity increases strongly by about 70 % (red diamonds, Figure 5.7).

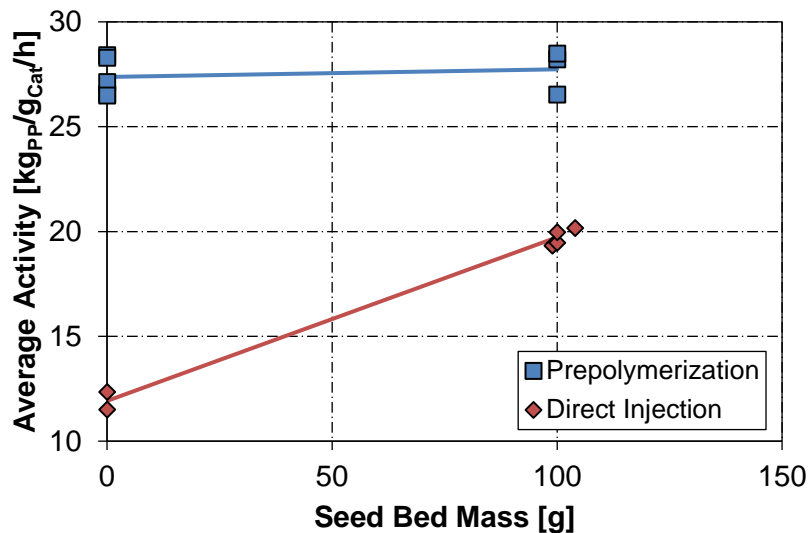


**Figure 5.7:** Effect of the seed bed mass on the activity of catalyst A. Prepolymerization refers to injection of catalyst at 40 °C, direct injection at 80 °C. Reaction conditions: 80 °C, 28.5 bar, 100 mg H<sub>2</sub>.

The observed results can be explained by improved heat transfer in presence of a seed bed. As expected from theory, overheating is not an issue in case of the prepolymerization step. Therefore, improved heat transfer does not change the polymerization rate and the activities in absence and presence of a bed material are identical. For the case of direct injection of catalyst at the reaction temperature of 80 °C, overheating is much likely to occur and thermal deactivation of possible active sites decreases the activity level. In presence of a seed bed, heat transfer is improved by conduction from relatively hot, small catalyst particles to relatively cold, large seed bed PP particles. The catalyst thus shows a higher activity and the difference to the prepolymerization activity is reduced.

The variation of the initial temperature was also performed in presence of a seed bed. For catalyst A, generally a higher activity was observed for all injection temperatures except for 40 °C (prepolymerization), where the activities are identical (Figure 5.8). The highest relative and absolute difference is found at 80 °C (direct injection). For catalyst B, this is also the case. However, the loss in activity with increasing initial reactor temperature is not linear as for catalyst A, but shows a sharp drop between 60 and 80 °C.

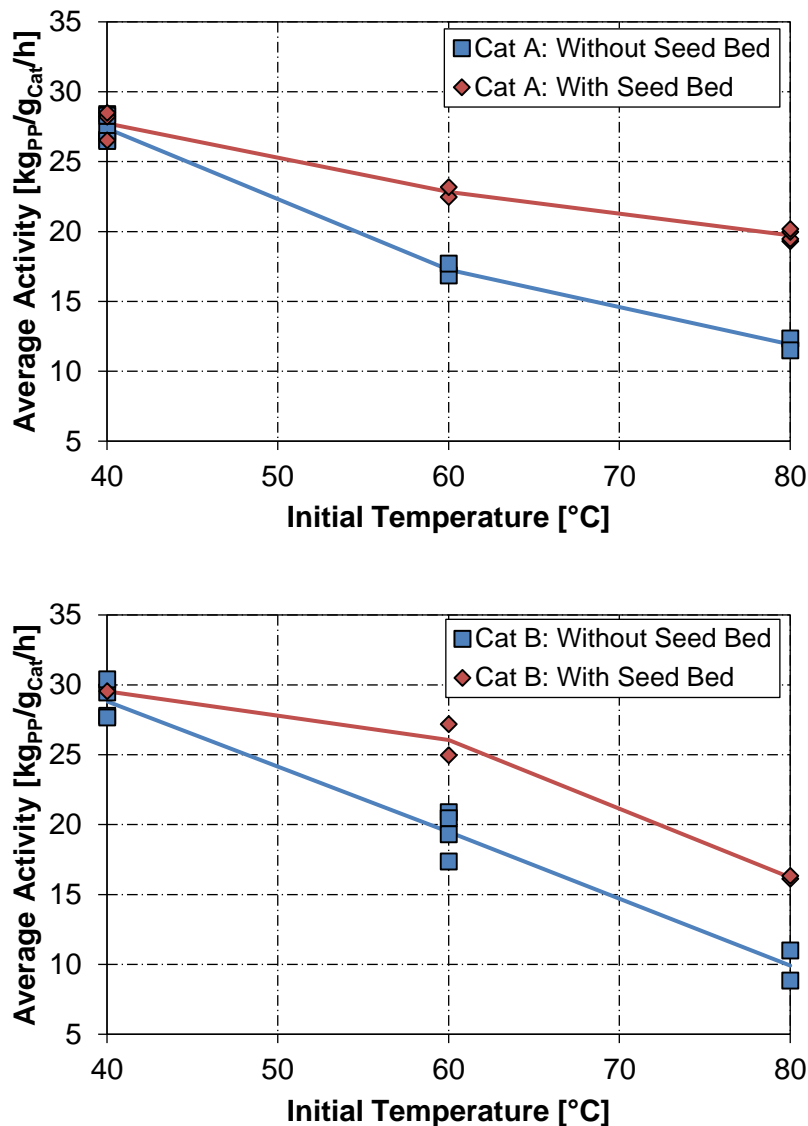


**Figure 5.8:** Effect of the initial reactor temperature on the average activity of catalyst A (top) and B (bottom) in absence and presence of 100 g seed bed. Reaction conditions: 80 °C, 28.5 bar, 100 mg H<sub>2</sub>.

As presented before, when comparing the two catalysts in absence of a seed bed, there is almost no difference in the activity response (Figure 5.6). However, in presence of a seed bed, the comparison turns out to give very different results (Figure 5.9). At an initial temperature of 40 °C, the activities are identical. When increasing the starting temperature to 60 °C, catalyst B shows a higher activity which is close to the prepolymerization activity level, whereas the activity of catalyst A decreases by about 20 %. Between 60 and 70 °C the largest difference in the activity response of the two catalysts can be found: Whereas the activity of catalyst A continues to drop linearly, a sharp drop is observed for catalyst B. This uneven decrease causes the activity level of catalyst B to drop below the one of catalyst A above initial temperatures of 70 °C. Curiously, a further increase of the initial temperature from 70 to 80 °C is not changing the activity of both catalysts which is difficult to explain by

theory. It might be that a certain threshold in the initial polymerization rate is achieved which negatively effects fragmentation and distribution of the catalyst active sites in the growing polymer particle.

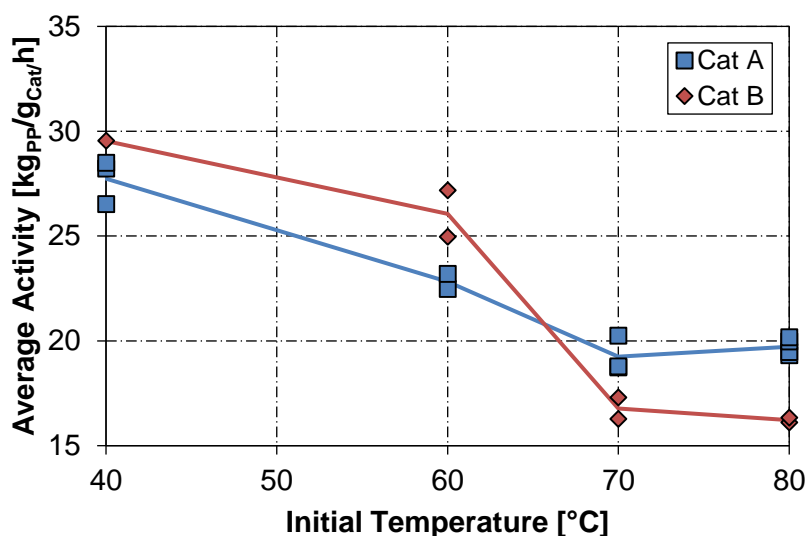


**Figure 5.9:** Effect of the initial reactor temperature on the average activity in presence of 100 g seed bed for catalyst A and B. Reaction conditions: 80 °C, 28.5 bar, 100 mg H<sub>2</sub>.

From the results of the seed bed polymerizations, it can be concluded that a very different activity response of the two catalysts is found. For the case of prepolymerization, the activity remains identical. However, at high initial temperatures (direct injection), the activity increases largely in presence of a seed bed by about 60 % for both catalysts. Furthermore, the activity responses with respect to the initial temperature are different and catalyst A proves to be more active at high initial temperatures.

When performing kinetic investigations of newly developed catalysts in lab-scale, the presented seed bed polymerization method shows to be very important in order to correctly capture the kinetic characteristics of the catalysts relevant for the industrial scale. In an industrial, continuous gas phase polymerization plant, the fresh catalyst enters a reactor full of grown polymer particles. This is much alike the presented seed bed polymerization experiments. Therefore, when transferring the lab-scale results to the next larger scale, the seed bed results should give a better prediction of the polymerization kinetics. When the catalyst is prepolymerized to a large extent (high Prepo degree), the seed bed experiments are not necessary. However, when no prepolymerization step is used or the catalyst is only shortly prepolymerized (low Prepo degree), the characteristic kinetics are much likely to be found by the seed bed experiments. As a concrete example, catalysts A and B would much likely perform identical using a prepolymerization step, but when no such step is applied, catalyst A should give the higher activity. Furthermore, when looking at the initial temperature

of 60 °C (Figure 5.9), it might be interpreted that a catalyst B of low Prepo degree could give a higher polymerization rate based on the assumption that this initial temperature resembles a short prepolymerization step. However, this would have to be verified in separate experiments.

Besides the effect of the seed bed on the activity, also the morphology of the resulting powders was analyzed (Figure 5.10). In absence of a seed bed, it was found that for the prepolymerization step, the particles are spherically shaped resembling the preferred powder morphology (lower chance for fine generation, higher bulk density). In contrast, when injecting the catalyst directly under the main reaction temperature, poor particle morphology is generated. Non-spherical particles were obtained that can be described as flakes and the effect of sheeting was observed. These observations are in agreement with the results of Kettner [22]. She found that by performing a prepolymerization step, the formed prepolymer replicated the spherical catalyst particle. During the main polymerization stage, the particle maintained its shape and the polymer particle grew regularly. In contrast, polymerization without a polymerization step led to non-spherical particles.

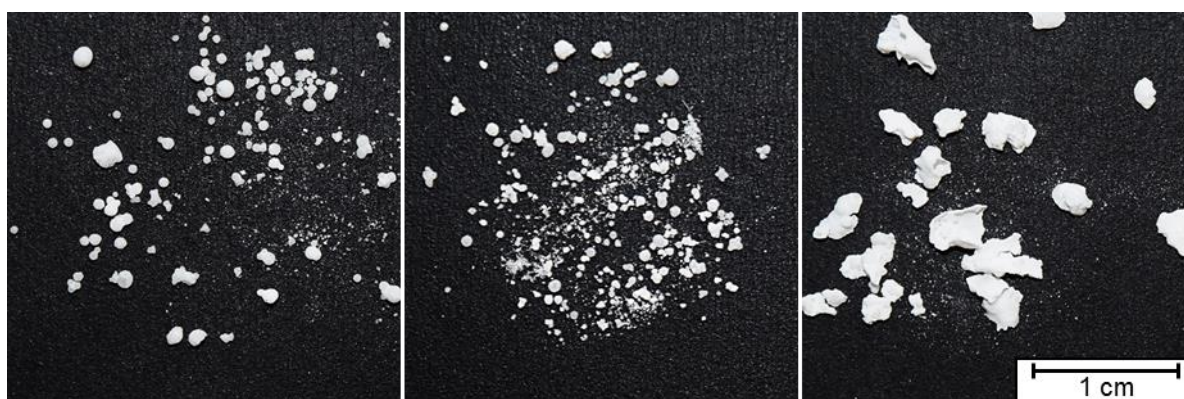


**Figure 5.10:** Effect of the seed bed on the particle morphology for catalyst A. From left to right: prepolymerization, seed bed polymerization, direct injection without a seed bed. Reaction conditions: 80 °C, 28.5 bar, 100 mg H<sub>2</sub>.

When a seed bed is used for catalyst injection at the main reaction temperature (SB polymerization method), the resulting PP particles seem rather like the one from the prepolymerization method (Figure 5.10). They seem spherical, but more irregular. The particle morphology of the seed bed experiment can be seen as an intermediate between the two extremes of good (prepolymerization) and poor particle morphology (direct injection). Note that the resulting powder of each seed bed polymerization is a mixture of the actual bed material and the freshly produced PP particles. However, the original seed bed particles can be easily identified due to the different particle shape. The bed material particles were taken from the previous prepolymerization experiment and show a smooth surface whereas the freshly produced particles have a rough surface. It can be concluded that not only the

activity, but also the morphology of the PP particles is improved in presence of a seed bed when the catalyst is directly injected under main reaction conditions. This is an important aspect when considering that the seed bed polymerization method resembles the situation of the continuous industrial scale. The particle morphology generated by a newly developed catalyst can thus be analyzed in lab-scale by this method and included as a criterion for catalyst development.

As shown and discussed in the preceding passages, the use of a seed bed can have a strong effect on the catalyst activity, especially when the catalyst is directly injected under main reaction conditions. In presence of a seed bed, not only is the activity of the individual catalyst influenced, but also different conclusions had to be made for the comparison of catalyst A and B. In order to extend the analysis of the seed bed effect, the seed bed mass variation was also studied for catalysts C and D. The focus was now shifted to two injection temperatures: the initial temperature of 40 °C which is defined as prepolymerization in this work and direct injection at the main reaction temperature.

When comparing the three catalysts A, C and D, it can be seen that there is a minor tendency of increasing activity with increasing seed bed mass for the prepolymerization method (Figure 5.11). The maximum increase is clearly below 10 % and within the experimental error. Generally, it can be concluded that the seed bed mass has no effect on the activity for the prepolymerization method. The reason was given before in section 5.1.4. During prepolymerization, catalyst overheating is avoided. The low initial temperature assures controlled catalyst fragmentation for highly active catalysts because of the accompanied low polymerization rate. Furthermore, the heat transfer area of the particle is increased by the growth of the particle before it is exposed to high temperatures and thus to high rates of heat generation. The improved heat transfer conditions which are introduced by the seed bed thus do not affect the activity.



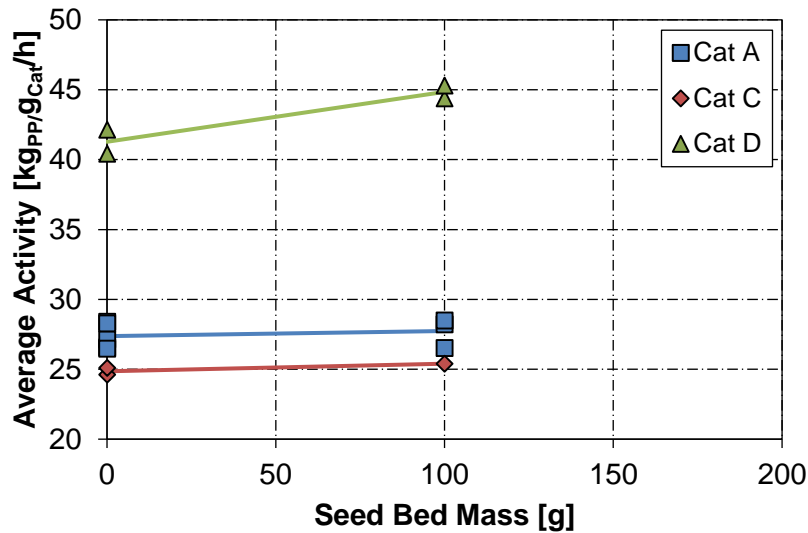


**Figure 5.11:** Seed bed mass variation for prepolymerization experiments of catalysts A, C and D. Reaction conditions: 80 °C (Cat A) or 75 °C (Cat C&D), 28.5 bar, 100 mg H<sub>2</sub>.

The picture is quite different when the catalyst is injected directly under the main reaction conditions (high temperature). Here, improved heat transfer due to the presence of a seed bed should have an effect on highly active catalysts since catalyst overheating is attenuated. This effect can be clearly seen for all three catalysts in Figure 5.12. The activity increases first steeply from 0 to 100 g seed bed for all catalysts. Then the gradient levels off at 150 g.

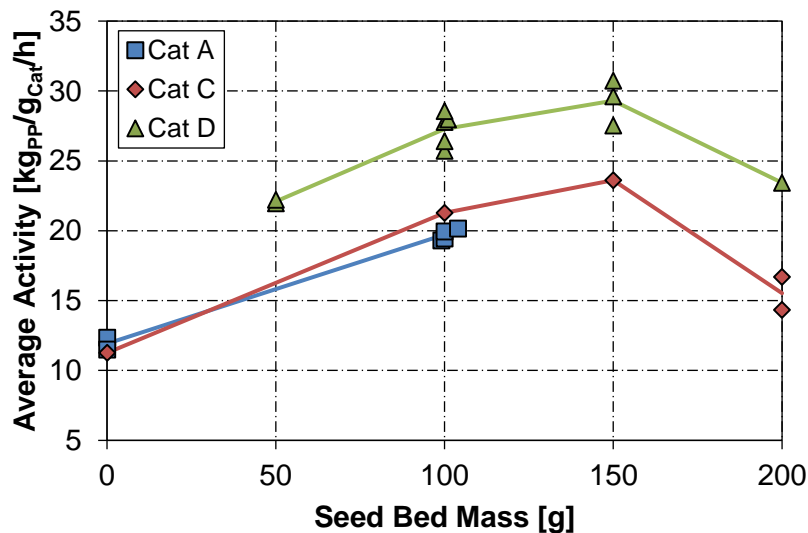


**Figure 5.12:** Seed bed mass variation for direct injection experiments of catalysts A, C and D. Reaction conditions: 80 °C (Cat A) or 75 °C (Cat C&D), 28.5 bar, 100 mg H<sub>2</sub>.

The experimental results can be explained by the improved heat transfer in presence of a seed bed. The more seed bed particles are present, the higher the chance for fresh and hot catalyst particles to transfer heat by conduction to large and cold seed bed PP particles. When the content of bed material reaches a certain threshold, enough particles are present

to evacuate the heat from the fresh catalyst particles and further addition of seed bed should not improve the heat transfer and thus the activity. From theory, a decrease in activity should not be expected and is in contrast with the experimental observations for seed bed masses above 150 g. However, for the seed bed experiments with high mass of bed material, plugging in the injection pipe and polymer chunks were observed. Thus some of the catalyst particles overheated due to agglomeration. Therefore, these catalyst particles became inactive and overall less catalyst particles contributed to the production of PP resulting in a lower yield. It can be concluded that high seed bed masses put an experimental limit to reactor operation. Note that this occurs at relatively low solid contents of the reactor. Assuming a bulk density of  $400 \text{ kg/m}^3$ , the solid volume fraction of the reactor amounts up to 10 vol% before the polymerization reaction and rises up to 30 vol% at the end of reaction. This is much lower than in commercial plants. Nevertheless, operational problems were observed starting at 200 g of seed bed.

Using the seed bed variation results, a standard seed bed mass of 100 g was selected. The activity difference between 100 and 150 g of seed bed is almost negligible. Furthermore, as seen at 200 g of bed material, with increasing bed support, the chance of agglomeration increases. Additionally, the seed bed content in the final product remains between 20 and 40 wt% by using a relatively low mass of seed bed of 100 g.

### 5.1.5 Hydrogen variation

Once the seed bed polymerization procedure had been established, a detailed kinetic analysis of the three different Ziegler-Natta catalysts A, C and D was conducted. The objective of this study is to analyze the kinetic response of these catalysts under industrial relevant conditions, in particular the effect of the hydrogen concentration which is an important parameter in industry. For all conditions, the prepolymerization method (catalyst injection at  $40 \text{ }^\circ\text{C}$  in absence of a seed bed) is compared to the seed bed polymerization method (catalyst injection at the main reaction temperature in presence of a seed bed) in order to examine the individual catalyst response to overheating. The seed bed polymerization experiment better resembles the situation of a continuous industrial plant without a prepolymerization reactor than the direct catalyst injection method in absence of bed material. The prepolymerization method should simulate the catalyst behavior in a plant operating with a prepolymerization reactor. From the comparison of these two methods, conclusions can be made on how the tested catalysts would perform in industrial scale and valuable information for catalyst design can be obtained before testing the catalysts at larger scale.

One of the most important kinetic aspects in the polymerization of propylene is the individual catalyst response to hydrogen. Hydrogen acts as chain transfer agent and is used to control the molecular weight and thus the MFR of the final PP product. Furthermore, the hydrogen concentration may affect the activity of the catalyst. In the following section, the effect of hydrogen on the activity and the MFR response of the three different Ziegler-Natta catalysts A, C and D is discussed.

The hydrogen mass was varied from 0 to 400 mg for the standard reaction conditions of 28.5 bar and 80 °C (Cat A) or 75 °C (Cat C&D). Comparing the seed bed polymerization results (Figure 5.13), all three catalyst show a rate enhancement with increasing hydrogen up to a plateau. However, this rate enhancement differs from catalyst to catalyst. For catalyst A, the activity is doubled from 0 to 50 mg hydrogen and the activity remains unchanged at 20 kg<sub>PP</sub>/g<sub>Cat</sub>/h for higher hydrogen masses. Catalyst C also shows a sharp increase in activity from 5 to 20 kg<sub>PP</sub>/g<sub>Cat</sub>/h for hydrogen mass of 0 to 50 mg, respectively. Further addition of hydrogen only partially enhances the polymerization rate. For catalyst D, this is also the case except that the plateau is reached at a higher hydrogen mass of about 100 mg.

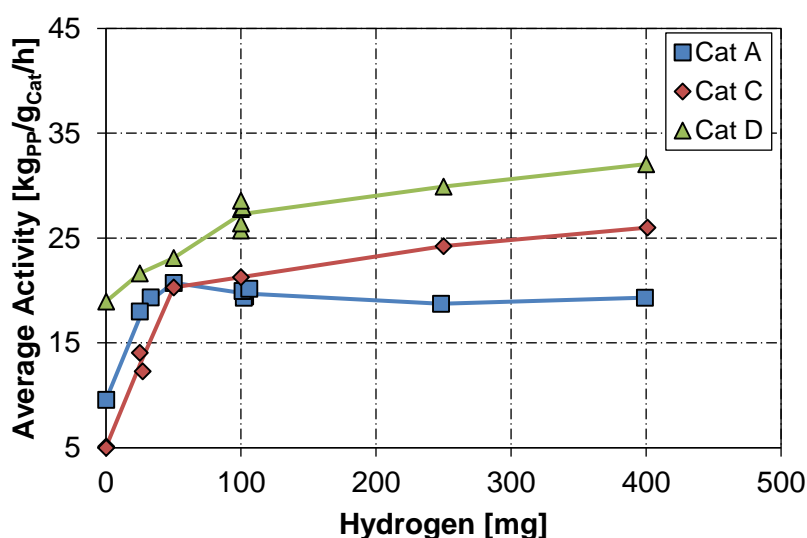


**Figure 5.13:** Hydrogen mass variation for the seed bed polymerization experiments of catalysts A, C and D. Reaction conditions: 80 °C (Cat A) or 75 °C (Cat C&D), 28.5 bar.

The observed effect can be explained by the dormant site theory. It is assumed that by the 2,1-misinsertion of monomer into a growing polymer chain a dormant chain is created, which does not contribute to further chain growth. This dormant species can be freed by the addition of hydrogen resulting in a reactivated site. Thus, the more hydrogen is present, the more active chains will be available for further chain growth. Therefore, the higher the hydrogen concentration is, the higher the polymerization rate or activity is. At very high

hydrogen concentrations, this effect is vanishing since the concentration of dormant species becomes relatively small with respect to the overall number of active sites/chains.

When comparing the average activity of the three catalysts for the case of seed bed polymerization, it can be found that the activity increases from A to D. Catalyst A shows a maximum activity of about 20 kg<sub>PP</sub>/g<sub>Cat</sub>/h, whereas catalyst C initially shows the same activity level, but upon further hydrogen a maximum average activity of 26 kg<sub>PP</sub>/g<sub>Cat</sub>/h is found. Catalyst D clearly has the highest activity with a maximum of about 32 kg<sub>PP</sub>/g<sub>Cat</sub>/h. Thus the catalysts differ in their activity level by up to 50 %.

When comparing the catalysts in case of the prepolymerization method (Figure 5.14), similar results can be found: an activity enhancement with hydrogen up to a plateau. However, for catalyst A, a decline from 100 to 250 mg hydrogen can be observed. This was only found for this catalyst and only under the conditions of prepolymerization. This result goes in contrast with theory. The presence of excess hydrogen might have a negative effect on prepolymerization of catalyst A. As the effect is relatively small, it was not further analyzed.

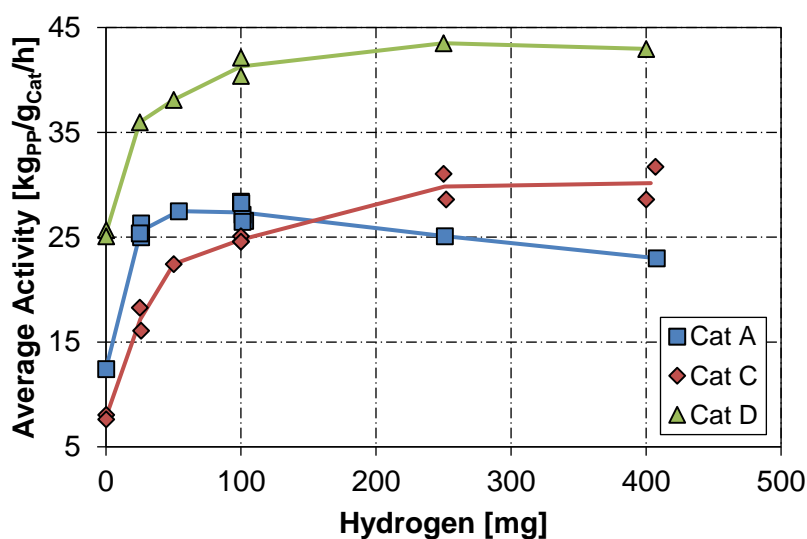


**Figure 5.14:** Hydrogen mass variation for the prepolymerization experiments of catalysts A, C and D. Reaction conditions: 80 °C (Cat A) or 75 °C (Cat C&D), 28.5 bar.

The catalyst's individual resistance to overheating (withstanding high initial polymerization rates without suffering loss in activity) or in other terms, its prepolymerization potential, can be analyzed when comparing the prepolymerization experiments with the seed bed ones (Figure 5.15). The activity difference between the prepolymerization and the seed bed experiments shows to be independent of the hydrogen concentration for the three catalysts as no clear hydrogen trend is visible. The activity difference is in the order of 4 to 14 kg<sub>PP</sub>/g<sub>Cat</sub>/h, respectively. Catalyst D shows the highest prepolymerization potential, i.e. a prepolymerization step for this catalyst is the most effective in enhancing the activity. For

catalyst C, a prepolymerization step is the least useful in terms of increasing the catalyst activity. On the other hand, this catalyst shows the highest resistance to overheating. This information is important for catalyst development in case a new catalyst should be designed for plants operating without a prepolymerization reactor.

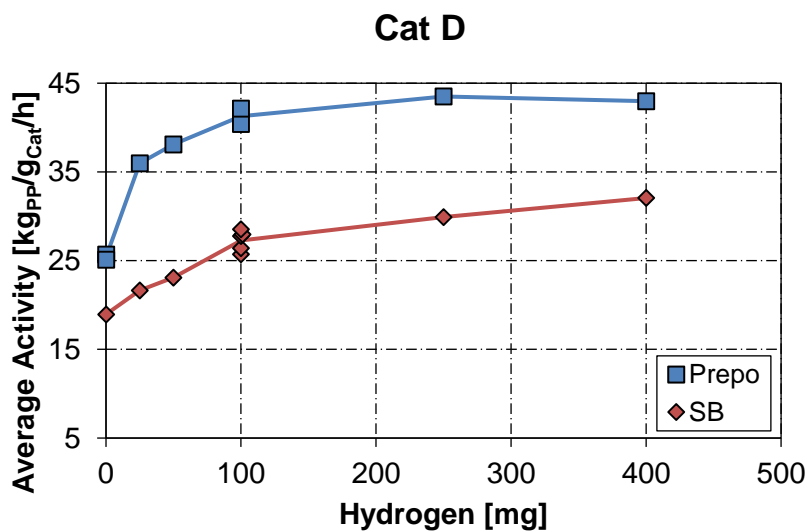
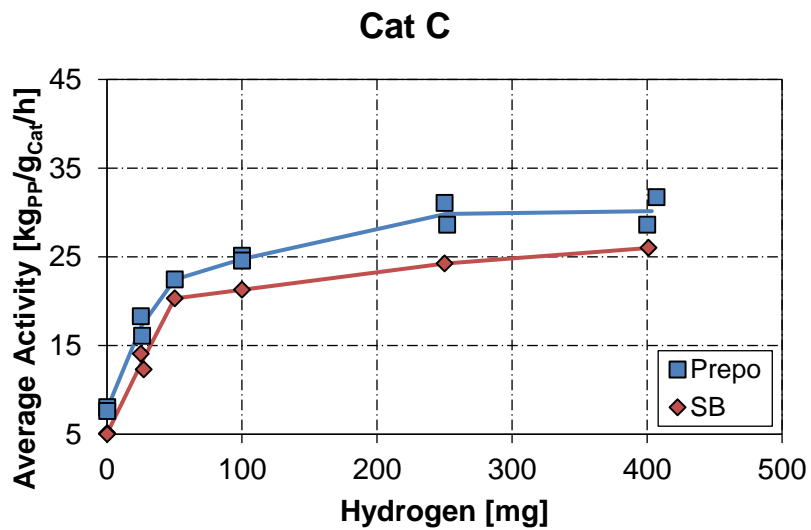
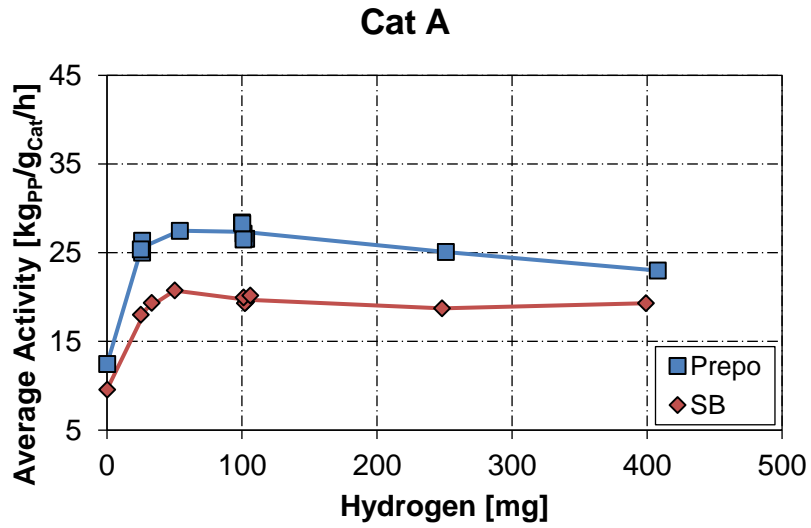


**Figure 5.15:** Hydrogen mass variation of catalyst A, C and D for prepolymerization and seed bed polymerization experiments. Reaction conditions: 80 °C (Cat A) or 75 °C (Cat C&D), 28.5 bar.

Since hydrogen acts as chain transfer agent in the polymerization of propylene, its effect on the molecular weight was analyzed by measuring the MFR of the produced PP. The hydrogen dependence of the MFR is compared for all three catalysts for both conditions of prepolymerization and seed bed polymerization in Figure 5.16. One important result is that the MFR of all three catalysts is independent of the initial reaction conditions. At any given hydrogen concentration, the prepolymerization and seed bed experiment lead to the same MFR. However, the three catalysts show a very different MFR response to the same hydrogen variation. Catalyst D shows the highest MFR over the entire hydrogen range. The MFR increases from 10 g/10 min at 25 mg hydrogen to about 130 g/10 min at 250 mg hydrogen. A similar strong increase is found for catalyst C, but at an about 50 % lower MFR level. Catalyst A shows similar MFR values at low hydrogen concentrations as catalyst C, but a less pronounced increase with higher hydrogen masses is found. The MFR at 250 mg hydrogen is below 40 g/10 min and overall catalyst A gives the lowest MFRs.

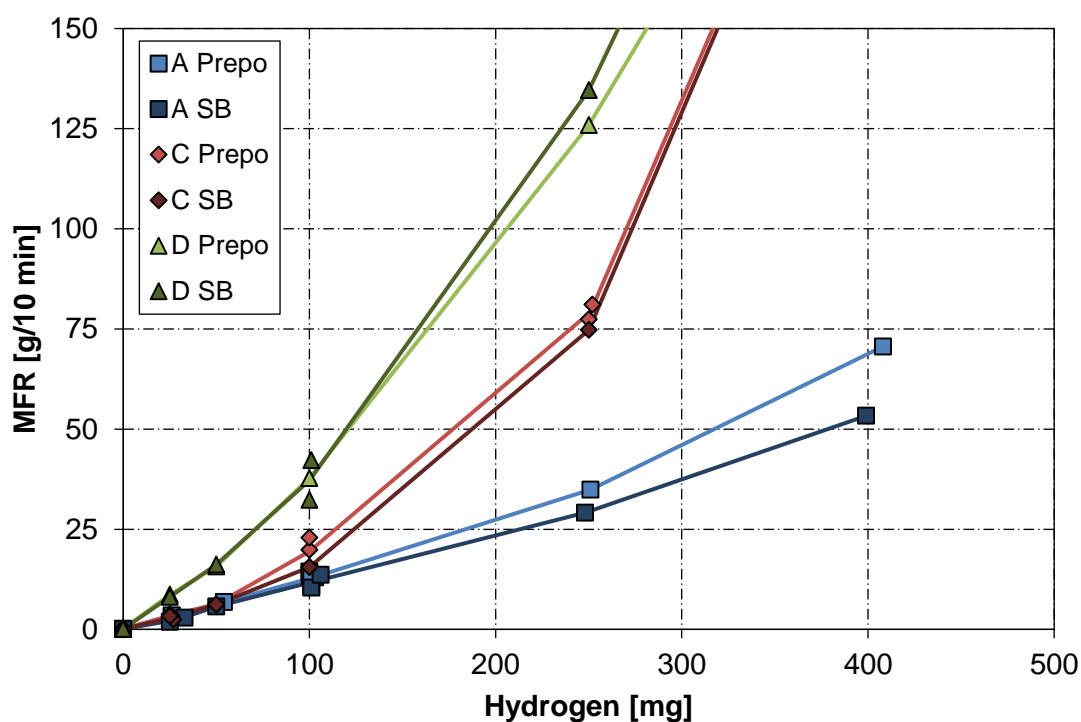


**Figure 5.16:** Hydrogen effect on MFR for the prepolymerization and seed bed polymerization experiments of catalysts A, C and D. Reaction conditions: 80 °C (Cat A) or 75 °C (Cat C&D), 28.5 bar.

Besides the average activity and the MFR, the recorded activity profiles of each experiment are adding valuable kinetic information about the catalysts. Since the activity is not directly accessible at the polymerization start, the activity profiles are presented only when isothermal and isobaric conditions are reached. This is generally after 20 min for the case of prepolymerization due to heat-up and further propylene feeding and after 10 min for seed bed polymerization experiments. The actual time to reach this stage depends on the

polymerization method, but also on the propylene consumption, e.g. larger amounts of a very active catalyst would lead to a delay in reaching isobaric conditions due to the high propylene conversion.

The activity profiles of catalysts A, C and D are compared for experiments with prepolymerization and a hydrogen mass of 100 mg (Figure 5.17). Catalyst D shows the highest activity over the whole reaction time, whereas catalyst A and C show an identical activity level. This is in agreement with the reported average activities (Figure 5.14). All three catalysts show a decay in activity over time which is typically observed for Ziegler-Natta catalysts in the polymerization of propylene. Generally, the relative activity loss with time is about the same for all catalysts. Catalyst A and C show the same deactivation behavior, whereas catalyst D shows a stronger absolute decay, but at a higher activity level. The same findings are valid for the seed bed polymerization experiments, although the activity differences are lower (Figure 5.18). Additionally, the activity decay seems to be less pronounced.

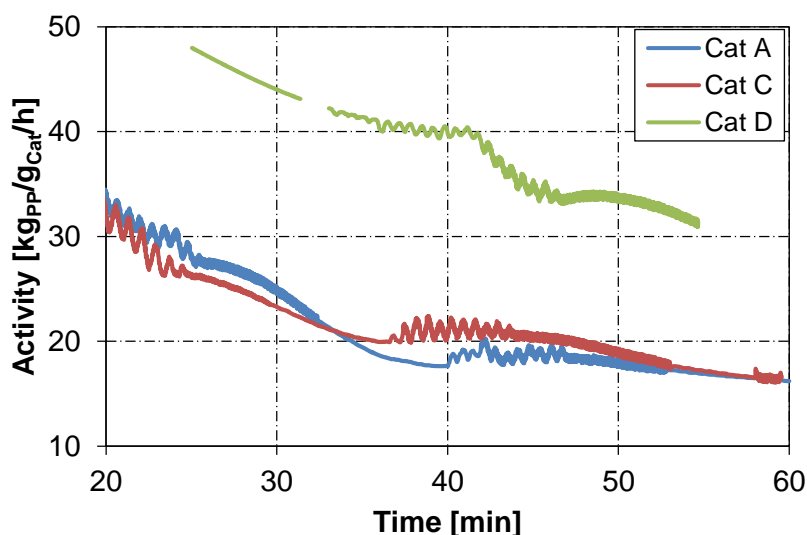


**Figure 5.17:** Activity profiles of catalysts A, C and D for the prepolymerization method. Reaction conditions: 80 °C (Cat A) or 75 °C (Cat C&D), 28.5 bar, 100 mg H<sub>2</sub>.



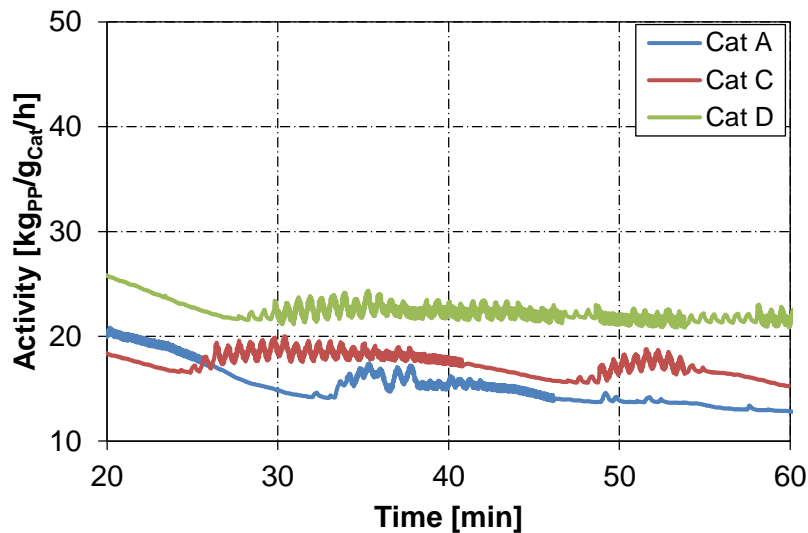


**Figure 5.18:** Activity profiles of catalysts A, C and D for the seed bed polymerization method. Reaction conditions: 80 °C (Cat A) or 75 °C (Cat C&D), 28.5 bar, 100 mg H<sub>2</sub>.

A relative comparison between all the activity profiles of different conditions can be made by normalizing the profiles by the corresponding average activities. Thereby it can be clearly stated that all three catalysts show the same relative deactivation behavior at 100 mg of hydrogen for the case of prepolymerization (Figure 5.19). This can also be observed for the seed bed polymerization experiments (Figure 5.20) with catalyst A showing a slightly faster decay with time and catalyst C a slightly slower one. The relative loss in activity shows to be more pronounced for the case of prepolymerization for all catalysts.

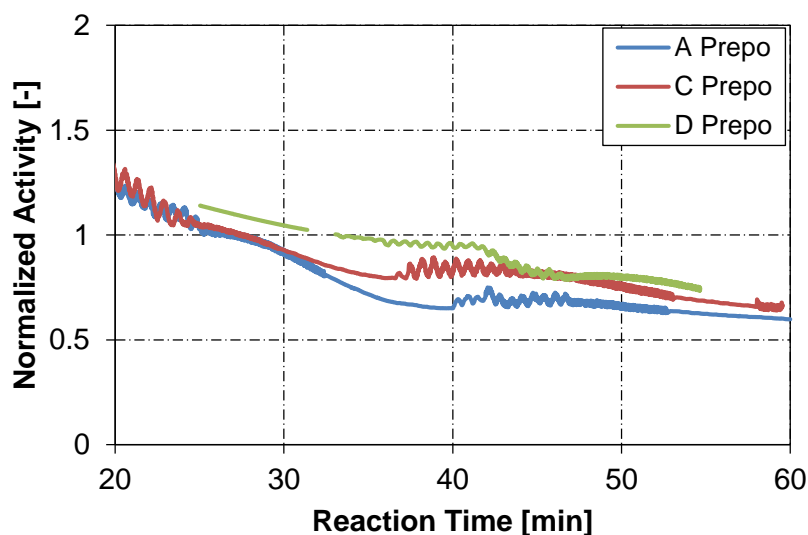


**Figure 5.19:** Normalized activity profiles of catalysts A, C and D for the prepolymerization method. Reaction conditions: 80 °C (Cat A) or 75 °C (Cat C&D), 28.5 bar, 100 mg H<sub>2</sub>.

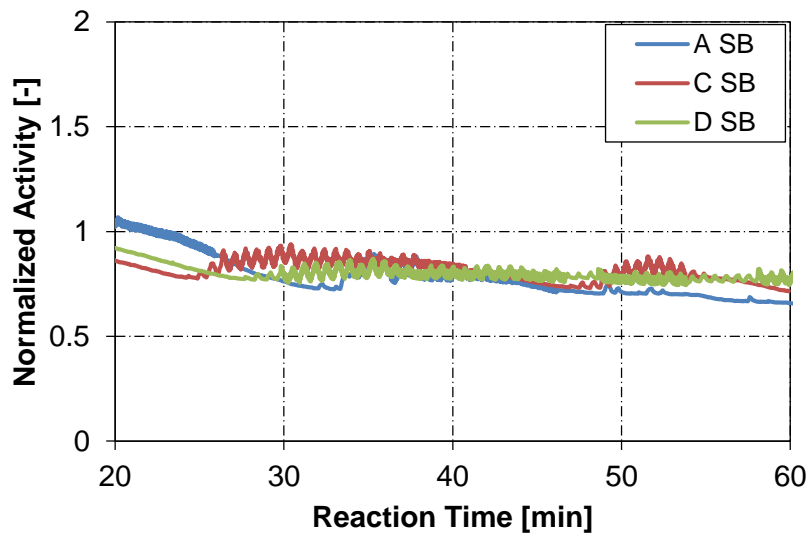


**Figure 5.20:** Normalized activity profiles of catalysts A, C and D for the seed bed polymerization method. Reaction conditions: 80 °C (Cat A) or 75 °C (Cat C&D), 28.5 bar, 100 mg H<sub>2</sub>.

The normalized activity profiles are also compared for the different hydrogen concentrations for the three catalysts for both methods of prepolymerization and seed bed polymerization (Figure 5.21 and Figure 5.22). Generally, it can be stated that for all catalysts hydrogen does not affect the deactivation behavior. A trend such as pronounced activity decay with increasing hydrogen mass is not visible. Furthermore, the tested catalysts show a very similar deactivation behavior independent of the polymerization method.

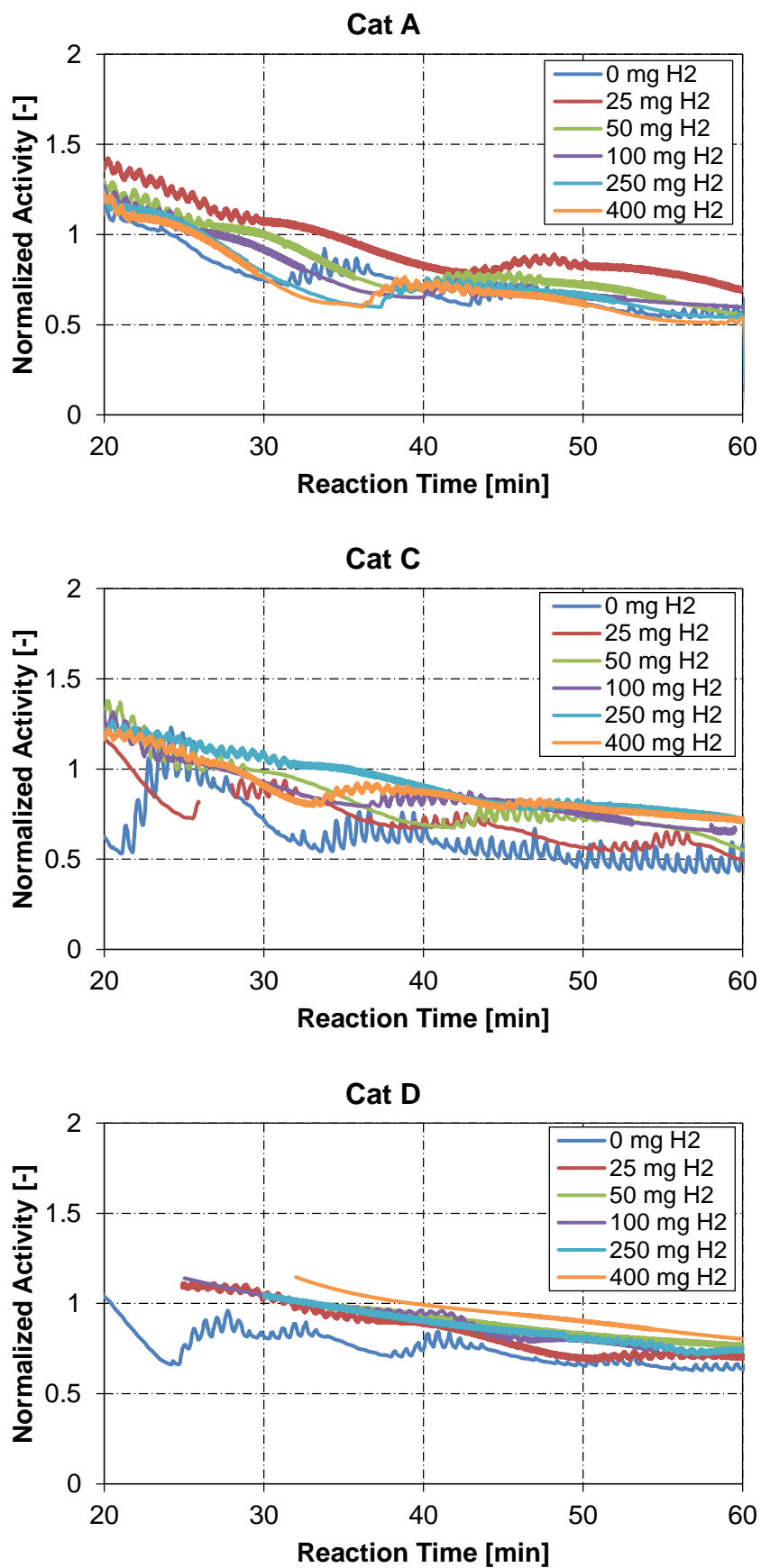


**Figure 5.21:** Normalized activity profiles of catalysts A, C and D for different hydrogen concentrations for the prepolymerization method. Reaction conditions: 80 °C (Cat A) or 75 °C (Cat C&D), 28.5 bar.

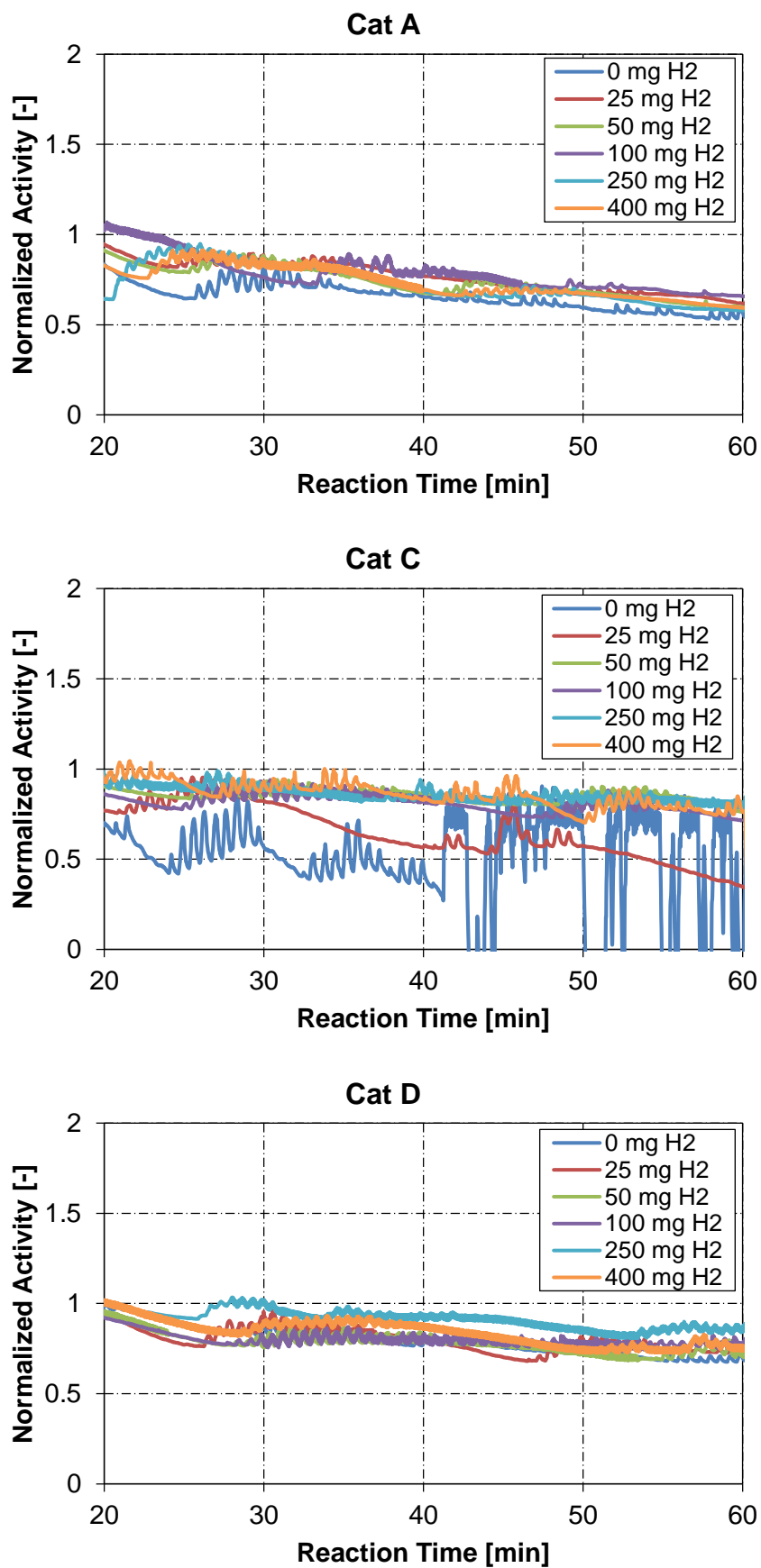


**Figure 5.22:** Normalized activity profiles of catalysts A, C and D for different hydrogen concentrations for the seed bed polymerization method. Reaction conditions: 80 °C (Cat A) or 75 °C (Cat C&D), 28.5 bar.

## 5.2 Crystallinity and particle morphology

### 5.2.1 Crystallinity by DSC

The crystallinity was measured for selected samples via differential scanning calorimetry (DSC). Generally, a good reproducibility was found for the DSC measurements and the error was estimated to be of about 1 wt%. The crystallinities of PP samples produced with catalysts A and C are about 40 wt%, whereas powders produced with catalyst D show a lower crystallinity of about 35 wt% (Table 5.1). The crystallinity is almost identical for the two methods of prepolymerization and seed bed polymerization.

**Table 5.1:** Crystallinities of selected PP powders as determined by DSC (first scan). PP powders were synthesized at 80 °C (Cat A) or 75 °C (Cat C&D), 28.5 bar and 100 mg hydrogen with the method of prepolymerization (Prepo) or seed bed polymerization (SB).

Polymerization Method	Catalyst	Crystallinity [wt%]
Prepo	A	40
	C	39
	D	35
SB	A	38
	C	39
	D	36

The here reported values refer to the nascent crystallinity of the PP powders directly after synthesis, i.e. there was no thermal treatment or processing and the first DSC scan was taken for crystallinity analysis. For the PP sample of catalyst A, a second DSC scan was also performed. This thermal treatment of melting and recrystallization caused the crystallinity to increase from 40 to 54 wt%. As for all semi-crystalline polymers, thermal treatment influences the crystallinity and in industry, the processing steps after the polymerization reactor will affect the final product crystallinity.

For catalyst A, the effect of hydrogen on the crystallinity was studied (Figure 5.23). At 25 and 100 mg hydrogen, the crystallinities are identical with about 38 to 41 wt%. Slightly higher crystallinities of 43 wt% are found at a hydrogen mass of 400 mg. Given the experimental error, it can be reasoned that the crystallinity is independent of the hydrogen concentration. Thus the PP crystallinity is not affected by the employed variations in the polymerization conditions (method of polymerization and hydrogen mass) and seems to be pre-determined by the catalyst.

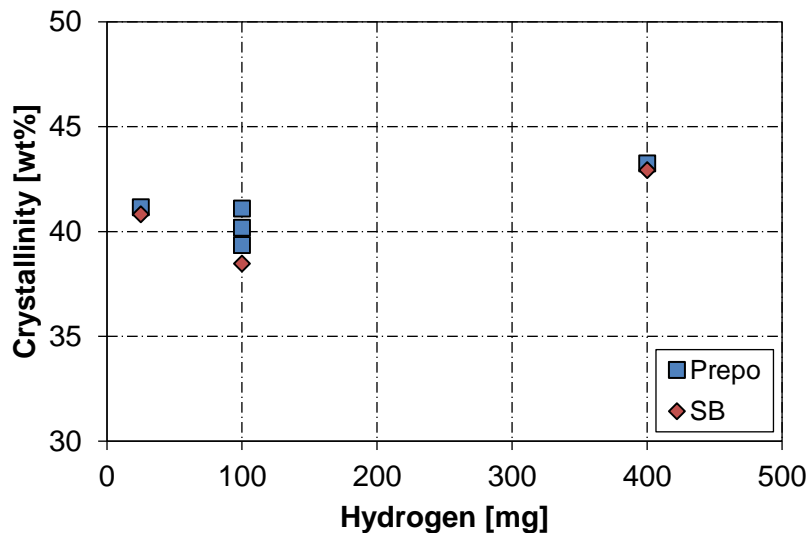


**Figure 5.23:** Effect of the hydrogen mass on the final polymer crystallinity as determined by DSC (first scan). PP powders were synthesized with catalyst A at 80 °C and 28.5 bar with the method of prepolymerization (Prepo) or seed bed polymerization (SB).

### 5.2.2 Particle morphology

Another important factor is the morphology of the produced polymer particles. Spherical and compact particles represent the desired particle morphology suitable for smooth process operation. Improper catalyst break-up upon polymerization leads to poor morphologies which might result in the undesired formation of fines.

Morphology is a rather qualitative quantity and was captured by different analytical methods in this thesis. Light and scanning electron microscopy (SEM) were used to visualize the particle shape and particle surface. Measurement of the particle porosity gave an estimate of the inner morphology. Additional information was gathered by particle size distribution (PSD) measurements. Furthermore, the bulk density was analyzed in order to quantitatively capture the morphology of the different PP samples. Although the bulk density is affected by various parameters (porosity, PSD, etc.) than solely the particle shape, in combination with the former techniques a simple and quantitative estimation of the powder morphology is possible.

Camera images were taken of PP powders produced with catalysts A, C and D (Figure 5.24). Particles produced via prepolymerization are all spherical independent of the used catalyst. The particles differ in size and a small amount of agglomerates can be identified. In contrast to the spherically shaped particles of the prepolymerization method, the PP particles produced by seed bed polymerization seem rather of irregular shape and clearly less

spherical. Note that the powder samples of the SB polymerization method are a mixture of the actual seed bed particles and the freshly produced polymer particles. However, having the images of the prepolymerization particles at hand, the original SB particles can be easily identified by their perfectly spherical nature. Based on the camera images, it can be stated that the prepolymerization method leads to spherical, regularly shaped particles and thus a good replication of the catalyst particles. Whereas under the SB polymerization injection conditions of higher temperatures, irregular, “popcorn-like” particles are produced and the original catalyst geometry is lost.

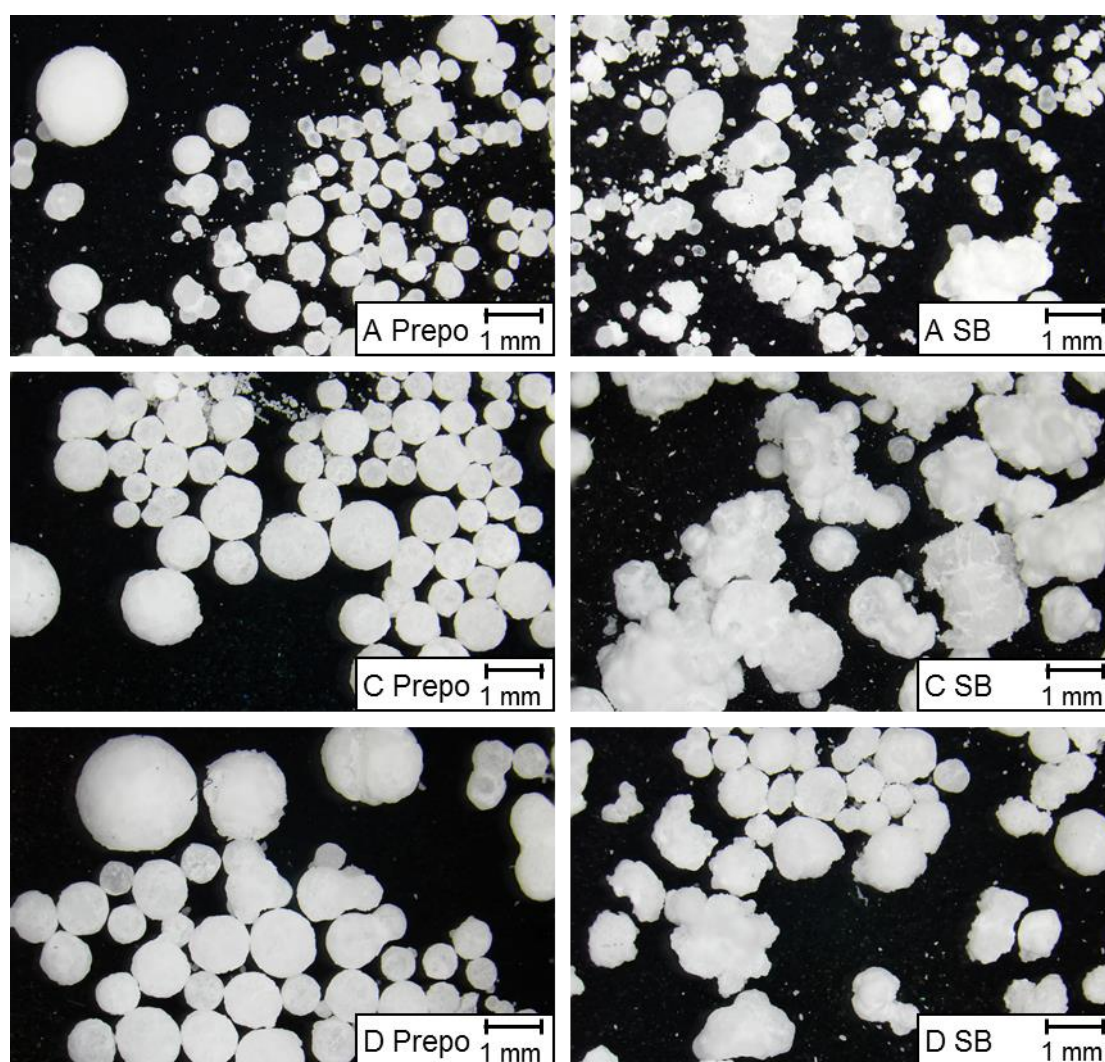


**Figure 5.24:** Camera images of selected PP samples synthesized with catalysts A, C and D using the method of prepolymerization (Prepo) or seed bed polymerization (SB). PP powders were synthesized at 80 °C (Cat A) or 75 °C (Cat C&D), 28.5 bar and 100 mg hydrogen.

A more detailed analysis of the particle shape and specifically surface structure was performed via scanning electron microscopy. Four levels of magnifications of particles synthesized with catalyst A using the method of prepolymerization are presented in Figure 5.25. The PP particles have all the same spherical shape. The surface appears smooth and cracks are not visible. Overall, the surface shows a low amount of irregularities. The particle



is not completely covered with a closed polymer skin, but small holes of different sizes are visible which possibly form the entrance of macro-pores. At very high magnifications, the multi-grain structure can be identified: The particle seems to consist of a vast number of grains of about 1  $\mu\text{m}$  in diameter. The grains themselves seem to be fused together and the particle can be described to consist of compact zones of agglomerated micro-grains or clusters of micro-grains as reported in literature [39, 68, 69].

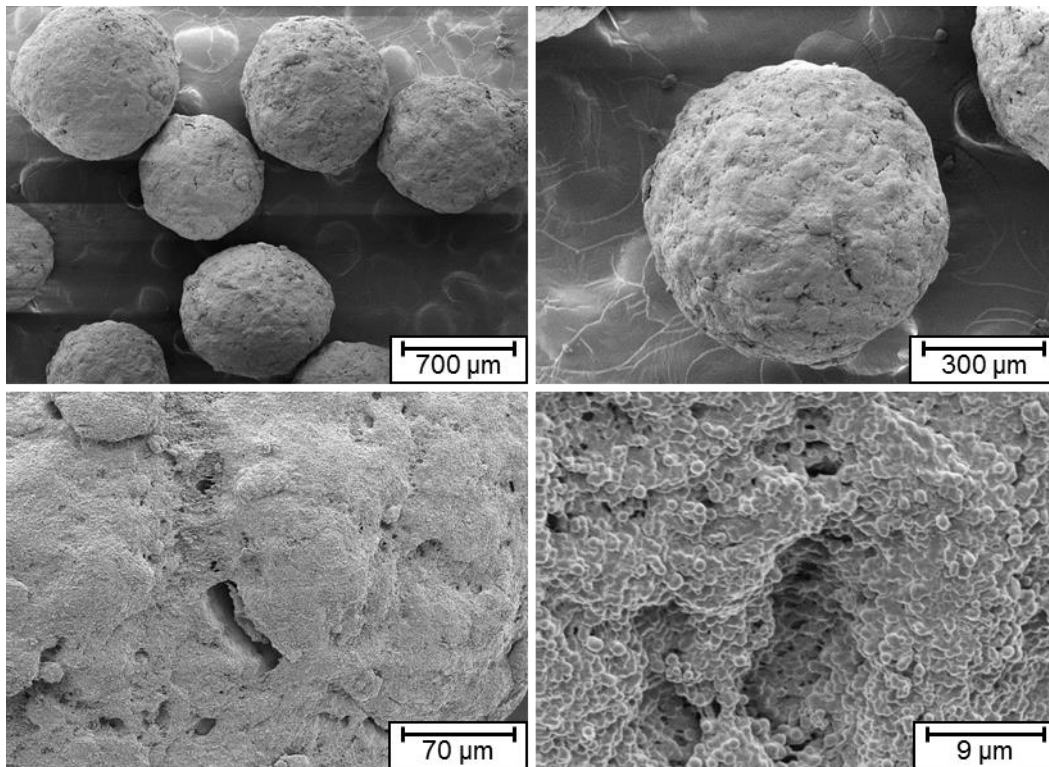


**Figure 5.25:** SEM images with four levels of magnification of PP particles synthesized with catalyst A using the method of prepolymerization. The sample was synthesized at 80 °C, 28.5 bar and 100 mg hydrogen.

When comparing the SEM images of powders produced with the different catalysts A, C and D, it is clear to see that spherical particles with a smooth surface are obtained by the method of prepolymerization for all catalysts (Figure 5.26). The seed bed polymerization method leads to non-spherical particles with rough surfaces. The non-spherical geometry combined with the irregular surface makes these particles more prone to attrition and particle breakup. This can cause the creation of fines increasing difficulties in plant operation.



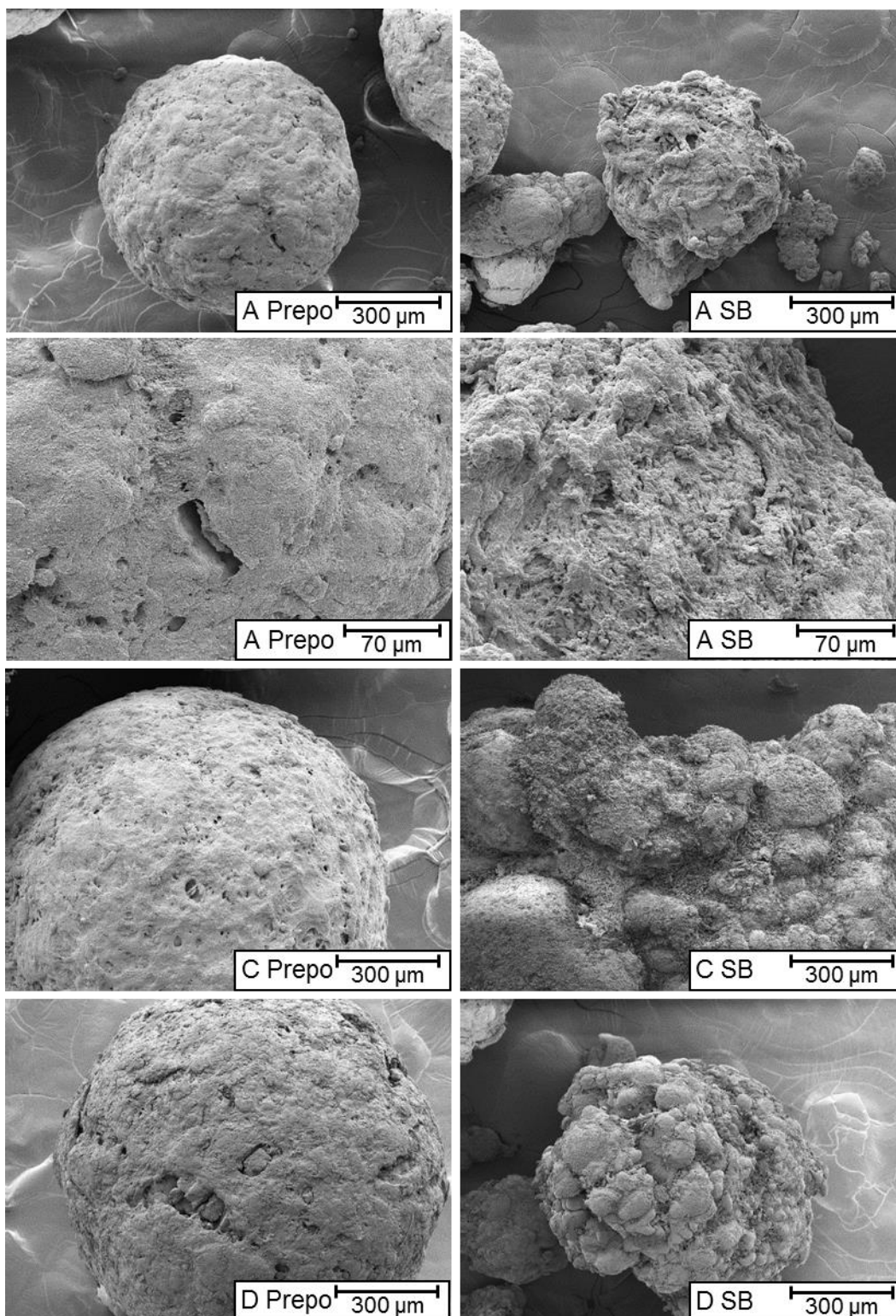


**Figure 5.26:** SEM images of selected PP samples synthesized with catalysts A, C and D using the method of prepolymerization (Prepo) or seed bed polymerization (SB). PP powders were synthesized at 80 °C (Cat A) or 75 °C (Cat C&D), 28.5 bar and 100 mg hydrogen.

The analysis of particle morphology by imaging techniques allowed to qualitatively study the particle shape and surface of selected samples, but may not be representative for the entire PP sample. Using bulk density measurements, the morphology can be characterized in a representative manner and quantitatively. Although not only the particle shape, but also other

factors influence the bulk density, in combination with the results of the camera images and SEM studies, detailed conclusions on the particle morphology may be drawn. Therefore, the bulk density was measured for various PP samples (Figure 5.27). The method of polymerization clearly affects the bulk density: Prepolymerization leads to high bulk densities, whereas seed bed polymerization gives lower bulk densities for each catalyst. Again it is mentioned that the PP powders produced by SB polymerization are a mixture of the seed bed and the freshly produced particles. The SB fraction was typically 30 wt%, but varied between 20 to 40 wt%. Thus, the bulk density of the SB polymerization experiment is rather an estimation of the true bulk density of the newly produced powder, but the analysis is still suited for a relative comparison.

The bulk densities are independent of the reactor hydrogen concentration, but differ from catalyst to catalyst. Catalyst A gives the highest bulk densities with on average  $510 \text{ kg/m}^3$  via the method of prepolymerization, whereas catalysts C and D give lower values of  $490$  and  $450 \text{ kg/m}^3$ , respectively. The absolute difference for the two polymerization methods of  $70 \text{ kg/m}^3$  is the same for all catalysts with average bulk densities for the SB method of  $450$ ,  $410$  and  $390 \text{ kg/m}^3$  for catalysts A, C and D, respectively. The bulk density of the prepolymerization method seems to be intrinsic for each catalyst, determined by factors such as porosity and PSD. However, the catalyst specific bulk density is lowered by the injection conditions, i.e. applying the method of SB polymerization decreases the bulk density by the same magnitude. Although the catalysts showed a very different heat resistance in terms of activity, the “morphology resistance” seems to be the same. For example, catalyst C showed the lowest difference in activity for the two methods of prepolymerization and SB polymerization, but the latter method nevertheless caused a reduction in bulk density in the same order as for the other catalysts.

Generally, the final particle shape is determined by the catalyst fragmentation step. The balance between the initial polymerization rate and mechanical properties of the support material determines how the catalyst fragments and thus the final particle morphology. [2, 4, 38] In case of SB polymerization, the higher reaction temperature causes a higher initial polymerization rate which is the likely reason for uneven catalyst fragmentation and loss of morphology control.

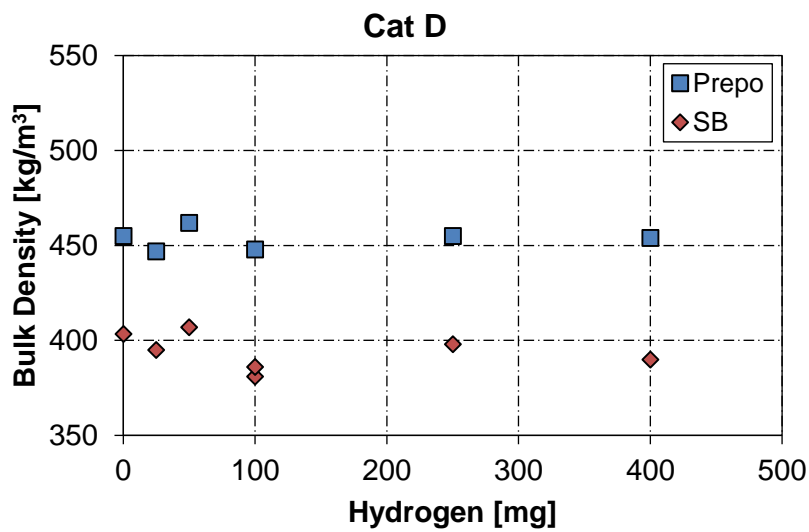
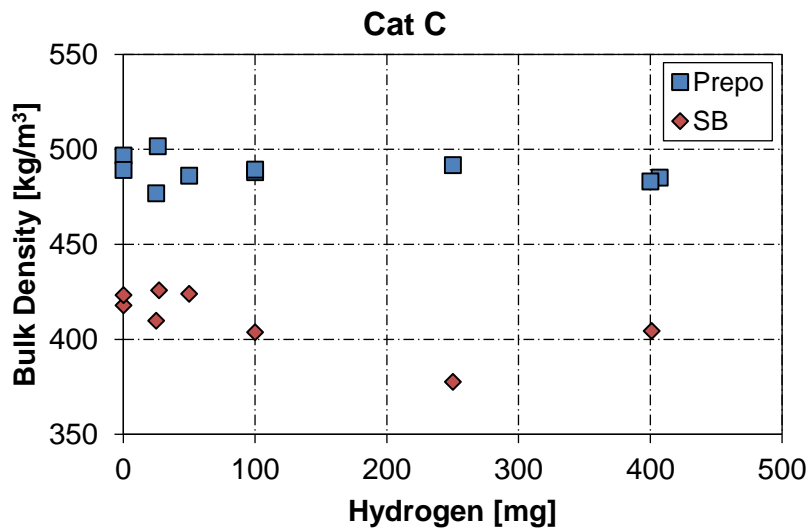
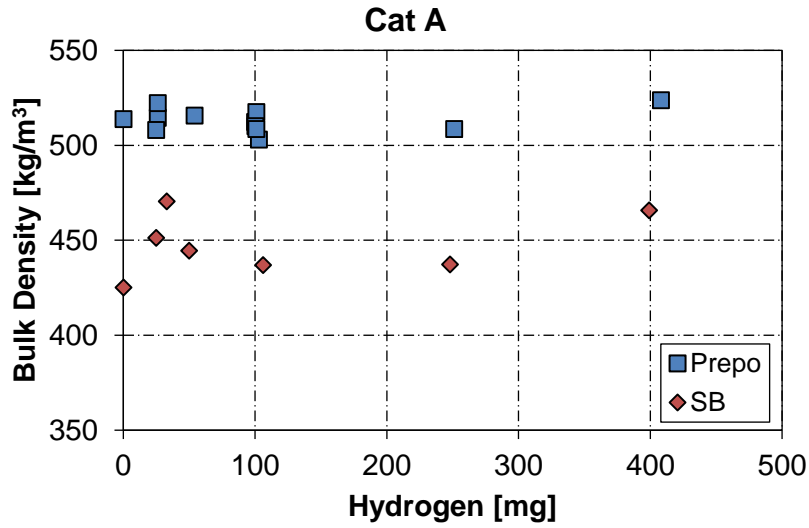


**Figure 5.27:** Effect of hydrogen on the bulk density. PP powders were synthesized at 80 °C (Cat A) or 75 °C (Cat C&D), 28.5 bar and 100 mg hydrogen with the method of prepolymerization (Prepo) or seed bed polymerization (SB).

Porosity was measured via mercury intrusion. The high pressures of up to 4000 bar applied during the measurement likely caused compression and/or deformation of the PP material leading to an over-estimation of the porosity results. However, a relative comparison should be still feasible. The determined porosities are in the range of 30 to 40 vol%. PP samples produced via prepolymerization have lower porosities than samples produced via SB polymerization (Table 5.2). Catalysts A and C give particles with porosities of 30 vol% for the method of prepolymerization and of 37 vol% for the SB method. PP powders produced with catalyst D give higher porosities of 34 and 43 vol% for the Prepo and SB method, respectively. A clear trend on the effect of the hydrogen concentration on the porosity was not found (Figure 5.28).

**Table 5.2:** Porosity of selected PP powders as determined by mercury intrusion. PP powders were synthesized at 80 °C (Cat A) or 75 °C (Cat C&D), 28.5 bar and 100 mg hydrogen with the method of prepolymerization (Prepo) or seed bed polymerization (SB).

Polymerization Method	Catalyst	Porosity [vol%]
Prepo	A	29
	C	31
	D	34
SB	A	38
	C	36
	D	43

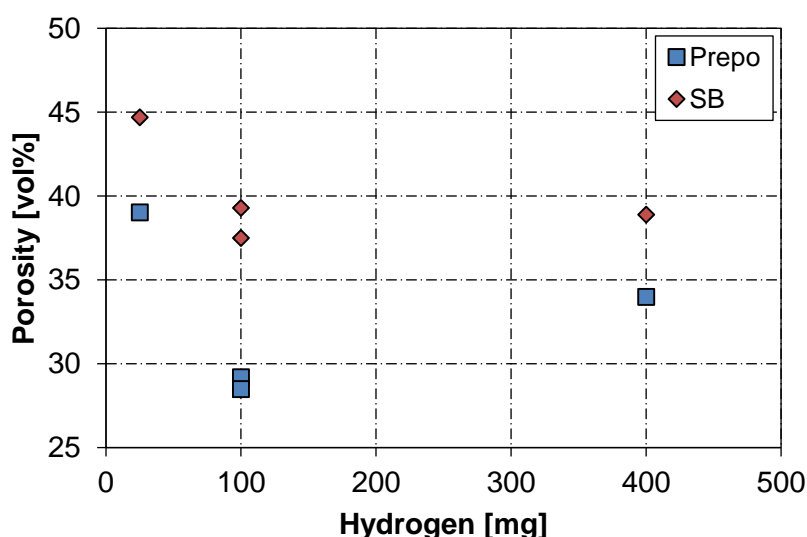


**Figure 5.28:** Effect of hydrogen on the particle porosity. PP powders were synthesized with catalyst A at 80 °C and 28.5 bar with the method of prepolymerization (Prepo) or seed bed polymerization (SB).

As a further characterization step, the particle size distribution (PSD) was measured by laser diffraction. PP powders of catalysts C and D show almost identical, symmetric PSDs with mean particle diameters of about 1100  $\mu\text{m}$  for both polymerization procedures (Figure 5.29, top). Catalyst A leads to PP particles of smaller size with a mean diameter of about 700  $\mu\text{m}$  and a less symmetric PSD. There is a certain difference between the prepolymerization and SB method for catalyst A in that the latter method gives a narrower PSD with a lower fraction of large particles. Breakage of large particles might be the reason for this discrepancy of Prepo and SB PSDs. For particles of catalyst A, also a tail at small particle diameters is observed for both polymerization methods indicating a certain amount of fines. This is also observed for catalysts C and D, but only for the SB method and less pronounced. A clear effect of hydrogen on the PSD is not found when analyzing the samples produced with catalyst A (Figure 5.29, bottom).

Based on the experimental investigations by particle shape and surface imaging, bulk density, porosity and PSD measurements, it can be concluded that the particle morphology is affected by mainly one factor which is the initial polymerization conditions. The low-rate prepolymerization conditions lead to a good morphology with regularly shaped, spherical particles with a smooth surface. Contrary, the higher reaction temperature at the polymerization start in case of SB polymerization causes a higher initial reaction rate which leads to loss of morphology control. The catalyst particle is not perfectly replicated and irregular, non-spherical particles with rough surfaces are obtained. The resulting bulk densities are lower and porosities are higher as a consequence of the faster fragmentation process. Although the three catalysts showed very different heat resistances, the loss of morphology is approximately equal for all catalysts and there is no distinguishable "morphology resistance", e.g. catalyst C showed the lowest activity difference between the Prepo and SB method, but the same reduction in bulk density as the other catalysts. The PSDs are rather similar for the two polymerization methods. Therefore, it can be concluded that the fast initial polymerization rates of the SB method do not lead to an extensive breakup. The particles maintain their integrity and only low amounts of fines are generated. Rather, the SB method leads to a poor morphology of the individual particle likely because of uneven fragmentation. The final powder bulk density was found to be catalyst specific, whereas the reduction of it by the SB method was equal for all catalysts. Interestingly, this catalyst specific bulk density differed in the same order as the bulk density difference of the two polymerization methods, e.g. the bulk densities of catalyst A and D were the same with 450  $\text{kg/m}^3$  for the SB and Prepo method, respectively.

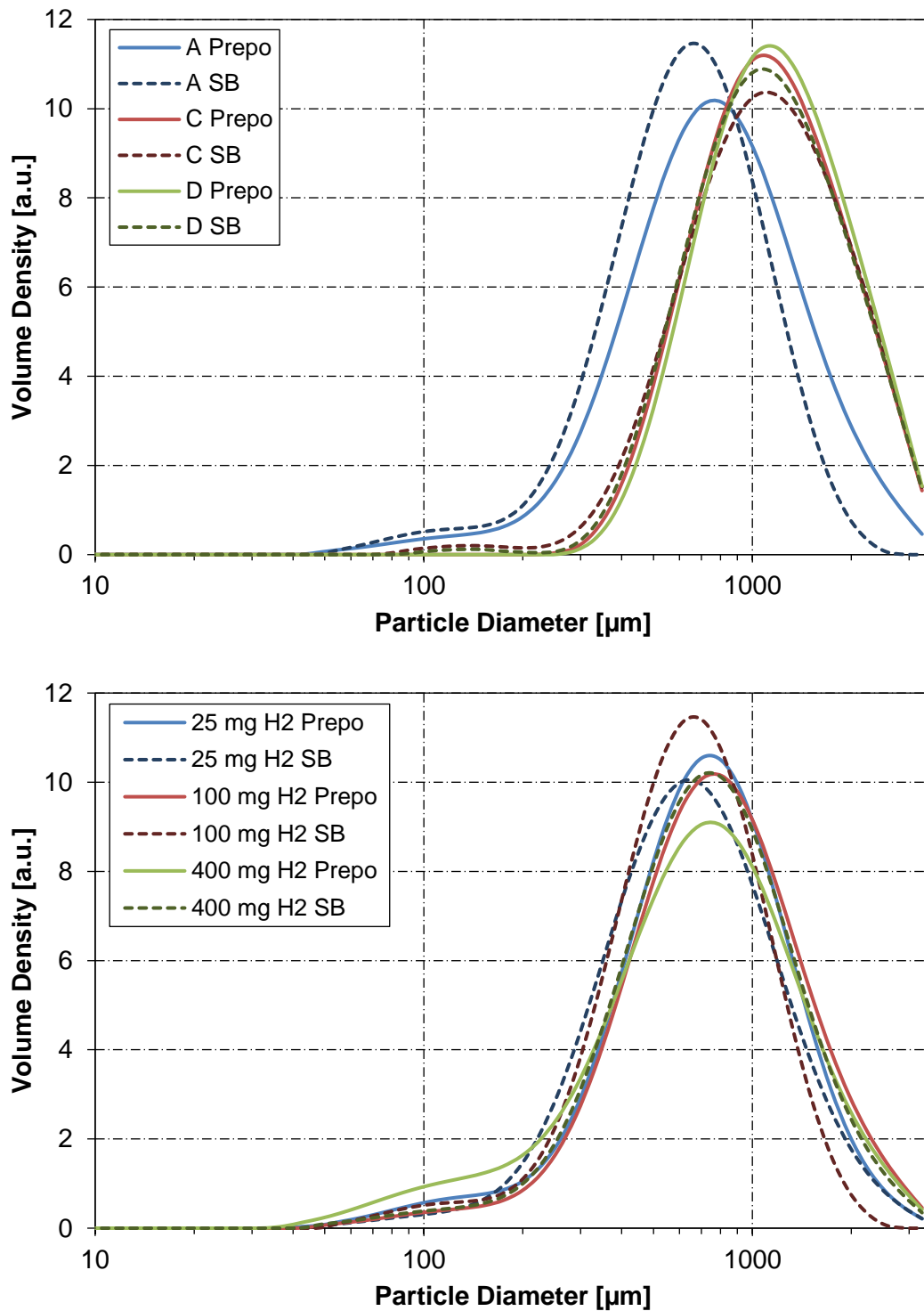


**Figure 5.29:** Particle size distribution of selected PP powders. Top: Comparison of powders produced with catalysts A, C and D. Bottom: Hydrogen variation for samples produced with catalyst A. PP powders were synthesized at 80 °C (Cat A) or 75 °C (Cat C&D), 28.5 bar and 100 mg hydrogen with the method of prepolymerization (Prepo) or seed bed polymerization (SB).

## 6 Solubility and Diffusion of Propylene in Polypropylene

Sorption experiments of propylene in selected PP samples were conducted in a high pressure magnetic suspension balance. One objective was to obtain correct solubility data which are needed for the calculation of reaction rates (section 7) since literature results for the propylene solubility in PP deviate (see below). The second objective aims at determining the transport properties of the PP particles. These are characteristic for a given PP powder and can be used to identify possible mass transfer limitations during reaction (section 6.5.2).

### 6.1 Comparison of literature solubility data

In this section, the solubility data of propylene in PP which was found in the open literature for experiments conducted at elevated pressures is compared. Contrary to mass transport properties which can be very different from sample to sample since mass transfer is greatly affected by the particle morphology [23, 40, 52, 55, 56, 58], the equilibrium solubility should only be affected by temperature, pressure and polymer density (thus polymer crystallinity). The effect of polymer density on the solubility of different gases in PE was studied by the group of Kosek [113, 114] showing that the amorphous solubility decreases with increasing polymer crystallinity. This was explained by the concept of elastic constraints in which the amorphous phase of a semi-crystalline polymer is constrained by the surrounding crystallites. It suggests that the higher the crystallinity of a polymer, the more constrained will be the amorphous phase leading to a lower gas solubility.

Contrary to the broad density range found for PE, state-of-the-art PP grades show a very narrow density range and thus the gas solubility should only differ slightly from sample to sample. However, in contrast to this assumption, literature solubilities show high deviations (Figure 6.1). Depending on the literature source, the amorphous solubility may differ by more than a factor of two. However, this is a crucial variable for kinetic modeling as it is proportional to the effective concentration of the monomer (see Equation (2.3)) which is directly linked to the polymerization rate. In view of the available literature data, the selection of the solubility values for modeling purposes seems arbitrary. Therefore, based on these findings, it was believed that a further experimental study on the solubility of propylene in PP combined with a critical review of literature data was necessary.

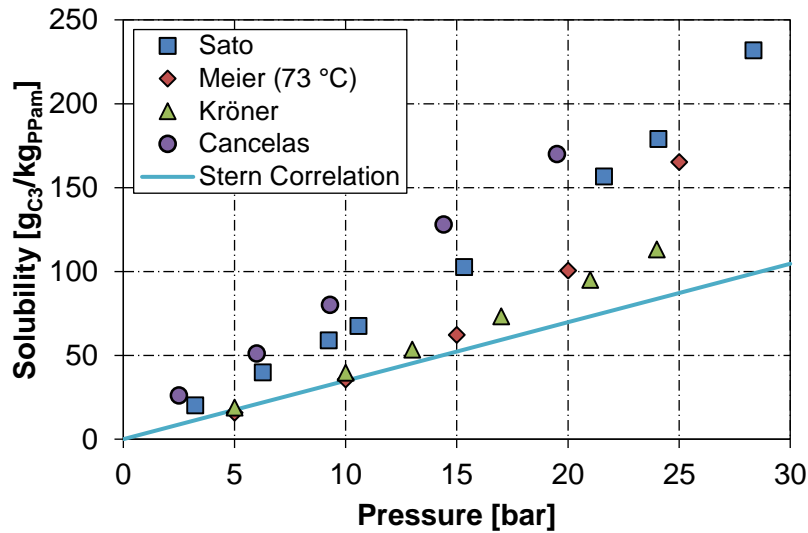


**Figure 6.1:** Comparison of literature solubility data at 70 °C of Sato [53], Meier [18], Kröner [58] and Cancelas [59] with the Stern correlation [64, 65]. The literature data was recalculated in terms of amorphous solubility (see appendix) for better comparison.

## 6.2 Experimental method

### 6.2.1 Magnetic suspension balance and operational procedure

Sorption experiments were performed by the gravimetric method using a high pressure magnetic suspension balance (*Rubotherm*, Figure 6.2). Detailed descriptions of the balance and experimental procedures can be found in [23] and [58]. The pressure chamber can be operated up to 25 bar and 80 °C. Isothermal conditions are ensured by jacket heating (*Lauda* E300 thermostat). Monomer is fed from the preheated ballast reservoir to the pressure chamber via a needle valve.

The sorption experiments were conducted as described in [23]. One to two grams of polymer were used for each experiment. The chamber was heated up to the desired temperature and vacuum was applied for one hour in order to remove traces of sorbed gases from the polymer sample. Propylene was fed via the needle valve to the pressure chamber requiring about 10 seconds for each pressure step. A small temperature rise usually occurred upon propylene feeding, but isothermal conditions were typically reached within one minute.



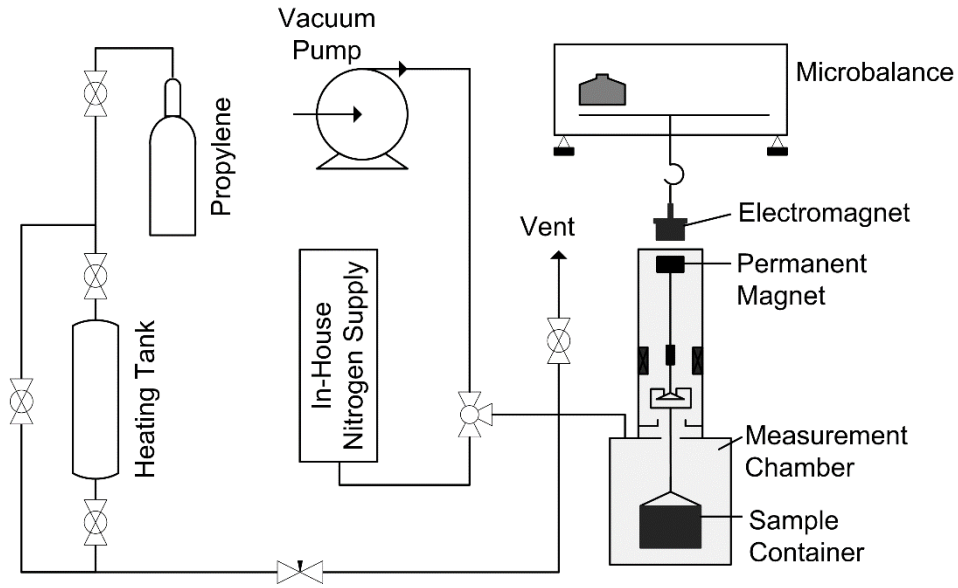


**Figure 6.2:** Flow sheet of the high pressure magnetic suspension balance.

## 6.2.2 Buoyancy force correction and polymer swelling

The measured balance weight  $m_{bal}$  has to be corrected for the buoyancy force:

$$m_{corr} = m_{bal} + \rho_{gas}(V_{con} + V_{PP}) \quad (6.1)$$

The gas density  $\rho_{gas}$  of propylene was calculated at each time step by a virial equation which Kröner [23] fitted to experimental gas densities of propylene between 50 and 80 °C up to a pressure of 30 bar with a maximum deviation of 1 %. The container volume  $V_{con}$  (all metal parts on which the buoyancy force acts on) was determined in a blank measurement in which the container was subjected to nitrogen at different pressures. The polymer volume  $V_{PP}$  is given by the sum of the polymer volume at vacuum conditions  $V_{PP,0}$  and the increase in volume by swelling  $\Delta V_{swell}$ :

$$V_{PP} = V_{PP,0} + \Delta V_{swell} \quad (6.2)$$

The polymer volume at vacuum can be calculated from the polymer mass at vacuum and the polymer density. The polymer density at vacuum conditions  $\rho_{PP,0}$  was calculated as:

$$\rho_{PP,0}(T) = v_{cr}\rho_{cr}(T) + (1 - v_{cr})\rho_{am}(T) \quad (6.3)$$

The temperature effect on the polymer density was considered by using the temperature-dependent amorphous  $\rho_{am}(T)$  and crystalline densities  $\rho_{cr}(T)$  (see appendix), whereas the

crystalline volume fraction was assumed to be constant. DSC measurements revealed that the crystallinity only increased by 2 wt% when the sample was exposed to 90 °C for 1 h and remained constant at a temperature of 70 °C supporting the made assumption.

The effect of swelling becomes important at elevated pressures. Bobak et al. [56] examined swelling of PP by propylene at 85 °C up to 26 bar by video-microscopy. The swelling volume could be well fit to the following linear equation:

$$\Delta V_{swell} = 1.7844 S V_{PP,0} \quad (6.4)$$

Further studies from the same research group [121] on the swelling of ethylene in PE showed that there is no temperature dependence of the swelling which suggests that the above correlation might be used for other temperatures than 85 °C. Note that a strong effect of the PE density on swelling was observed in their study, however, contrary to PE, the densities of PP synthesized with state-of-the-art ZN catalysts show a very narrow range and swelling should be similar for all of these type of PP samples.

Another study on swelling was conducted by Sato et al. [54] in which the elongation of a PP film was studied in a high pressure observation cell. The experimental swelling data was underestimated by using the Sanchez-Lacombe EoS, but could be well described by additivity of saturated propylene volume and polymer volume:

$$\Delta V_{swell} = \left[ \frac{\frac{w_{cr}}{\rho_{cr}(T,P)} + \frac{w_{am}}{\rho_{am}(T,P)} + \frac{w_{am}}{\rho_{C3}^{liq}(T,P_{vap})} S_{am}}{\frac{w_{cr}}{\rho_{cr}(T,0)} + \frac{w_{am}}{\rho_{am}(T,0)}} - 1 \right] V_{PP,0} \quad (6.5)$$

Neglecting the pressure effect on the amorphous and crystalline densities of the polymer in the numerator, the swelling can be simplified to:

$$\Delta V_{swell} = \frac{\rho_{PP,0}(T)}{\rho_{C3}^{liq}(T,P_{sat})} S V_{PP,0} \quad (6.6)$$

Thus this expression for swelling involves a temperature-dependent factor, whereas the experimental correlation of Bobak et al. [56] simply uses the constant factor of 1.7844. The two correlations are compared in Figure 6.3. As can be clearly seen, linear additivity leads to higher swelling. At 50 °C, linear additivity and the correlation of Bobak et al. [56] are very similar, whereas at higher temperatures, the deviation increases. However, when Sato et al. [54] studied the swelling behavior at 50 and 75 °C, linear additivity could well describe the swelling at 50°C, but over-predicted the swelling by about 12 % at the higher temperature of 75 °C. When considering this mismatch, the swelling curves of Sato et al. [54] are identical at

50 and 75 °C (Figure 6.3) suggesting no temperature effect. Furthermore, the two curves are close to the one of Bobak et al. [56]. It can thus be concluded that swelling of propylene in PP can be considered temperature independent based on the available experimental data. Nevertheless, further experimental swelling studies should be conducted to verify this conclusion.

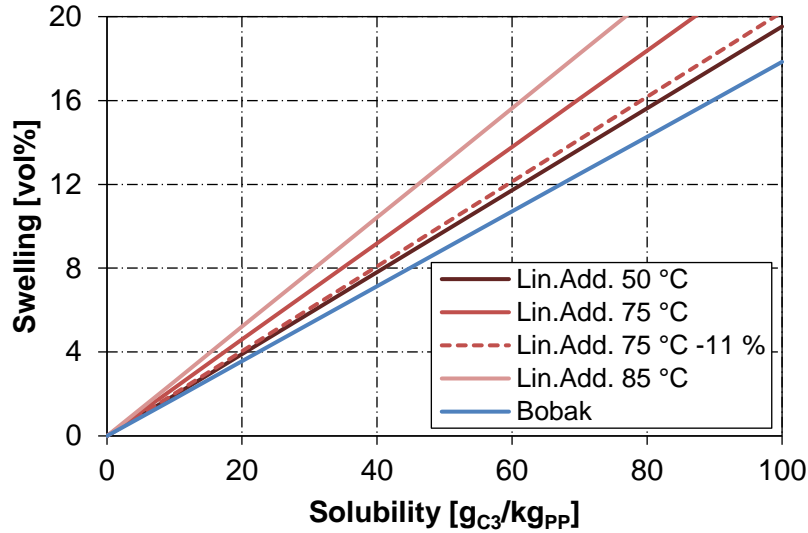


**Figure 6.3:** Comparison of the experimental correlation for swelling of propylene in PP of Bobak et al. [56] with linear additivity of polymer and monomer volumes as experimentally observed by Sato et al. [54]. A constant polymer density of 890 kg/m<sup>3</sup> was used in the calculations since the temperature effect on polymer density was found to be negligible.

Eventually, depending on the applied swelling correlation, the solubility can be calculated. In case swelling is neglected, the sorbed mass of propylene is simply calculated by subtracting the mass of the container  $m_{con}$  (mass of all metal parts at vacuum which was obtained via a blank measurement) and the sample mass at vacuum from the corrected mass  $m_{corr}$ :

$$m_{C3} = m_{corr} - m_{con} - m_{PP} \quad (6.7)$$

As the sorption experiments were conducted at elevated pressures, swelling should be considered. Based on the conclusion about the swelling behavior of propylene in PP, in this work the correlation of Bobak et al. [56] was used for all temperatures. When considering this swelling correlation, the sorbed propylene mass is given by:

$$m_{C3} = \frac{m_{corr} - m_{con} - m_{PP}}{1 - 1.7844 \frac{\rho_{gas}}{\rho_{PP,0}}} \quad (6.8)$$

Eventually, the solubility and amorphous solubility can be calculated by Equations (2.1) and (2.2).

### 6.2.3 Experimental plan

The experimental study can be divided into two objectives: the determination of solubility data and the evaluation of the particle's mass transport properties. The experimental results are accordingly presented in two separate sections: equilibrium solubility and diffusion. The latter was obtained from the slope of the mass uptake profile, whereas the former was received from the (average) values of the sorption curve at long measurement times, i.e. when the balance weight did not increase any longer (Figure 6.4).

Different samples were analyzed at various conditions to study the influence of the sample, temperature and pressure on the solubility of propylene in PP (Table 6.1). To study the effect of the sample characteristics, various samples were analyzed up to 25 bar at 70 °C (for comparison as most literature data are available for 70 °C). Additionally, sample A was measured in a temperature range from 40 to 80 °C. For mass transport analysis, selected samples were studied at the corresponding reaction temperatures (section 6.5.1).

Note that a large amount of the experiments was conducted as part of the master thesis of Klabunde [122]. The respective experiments are labelled and her contribution to this section is greatly acknowledged.

**Table 6.1:** Samples and experimental plan for solubility measurements. PP powders were synthesized at 80 °C (Cat A&B) or 75 °C (Cat C&D), 28.5 bar and 100 mg hydrogen with the method of prepolymerization (Prepo).

Sample	Catalyst	Polymerization Method	DSC-Crystallinity [wt%]	Sorption Temperature [°C]
A	A	Prepo	40	40-70 <sup>1</sup> ; 80
A-Film	A	Pressed film of sample A	53	70 <sup>1</sup>
B	B	Prepo	-	70
C	C	Prepo	39	70 <sup>1</sup>
D	D	Prepo	35	70 <sup>1</sup>
E <sup>2</sup>	anonymous	Bulk phase	-	70 <sup>1</sup>

<sup>1</sup>Experiments were performed by Klabunde [122]

<sup>2</sup>Sample from a different research project

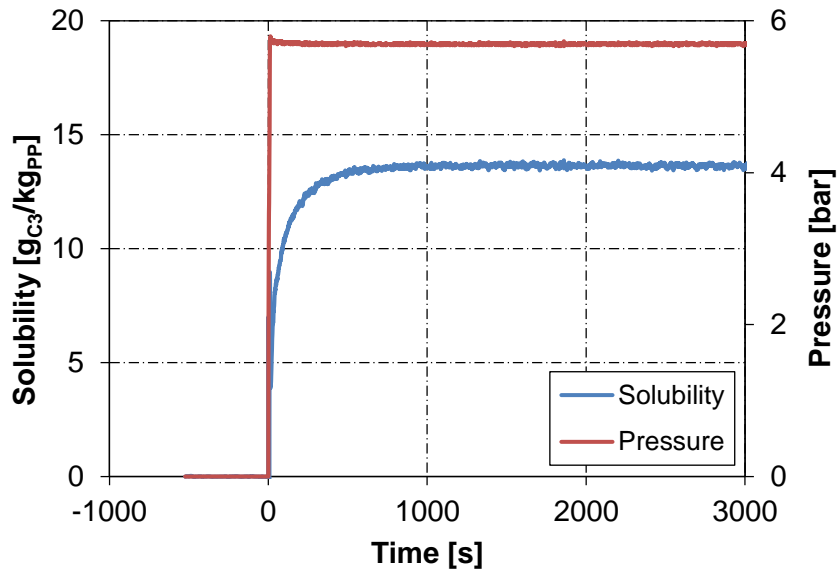


Figure 6.4: Sorption curve of sample A at 70 °C.

### 6.3 Equilibrium solubility results

#### 6.3.1 Solubility

The reproducibility of the measurements was tested by measuring the total solubility of sample A in three separate experiments (Figure 6.5). For the solubility measurements, a good reproducibility was found with almost no deviations between the different reproduced isotherms.

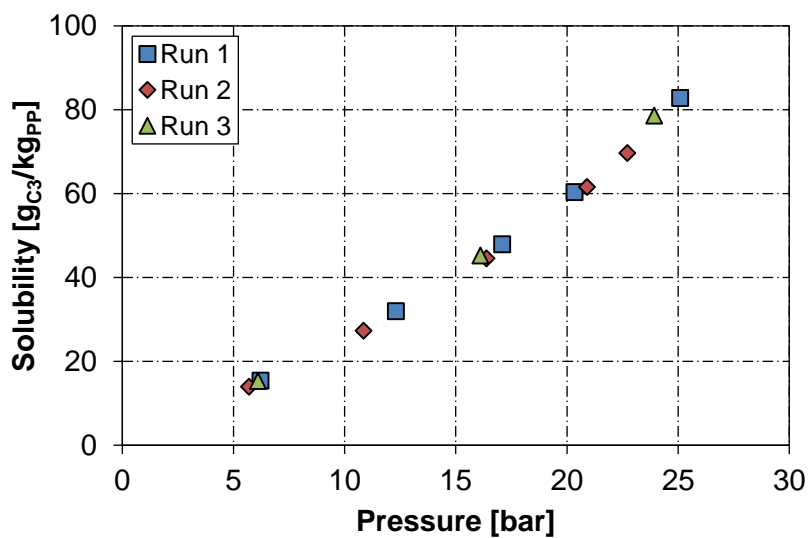
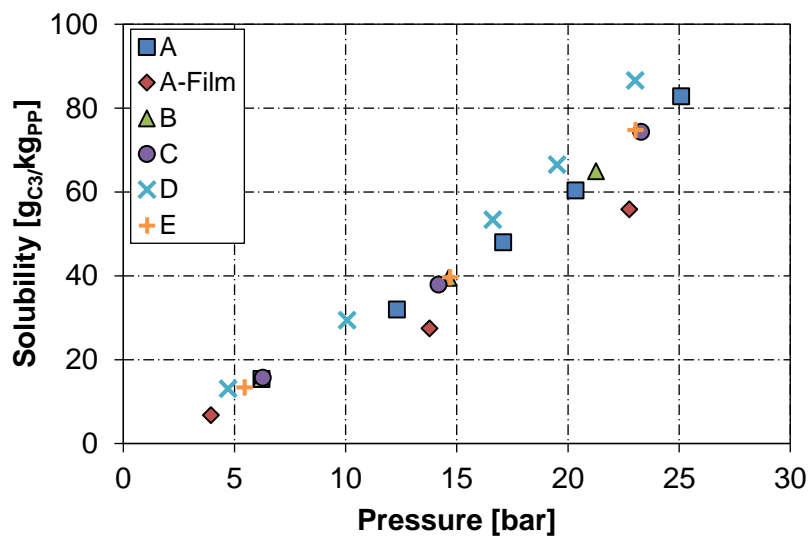


Figure 6.5: Reproducibility for the solubility of propylene in sample A at 70 °C.

Various different samples were measured at 70 °C to study the effect of the sample influence on the solubility. Samples A, B, C and E show the same solubility isotherms although these samples were produced with different catalysts and at different conditions (Figure 6.6). Sample D shows a slightly higher solubility which was expected because of the lower crystallinity of 35 wt% (DSC) in contrast to the crystallinities of sample A and C of 40 wt%. The produced film of sample A showed a lower propylene solubility than all the other samples. This can be explained by the thermal treatment of the PP powder which caused an increase in crystallinity (53 wt%) and thus a lower solubility since monomer is only absorbed in the amorphous polymer fraction. Comparing the solubilities at 23 bar indicates that a higher difference in crystallinity leads to a higher difference in solubility.

The temperature dependence on the propylene solubility in PP was studied for sample A (Figure 6.7). The solubility decreases with increasing temperature and the solubility isotherms all show a non-linear increase with pressure.



**Figure 6.6:** Solubility of propylene in PP at 70 °C for various samples.

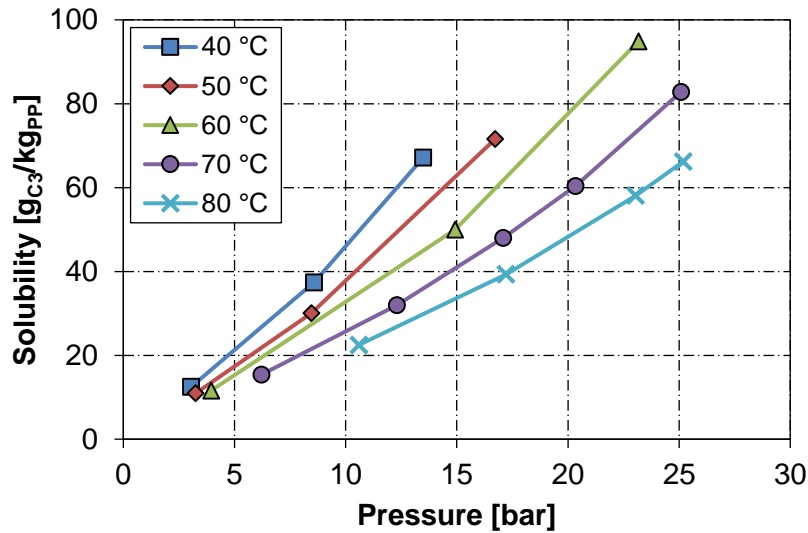


**Figure 6.7:** Solubility of propylene in sample A at temperatures between 40 and 80 °C.

### 6.3.2 Comparison of solubility results with literature data

As shown in section 6.1, literature solubility data of propylene in PP can deviate by a factor of more than two when comparing the amorphous solubility. In the following, the solubility presented in mass of propylene per mass of the entire sample is compared, i.e. crystallinity determination is not needed. In this way, assuming that the literature solubility data was correctly determined, the qualitative crystallinity difference between the various samples is directly visible since the solubility of samples with different crystallinity will be different. Only sample A is used for comparison with literature data since it well represents most of the PP powders studied in this work.

The comparison of the solubility isotherm at 70 °C of literature data and sample A reveal good agreement (Figure 6.8). Up to a pressure of 15 bar, the solubilities are identical. Above 20 bar, a difference in solubility is found: The reported values of Meier et al. [18] and Kröner and Bartke [58] agree well with the solubility of sample A, whereas the solubility of Sato et al. [53] and Cancelas et al. [59] is slightly lower suggesting a higher crystallinity of their samples. The comparison at other temperatures reveals very similar results of this work and literature solubilities (Figure 6.9). The solubility isotherms of sample A and the ones from Meier et al. [18] at 40 and 60 °C are almost identical, except for the last solubility value close to the vapor pressure, which is always higher for the isotherms of Meier et al. [18]. At 50°C, the compared isotherms are all identical up to a pressure of 10 bar. At higher pressures, the deviations increase with the solubility of sample A falling in between the results of Sato et al. [53] and Meier et al. [18]. Note that the chosen correlation for swelling becomes important

at elevated pressure. Here, Sato et al. [53] used the Sanchez-Lacombe EoS for swelling correction which underestimated the swelling by linear additivity as considered by Meier et al. [18]. The isotherms at around 85 °C show the highest deviations. However, the results of this work and the ones of Bobak et al. [56] agree well and the lower solubility of Sato et al. [53] can be explained by the generally lower solubility found at all temperatures (likely due to a higher crystallinity) and the higher temperature of 90 °C.

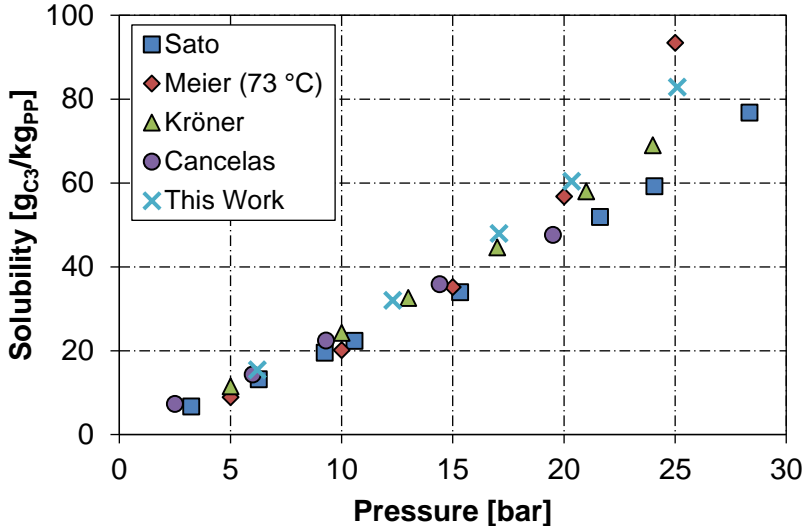


**Figure 6.8:** Comparison of the solubility of propylene in PP for sample A and literature values at 70 °C. Literature data were taken from the publications of Sato et al. [53], Meier et al. [18], Kröner and Bartke [58] and Cancelas et al. [59].



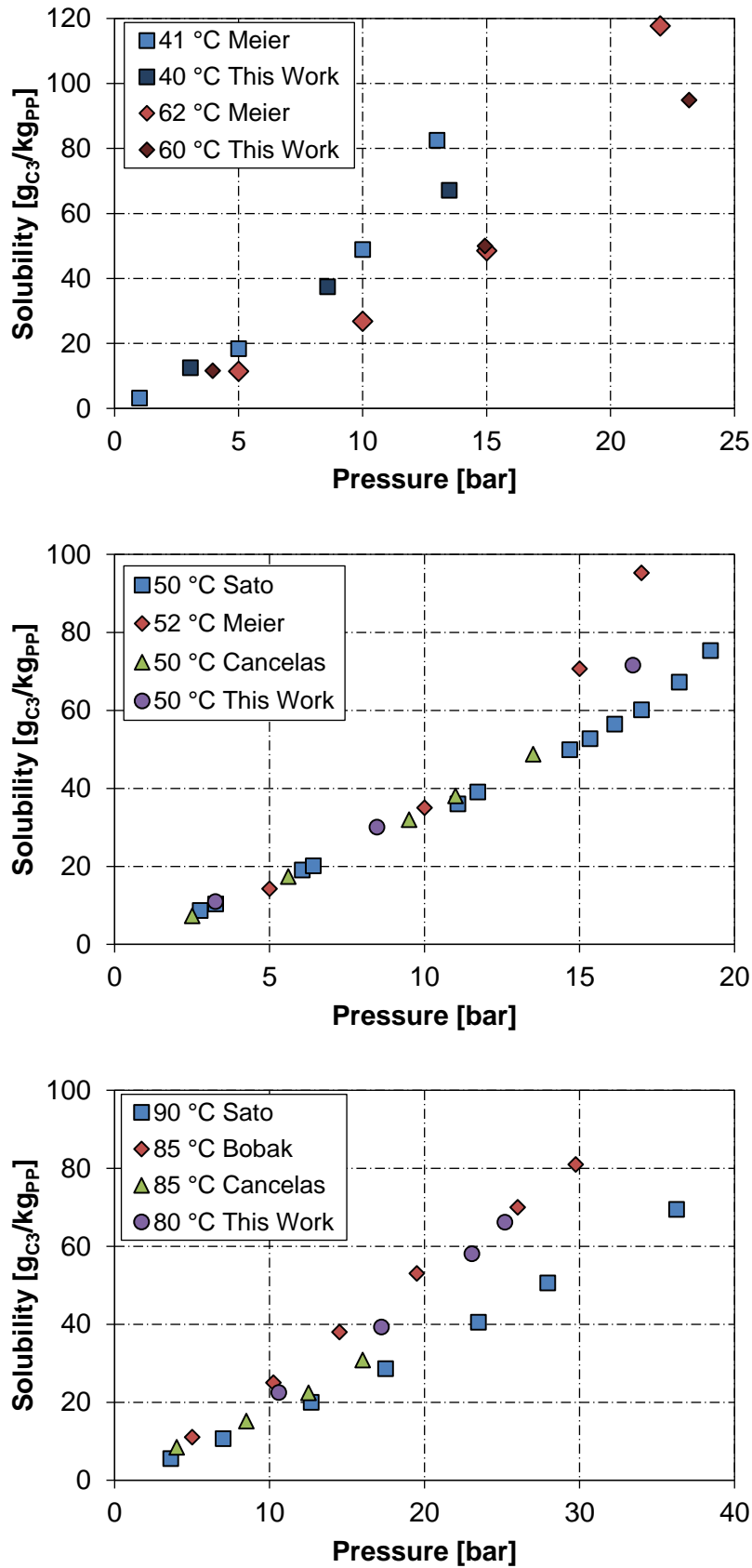


**Figure 6.9:** Comparison of the solubility of propylene in PP for sample A and literature values at 40, 50, 60 and between 80 to 90 °C. Literature data was taken from the publications of Sato et al. [53], Meier et al. [18], Bobak et al. [56] and Cancelas et al. [59].

Based on the results of the various samples studied in this work and the literature results, it can be concluded that the solubility of propylene in PP does only vary little from sample to sample in accordance with the small density range of PP grades produced with state-of-the-art Ziegler-Natta catalysts. Some variations may be found, but large differences are not expected (contrary to PE).

The strong deviations found for the reported amorphous solubility can thus be ascribed to the assigned crystallinities. Therefore, in order to determine the crystallinity with high accuracy, sample A and D were analyzed by three different methods: DSC, WAXS and density (via He-pycnometry). All three different methods gave different crystalline mass fractions of 40, 46 and 56 wt% for sample A (Table 6.2). The same trend is found for sample D with all methods indicating a lower crystallinity in agreement with the solubility isotherm of sample D. DSC gave very accurate results in terms of reproducibility, but relies on the chosen value for the theoretical enthalpy of fusion of 100 % crystalline PP. Furthermore, Kong and Hay [123] argued that a simple integration of the DSC heat endotherm may give wrong results and a more sophisticated analysis is needed to obtain the correct DSC crystallinity which should agree with values obtained by for instance WAXS or the density method. For WAXS measurements, a good reproducibility was found and the largest error in crystallinity determination is likely caused by the analysis of the XRD spectra. The density of the porous PP powders was measured via He-pycnometry. A higher crystallinity than by DSC was obtained which was also reported by Sato et al. [54]. This method showed the highest inaccuracy in terms of reproducibility and for sample D, also crystallinity values that agreed well with the ones by WAXS were found. Overall, the crystallinity seems to be dependent on the selected method. However, deviations in this work are much smaller than the ones found in the publications about propylene solubility. For the calculation of the amorphous solubility and the monomer concentration in the amorphous phase, the WAXS results are used as they fall in between the other two methods with a deviation of about 10 %.

**Table 6.2:** Crystalline mass fractions of sample A and D as determined by DSC, WAXS and density (via He-pycnometry). The values in brackets correspond to the deviations found by two separate measurements.

Sample	Crystalline Mass Fraction [wt%]		
	DSC	WAXS	Density
A	40 ( $\pm 1$ )	46 ( $\pm 1$ )	56 ( $\pm 5$ )
D	35 ( $\pm 1$ )	43 ( $\pm 1$ )	53 ( $\pm 12$ )

It can be concluded that literature amorphous solubility results were found to largely disagree by a factor of more than two. The reason for this is the determined crystallinity value of the studied samples. When the solubility as mass of propylene per mass of PP is compared, literature data and solubility results of this work are very similar suggesting that the compared samples all should have almost identical densities and thus crystallinities. This is supported by the various samples studied in this work. Crystallinity results of the different methods DSC, WAXS and density deviate to a certain extent and the crystallinity can only be described with a minimum error of about 10 %.

### 6.3.3 Effective propylene concentration

Based on the solubility results and the determined crystallinity of sample A, the propylene concentration in the amorphous polymer phase can be calculated. This effective monomer concentration is directly linked to the polymerization rate and therefore crucial for kinetic modeling. The experimental propylene concentration in the amorphous phase, incorporating the effect of swelling according to Bobak et al. [56], is calculated as:

$$c_{am} = \frac{n_{C3}}{V_{am,0} + \Delta V_{swell}} = \frac{S \rho_{PP,0}(T)}{MW_{C3}[1 - v_{cr} + 1.7844 \cdot S]} \quad (6.9)$$

The amorphous concentration is compared to the literature correlation of Stern [64, 65] in Figure 6.10. At low pressures, the experimental results agree well with the literature correlation, whereas with rising pressure, the deviation increases. Stern et al. [64] proposed a correlation to estimate when the deviation from Henry's law becomes larger than 5 %. At 70 °C, this correlation gives a pressure of 9.2 bar for propylene above which deviations should become larger than 5 % due to plasticizing effects of the penetrant. This can qualitatively be seen in the Figure 6.10. At low pressures Henry's law is applicable, whereas at high pressures, a non-linear increase in concentration is caused by interactions of penetrant and polymer for which other thermodynamic models should be used. The experimentally determined concentrations are about 20 % higher in the low-pressure region and up to 35 % at 25 bar. Note that Hutchinson and Ray [65] fitted the Stern correlation based on experimental solubilities of gases in polyethylene and not polypropylene which might explain the found deviations at low pressures.

The effect of temperature on the amorphous concentration is presented in Figure 6.11. The propylene concentration decreases with increasing temperature like the solubility, but increases less non-linearly with pressure over the studied temperature range.

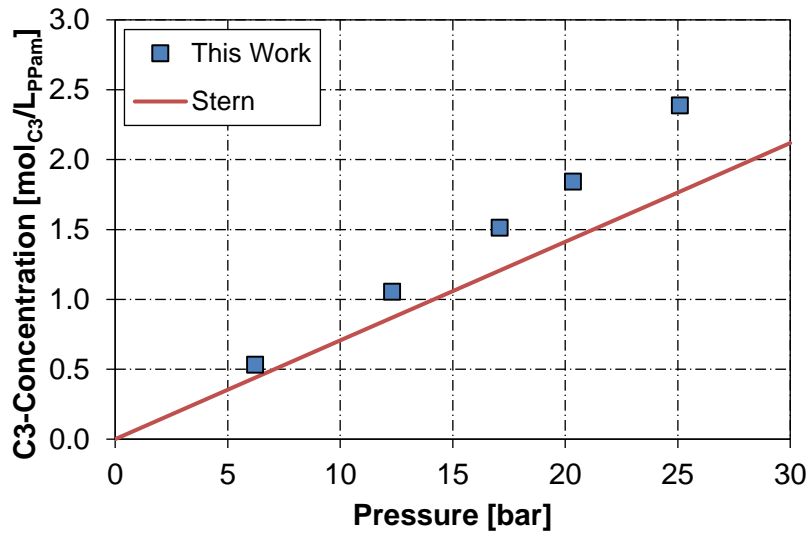


**Figure 6.10:** Comparison of the experimental propylene concentration in the amorphous polymer phase for sample A at 70 °C with the Stern correlation [64, 65].

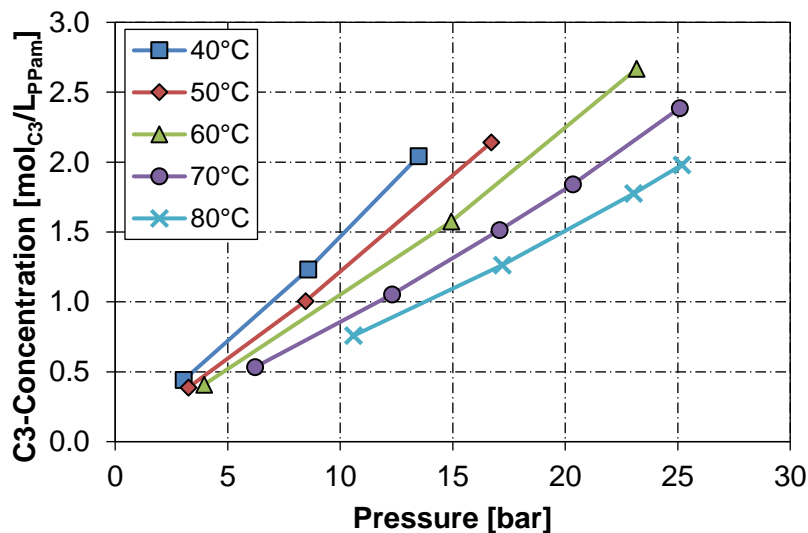


**Figure 6.11:** Concentration of propylene in the amorphous PP polymer phase for sample A for different temperatures.

## 6.4 Thermodynamic modeling

### 6.4.1 Sanchez-Lacombe and PC-SAFT equations of state

Both the Sanchez-Lacombe and the PC-SAFT model were tested in order to describe the equilibrium solubility of propylene in PP. The SL EoS was implemented in the open-source software GNU Octave 5.1.0 [124] which is largely compatible with MATLAB®. The involved equations can be found in the publication of Neau [125]. Different methods for the calculation

of mixtures exist for the SL EoS. Although the formulation of the chemical potential by McHugh and Krukoni [126] is commonly used [60, 104, 107–109, 127], in this work the fugacity coefficient as derived by Neau [125] is applied which should be used for thermodynamically consistent phase equilibrium calculations. Quadratic mixing rules were used for the characteristic volume  $v^*$  and energy  $\varepsilon^*$  of the mixture:

$$v^* = \sum \sum \phi_i \phi_j v_{ij}^* \quad (6.10)$$

$$\varepsilon^* v^* = \sum \sum \phi_i \phi_j \varepsilon_{ij}^* v_{ij}^* \quad (6.11)$$

with

$$v_{ij}^* = \frac{1}{2}(v_i^* + v_j^*) \quad (6.12)$$

and

$$\varepsilon_{ij}^* = \sqrt{\varepsilon_i^* \varepsilon_j^* (1 - k_{ij})} \quad (6.13)$$

For the PC-SAFT EoS, the open-source GNU Octave (or MATLAB®) programs [128, 129] provided by the High Pressure Process Group of the University of Valladolid were used which are based on the original PC-SAFT publication of Gross and Sadowski [110].

The solubility was calculated from the thermodynamic equilibrium at a given temperature and pressure which is determined by the point of equal fugacities in the gas and liquid phase:

$$f_i^{gas} = f_i^{liq} \quad (6.14)$$

Note that within the model framework, the amorphous polymer phase is considered as the liquid phase. The semi-crystalline nature of the polymer phase is thus neglected and crystallinity cannot be described by the thermodynamic model.

Using the fugacity coefficient  $\varphi$ , the point of equal fugacities can be expressed for propylene by:

$$\varphi_{C3}^{gas} y_{C3} = \varphi_{C3}^{liq} x_{C3} \quad (6.15)$$

Assuming the amount of polymer in the gas phase is negligible, the molar fraction of propylene in the gas phase becomes one and the solubility of propylene in PP can be calculated by solving the following equation:

$$\varphi_{C3}^{pure} = \varphi_{C3}^{liq} x_{C3} \quad (6.16)$$

where  $\varphi_{C3}^{pure}$  refers to the fugacity coefficient of pure propylene.

#### 6.4.2 Pure component parameters and density calculations

Three characteristic parameters are needed to describe a pure component for both the SL and the PC-SAFT model. Literature parameters for the SL and PC-SAFT EoS are listed in Table 6.3 and Table 6.4, respectively. As an example, the gas density of propylene at 80 °C is presented in Figure 6.12 for the different literature parameters. Both models describe the vapor density very accurately. The PC-SAFT clearly best agrees with the experimental data. Generally, the PC-SAFT equation is superior in describing the propylene density close to the critical point as pointed out by Krallis and Kanellopoulos [104]. At high pressures, the SL EoS shows higher deviations from the experimental propylene gas density. The very similar parameters of Sato et al. [54] and Krallis and Kanellopoulos [104] give almost the same simulation results, whereas the parameters of Khare [130] tend to slightly better describe the experimental gas density at 80 °C. It can be concluded that all literature parameters for the SL EoS give accurate results and the selection of a given set of parameters is arbitrary. For further SL simulations of the propylene solubility, the parameters of Khare [130] are chosen as they seem to better describe the propylene gas density close to the critical temperature which are the relevant conditions for the studied gas phase polymerizations (75 and 80 °C at 28.5 bar).

**Table 6.3:** Literature pure component parameters of propylene and polypropylene for the Sanchez-Lacombe EoS.  $T^*$ ,  $P^*$  and  $\rho^*$  denote the characteristic temperature, pressure and closed-packed mass density, respectively.

Component	$T^*$ [K]	$P^*$ [bar]	$\rho^*$ [kg/m <sup>3</sup> ]	Reference
Propylene	345.4	3788	755	[54]
	356	3790	755	[104]
	360.43	3100	670.83	[130]
PP	690.6	3007	885.6	[54]
	724.3	2800	938.87	[130]

**Table 6.4:** Literature pure component parameters of propylene and polypropylene for the PC-SAFT EoS.  $m$ ,  $\sigma$ ,  $\varepsilon$ ,  $k_B$  and  $M_n$  denote the number of segments per molecule, segment diameter, energy related to the interaction of two segments, Boltzmann constant and number average molecular weight, respectively.

Component	$m$ [-]	$\sigma$ [Å]	$\varepsilon/k_B$ [K]	$m/M_n$ [mol/g]	Reference
Propylene	1.9597	3.5356	207.19	-	[110]
PP	-	4.147	298.6	0.0253	[79]
	-	4.1	217.0	0.02305	[111]

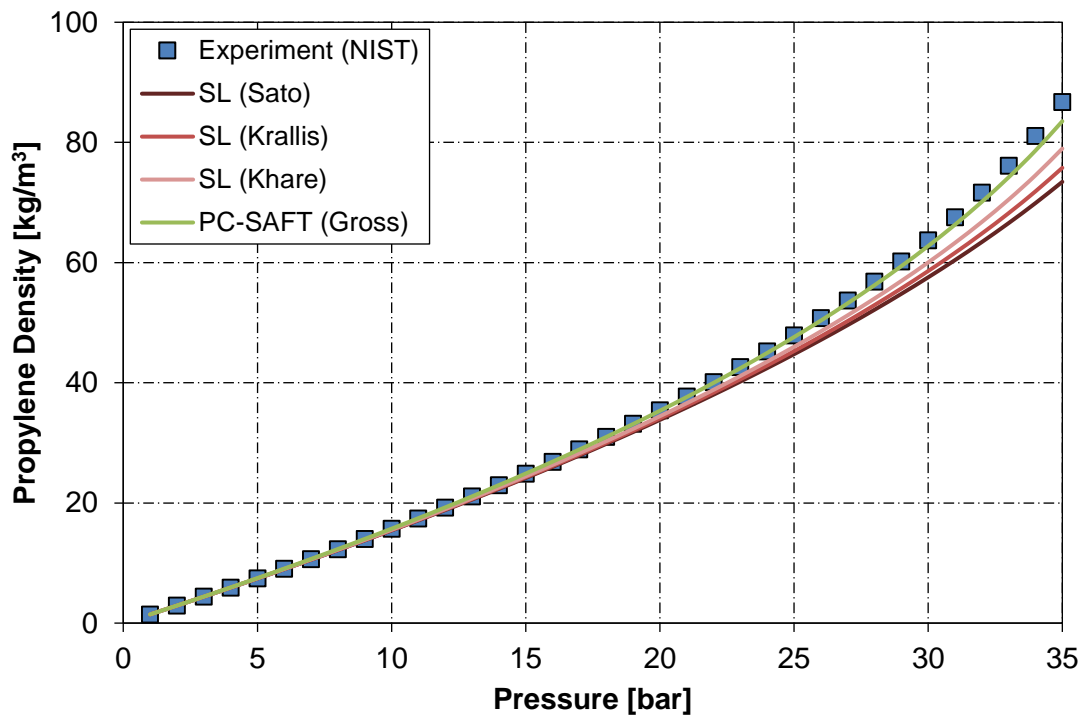


**Figure 6.12:** Comparison of the experimental gas density of propylene at 80 °C [131] with the SL and PC-SAFT EoS using the literature parameters of Sato et al. [54], Krallis and Kanellopoulos [104], Khare [130] and Gross and Sadowski [110].

The experimental densities of amorphous and semi-crystalline PP are compared with the SL and PC-SAFT model using the different literature pure component parameters in Figure 6.13. As can be clearly seen, both the SL with the parameters of Sato et al. [54] and the PC-SAFT EoS with the parameters Khare et al. [79] well describe the experimental amorphous density. The proposed parameters of Khare [130] for the SL model are the matter of choice when simulating the semi-crystalline PP density, whereas the parameters of Gross and Sadowski [111] do not accurately describe the experimental densities. Since the model approach is to only consider the solubility of propylene in the amorphous polymer phase, the parameters of Sato et al. [54] (SL) and Khare et al. [79] (PC-SAFT) were chosen for further simulations. Combining the EoS based amorphous density with the crystalline density (Tait

equation) offers a valid method to calculate the semi-crystalline density of PP if needed (see appendix).

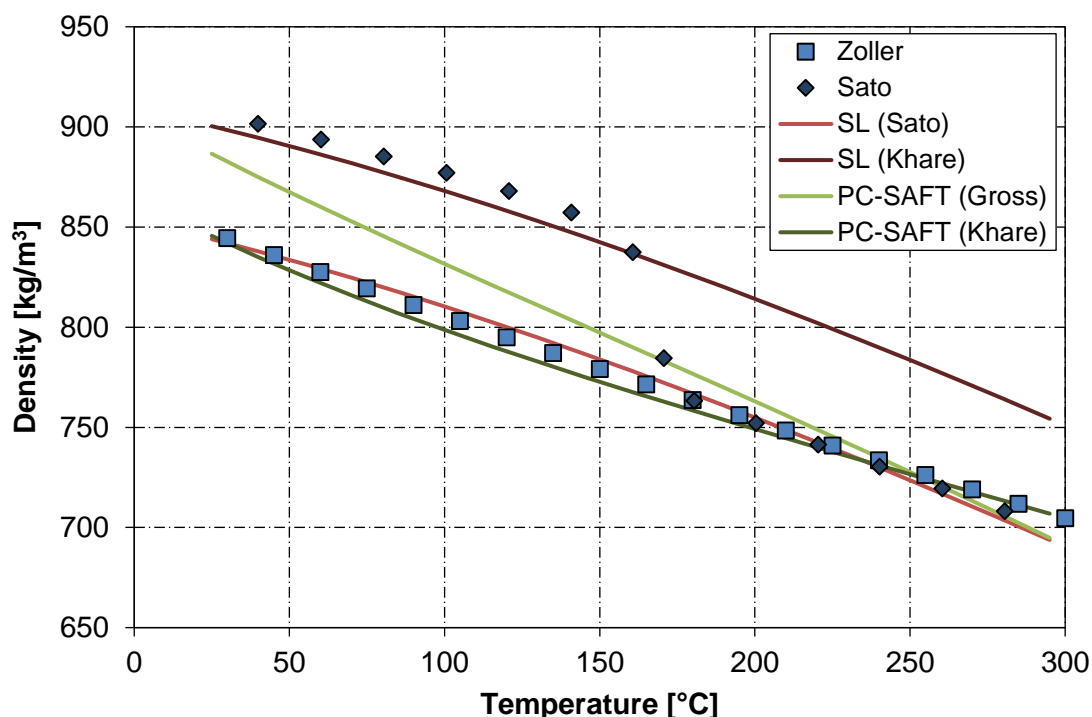


**Figure 6.13:** Comparison of the experimental PP densities with the SL and PC-SAFT EoS. The experimental amorphous density was taken from Zoller [132], the semi-crystalline density from Sato et al. [133] and the pure component parameters from Sato et al. [54] and Khare [130] (SL) and Gross and Sadowski [111] and Khare et al. [79] (PC-SAFT). The polymer was assumed to be monodisperse with a number average molecular weight of 50 kg/mol.

### 6.4.3 Simulation of amorphous solubility and concentration

The simulation of the solubility of propylene in amorphous PP is discussed for the SL and PC-SAFT EoS in the following. The pure component parameters for propylene and PP were taken from Khare [130] and Sato et al. [54] for the SL model and Gross and Sadowski [110] and Khare et al. [79] for the PC-SAFT model, respectively, based on the previous density analysis. One binary interaction parameter (BIP), i.e.  $k_{ij} = k$ , is used as fitting parameter. PP was modelled as a monodisperse polymer with a number average molecular weight of 50 kg/mol for all simulations.

The experimental amorphous solubility isotherm of sample A at 70 °C, which was carefully studied and for which the solubility comparison revealed good agreement with various literature data, was compared to simulations of the SL and PC-SAFT EoS. Both models cannot predict a-priori ( $k = 0$ ) the amorphous solubility and a fit of the binary interaction parameter to the experimental data was required. The BIPs of 0.0794 and 0.0185 for the SL



and PC-SAFT model, respectively, support the higher predictive capabilities of the latter EoS since the adjusted BIP is closer to zero. The fitted models can both well describe the experimental results (Figure 6.14). The SL EoS represents the experimental results very accurately with an average relative deviation (ARD) of less than 1 %. The PC-SAFT EoS shows a higher ARD of 9 % and seems to over-predict the solubility at higher pressures. The same conclusion can be drawn for the propylene concentration in the amorphous polymer fraction (Figure 6.15) with identical ARDs.

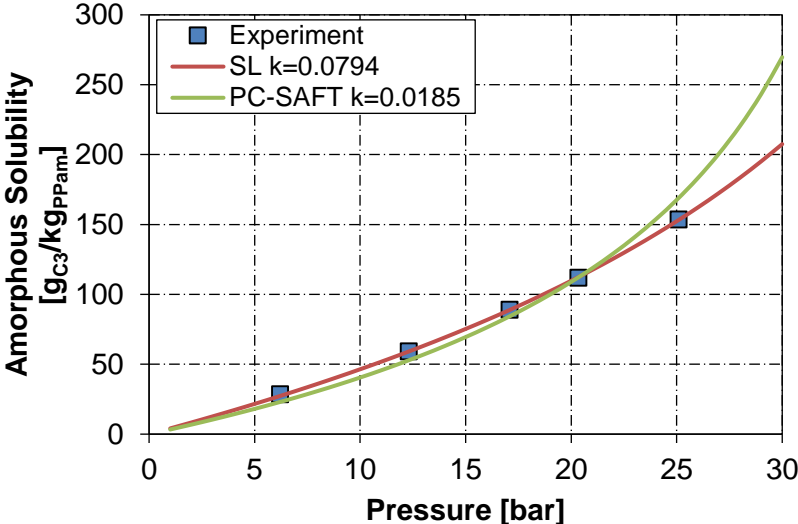


**Figure 6.14:** Comparison of the experimental amorphous solubility at 70 °C with the SL and PC-SAFT EoS. *k* denotes the binary interaction parameter.

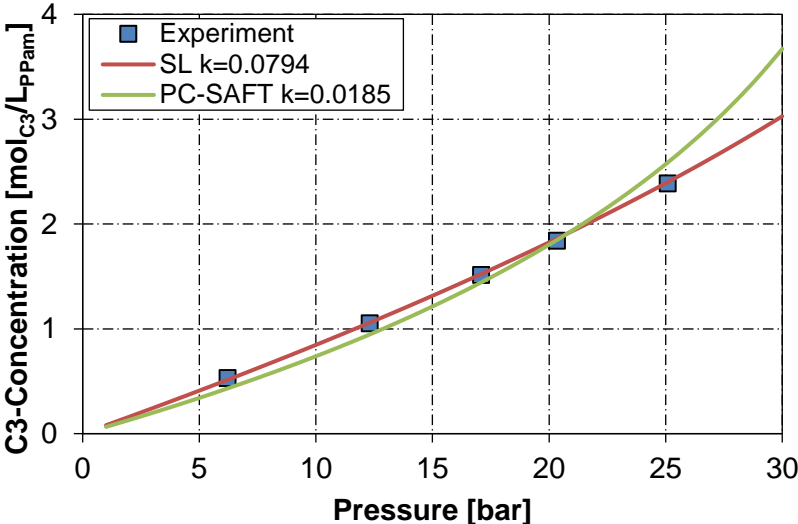


**Figure 6.15:** Comparison of the experimental propylene concentration in the amorphous PP phase at 70 °C with the SL and PC-SAFT EoS. *k* denotes the binary interaction parameter.

Although the two models were solely fitted to the experimental solubility data, the monomer concentration is described with the same accuracy because the decrease in amorphous

polymer density with increasing propylene pressure is perfectly predicted by both EoS models (Figure 6.16). Note that the experimental amorphous PP density was calculated based on the temperature-dependent PP density (see appendix) combined with the swelling correlation of Bobak et al. [56] as:

$$\rho_{am} = \frac{m_{C3} + m_{am}}{V_{am,0} + \Delta V_{swell}} = \frac{(S + 1 - w_{cr})\rho_{PP,0}(T)}{1 - v_{cr} + 1.7844 \cdot S} \quad (6.17)$$

Since the polymer density upon propylene sorption is described accurately, also the polymer swelling is well captured by both models (Figure 6.17). The experimental swelling was calculated based on the empirical correlation of Bobak et al. [56] and compared to the model swelling which is given by [121]:

$$\frac{V_{PP}}{V_{PP,0}} = \frac{V_{am} + V_{cr}}{V_{am,0} + V_{cr}} = (1 - w_{cr})(1 + S_{am}^{EoS}) \frac{\rho_{PP,0}}{\rho_{am}^{EoS}} + w_{cr} \frac{\rho_{PP,0}}{\rho_{cr}} \quad (6.18)$$

The crystalline PP density was calculated by the Tait equation using the parameters of Sato et al. [54]. The PP density prior to swelling  $\rho_{PP,0}$  was calculated by combining the density of the crystalline and the amorphous (based on EoS) phase (see appendix). Although the PC-SAFT slightly better predicts the swollen polymer density, the lower accuracy in describing the solubility and the original amorphous density prior to swelling leads to a better agreement of the SL EoS simulation results and the experimental swelling data.

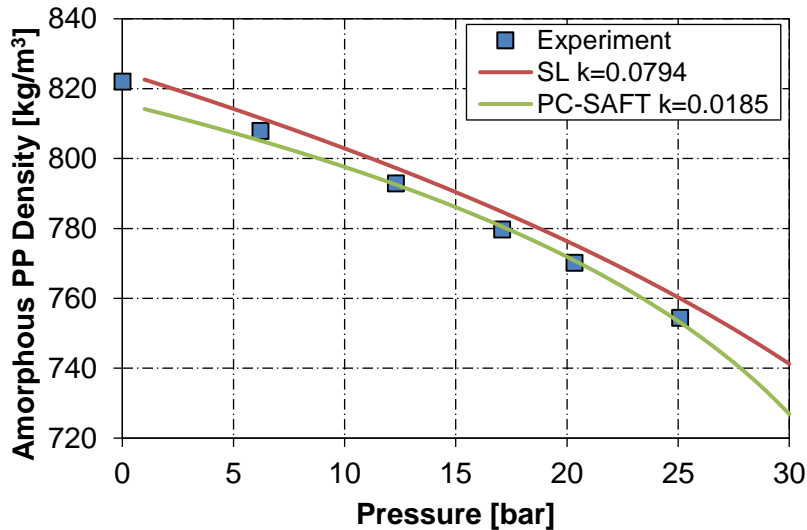


**Figure 6.16:** Comparison of the experimental amorphous PP density as function of the propylene pressure at 70 °C with the SL and PC-SAFT EoS. The experimental amorphous PP density was calculated based on the temperature-dependent PP density (see appendix) combined with the swelling correlation of Bobak et al. [56].  $k$  denotes the binary interaction parameter.

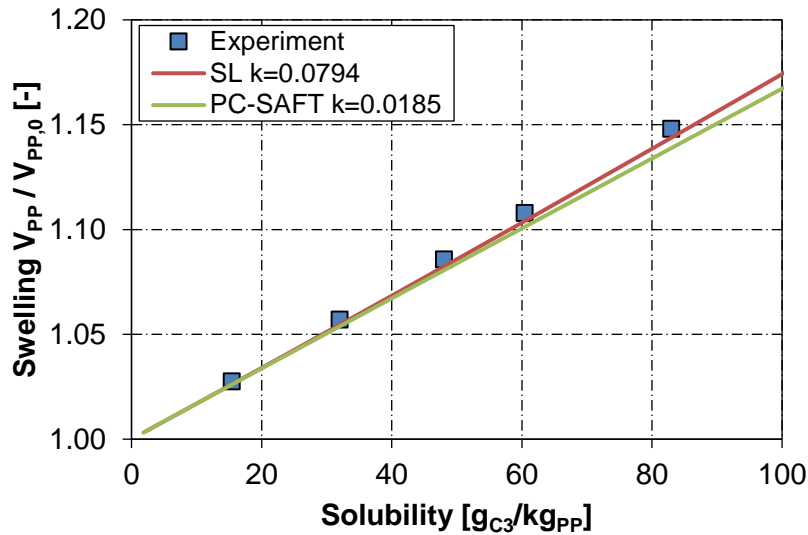


**Figure 6.17:** Comparison of the experimental swelling as function of the solubility at 70 °C with the SL and PC-SAFT EoS. The experimental data is based on the swelling correlation of Bobak et al. [56].  $k$  denotes the binary interaction parameter.

Using the obtained BIPs from the parameter estimation at 70 °C, the solubility isotherms were simulated and compared to the experimental ones (Figure 6.18). Both EoS models show good predictions at 60 and 80 °C, but an increased mismatch is found at lower temperatures, i.e. the mismatch increases the further the temperature of prediction differs from the temperature at which the BIP was estimated. The SL EoS represents the experimental solubility data with an ARD of 6 % and the PC-SAFT model with an ARD of 13 %. The latter model better captures the low temperature solubility at higher pressures, but the inaccuracy at lower pressures causes an overall higher relative deviation. Thus based on the available experimental data and a constant BIP, the SL EoS is more suitable in modeling the propylene solubility in PP.

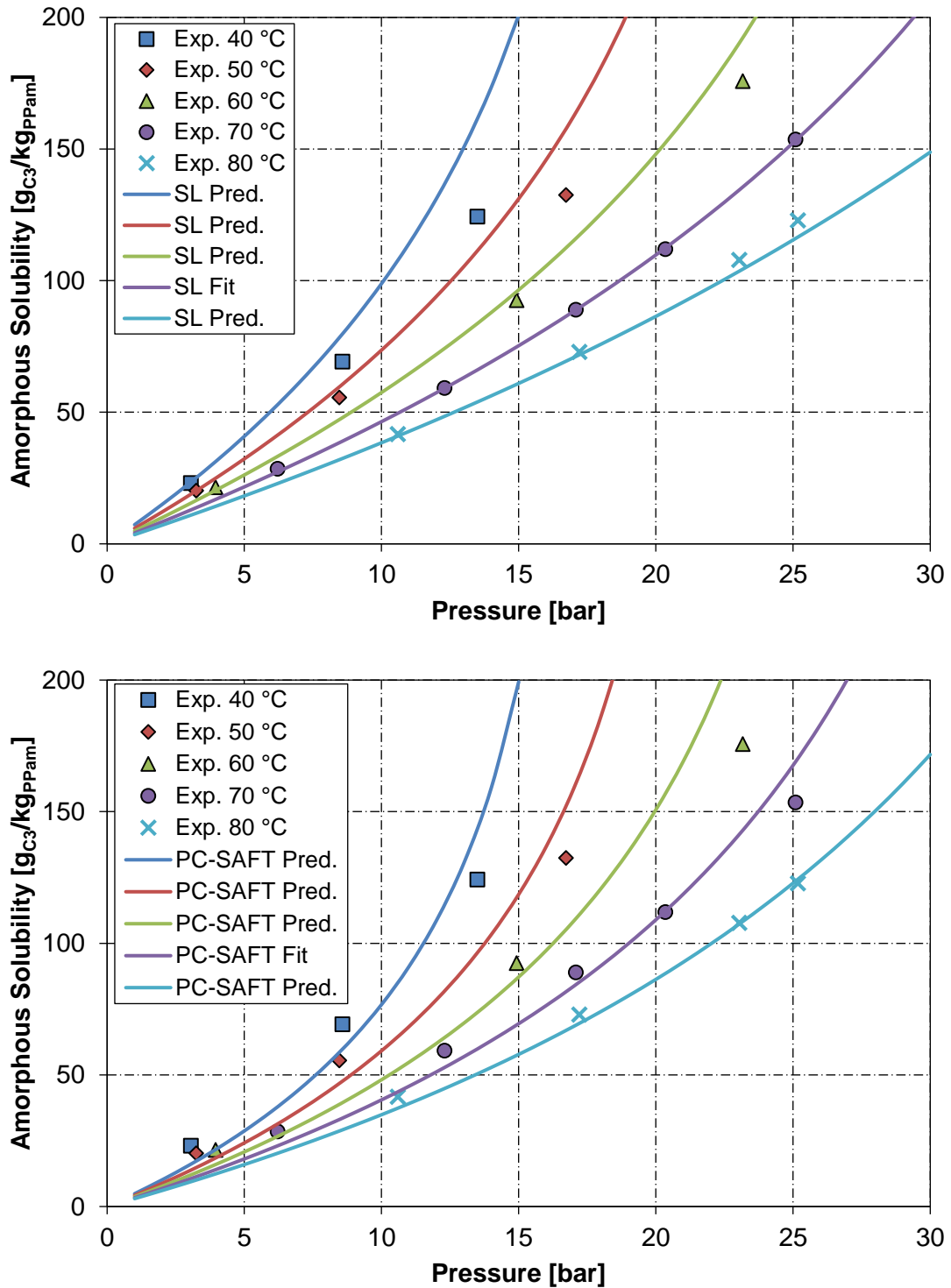


**Figure 6.18:** Comparison of the experimental amorphous solubility isotherms with the SL (top) and PC-SAFT (bottom) EoS predictions using the BIPs of 0.0794 and 0.0185, respectively, which were obtained by model fitting at 70 °C.

To improve the SL model description of the solubility, a temperature-dependent BIP can be used. Thus instead of one, two parameters can be used to capture the solubility of propylene in PP with higher accuracy using the SL EoS. The BIP  $k$  can be expressed by a linear temperature dependence (Figure 6.19) as:

$$k = -0.0757 \cdot T_r + 0.1664 \quad (6.19)$$

with

$$T_r = \frac{T}{298.15 \text{ K}} \quad (6.20)$$

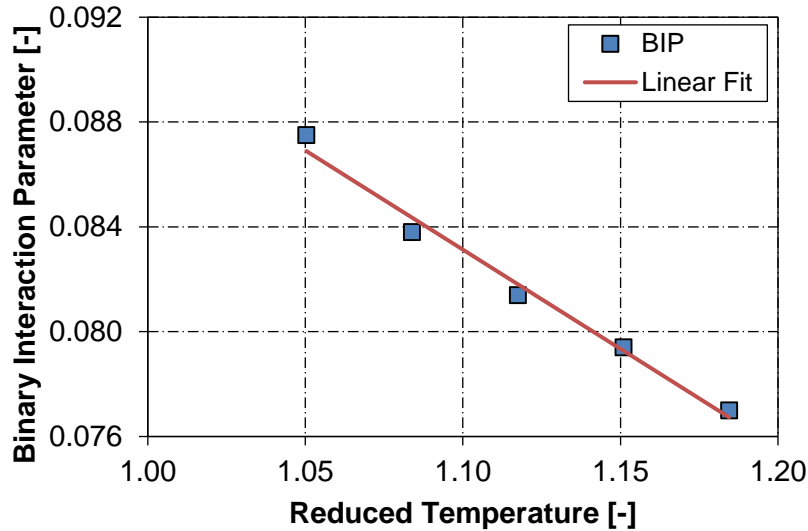


**Figure 6.19:** Dependency of the SL BIP on temperature for the system propylene/PP and linear fit ( $R^2=0.986$ ).

The agreement of experimental and model solubility is further improved by using the proposed temperature-dependent BIP which is resembled by an ARD of 3 % (Figure 6.20). Although only the solubility isotherms were fitted, the propylene concentration is predicted with the same ARD of 3 % because of the correct swelling description by the model (Figure 6.21).

Note that the swelling may not always be predicted correctly by the EoS [54, 121]. For example, Sato et al. [54] found an underestimation of the experimental swelling by about 20 % using the SL model. Inaccuracy in density modeling however causes inaccurate calculation of the effective monomer concentration relevant for polymerization kinetics. The difference found in swelling prediction between the work of Sato et al. [54] and this work, although in both cases the SL EoS was used, could be explained by the chosen method for equilibrium calculation and the experimental data. Instead of using formulations for the chemical potential, in this work the thermodynamically consistent equations for the fugacity coefficients were used. Furthermore, the experimental swelling was considered to be temperature independent as concluded in section 6.2.2.

It can be stated that here obtained results based on detailed experimental as well as thermodynamic modeling studies provide valuable information for process modeling of PP production plants.

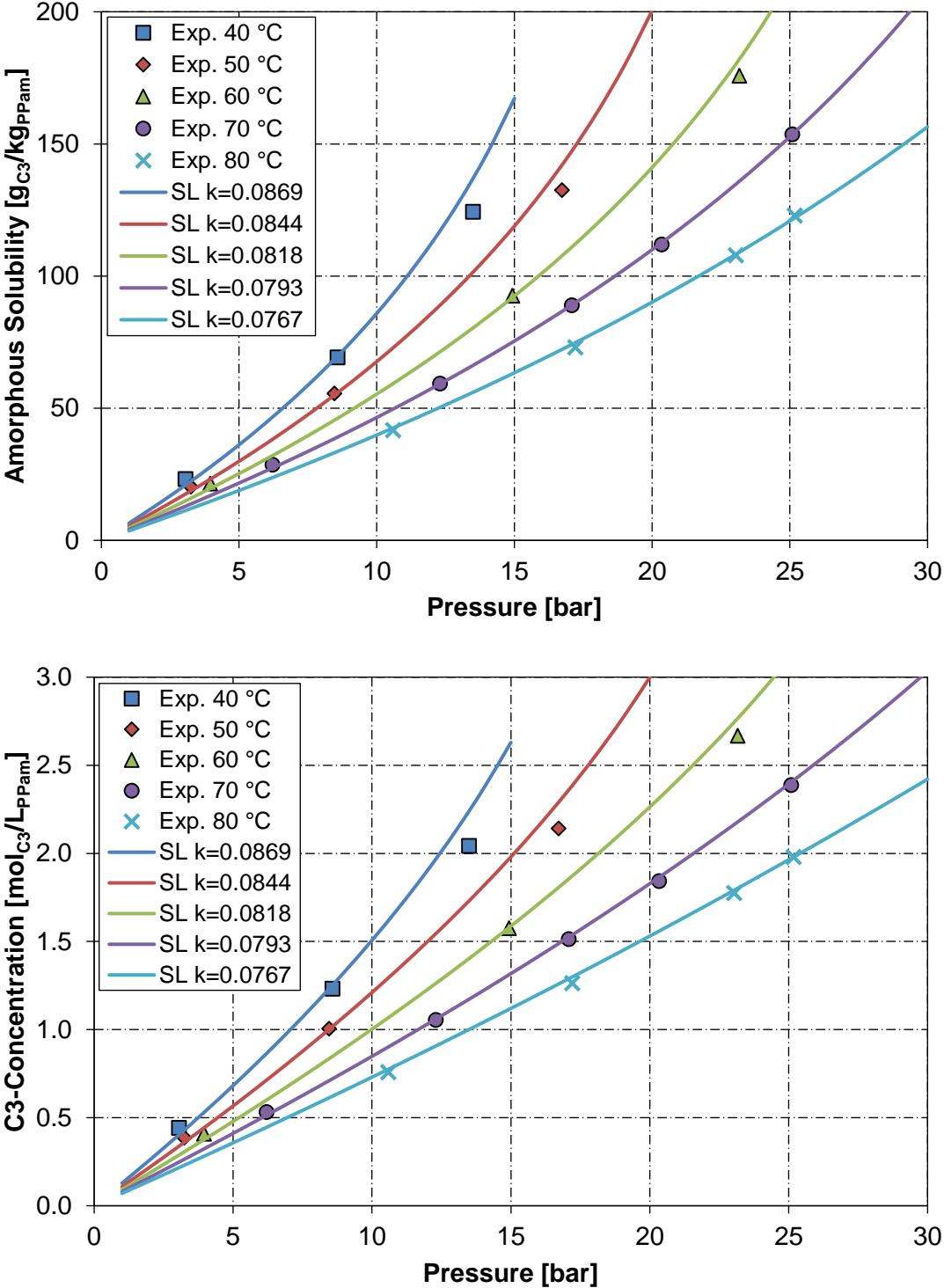


**Figure 6.20:** Comparison of the experimental amorphous solubility (top) and propylene concentration (bottom) with the SL EoS simulations using a temperature-dependent binary interaction parameter *k*.

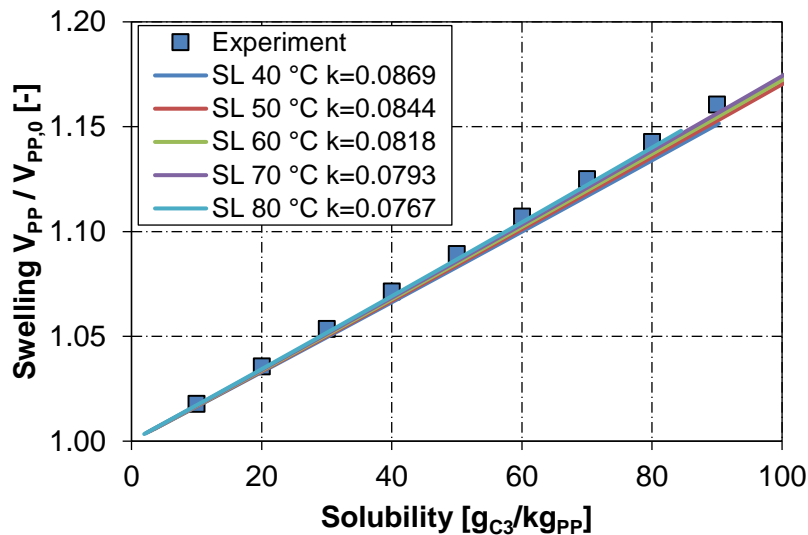


**Figure 6.21:** Comparison of the experimental polymer swelling with the SL EoS simulations using a temperature-dependent binary interaction parameter  $k$ . The experimental swelling was calculated based on the swelling correlation of Bobak et al. [56].

## 6.5 Diffusion results

### 6.5.1 Sorption curves

Not only the equilibrium solubility can be obtained from sorption experiments, but moreover important information about the mass transfer within the analyzed PP particles can be gathered from sorption curves, i.e. the mass uptake over time. Mass transport in these porous particles is largely influenced by the specific interior particle morphology, that is, the distribution of pore and polymer space. [56] Therefore, mass transport properties are characteristic for a given PP powder. Once these properties are known, the effect of mass transport on the actual polymerization rate can be analyzed and possible mass transfer limitations can be detected. Such limitations are undesirable since they not only reveal that the intrinsic catalyst activity is not fully exploited, but they can also cause inferior product properties due to property gradients within the growing polymer particles.

To experimentally study mass transfer close to the relevant polymerization conditions, six selected powder samples were investigated in the magnetic suspension balance at the reaction temperatures of 75 and 80 °C up to a pressure of 23 bar (Table 6.5). The objective was to identify the characteristic mass transport properties of each sample in order to test possible mass transfer limitations.

**Table 6.5:** Overview of selected samples for which mass transfer was studied. PP powders were synthesized at 80 °C (Cat A) or 75 °C (Cat C&D), 28.5 bar and 100 mg hydrogen with the method of prepolymerization (Prepo) or seed bed polymerization (SB).

Polymerization Method	Catalyst	Sorption Temperature [°C]
Prepo	A	80
	C	75
	D	75
SB	A	80
	C	75
	D	75

The experimental raw data, i.e. the course of the balance mass over time, was recalculated in terms of solubility and then expressed as normalized mass profiles for each pressure step:

$$\frac{m_{C3}(t)}{m_{C3,eq}} = \frac{S(t) - S(t=0)}{S(t \rightarrow \infty) - S(t=0)} \quad (6.21)$$

As an example, the sorption curves of the PP powder produced with catalyst D are shown in Figure 6.22 for two different pressure steps. Both curves show a very similar mass uptake over time with more than 90 % of the equilibrium mass  $m_{C3,eq}$  reached after about 2 min. Although the two profiles were recorded for different pressure steps, they seem identical from about 30 s onwards. Note that the measurement signal of the balance is not reliable for the first seconds upon pressure increase due to oscillations and should therefore not be used for analysis since pressure and temperature need to stabilize yet. Thus, for the presented sample, no clear difference in the mass uptake rate between the pressure step at low (0 to 11 bar) or high (17 to 23 bar) pressures was found. Overall, this was found for all analyzed powders. Furthermore, the difference in initial and final pressure of a pressure step did not influence the normalized mass curves, i.e. a pressure step from 0 to 6 bar or 0 to 11 bar resulted in the same normalized mass uptake over time. This leads to the following first conclusions: The mass uptake over time is independent of both the magnitude of the pressure step and the pressure at which the pressure step was conducted.



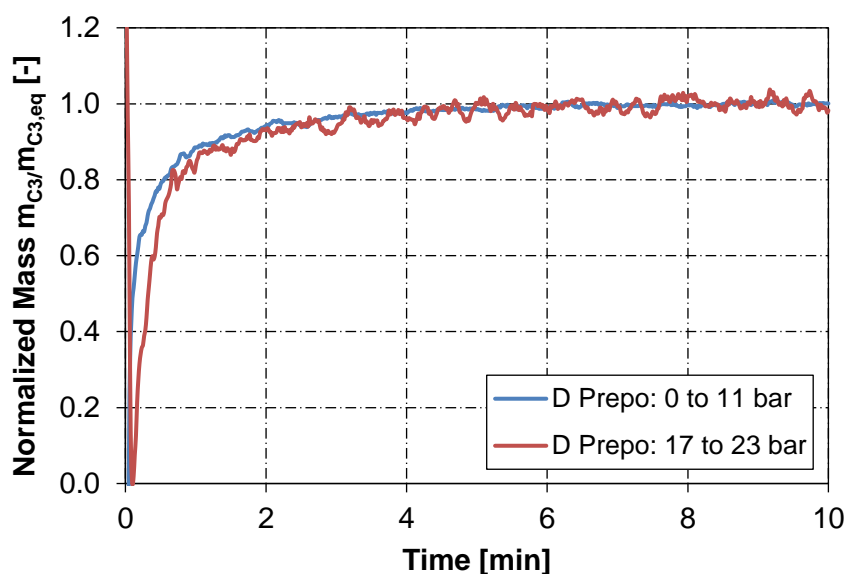


**Figure 6.22:** Comparison of sorption curves at 75 °C for a pressure step at low pressures from 0 to 11 bar and at high pressures from 17 to 23 bar. The analyzed sample powder was synthesized with catalyst D using the method of prepolymerization at reaction conditions of 75 °C, 28.5 bar and 100 mg hydrogen.

Comparing the sorption curves of the different powder samples (Figure 6.23), it is interesting to find that all curves are very similar indicating comparable transport properties of all studied PP particles, even despite the different measurement temperatures for catalyst A (80°C) vs. catalyst C and D (75°C). When looking closely at the normalized mass uptake profiles, minor deviations are found. Both powders of catalyst D show a slightly faster mass increase, whereas the sample produced with catalyst C using the method of prepolymerization reveals a slightly slower mass uptake. But generally speaking, all mass uptake profiles seem alike – even for the different polymerization methods. Surprisingly, although the outer morphology is very different for the powders produced with the method of prepolymerization and seed bed polymerization (section 5.2.2), the resulting mass transfer behavior seems to be comparable, which might be a hint, that interior particle morphology of the studied samples particles is comparable.

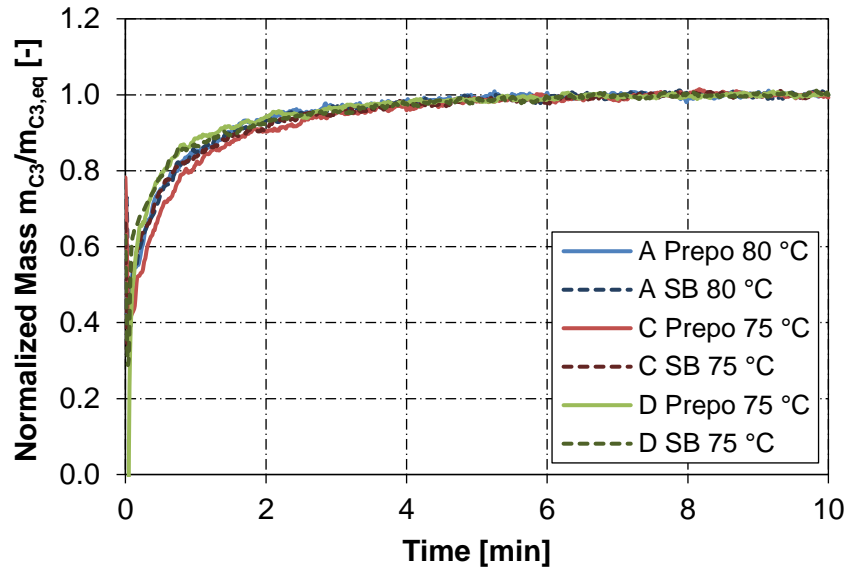


**Figure 6.23:** Comparison of sorption curves at 75 and 80 °C for a pressure step from 0 to 11 bar of PP powders synthesized with catalysts A, C and D. The analyzed samples were synthesized with the method of prepolymerization (Prepo) or seed bed polymerization (SB) at reaction conditions of 80 °C (Cat A) or 75 °C (Cat C&D), 28.5 bar and 100 mg hydrogen.

## 6.5.2 Effective diffusion coefficients and test for mass transfer limitations

Effective diffusion coefficients can be estimated from the experimental sorption curves and later on, these can be used to identify possible mass transfer limitations by balancing diffusion and reaction. Mass transfer in the spherical PP particles can be mathematically depicted as diffusion in a sphere. For a constant diffusion coefficient  $D$ , the diffusion equation is given by [134]:

$$\frac{\partial c}{\partial t} = D \left( \frac{\partial^2 c}{\partial r^2} + \frac{2}{r} \frac{\partial c}{\partial r} \right) \quad (6.22)$$

The diffusion equation is only strictly valid for pore-free particles, which is here not the case. Hence, the used diffusion coefficient cannot be seen as molecular diffusion coefficient, but as an effective diffusion coefficient taking into account particle morphology.

In case of a constant surface concentration and an initially uniform concentration throughout the sphere, the total amount of diffusing substance entering the sphere is given by Crank [134] as:

$$\frac{m_{C3}(t)}{m_{C3,eq}} = 1 - \frac{6}{\pi^2} \sum_{n=1}^{\infty} \frac{1}{n^2} \exp\left(-\frac{Dn^2\pi^2 t}{R^2}\right) \quad (6.23)$$

This solution can be directly applied to fit the experimental mass uptake curve (Figure 6.24). For the sphere radius  $R$ , the particle radius obtained from the PSD measurements, i.e. via the D50 value, was taken for each powder sample. The effective diffusion coefficient is used as the fitting parameter which comprises the characteristic powder morphology and is thus only valid for the specific sample. The estimated diffusion parameters are summarized in Table 6.6. The parameters are in the order of  $2 \cdot 10^{-10} \text{ m}^2/\text{s}$  for powders of catalyst A. PP particles synthesized with catalysts C and D have slightly higher diffusion coefficients in the range of 5 to  $7 \cdot 10^{-10} \text{ m}^2/\text{s}$ , indicating more favorable internal structures with respect to mass-transfer. In agreement with the conclusions from the experimental mass uptake curves, the effective diffusion coefficients are independent of the pressure step and polymerization method (Prepo or SB). The estimated effective diffusion coefficients are comparable in magnitude to reported literature values for porous PP particles of  $2.3$  to  $3.5 \cdot 10^{-10} \text{ m}^2/\text{s}$  at  $85^\circ\text{C}$  [56] and  $0.2$  to  $1.6 \cdot 10^{-10} \text{ m}^2/\text{s}$  at  $70^\circ\text{C}$  [57]. A direct comparison is however not possible since the individual particle morphology is part of the estimated diffusion coefficient.

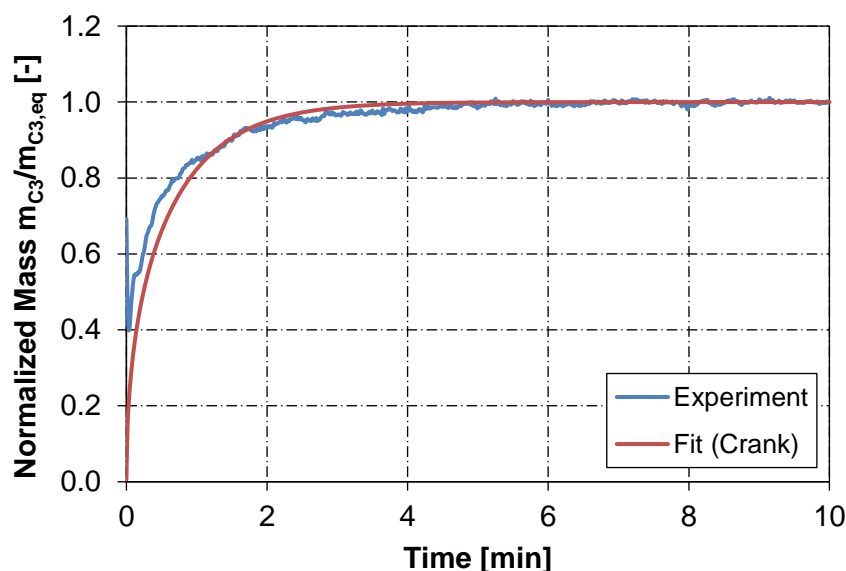


**Figure 6.24:** Comparison of the experimental sorption curve ( $80^\circ\text{C}$ , pressure step from 0 to 11 bar) with the model fit using Crank's solution for diffusion in a sphere. The analyzed sample powder was synthesized with catalyst A using the method of prepolymerization at reaction conditions of  $80^\circ\text{C}$ , 28.5 bar and 100 mg hydrogen.

**Table 6.6:** Estimated effective diffusion coefficients  $D_{eff}$  from sorption curves at 80 °C (Cat A) and 75 °C (Cat C&D) for a pressure step from 0 to 11 bar and from 17 to 23 bar. PP powders were synthesized at 80 °C (Cat A) or 75 °C (Cat C&D), 28.5 bar and 100 mg hydrogen with the method of prepolymerization (Prepo) or seed bed polymerization (SB).  $R_{particle}$  denotes the particle radius as obtained by PSD measurements (via D50).

Polymerization Method	Catalyst	$R_{particle}$ [μm]	$D_{eff}$ [ $10^{-10}$ m <sup>2</sup> /s]	
			0 to 11 bar	17 to 23 bar
Prepo	A	379	3.0	2.1
	C	560	5.0	6.0
	D	580	7.0	6.5
SB	A	317	2.0	1.9
	C	550	6.0	7.0
	D	555	6.0	5.5

It has to be mentioned that the model of diffusion in a sphere cannot accurately describe the experimental mass uptake curve and a small discrepancy between experiment and model is found for all curves (Figure 6.24 represents this minor mismatch as an example). Main reason for the observed differences is likely the strong simplification of particle morphology in the mass transfer model used here. Kröner [23] found out, that for PP particles, the particle diameter is not the relevant length scale for diffusion and assumed that clusters of micrograins within the porous particle are the relevant domain for mass transfer. Bobak et al. [56] studied experimental mass uptake curves of porous PP particles and found out, that these could not be described by a simple Fick's model (i.e. diffusion in a sphere) consisting of one diffusion coefficient and just one effective diffusion length, but rather two diffusion lengths were needed. The model thus considered two different sizes of compact polymer granules which better resembled the real particle morphology. However, to keep it simple and since the discrepancy between experiment and model found in this work is relatively small, the estimated diffusion coefficients will be used for further analysis.

In the following, a simple, pseudo-stationary model that accounts both for diffusion and chemical reaction in a spherical particle is used for a rough estimation of the balance between reaction and mass-transfer at a polymerization time of 60 min. Analogous to classical models of pore diffusion and surface reaction in solid catalyst pellets [135, 136], the polymerization can be expressed as a balance of monomer diffusion in the spherical PP particle and consumption of monomer by the polymerization reaction [137]. Simplifying the latter process to a first-order reaction, i.e. reducing the rate of polymerization  $r_p$  to:

$$r_p = k_p c_{am} c_P^* = k_r c_{C3} \quad (6.24)$$

the steady-state mass balance of monomer in the spherical polymer particle can be described by:

$$D_{eff} \left( \frac{\partial^2 c_{C3}}{\partial r^2} + \frac{2}{r} \frac{\partial c_{C3}}{\partial r} \right) - k_r c_{C3} = 0 \quad (6.25)$$

with the boundary conditions:

$$c_{C3}(r = R_{particle}) = c_{C3,eq} \quad \text{and} \quad \left. \frac{\partial c_{C3}}{\partial r} \right|_{r=0} = 0 \quad (6.26)$$

Using the dimensionless variables:

$$\psi = \frac{c_{C3}}{c_{C3,eq}} \quad \text{and} \quad \lambda = \frac{r}{R_{particle}} \quad (6.27)$$

the mass balance can be written as [135]:

$$\frac{\partial^2 \psi}{\partial \lambda^2} + \frac{2}{\lambda} \frac{\partial \psi}{\partial \lambda} - \phi_{Thiele}^2 \psi = 0 \quad (6.28)$$

with the Thiele modulus:

$$\phi_{Thiele} = R_{particle} \sqrt{\frac{k_r}{D_{eff}}} \quad (6.29)$$

Based on the Thiele modulus, the effectiveness factor  $\eta$ , which corresponds to how much the reaction rate is lowered because of diffusion resistance, can be calculated as [135, 136]:

$$\eta = \frac{3}{\phi_{Thiele}^2} (\phi_{Thiele} \coth \phi_{Thiele} - 1) \quad (6.30)$$

Hence, three parameters are needed to calculate the effectiveness factor and detect possible diffusion resistances. The effective diffusion coefficient  $D_{eff}$  was already obtained by fitting the experimental sorption curves and the particle radius  $R_{particle}$  by PSD measurements. However, these are only valid for the end of the polymerization reaction, i.e. at a reaction time of 60 min, as these parameters correspond to the final polymer product. Therefore, the effectiveness factor is only calculated for the end of the reaction. The first-order kinetic rate coefficient  $k_r$  can be calculated from the intrinsic activity  $A_{int}$  and yield  $y$ . Defining the intrinsic activity as:

$$A_{int} = \frac{k_r c_{C3,eq} MW_{C3} V_{PP}}{m_{Cat}} \quad (6.31)$$

the rate coefficient can be obtained by:

$$k_r = \frac{A_{int}\rho_{PP}}{c_{C3,eq}MW_{C3}(S+1)y} = \frac{A_{int}\rho_{am}}{c_{am,eq}MW_{C3}(S_{am}+1)(1-w_{cr})y} \quad (6.32)$$

The amorphous propylene concentration  $c_{am,eq}$ , amorphous polymer density  $\rho_{am}$  and amorphous equilibrium solubility  $S_{am}$  were calculated for the relevant reaction conditions of 75 or 80 °C and 28.5 bar using the SL EoS with temperature-dependent BIP. The intrinsic activity was calculated iteratively so that the product of intrinsic activity and effectiveness factor, i.e. the activity reduced by diffusional limitations, was equal to the experimentally observed activity  $A_{exp}$  at 60 min (taken from the activity profiles):

$$A_{exp}(t = 60 \text{ min}) = \eta A_{int} \quad (6.33)$$

The comparison of the effectiveness factors and of the intrinsic and experimental activities are presented in Table 6.7. For calculations of  $\eta$ , the lowest diffusion coefficient of the two sorption pressure steps was chosen.

**Table 6.7:** Effectiveness factors  $\eta$  based on a pseudo-stationary diffusion-reaction model. The reported effective diffusion coefficients  $D_{eff}$ , intrinsic activities  $A_{int}$  and experimental activities  $A_{exp}$  as well as the calculated effectiveness factors are only valid for a reaction time of 60 min. PP powders were synthesized at 80 °C (Cat A) or 75 °C (Cat C&D), 28.5 bar and 100 mg hydrogen with the method of prepolymerization (Prepo) or seed bed polymerization (SB).  $R_{particle}$  denotes the particle radius as obtained by PSD measurements (via D50).

Polym.	Catalyst	$R_{particle}$	$D_{eff}$	Yield	$A_{int}$	$\eta$	$A_{exp}$
Method		[ $\mu\text{m}$ ]	[ $10^{-10} \text{ m}^2/\text{s}$ ]	[ $\text{kg}_{PP}/\text{g}_{Cat}$ ]	[ $\text{kg}_{PP}/\text{g}_{Cat}/\text{h}$ ]	[%]	[ $\text{kg}_{PP}/\text{g}_{Cat}/\text{h}$ ]
Prepo	A	379	2.1	27.4	18	91	16
	C	560	5.0	24.8	17	92	16
	D	580	6.5	41.3	32	93	30
SB	A	317	1.9	19.7	14	92	13
	C	550	6.0	21.3	16	93	15
	D	555	5.5	27.3	23	91	21

The model results reveal that diffusion limitations at the end of the polymerization reaction are very small with high effectiveness factors of 91 to 93 % for the analyzed PP powders. In other words, less than 10 % of the catalyst's intrinsic activity are "lost" due to diffusional resistances which cause a reduction in activity of 1 to 2  $\text{kg}_{PP}/\text{g}_{Cat}/\text{h}$ . The obtained effectiveness factors are almost identical to the value of Kröner [23] who studied the effect of diffusion on polymerization kinetics in detail. In his work, the effectiveness factor was calculated over the course of the reaction and increased from 75 % at the beginning of the reaction to 93 % after one hour of homopolymerization. The average effectiveness factor was about 90 % and thus close to the final value. Given the fact that the conditions which Ziegler-

Natta catalysts face at the very beginning of reaction determine the overall activity and particle morphology, it is reasonable to assume that the here calculated effectiveness factors will be very similar to the average effectiveness factors of the entire reaction. Therefore, diffusion limitations can be assumed to be negligible for the studied polymerizations of this work.

In summary, effective diffusion coefficients were estimated from experimental sorption curves and used in a simplified diffusion-reaction model to calculate effectiveness factors which quantify the reduction in activity due to diffusion limitations. All calculated factors were above 90 % independent of the polymerization method suggesting negligible diffusion limitations. Interestingly, although the outer morphology was largely affected by the chosen method of polymerization as discussed previously, the interior morphology governing the mass transport properties was found to be alike for the two methods of prepolymerization and seed bed polymerization.

## 7 Kinetic Model

Objective of the model development is to characterize the three experimentally studied Ziegler-Natta catalysts A, C and D by their specific kinetic parameters. A simplified kinetic model is therefore derived in order to describe the polymerization kinetics of the catalysts. The two main targets are the correct description of the catalyst activity and the melt flow rate as a function of the reaction conditions, specifically the hydrogen concentration. The final model including the estimated parameters is useful for catalyst development as it allows to compare the catalysts based on the kinetic parameters rather than the experimental raw data. Furthermore, the kinetic model may be coupled with process models allowing simulation studies on the catalyst performance in the pilot and/or commercial scale supporting process and product development.

Modeling of the propylene polymerization of Ziegler-Natta catalysts can become relatively complex when accounting for all possible aspects such as multiple active sites, various kinetic reaction steps as well as different length scales (section 2.4). However, since the overall aim is to obtain the catalyst-specific rate constants based on the conducted experiments, the model is largely reduced to only describe the experimentally observed results focusing on micro-scale effects. Ultimately, it is a simplified, phenomenological kinetic model.

The model is implemented in the commercial software gPROMS® ModelBuilder 5.1 (*Process Systems Enterprise*). The kinetic parameters are estimated based on the experimentally obtained data, that is, the activity profiles, the yields and the weight-average molecular weights which were calculated from the MFRs via an empirical equation (Equation (4.2)).

### 7.1 Derivation of the kinetic model

#### 7.1.1 Model assumptions

The kinetic model involves a number of assumptions. First, the multi-site nature of Ziegler-Natta catalysts is neglected by only considering one type of active catalyst site. Multiple sites are commonly used to model the broad MWD of ZN catalysts or to account for particular polymerization kinetics that can only be modeled with more than one catalyst site. Neither case applies to this work as no MWDs were measured and the reaction kinetics can be described with one type of site.



Since the model only focuses on the micro-scale, phenomena of other length scales are neglected. At the particle scale, it is assumed that heat and mass transfer do not influence the polymerization kinetics, i.e. there are no transport limitations. The assumption of negligible diffusion limitations is supported by the study of the sorption curves (section 6.5). The effect of particle heat transfer on the activity was indirectly observed experimentally, however, the different activity levels of the prepolymerization and seed bed polymerization methods are simply described by a different number of active sites. At the macro-scale, ideal mixing and good heat removal can be assumed, since the polymerization experiments were conducted in a small lab-scale reactor. Isothermal and isobaric conditions are assumed throughout the reaction, which is close to reality in the semi-batch experiments performed in this study, at least at the main-stage conditions. The heat-up stage of the prepolymerization experiments is neglected and the catalysts are modeled to be injected directly at the main reaction conditions and polymerized for one hour at constant temperature and pressure.

To summarize, the following three main assumptions are made:

- Only one type of catalyst site is considered.
- Isothermal and isobaric conditions are assumed throughout the entire reaction time of one hour.
- Mass and heat transfer effects are neglected.

Based on the experimental results, a kinetic scheme consisting of a set of standard reaction steps has to be chosen. The experimental findings are therefore shortly summarized in the following:

- All catalysts show an enhancement in polymerization rate with increasing hydrogen mass. This hydrogen response is different for each catalyst.
- The MFR is different for each catalyst and increases with the hydrogen concentration.
- The deactivation behavior seems to be independent of the hydrogen amount.
- For the prepolymerization method, a larger catalyst activity is found for all catalysts. However, only the activity level seems to be changed by this method, whereas rate enhancement by hydrogen, MFR and deactivation appear to be unaffected.

### 7.1.2 Kinetic scheme

Based on the experimental findings, the kinetic scheme is derived from standard reaction steps commonly applied in kinetic modeling of coordinative olefin polymerization (section 2.4.2). The effect of rate enhancement by hydrogen is considered by employing the three main reaction steps of the dormant site theory. The molecular weight response is modeled by using two different transfer reactions. The difference in the activity level between the method of prepolymerization and seed bed polymerization is described by different numbers of active catalyst sites.

The applied kinetic scheme is presented in Table 7.1. The activation of Ziegler-Natta catalysts usually occurs by the reaction with the cocatalyst. In large excess of TEA as in all conducted experiments, this is equivalent to a spontaneous activation step from the mathematical point of view since the concentration of the cocatalyst can be considered constant:

$$\frac{d[S_p]}{dt} = -k_{aco}[CoCat][S_p] \approx -k_a[S_p] \quad (7.1)$$

The spontaneously activated catalyst site reacts further with propylene to form an active chain with a length of one. By propagation, this living chain grows by monomer addition. The experimentally observed change in MFR and thus molecular weight upon hydrogen mass variation is incorporated by chain transfer reaction to hydrogen. In that, the living chain reacts with hydrogen to form a dead polymer chain and a vacant active site which can further contribute to chain growth. In absence of hydrogen, the model would overpredict the molecular weight without an additional transfer step. Therefore, spontaneous chain transfer (e.g.  $\beta$ -hydride elimination) is included as a further transfer reaction. Here, a living chain reacts to form a vacant active site and a dead polymer chain. Other transfer steps such as chain transfer by cocatalyst or monomer are not considered, but could also be implemented. As no detailed microstructural analysis was performed and modeling of this is not the objective, for simplicity, only spontaneous chain transfer was implemented into the kinetic model.

All activity profiles show a decay over time which is explained by catalyst deactivation. Deactivation can occur by different species. Since the comparison of the normalized activity profiles for different hydrogen concentrations do not indicate a hydrogen effect, hydrogen is excluded to participate in deactivation. The deactivating effect of poisons is assumed to be negligible due to the use of excessive amounts of TEA which acts as scavenger. To conclude, the deactivation step is thought to occur simply spontaneously in which a living

polymer chain forms a dead chain and a dead site or a vacant active site turns into a dead catalyst site.

**Table 7.1:** Reaction steps of the phenomenological kinetic model. In this scheme,  $S_p$ ,  $S_a$ ,  $M$ ,  $P_n$ ,  $H_2$ ,  $D_n$ ,  $S_d$  and  $P_n^{dorm}$  are symbols for the potential catalyst site, active catalyst site, monomer, living polymer of length  $n$ , hydrogen, dead polymer of length  $n$ , dead catalyst site and dormant polymer of length  $n$ , respectively.

Reaction Step	Chemical Equation
Activation	$S_p \xrightarrow{k_a} S_a$
Initiation	$S_a + M \xrightarrow{k_i} P_1$
Propagation	$P_n + M \xrightarrow{k_p} P_{n+1}$
Transfer	
• by hydrogen	$P_n + H_2 \xrightarrow{k_{trH}} S_a + D_n$
• spontaneous	$P_n \xrightarrow{k_{trSp}} S_a + D_n$
Deactivation	
	$P_n \xrightarrow{k_d} S_d + D_n$
	$S_a \xrightarrow{k_d} S_d$
	$P_n^{dorm} \xrightarrow{k_d} S_d + D_n$
Dormant Chain Formation	
	$P_n + M \xrightarrow{k_{dorm}} P_{n+1}^{dorm}$
	$S_a + M \xrightarrow{k_{dormi}} P_1^{dorm}$
Reactivation	
• by hydrogen	$P_n^{dorm} + H_2 \xrightarrow{k_{reH}} S_a + D_n$
• by monomer	$P_n^{dorm} + M \xrightarrow{k_{reM}} P_{n+1}$

The experimentally observed rise in activity with increasing hydrogen mass is employed by the kinetic steps of the dormant site theory. It assumed that dormant polymer chains are formed by the 2,1-misinsertion of a propylene molecule into a growing polymer chain. The active center is now sterically hindered leading to a much lower reactivity. This dormant species can be reactivated by the small hydrogen molecule resulting in an active catalyst site and a dead polymer chain. If no further reactivation step were included, the model would predict an enhanced decay in activity in absence of hydrogen. This is because the concentration of dormant species would increase over reaction time and thus the concentration of active species would decrease leading to a pronounced loss of activity. As this was not observed in the experiments, reactivation by monomer is also considered. Here, a monomer unit is added to the dormant chain by a regio-regular 1,2-insertion leading to a living chain. Note that for completion, a further step for dormant site formation is added by

allowing vacant active sites to undergo 2,1-misinsertion. Furthermore, the dormant chains are also considered to deactivate. Although this reaction step is not commonly employed in literature [27, 36, 81], it is used here based on the experimental finding that all activity profiles show the same relative decay independent of the hydrogen concentration (section 5.1.5). The dormant site theory describes an equilibrium between living and dormant chains. At low hydrogen concentrations, this equilibrium is shifted towards a low concentration of living chains resulting in a lower activity and also a less pronounced absolute activity decay. However, the relative deactivation is only dependent on the deactivation constant and is therefore the same at all hydrogen concentrations. This is only valid when also the dormant chains deactivate because otherwise they would function as a reservoir for the living chains. The decrease in living chains would be counteracted by the reactivation of dormant chains in drive of the equilibrium. At low hydrogen concentrations, a higher reservoir is available due to the higher dormant chain concentration and thus the deactivation would be less pronounced than at high hydrogen concentrations. Therefore, to obtain the same relative decay, the deactivation of dormant chains was used in the kinetic scheme.

All necessary reaction steps were included which should describe the experimentally observed phenomena. A further simplification which was made is that all vacant active sites that are formed through the selected reaction steps (activation, chain transfer and reactivation) are identical. This is not the reality as some sites are for instance actually hydride catalyst sites. However, this is a simplification typically used in coordinative polymerization modeling. [14, 72]

### 7.1.3 Mass balances

From the developed kinetic scheme, the mass balances are derived for each reactive species in the following. The potential catalyst sites are simply consumed by the spontaneous activation step:

$$\frac{d[S_p]}{dt} = -k_a[S_p] \quad (7.2)$$

For the vacant active sites, all reaction steps in which these are formed or consumed have to be considered. They are formed by activation, chain transfer, reactivation and are consumed by initiation, deactivation and dormant chain formation. The vacant active site balance, applied over the proposed kinetic scheme, leads to the equation:

$$\frac{d[S_a]}{dt} = k_a[S_p] - (k_i[M] + k_d + k_{dormi}[M])[S_a] + k_{tr}L_0 + k_{reH}[H_2]L_0^{dorm} \quad (7.3)$$

with

$$k_{tr} = k_{trH}[H_2]^{0.5} + k_{trSp} \quad (7.4)$$

$$L_0 = \sum_{n=1}^{\infty} [P_n] \quad (7.5)$$

$$L_0^{dorm} = \sum_{n=1}^{\infty} [P_n^{dorm}] \quad (7.6)$$

Following the same procedure of balancing the chemical species over the kinetic scheme, the mass balances of each remaining reactant were derived.

Dead catalyst sites:

$$\frac{d[S_a]}{dt} = k_d([S_a] + L_0 + L_0^{dorm}) \quad (7.7)$$

Living polymer chains of length one:

$$\frac{d[P_1]}{dt} = k_i[M][S_a] - (k_p[M] + k_{tr} + k_d + k_{dorm}[M])[P_1] \quad (7.8)$$

Living polymer chains of length  $n \geq 2$ :

$$\begin{aligned} \frac{d[P_n]}{dt} = & k_p[M][P_{n-1}] - (k_p[M] + k_{tr} + k_d + k_{dorm}[M])[P_n] \\ & + k_{reM}[M]P_{n-1}^{dorm} \end{aligned} \quad (7.9)$$

Dormant polymer chains of length one:

$$\frac{d[P_1^{dorm}]}{dt} = k_{dormi}[M][S_a] - (k_{re} + k_d)[P_1^{dorm}] \quad (7.10)$$

with

$$k_{re} = k_{reH}[H_2] + k_{reM}[M] \quad (7.11)$$

Dormant polymer chains of length  $n \geq 2$ :

$$\frac{d[P_n^{dorm}]}{dt} = k_{dorm}[M][P_{n-1}] - (k_{re} + k_d)[P_n^{dorm}] \quad (7.12)$$

Dead polymer chains:

$$\frac{d[D_n]}{dt} = (k_{tr} + k_d)[P_n] + (k_{reH}[H_2] + k_d)[P_n^{dorm}] \quad (7.13)$$

Hydrogen:

$$\frac{d[H_2]}{dt} = -k_{trH}[H_2]^{0.5}L_0 - k_{reH}[H_2]L_0^{dorm} \quad (7.14)$$

Note that in the mass balances, the hydrogen concentration is raised to the power of one half in case of the chain transfer step by hydrogen because in the literature, the reaction order of hydrogen for the transfer reaction via supported catalysts is reported as 0.5. [7, 138, 139]

Since within the model a constant pressure and therefore a constant propylene concentration is assumed, no mass balance is needed for the monomer. The mass production rate of polypropylene is obtained by taking account of all reaction steps in which monomer is consumed:

$$\frac{dm_{PP}}{dt} = (k_pL_0 + k_i[S_a] + k_{dorm}L_0 + k_{reM}L_0^{dorm})[M]MW_{C3}V_R \quad (7.15)$$

The catalyst activity and yield is given by:

$$A = \frac{1}{m_{Cat}} \frac{dm_{PP}}{dt} \quad (7.16)$$

$$y = \frac{m_{PP}}{m_{Cat}} \quad (7.17)$$

#### 7.1.4 Method of moments and molecular weight averages

The derived mass balances for the reactive species form a large set of ordinary differential equations (ODEs). Different numerical solution techniques exist for such systems and were compared by Deuflhard and Wulkow [140] or Bartke and Reichert [96]. One common technique to solve the ODE-system with low numerical effort is the method of moments [14, 72, 74], by which however only polymer weight averages and not the complete molecular weight distribution is obtained. Since in this work the polymer samples were only

characterized by the weight average molecular weight (indirectly via the MFR), the solution technique of choice is obviously the method of moments. Furthermore, this method can be readily extended to model the broad MWD of ZN catalysts. [72]

The method of moments is a statistical technique by which polymer chain averages such as the number average molecular weight  $M_n$ , the weight average molecular weight  $M_w$  and the polydispersity index  $PDI$  can be calculated. The moments are averages of the polymer chain concentrations that are weighted by their chain length. In the following, moments of the corresponding number chain length distribution are defined.

Moments for the living polymers or “live moments”:

$$L_i = \sum_{n=1}^{\infty} n^i [P_n] \quad (7.18)$$

Moments for the dormant polymers or “dormant moments”:

$$L_i^{dorm} = \sum_{n=1}^{\infty} n^i [P_n^{dorm}] \quad (7.19)$$

Moments for the dead polymers or “dead moments”:

$$D_i = \sum_{n=2}^{\infty} n^i [D_n] \quad (7.20)$$

Moments for all polymers or “bulk moments”:

$$B_i = L_i + L_i^{dorm} + D_i \quad (7.21)$$

The zeroth, first and second moment are sufficient to calculate the following average properties:

$$M_n = MW_{C3} \frac{B_1}{B_0} \quad (7.22)$$

$$M_w = MW_{C3} \frac{B_2}{B_1} \quad (7.23)$$

$$PDI = \frac{M_w}{M_n} \quad (7.24)$$

Using the definition of the moments, the mass balances for the different types of polymer chains (Equations (7.8) to (7.13)) can be reduced to the following set of equations.

Zeroth moments:

$$\frac{dL_0}{dt} = k_i[M][S_a] - (k_{tr} + k_d + k_{dorm}[M])L_0 + k_{reM}[M]L_0^{dorm} \quad (7.25)$$

$$\frac{dL_0^{dorm}}{dt} = k_{dormi}[M][S_a] - (k_{re} + k_d)L_0^{dorm} + k_{dorm}[M]L_0 \quad (7.26)$$

$$\frac{dD_0}{dt} = (k_{tr} + k_d)L_0 + (k_{reH}[H_2] + k_d)L_0^{dorm} \quad (7.27)$$

First moments:

$$\begin{aligned} \frac{dL_1}{dt} = k_i[M][S_a] - (k_{tr} + k_d + k_{dorm}[M])L_1 + k_p[M]L_0 \\ + k_{reM}[M](L_0^{dorm} + L_1^{dorm}) \end{aligned} \quad (7.28)$$

$$\frac{dL_1^{dorm}}{dt} = k_{dormi}[M][S_a] - (k_{re} + k_d)L_1^{dorm} + k_{dorm}[M](L_0 + L_1) \quad (7.29)$$

$$\frac{dD_1}{dt} = (k_{tr} + k_d)L_1 + (k_{reH}[H_2] + k_d)L_1^{dorm} \quad (7.30)$$

Second moments:

$$\begin{aligned} \frac{dL_2}{dt} = k_i[M][S_a] - (k_{tr} + k_d + k_{dorm}[M])L_2 + k_p[M](L_0 + 2L_1) \\ + k_{reM}[M](L_0^{dorm} + 2L_1^{dorm} + L_2^{dorm}) \end{aligned} \quad (7.31)$$

$$\frac{dL_2^{dorm}}{dt} = k_{dormi}[M][S_a] - (k_{re} + k_d)L_2^{dorm} + k_{dorm}[M](L_0 + 2L_1 + L_2) \quad (7.32)$$

$$\frac{dD_2}{dt} = (k_{tr} + k_d)L_2 + (k_{reH}[H_2] + k_d)L_2^{dorm} \quad (7.33)$$

### 7.1.5 Catalyst site, monomer and hydrogen concentration

Different species concentrations are required for model calculations. For the initial conditions, the potential active catalyst site concentration is needed which was defined as the total concentration of potential catalyst sites in the reactor:

$$[S_p](t = 0) = \frac{m_{Cat}W_{Ti}X_{active}}{MW_{Ti}V_R} \quad (7.34)$$



In the propylene polymerization with Ziegler-Natta catalysts, the titanium atoms distributed on the catalyst support act as active sites. However, not all but only 1 to 10 % of these are believed to participate in the polymerization reaction and an exact determination is not possible so far. [4] Therefore, the term  $x_{active}$  is included in the above equation which expresses the fraction of active titanium and which needs to be estimated.

The effective monomer concentration at the catalyst sites should be used in the calculation of reaction rates which is the monomer concentration in the amorphous polymer phase. For this purpose, the Sanchez-Lacombe EoS with temperature-dependent binary interaction parameter was chosen since it could well describe the experimentally determined concentration of propylene in amorphous PP (section 6.4.3). The kinetic model is thus combined with an advanced thermodynamic model relevant for process modeling.

Due to lack of experimental data on the solubility of hydrogen in PP, the hydrogen concentration in the gas phase was chosen for the rate expressions:

$$[H_2] = \frac{m_{H_2}}{MW_{H_2} V_R} \quad (7.35)$$

For the here used relatively low amounts of hydrogen, the gas phase hydrogen concentration should be directly proportional to the concentration in the amorphous phase. Additionally, the complexity of the thermodynamic calculations is clearly reduced.

Although the solubility of hydrogen in the polymer phase was neglected, the gas composition was modeled via the SL EoS using a BIP of zero (Table 7.2 and Table 7.3).

As a constant reaction pressure of 28.5 bar was used throughout all polymerization experiments, but the hydrogen mass was varied, the propylene partial pressure and thus the effective monomer concentration was affected which was considered within the thermodynamic model (Figure 7.1).

**Table 7.2:** Literature pure component parameters of hydrogen, propylene and polypropylene for the Sanchez-Lacombe EoS as used for the kinetic model.  $T^*$ ,  $P^*$  and  $\rho^*$  denote the characteristic temperature, pressure and closed-packed mass density, respectively.

Component	$T^*$ [K]	$P^*$ [bar]	$\rho^*$ [kg/m <sup>3</sup> ]	Reference
Hydrogen	45.89	1000	142.66	[130]
Propylene	360.43	3100	670.83	[130]
PP	690.6	3007	885.6	[54]

**Table 7.3:** Binary interaction parameters for the Sanchez-Lacombe EoS as used for the kinetic model.

Binary System	BIP [-]	Reference
Hydrogen/Propylene	$k = 0$	-
Propylene/PP	$k = -0.0757 \frac{T}{298.15 K} + 0.1664$	this work

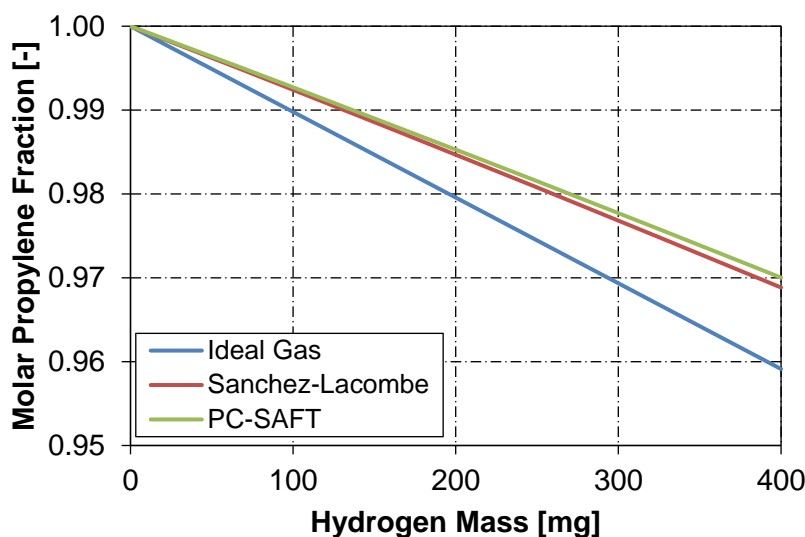


**Figure 7.1:** Molar vapor phase fraction of propylene as function of the used hydrogen mass for the polymerization conditions of 80 °C and 28.5 bar. Pure component parameters for the SL and PC-SAFT EoS were taken from Khare [130] and Gross and Sadowski [110], respectively. The BIP was set to zero for both EoS models.

## 7.2 Model implementation and parameter estimation

The derived set of equations was implemented in the software gPROMS® ModelBuilder 5.1 (*Process Systems Enterprise*). The available parameter estimation tool was used to determine the kinetic rate coefficients as well as the fraction of active sites. These parameters were estimated based on the experimental results, meaning the activity profiles, yields and weight average molecular weights (obtained via the MFR). Here, MFR values obtained at 0 mg hydrogen were not used as well as values above 150 g/10 min due to high measurement errors. Additionally, to reduce the computational effort, the activity profiles were represented by 4 to 5 data points (Figure 7.2). The experimental error was assumed to be of 10 % for the yield and molecular weight, whereas a higher error of 15 % was chosen for the activity profiles as these showed some oscillations caused by the pressure controller.

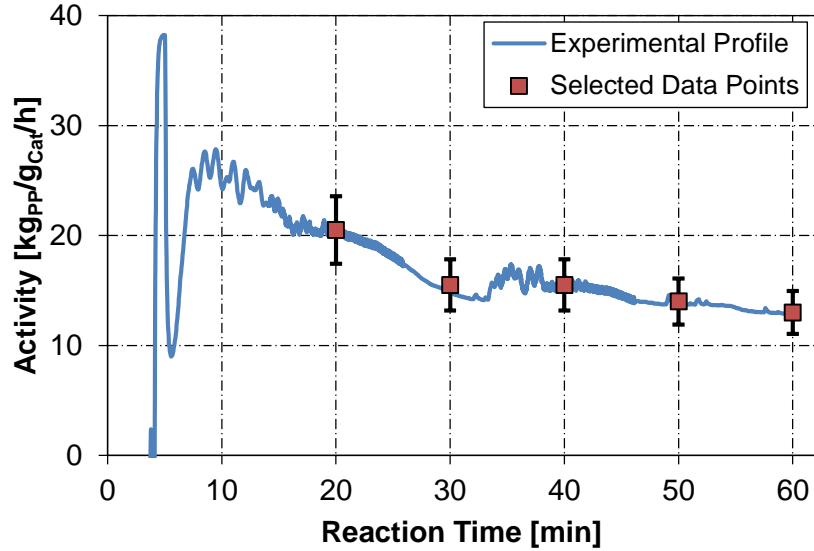


**Figure 7.2:** Example of the reduction of the continuous activity profile to selected data points as used for parameter estimation.

Some of the kinetic rate coefficients such as the activation and initiation constant cannot be estimated with the available experimental data or they are strongly correlated (e.g. the dormant site theory rate constants). Therefore, the following assumptions were made:

$$k_i = k_p \quad \text{and} \quad k_{dormi} = k_{dorm} \quad (7.36)$$

Furthermore, the values of the rate coefficients for activation, propagation and formation of dormant chains were pre-defined (Table 7.4). The activation constant was set to  $10^5$  /s and thus to the same magnitude as the propagation constant. This results in an instantaneous activation and a change of this constant by a few orders of magnitude would not affect the simulation results. The fraction of active titanium and the propagation rate coefficient are highly correlated. The latter parameter was taken from the work of Kettner [22] who studied ZN catalyst kinetics under very similar conditions. The three kinetic constants used within the simplified dormant site theory cannot be estimated from the available experimental data, but only the ratios of these. If experimental results on the regio-regularity or chain end groups of the produced polymer were available, the three constants could be independently determined. As this is not the case, the value of  $k_{dorm}$  was set to  $10^{-3}$  L/mol/s. This value was chosen so that the value of  $k_{reH}$  was in the same order of magnitude as  $k_{trH}$  (or lower). Busico et al. [25] argued that these two coefficients should be of about unity. Simplified speaking, from the point of modeling, only the ratios of the three dormant site constants determine the simulation results. For instance,  $k_{dorm}$  could also be set to 1 L/mol/s which would result in a number of *n*-butyl chain ends of about 6 to 14 % as experimentally determined by Chadwick et al. [25]. However, in this case, the kinetic constant  $k_{reH}$  would become magnitudes higher than  $k_{trH}$  and even higher than the propagation rate coefficient.

**Table 7.4:** Pre-defined rate coefficients to break parameter correlations. The kinetic constant for propagation  $k_p$  was taken from Kettner [22].  $k_a$  and  $k_{dorm}$  refer to the rate constants for activation and dormant chain formation, respectively.

Parameter	Value	Unit
$k_a$	$10^5$	1/s
$k_p$ (75 °C)	$2.19 \cdot 10^5$	L/mol/s
$k_p$ (80 °C)	$2.89 \cdot 10^5$	L/mol/s
$k_{dorm}$	$10^{-3}$	L/mol/s

The parameter estimation was performed in a step-wise procedure. The fraction of active titanium  $x_{active}$  and the deactivation constant  $k_d$  were first estimated from experimental results at high hydrogen concentrations while setting  $k_{dorm}$  to zero. In a next step, the dormant site parameters were estimated based on the experimental activity profiles and yields. In the last step, the transfer constants were determined from the molecular weight data. These steps were repeatedly carried out and a final simultaneous estimation of all parameters was performed. Since a local optimizer is used within gPROMS® for parameter estimation, each step was carefully rechecked and different initial guesses were investigated to find the best fit. Nevertheless, it cannot be guaranteed that the global optimum was found. Note that not all experimental data was used for parameter estimation, but some was kept for model validation, i.e. parts of the experimental results were used for model fitting and parts for comparison of model predictions with experimental data.

A detailed comparison between simulated and experimental data follows in the next section 7.3.

The obtained kinetic parameters are summarized in Table 7.5. The different polymerization procedures could be well described with the same set of rate coefficients by just using a different number of active sites. This was already indicated by the comparison of the experimental results: Each catalyst showed different polymerization kinetics, but the difference between prepolymerization and seed bed polymerization was simply a different activity level. When either polymerization method was fitted individually, very similar kinetic constants were obtained. Merely the deactivation constant showed some disagreement. Nevertheless, with slightly less accuracy, the experiments could be described with one set of kinetic constants for each catalyst and an individual fraction of active sites for each catalyst and polymerization procedure.

**Table 7.5:** Parameter estimation results for catalysts A, C and D.  $x_{active}$  and  $w_{Ti}$  are symbols for the active fraction of titanium and the weight fraction of titanium, respectively.  $k_a$ ,  $k_i$ ,  $k_p$ ,  $k_d$ ,  $k_{trH}$ ,  $k_{trSp}$ ,  $k_{dorm}$ ,  $k_{dormi}$ ,  $k_{reH}$  and  $k_{reM}$  denote the rate constants for activation, initiation, propagation, deactivation, transfer to hydrogen, spontaneous transfer, dormant chain formation, dormant chain initiation, reactivation by hydrogen and reactivation by monomer, respectively.

Parameter	Cat A		Cat C		Cat D		Unit
	Prepo	SB	Prepo	SB	Prepo	SB	
$x_{active} \cdot w_{Ti}$	$1.88 \cdot 10^{-2}$	$1.26 \cdot 10^{-2}$	$3.09 \cdot 10^{-2}$	$2.34 \cdot 10^{-2}$	$3.83 \cdot 10^{-2}$	$2.43 \cdot 10^{-2}$	wt%
$k_a^*$	$10^5$		$10^5$		$10^5$		1/s
$k_i^*$	$2.89 \cdot 10^5$		$2.19 \cdot 10^5$		$2.19 \cdot 10^5$		L/mol/s
$k_p^*$	$2.89 \cdot 10^5$		$2.19 \cdot 10^5$		$2.19 \cdot 10^5$		L/mol/s
$k_d$	$2.21 \cdot 10^{-4}$		$1.96 \cdot 10^{-4}$		$1.46 \cdot 10^{-4}$		1/s
$k_{trH}$	88.7		133		128		$L^{0.5}/mol^{0.5}/s$
$k_{trSp}$	10.0		4.20		8.33		1/s
$k_{dorm}^*$	$10^{-3}$		$10^{-3}$		$10^{-3}$		L/mol/s
$k_{dormi}^*$	$10^{-3}$		$10^{-3}$		$10^{-3}$		L/mol/s
$k_{reH}$	551		$4.45 \cdot 10^{-1}$		$7.62 \cdot 10^{-1}$		L/mol/s
$k_{reM}$	$5.57 \cdot 10^{-4}$		$1.49 \cdot 10^{-4}$		$8.31 \cdot 10^{-4}$		L/mol/s

\*These constants were not estimated and are just shown for completion.

The estimated parameters can be used for a quantitative comparison. The initial active catalyst mass fraction (product of  $x_{active}$  and  $w_{Ti}$ ) increases from catalyst A over C to D in agreement to the experimentally observed activities. The ratio of these products for the two different methods of prepolymerization and seed bed polymerization gives an quantitative estimation of the prepolymerization potential or catalyst resistance to overheating. The prepolymerization potential is highest for catalyst D with about 60 % increase, whereas lower values are obtained for catalysts A and C of about 49 and 32 %, respectively. For catalyst C, a prepolymerization step is least beneficial in terms of activity enhancement. The deactivation constants are in the range of  $1.5$  to  $2.2 \cdot 10^{-4}$  /s and thus fairly similar. Catalyst C and D have the same molecular weight response upon changes in the hydrogen concentration as can be seen in the almost identical chain transfer constant  $k_{trH}$  of about  $130 L^{0.5}/mol^{0.5}/s$ . The different MFR results can be explained by different values in  $k_{trSp}$ . Catalyst A shows a less pronounced response to hydrogen with smaller  $k_{trH}$  of about  $90 L^{0.5}/mol^{0.5}/s$  and similar  $k_{trSp}$  as catalyst D. Catalyst A shows to be most sensitive to hydrogen in terms of rate enhancement with the clearly highest value in  $k_{reH}$ . Catalyst C and D have much lower hydrogen reactivation constants. The ratio of  $k_{dorm}$  to  $k_{reM}$  is equal to the ratio of dormant to living chains in absence of hydrogen (quasi-steady-state approximation). This ratio is a measure on how much the activity is increased from zero hydrogen to the

plateau activity level. It is highest for catalyst C meaning that this catalyst shows the highest total activity enhancement by hydrogen, whereas catalyst D shows the lowest hydrogen influence on the activity.

The standard deviation for the estimated parameters of catalyst A is on average 43 %. The highest values of 44 and 185 % were found for the reactivation constants  $k_{reM}$  and  $k_{reH_2}$ , respectively. Clearly, this is caused by the lack of experimental data between the hydrogen masses of 0 and 25 mg. The detailed activity enhancement by hydrogen up to the plateau level is not fully captured by the experimental results and thus leads to high standard deviations for the dormant site theory rate constants. Excluding these two standard deviations, the average standard deviation was found to be of 15 % showing that the other parameters could be precisely estimated. For catalyst D, the average standard deviation was 24 % with a high value of 55 % found for the hydrogen reactivation constant indicating that a relatively large amount of experimental data points is needed to estimate this constant with higher accuracy. Note that only part of the experimental data was used for parameter estimation and the standard deviations should become smaller when including more experimental results. For catalyst C, the highest amount of experimental data was used for parameter estimation and the standard deviation was about 15 % on average.

A comparison of the determined rate coefficients with literature values is difficult because each catalyst shows individual polymerization kinetics. Thus, only an order of magnitude comparison should be performed. The here used rate constants for propagation fall in between reported values of 0.5 and  $4.6 \cdot 10^5$  L/mol/s of Kröner [23] and Reginato et al. [75], respectively. The deactivation constants are similar to literature values of 1.0 to 2.7 [36], 1.7 [23], 2.1 [22] and  $3.2 \cdot 10^{-4}$  /s [75]. The obtained chain transfer to hydrogen constants lie in between reported values of 42 [22] and  $718 \text{ L}^{0.5}/\text{mol}^{0.5}/\text{s}$  [75]. The ratio of  $k_{dorm}$  to  $k_{reM}$  is clearly catalyst dependent as each ZN catalyst shows a different activity response towards hydrogen. Nevertheless, the here obtained ratios of 1.8, 6.7 and 1.2 for catalysts A, C and D, respectively, are in the range of literature ratios of 0.9 [22] and 8.0 [81]. Overall, it can be concluded that the estimated rate coefficients are of reasonable magnitude and are similar to literature constants.

Both the fitted and validated model results agree well with experimental data (Figure 7.3). The deviations between experiment and simulation are on average below 10 %. Although only shown for the experimental yield and weight average molecular weight, this also holds for the activity profiles. Note that the deviations are on average below 10 % both for the experiments which were used for model fitting as well as the ones kept for model validation, i.e. the model predictions agree well with selected experimental results.

The proposed kinetic model is thus sufficient to describe the experimental results using one set of kinetic rate constants for each catalyst and a different fraction of active catalyst sites for the specific polymerization method. The comparison reveals that for all catalysts, the molecular weight is very accurately described within the model using only two kinetic constants for chain transfer. Generally, three molecular weight results of each polymerization method were needed for satisfying model predictions. The experimental yield is slightly less accurately described with a few values showing more than 10 % deviation. Here, for each catalyst a varying amount of data points was needed for model fitting in order to correctly predict the plateau activity at high hydrogen concentrations, e.g. for catalyst C only the experimental yield at 400 mg could be used for model validation.

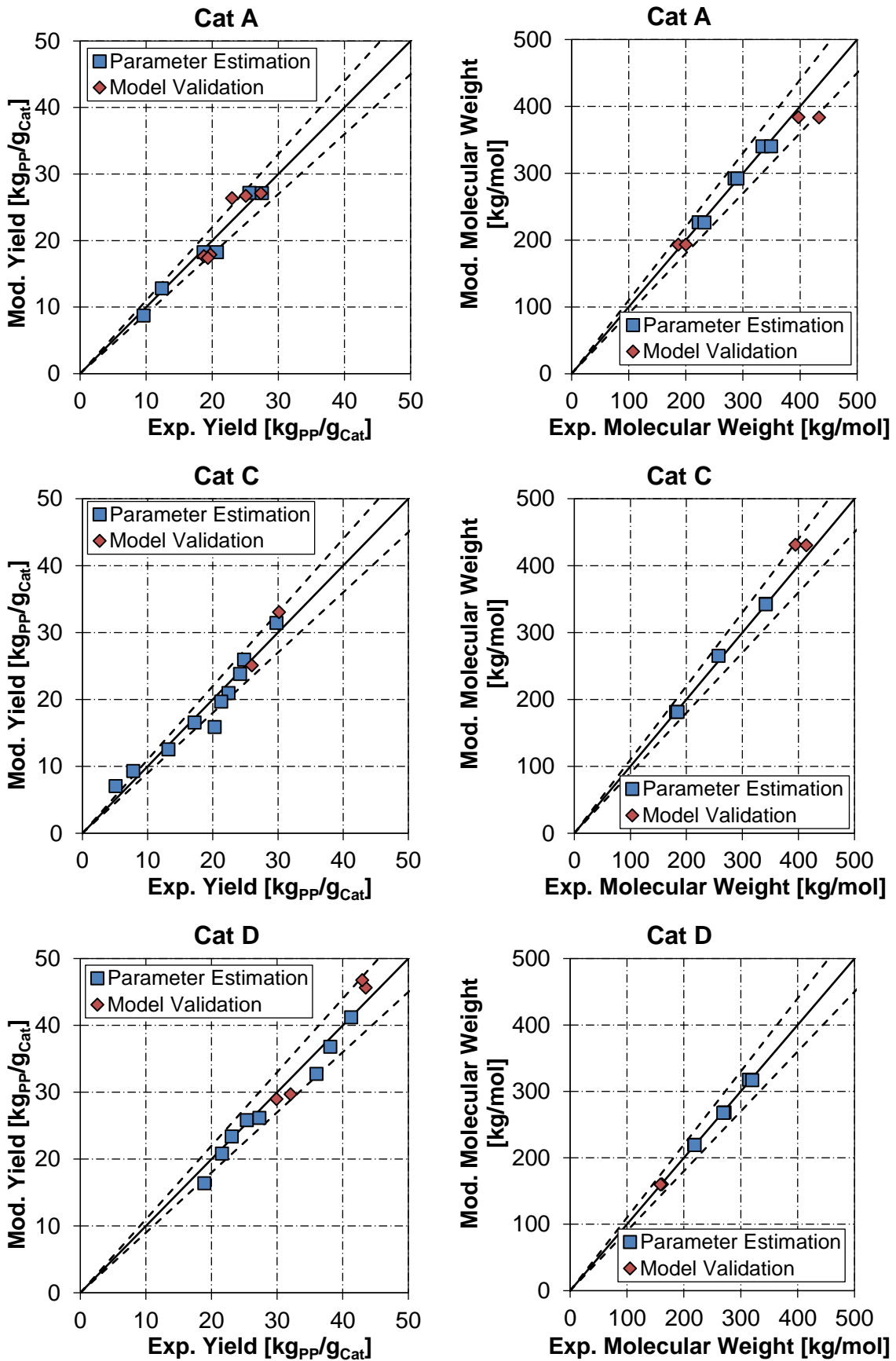


**Figure 7.3:** Comparison of model fit (blue squares) and prediction (red diamonds) with experimental yield and molecular weight. Dashed lines indicate 10 % deviation.



### 7.3 Comparison of experiment and simulation

In this section, the experimental results are compared with the simulation results in form of overlay charts. The rate enhancement of the activity with increasing hydrogen is well captured by the validated kinetic model for all three catalysts both for the method of prepolymerization and seed bed polymerization (Figure 7.4). Whereas for catalysts C and D the experimental rise in activity with increasing hydrogen mass up to the plateau level can be compared in detail with the simulation results, the fast rate enhancement of catalyst A from 0 to 25 mg hydrogen and therefore lack of experimental data does not allow this. The experimental MFR is well described by the model (Figure 7.5). Average deviations were found to be of 15, 10 and 3 % for catalysts A, C and D, respectively, and thus in range with the observed experimental error. Selected experimental activity profiles at 0, 100 and 400 mg hydrogen for both polymerization methods are compared with simulated activities in Figure 7.6 and Figure 7.7. The highest deviation is found for the activity profile of catalyst A at 400 mg hydrogen for the case of prepolymerization. Here, the model largely over-predicts the activity level. This is because experimentally, a decline in activity was observed for catalyst A at high hydrogen masses. As this phenomena was only observed for catalyst A and the method of prepolymerization, no kinetic step was considered within the model to account for this effect. Overall, the simulated activity profiles agree well with the experimental ones showing little mismatch.

In conclusion, the validated kinetic model is capable of accurately describing the key variables activity and MFR for all three catalysts for both polymerization procedures. It therefore adds valuable information for process development allowing to analyze the dynamic performance of these catalysts in industrial scale. Moreover, the prepolymerization potential can be studied. Since the model was only validated for experiments performed at a fixed temperature and pressure, further experiments at different pressures and temperatures would be useful to widen the model capabilities. The effect of temperature can be easily incorporated within the kinetic model by making use of the Arrhenius equation for the rate coefficients. Activation energies could be obtained from a number of experiments performed at different temperatures. The main effect of pressure is the change in effective monomer concentration which is in principle already incorporated in the model as part of the SL EoS, but should be validated based on selected experiments at different pressures.

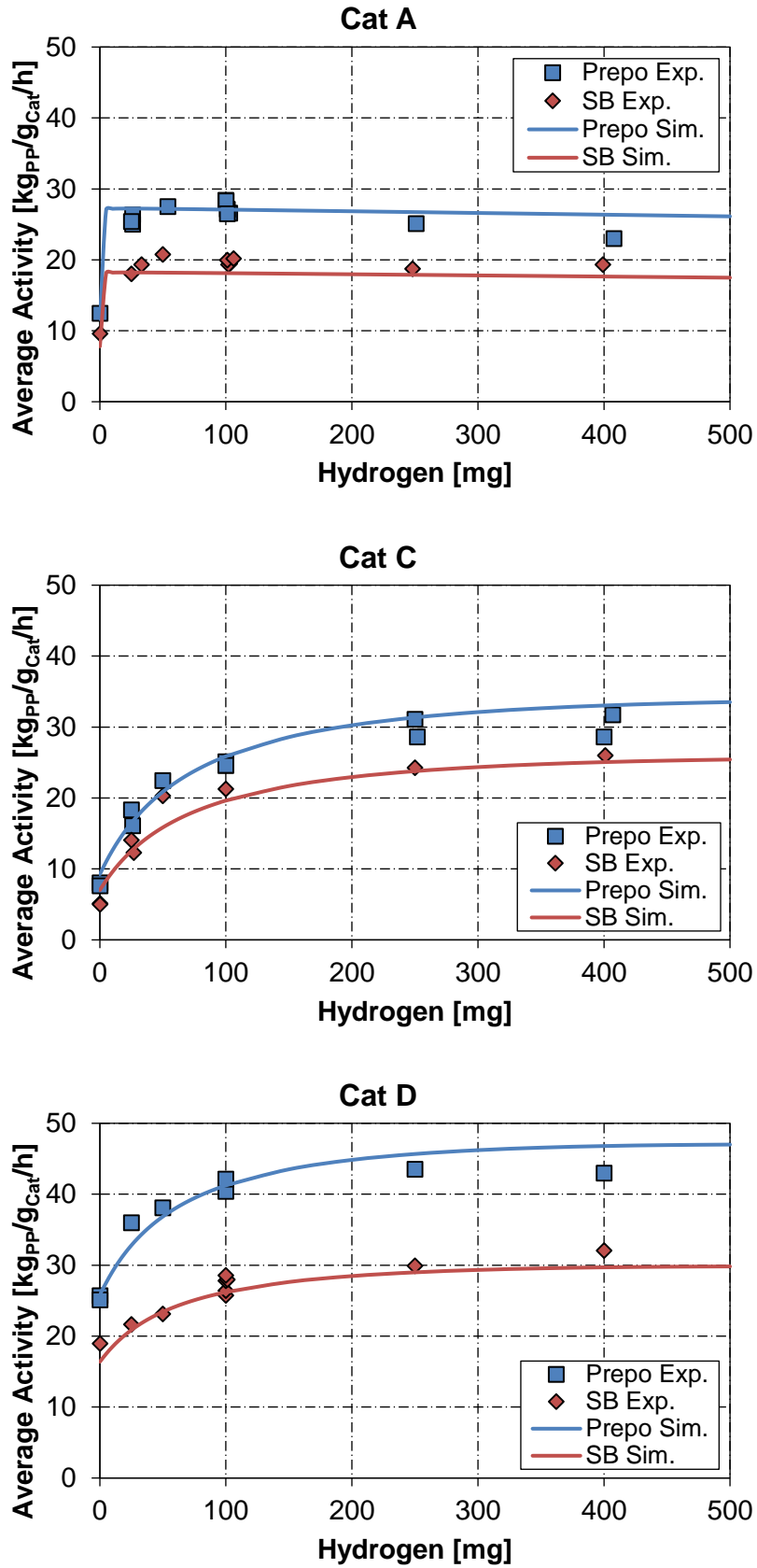


**Figure 7.4:** Comparison of experimental and simulated average activities of catalysts A, C and D. Reaction conditions: 80 °C (Cat A) or 75 °C (Cat C&D) and 28.5 bar.

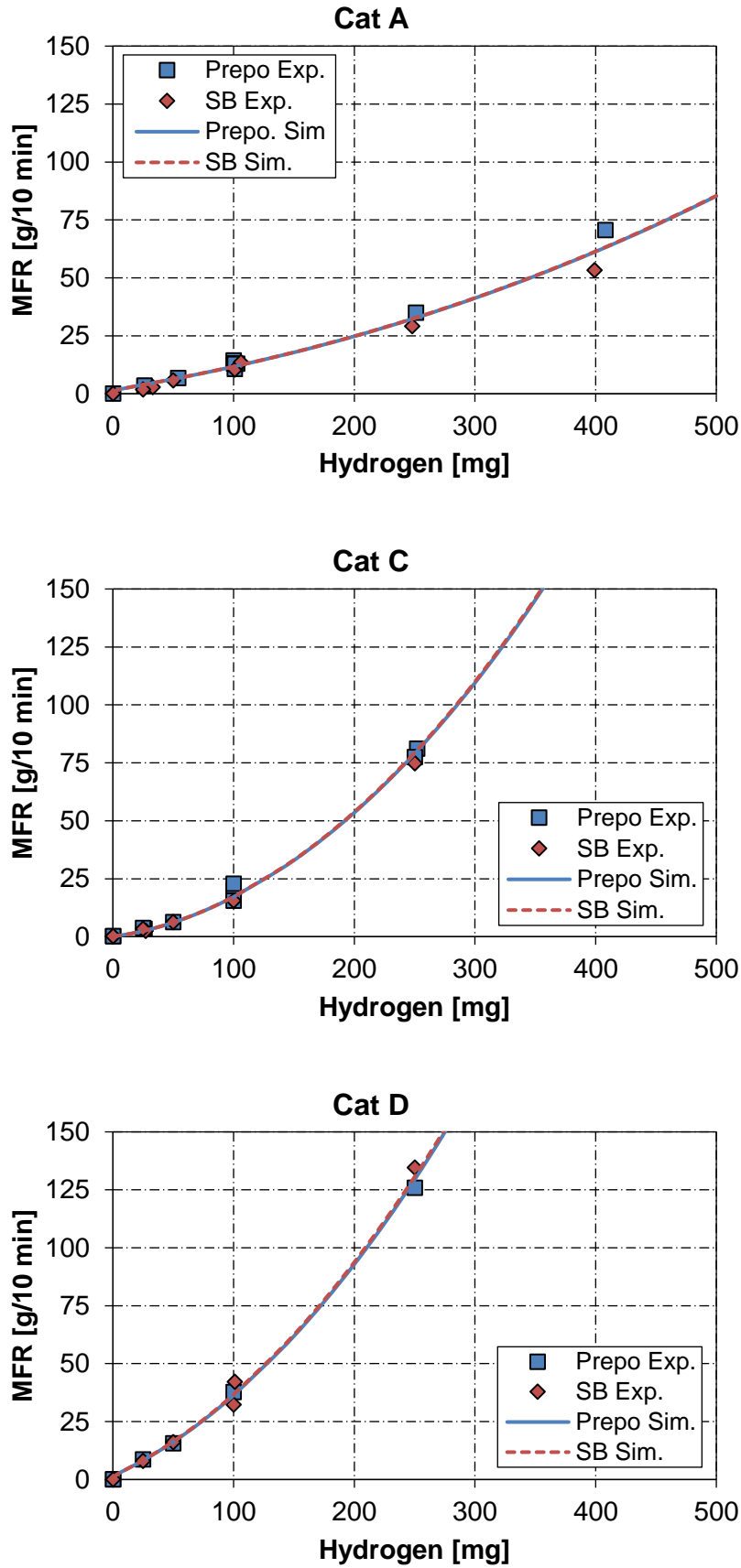


**Figure 7.5:** Comparison of experimental and simulated MFR of catalysts A, C and D. Reaction conditions: 80 °C (Cat A) or 75 °C (Cat C&D) and 28.5 bar.

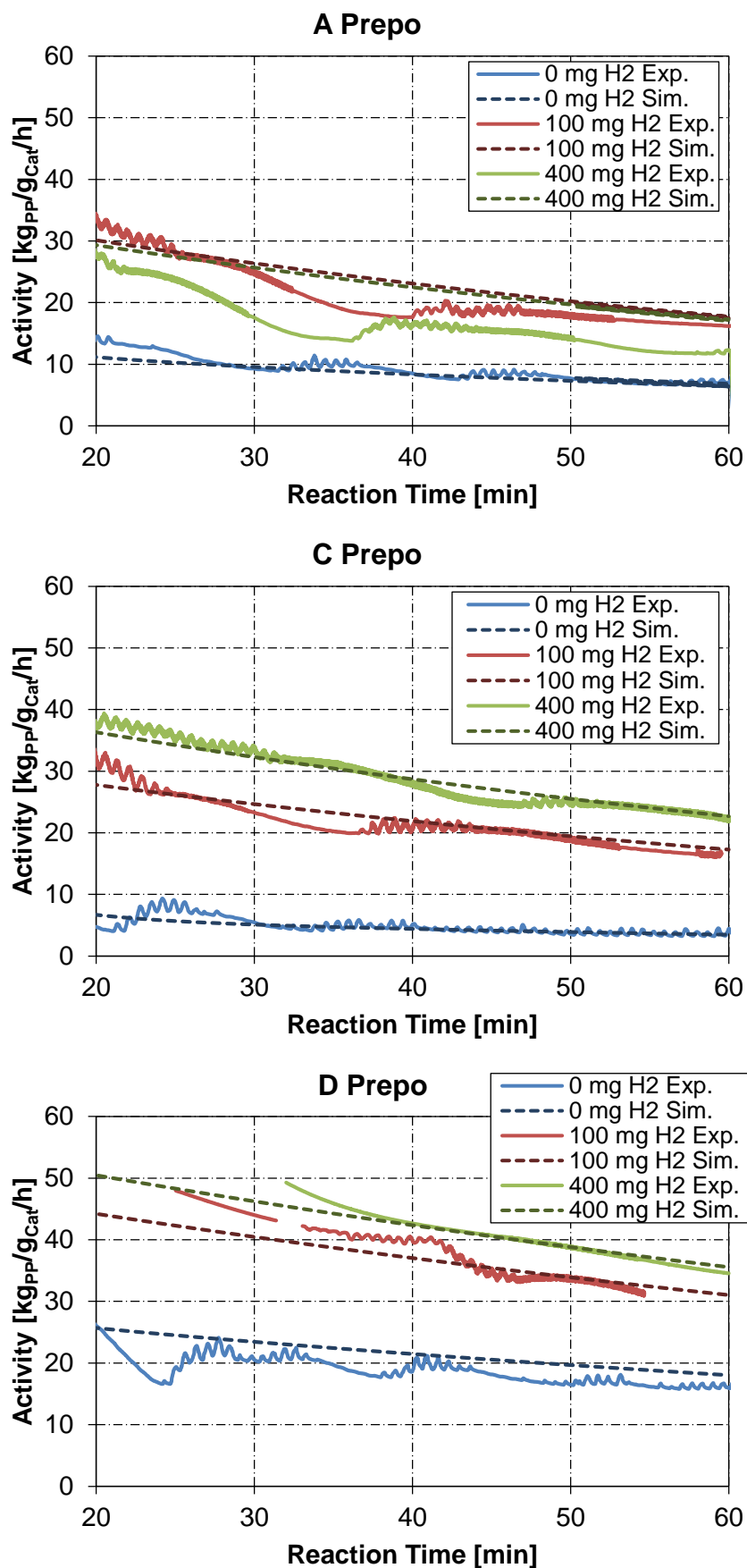


**Figure 7.6:** Comparison of experimental and simulated activity profiles of catalysts A, C and D for selected hydrogen masses of 0, 100 and 400 mg for the prepolymerization method. Reaction conditions: 80 °C (Cat A) or 75 °C (Cat C&D) and 28.5 bar.

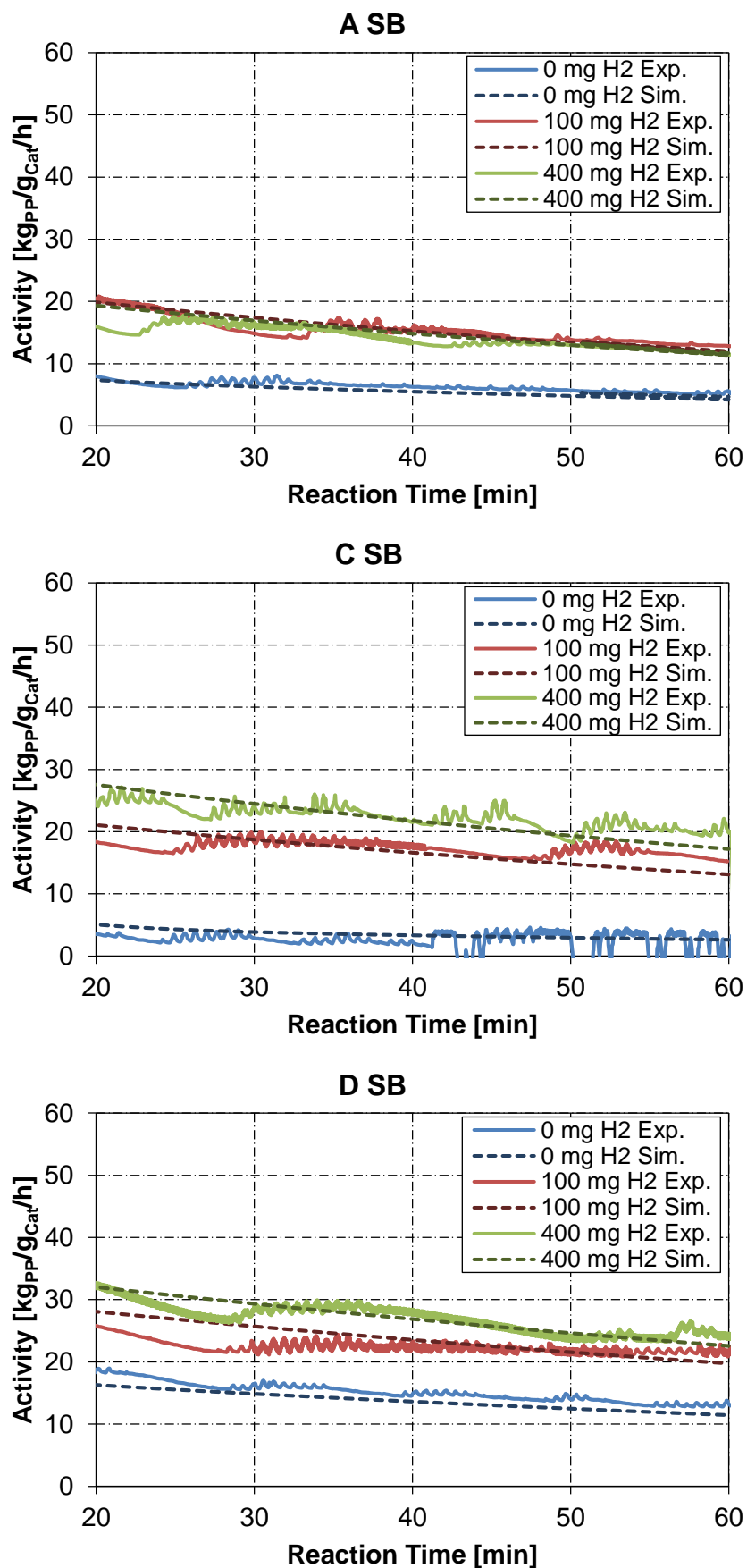


**Figure 7.7:** Comparison of experimental and simulated activity profiles of catalysts A, C and D for selected hydrogen masses of 0, 100 and 400 mg for the seed bed polymerization method. Reaction conditions: 80 °C (Cat A) or 75 °C (Cat C&D) and 28.5 bar.

## 8 Summary

The objective of this work was to investigate the kinetics of four Ziegler-Natta catalysts in the gas phase polymerization of propylene under industrial relevant conditions. The main aspect was to study conditions that resemble the situation in continuous industrial plants in terms of particle-particle heat transfer by performing seed bed polymerization experiments. The focus was placed on the effect of catalyst overheating by comparing two polymerization methods: prepolymerization and direct injection of catalyst at the main reaction conditions in presence of a seed bed.

Experiments were performed in a 5 L horizontal stirred tank reactor operated in semi-batch mode. Isobaric conditions were maintained via a pressure control loop allowing to monitor the catalyst activity over time. First experiments were conducted for catalysts A and B at the main reaction conditions of 80 °C, 28.5 bar and 100 mg hydrogen. The effect of the initial temperature was studied between 40 and 80 °C revealing that a lower initial temperature led to a higher catalyst activity. Both catalysts showed almost identical kinetic behavior and prepolymerization (initial temperature of 40 °C) increased the average activities to about 28 kg<sub>PP</sub>/g<sub>Cat</sub>/h in contrast to much lower activities of about 11 kg<sub>PP</sub>/g<sub>Cat</sub>/h obtained for the case of direct catalyst injection at the main reaction temperature. The use of 100 g PP seed bed was evaluated for the same conditions and showed a strong increase in activity for the latter case of direct injection. The activity increased for catalyst A by 65 % simply by the addition of a seed bed. Variation of the initial temperatures was therefore conducted again in presence of a seed bed and revealed that the activity of both catalysts differed with catalyst A being more heat resistant, i.e. showing a lower decline in activity with increasing initial temperature. For the case of prepolymerization, the activity of both catalysts remained unchanged leading to the conclusion that merely improved heat transfer was the reason for the enhanced activities observed at higher initial temperatures. Particle-particle heat transfer led to improved evacuation of heat from small catalyst particles to large PP bed particles reducing catalyst overheating and thus improving both activity and particle morphology. No effect on the activity or morphology was observed for prepolymerization because at low initial temperatures overheating should not be an issue. Based on the seed bed polymerization results, it was concluded that studying kinetics of new ZN catalysts in lab-scale should be performed in a presence of a seed bed in order to obtain results that would be more applicable to the continuous gas phase pilot or commercial scale.

After establishment of the seed bed polymerization method, a detailed kinetic study was conducted for catalysts A, C and D with focus on the effect of hydrogen as well as the initial temperature by comparing prepolymerization and seed bed polymerization (catalyst injection

directly at the main reaction temperature). The average activity was found to be highest for catalyst D with a maximum activity of 44 kg<sub>PP</sub>/g<sub>Cat</sub>/h and lowest for catalyst A with a maximum of 28 kg<sub>PP</sub>/g<sub>Cat</sub>/h. It turned out that the effect of the polymerization method and thus initial temperature was merely a change in the overall catalyst activity. All catalysts showed a higher overall activity level for the method of prepolymerization, but the difference in activity for the two methods varied from catalyst to catalyst. Catalyst C showed the lowest difference and thus highest heat resistance, whereas catalyst A and D showed an increase in activity by about 50 %. All three catalysts showed a rate enhancement with increasing hydrogen concentration which was catalyst specific. The sensitivity in activity towards hydrogen was highest for catalyst A and lowest for catalyst C. The plateau activity value was already reached at 25 mg hydrogen for catalyst A, but only at 250 mg for catalyst C. The overall effect of hydrogen on the activity was strongest for catalyst C with an increase from about 5 to 30 kg<sub>PP</sub>/g<sub>Cat</sub>/h for hydrogen masses of 0 and 400 mg, respectively. For catalysts A and D, the effect was less pronounced, but still activity increased by factor two upon raising the hydrogen concentration. The analysis of the kinetic profiles revealed that a similar deactivation behavior was observed for all catalysts independent of the hydrogen concentration. The activity profiles of the seed bed polymerization method showed a slightly lower relative decline in activity for all catalysts. Generally, the deactivation behavior was not found to be strongly catalyst specific. The MFR increased with hydrogen, but differently for the three catalysts. The MFR was about 12, 18 and 38 g/10 min at 100 mg hydrogen for catalysts A, C and D, respectively. Catalysts A and C both showed similar MFR values at low hydrogen amounts, but the MFR increased much stronger for catalyst C. Catalyst D showed a similar relative increase as catalyst C and the highest MFR values. The MFR was found to be unaffected by the polymerization method.

The particle morphology, which was studied by light microscopy, SEM, bulk density, porosity and PSD measurements, proved to be less catalyst specific, but rather depend on the polymerization method. Prepolymerization led to spherical, regular particles with smooth surfaces for all catalysts. Injecting the catalyst directly under main reaction conditions without a seed bed led to a complete loss of the spherical catalyst geometry and sheet like particles were obtained. In presence of a seed bed, the particle morphology was considered to be an intermediate between the two morphology extremes. The particles showed a close to spherical geometry, but were irregular and had a rough surface. Thus the initial polymerization rate determined the morphology which was lowest for prepolymerization. Improved heat transfer in presence of a seed bed reduced the initial polymerization rate leading to less pronounced loss of morphology at high initial temperatures. The PSDs were catalyst specific and unaffected by the polymerization method indicating particles produced by the seed bed polymerization method did not suffer breakage or fine formation although

they showed poorer morphology. The bulk density was found to be catalyst specific with about 510, 490 and 450 kg/m<sup>3</sup> for catalysts A, C and D, respectively, for the prepolymerization method. The seed bed polymerization method led to an almost equal reduction in bulk density by 70 kg/m<sup>3</sup>. It was concluded that prepolymerization clearly enhanced the morphology equally for all catalysts and there was no catalyst specific “morphology resistance”.

The experimental results gave valuable information for catalyst and process design. Generally, prepolymerization led to higher activity and better morphology, without changing the general polymerization kinetics such as rate enhancement with increasing hydrogen concentration and MFR response. However, important characteristics such as overall activity level and bulk density as well as the effect of prepolymerization on the activity were catalyst specific. Lab-scale studying of catalysts under conditions closer to the ones in industrial plants was concluded to be crucial for catalyst design and process development in order to facilitate the transition of new catalysts with enhanced properties to the commercial scale.

The solubility of propylene in PP was measured using a high pressure magnetic suspension balance. Various samples synthesized with different catalysts were studied at 70 °C and up to 25 bar showing very similar solubility. Additionally, one sample was measured between 40 and 80 °C revealing that the solubility decreased with increasing temperature. A detailed analysis of literature solubility data was conducted. When the amorphous solubility was compared, differences amounted up to a factor of two. Whereas a comparison of the solubility in mass of propylene per mass of PP showed almost identical results and literature data agreed well with the measured solubilities of this work. This led to the conclusion that commercial PP grades produced with modern ZN catalysts should all show similar solubility only dependent on temperature and pressure. Literature discrepancies could thus be explained by the applied crystallinity determination methods. The crystallinity was therefore estimated via DSC, WAXS and He-pycnometry. Although each method gave different results, these deviated in a small range of about 40 to 50 wt%. The mean value of 46 wt% as measured by WAXS was chosen for amorphous solubility and concentration calculations. A comparison with the well-known Stern correlation for the calculation of the amorphous concentration showed good agreement at low pressures, but up to 35 % higher experimental concentrations at high pressures.

Two state-of-the-art thermodynamic models relevant for process modeling were tested in describing the propylene/PP system based on the experimental sorption studies. Both the Sanchez-Lacombe (SL) and the PC-SAFT EoS could not predict a-priori the solubility, but fitting to experimental data was needed. The former EoS could very accurately describe the amorphous solubility at 70 °C with an average relative deviation (ARD) of 1 %, whereas the



latter resulted in an ARD of 9 %. Using the estimated binary interaction parameter (BIP) to predict the solubility between 40 to 80 °C revealed better performance of the SL model with an ARD of 6 %. Using a temperature-dependent BIP, the ARD could be further reduced to 3 %. The experimental concentrations were described with the same accuracy by both models, since the swelling of amorphous PP was very accurately predicted. Based on the model comparison, it was found that the SL EoS was better suited for modeling the solubility of propylene in PP.

A phenomenological kinetic model was developed in order to describe the polymerization kinetics. Basic kinetic reaction steps were chosen based on the experimental observations. Chain transfer was modeled to occur spontaneously and by hydrogen. The rate enhancement with increasing hydrogen concentration was considered by the dormant site theory. Here, the deactivation of dormant chains was also included which was typically not used in literature, but which was necessary to account for the same relative activity decay independent of the hydrogen concentration. The resulting mass balances were derived using the method of moments. The monomer concentration and gas composition were calculated using the SL EoS. The kinetic parameters were estimated based on the experimentally obtained yields, weight average molecular weights (indirectly obtained via MFR by an empirical correlation) and activity profiles. Parts of the experimental data were used for model validation. Individual kinetic rate constants were needed for each catalyst, but the method of prepolymerization and seed bed polymerization could be described with the same set of rate coefficients by only using a different number of active catalyst sites. Overall, the validated model could accurately describe the experimental results with an ARD below 10 and 15 % for the activity and MFR, respectively, and thus in the same order as the experimental errors. The validated model including estimated kinetic parameters and based on a thermodynamic EoS was considered to be well suited for further studies regarding catalyst and particularly process development.

## 9 Appendix

### 9.1 Data of the gas phase polymerization experiments

**Table 9.1:** Reproducibility. Reaction conditions: 80 °C, 28.5 bar, 100 mg H<sub>2</sub>, prepolymerization method.

Experiment	Cat	Hydrogen [mg]	Average Activity [kg <sub>PP</sub> /g <sub>Cat</sub> /h]	MFR [g/10 min]	Bulk Density [kg/m <sup>3</sup> ]
A1	A	100	28.4	14.4	512
A2	A	103	26.6	13.0	503
A3	A	101	27.1	10.8	518
A4	A	100	28.3	13.0	510
A5	A	101	26.5	12.8	509

**Table 9.2:** Variation of the initial temperature. Reaction conditions: 80 °C, 28.5 bar, 100 mg H<sub>2</sub>. Experiments A2 to A5 of Table 9.1 are not listed again.

Experiment	Cat	Initial Temperature [°C]	Average Activity [kg <sub>PP</sub> /g <sub>Cat</sub> /h]
A1	A	40	28.4
A7	A	60	16.8
A8	A	60	17.7
A9	A	80	12.3
A10	A	80	11.5
B1	B	40	27.8
B2	B	40	29.5
B3	B	40	27.7
B4	B	40	30.4
B5	B	60	20.9
B6	B	60	20.4
B7	B	60	19.3
B8	B	60	17.3
B9	B	80	8.8
B10	B	80	11.0

**Table 9.3:** Variation of the initial temperature in presence of a seed bed and seed bed mass variation experiments. Reaction conditions: 80 (Cat A&B) or 75 °C (Cat C&D), 28.5 bar, 100 mg H<sub>2</sub>. Experiments A2 to A5 of Table 9.1 are not listed again.

Experiment	Cat	Initial Temperature	SB Mass	Average Activity
		[°C]	[g]	[kg <sub>PP</sub> /g <sub>Cat</sub> /h]
A1	A	40	0	28.4
A11	A	40	100	28.2
A12	A	40	100	26.5
A13	A	40	100	28.5
A17	A	60	100	22.5
A18	A	60	100	23.2
A19	A	70	100	18.7
A20	A	70	100	18.8
A21	A	70	100	20.2
A14	A	80	99	19.3
A6	A	80	100	19.5
A15	A	80	100	20.0
A16	A	80	104	20.2
B11	B	40	100	29.5
B12	B	60	100	27.2
B13	B	60	100	25.0
B14	B	70	100	16.3
B15	B	70	100	17.3
B16	B	80	100	16.1
B17	B	80	100	16.3
C1	C	40	0	24.6
C2	C	40	0	25.1
C3	C	75	100	21.3
C4	C	75	150	23.6
C5	C	75	200	16.7
C6	C	75	200	14.3
C24	C	75	0	11.3
C25	C	40	100	25.4
D1	D	40	0	40.4
D2	D	40	0	42.1
D3	D	40	100	44.4
D4	D	40	100	45.3
D5	D	75	100	25.7

Experiment	Cat	Initial Temperature [°C]	SB Mass [g]	Average Activity [kg <sub>PP</sub> /g <sub>Cat</sub> /h]
D6	D	75	100	26.4
D7	D	75	100	27.8
D8	D	75	101	28.0
D9	D	75	100	28.6
D10	D	75	50	22.0
D11	D	75	50	22.2
D12	D	75	150	29.6
D13	D	75	150	30.8
D14	D	75	150	27.5
D15	D	75	200	23.4

**Table 9.4:** Hydrogen variation for the prepolymerization method. Reaction conditions: 80 °C (Cat A) or 75 °C (Cat C&D), 28.5 bar. Experiments A2 to A5 of Table 9.1 are not listed again.

Experiment	Cat	Hydrogen Mass [mg]	Average Activity [kg <sub>PP</sub> /g <sub>Cat</sub> /h]	MFR [g/10 min]	Bulk Density [kg/m <sup>3</sup> ]
A22	A	0	12.4	0.1	514
A23	A	26	26.3	3.3	514
A24	A	26	25.0	3.5	522
A25	A	25	25.4	-	508
A26	A	54	27.5	6.8	516
A1	A	100	28.4	14.4	512
A27	A	251	25.1	34.9	509
A28	A	408	23.0	70.6	524
C7	C	0	8.0	0.1	497
C8	C	0	7.6	0.1	489
C9	C	26	16.1	3.3	502
C10	C	25	18.3	3.7	477
C11	C	50	22.4	6.2	486
C1	C	100	24.6	19.9	488
C2	C	100	25.1	15.5	489
C13	C	252	28.6	81.1	-
C14	C	250	31.1	77.4	492
C15	C	407	31.7	234.0	485
C16	C	400	28.6	243.0	483
D16	D	0	25.7	0.1	-

Experiment	Cat	Hydrogen Mass [mg]	Average Activity [kg <sub>PP</sub> /g <sub>Cat</sub> /h]	MFR [g/10 min]	Bulk Density [kg/m <sup>3</sup> ]
D17	D	0	25.1	0.1	455
D18	D	25	36.0	8.7	447
D19	D	50	38.1	15.7	462
D1	D	100	40.4	-	-
D2	D	100	42.1	37.8	448
D20	D	250	43.5	125.9	455
D21	D	400	43.0	242.2	454

**Table 9.5:** Hydrogen variation for the seed bed polymerization method. Reaction conditions: 80 °C (Cat A) or 75 °C (Cat C&D), 28.5 bar, 100 g SB.

Experiment	Cat	Hydrogen Mass [mg]	Average Activity [kg <sub>PP</sub> /g <sub>Cat</sub> /h]	MFR [g/10 min]	Bulk Density [kg/m <sup>3</sup> ]
A29	A	0	9.6	0.1	425
A30	A	33	19.3	2.9	470
A31	A	25	18.0	1.9	451
A32	A	50	20.7	5.7	444
A6	A	103	19.5	-	-
A14	A	102	19.3	-	-
A15	A	101	20.0	10.4	-
A16	A	106	20.2	13.6	437
A33	A	248	18.7	29.1	437
A34	A	399	19.3	53.3	466
C17	C	0	5.1	0.1	418
C18	C	0	5.0	0.1	423
C19	C	27	12.3	2.4	426
C20	C	25	14.1	3.3	410
C21	C	50	20.3	6.2	424
C3	C	100	21.3	15.5	404
C22	C	250	24.2	74.8	378
C23	C	401	26.0	239.0	404
D22	D	0	18.9	0.1	403
D23	D	25	21.6	8.1	395
D24	D	50	23.1	16.2	407
D5	D	100	25.7	-	-
D6	D	100	26.4	-	-

Experiment	Cat	Hydrogen Mass [mg]	Average Activity [kg <sub>PP</sub> /g <sub>Cat</sub> /h]	MFR [g/10 min]	Bulk Density [kg/m <sup>3</sup> ]
D7	D	100	27.8	-	-
D8	D	101	28.0	42.2	381
D9	D	100	28.6	32.3	386
D25	D	250	29.9	134.6	398
D26	D	400	32.1	280.6	390

## 9.2 Experimental solubility data

Table 9.6: Reproducibility at 70 °C.

Experiment	Sample	Pressure [bar]	Solubility [g <sub>C3</sub> /kg <sub>PP</sub> ]
sA1	A	6.2	15.4
sA1	A	12.3	32.0
sA1	A	17.1	48.0
sA1	A	20.3	60.4
sA1	A	25.1	82.8
sA2	A	5.7	13.9
sA2	A	10.9	27.3
sA2	A	16.4	44.6
sA2	A	20.9	61.6
sA2	A	22.7	69.7
sA3	A	6.1	15.3
sA3	A	16.1	45.3
sA3	A	23.9	78.6

Table 9.7: Different samples at 70 °C.

Experiment	Sample	Pressure [bar]	Solubility [g <sub>C3</sub> /kg <sub>PP</sub> ]
sA1	A	6.2	15.4
sA1	A	12.3	32.0
sA1	A	17.1	48.0
sA1	A	20.3	60.4
sA1	A	25.1	82.8
sA-Film	A-Film	3.9	6.8

Experiment	Sample	Pressure [bar]	Solubility [g <sub>C3</sub> /kg <sub>PP</sub> ]
sA-Film	A-Film	13.8	27.5
sA-Film	A-Film	22.8	55.9
sB	B	6.2	15.4
sB	B	14.6	39.5
sB	B	21.3	64.9
sC	C	6.3	15.7
sC	C	14.2	37.9
sC	C	23.3	74.4
sD	D	4.7	13.0
sD	D	10.1	29.4
sD	D	16.6	53.4
sD	D	19.5	66.5
sD	D	23.0	86.6
sE	E	5.5	13.4
sE	E	14.7	39.6
sE	E	23.0	74.8

**Table 9.8:** Temperature variation for sample A.

Experiment	Temperature [°C]	Pressure [bar]	Solubility [g <sub>C3</sub> /kg <sub>PP</sub> ]
sA4	40	3.1	12.5
sA4	40	8.6	37.4
sA4	40	13.5	67.1
sA5	50	3.3	20.9
sA5	50	8.5	30.0
sA5	50	16.7	71.6
sA6	60	4.0	11.6
sA6	60	14.9	49.9
sA6	60	23.2	94.9
sA1	70	6.2	15.4
sA1	70	12.3	32.0
sA1	70	17.1	48.0
sA1	70	20.3	60.4
sA1	70	25.1	82.8

Experiment	Temperature [°C]	Pressure [bar]	Solubility [g <sub>C3</sub> /kg <sub>PP</sub> ]
sA7	80	10.6	22.5
sA7	80	17.2	39.3
sA7	80	23.0	58.1
sA7	80	25.2	66.2

### 9.3 Recalculation of literature solubility data

The literature solubility data is presented in different ways. For better comparison, the literature data was recalculated as follows.

The solubility of Sato et al. [53] was used as reported and the amorphous solubility was calculated based on the reported crystalline mass fraction of 66.9 wt%.

The solubility of Meier et al. [18] was calculated from the reported propylene volume fractions  $\phi_{C3}$ . These fractions were obtained by the Flory-Huggins equation which well described their experimental results based on the reported interaction parameter. After comparison with the reported graphs, only a limited number of data points per isotherm was chosen to represent their data. The amorphous solubility was calculated by:

$$S_{am} = \frac{\phi_{C3} \rho_{C3}^{liq}}{1 - \phi_{C3} \rho_{am,0}} \quad (9.1)$$

The solubility was calculated based on the reported crystallinity of 43.5 wt%.

The solubility isotherm of Bobak et al. [56] was evaluated from the presented graph and recalculated based on the reported crystallinity of 37 wt%.

Kröner and Bartke [55] reported the solubility in terms of monomer concentration in the amorphous polymer phase  $c_{am}$  including swelling. The amorphous solubility was recalculated as:

$$S_{am} = \frac{c_{am} MW_{C3}}{\rho_{am,0} - 1.7844 \cdot c_{am} MW_{C3} \frac{\rho_{am,0}}{\rho_{PP,0}}} \quad (9.2)$$

The densities were used as reported and the solubility was obtained from the reported crystallinity of 39 wt%.

The Stern correlation [64] was used to calculate the monomer concentration based on the parameters of [65] and the amorphous solubility was calculated by:



$$S_{am} = \frac{c_{am}MW_{C3}}{\rho_{am,0}} \quad (9.3)$$

#### 9.4 Density of amorphous and crystalline PP

The density of PP was experimentally determined by Zoller [132] and Sato et al. [54] (Figure 9.1). The reported density of Zoller [132] clearly represents the amorphous density and agrees well with the amorphous density given by Sato et al. [54]. Both authors used the Tait equation which could well describe the experimental amorphous ( $v_0 = 1.1606 \text{ cm}^3/\text{g}$  and  $\alpha_0 = 6.70 \cdot 10^{-4} / \text{K}$  [132]) and crystalline ( $v_0 = 0.943 \text{ cm}^3/\text{g}$  and  $\alpha_0 = 3.774 \cdot 10^{-4} / \text{K}$  [54]) densities:

$$\rho_{am/cr} = \frac{1}{v_0 e^{\alpha_0 T}} \quad (9.4)$$

Combining the amorphous and crystalline densities using Equation (6.3) well describes the semi-crystalline PP density (Figure 9.1).

The same approach of calculating the semi-crystalline PP density can be used when simulating the amorphous density based on the SL or PC-SAFT EoS and combining it with the crystalline density obtained via the Tait equation (Figure 9.2).

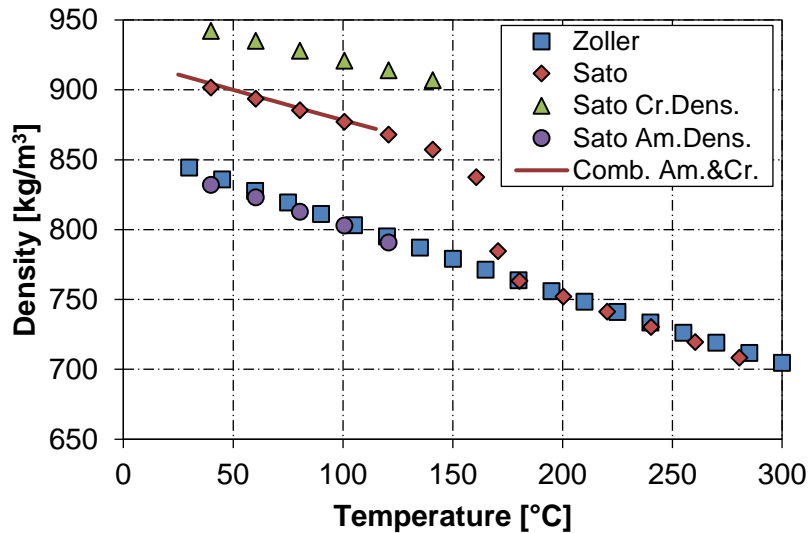


**Figure 9.1:** Experimental densities of polypropylene. Sato et al. [133] determined the PP density (red diamonds) and based on that calculated the crystalline density [54]. The reported values of the PP density of Zoller [132] clearly represent the amorphous density and agree well with the values for amorphous density of Sato et al. [54]. Combination of the amorphous and crystalline densities (red line) based on the respective Tait equations well describes the experimental PP density using the reported crystallinity of 66 wt%.

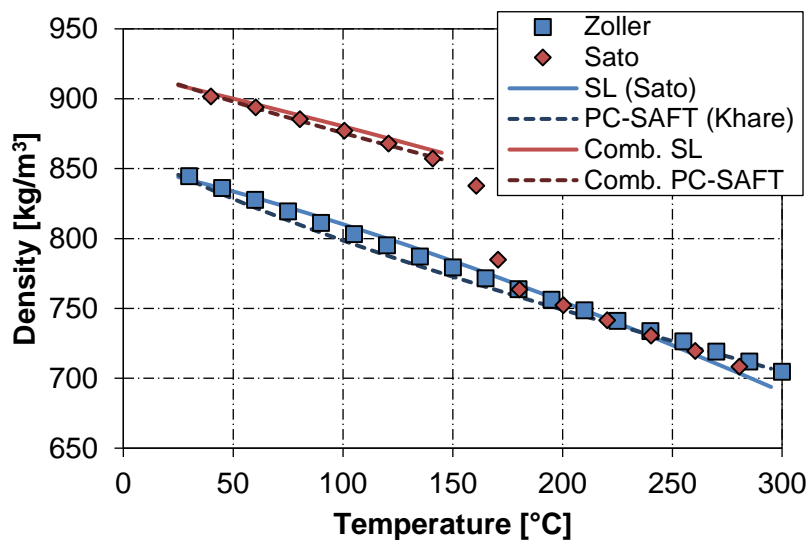


**Figure 9.2:** Combination of the EoS based amorphous density and the crystalline density to calculate the semi-crystalline PP density. The experimental amorphous density was taken from Zoller [132], the semi-crystalline density from Sato et al. [133] and the pure component parameters for the SL and PC-SAFT EoS from Sato et al. [54] and Khare et al. [79], respectively. Combination of the EoS simulation for the amorphous density and the crystalline density based on the Tait equation well describes the experimental semi-crystalline PP density using the reported crystallinity of 66 wt%.

## 10 Nomenclature

<b>Abbreviation</b>	<b>Description</b>
ARD	Average relative deviation
BIP	Binary interaction parameter
C3	Propylene
Cat	Catalyst
CoCat	Cocatalyst
CSTR	Continuous stirred tank reactor
DEAC	Diethylaluminum chloride
DSC	Differential scanning calorimetry
EoS	Equation of state
EPS	Expanded polystyrene
FBR	Fluidized bed reactor
M	Monomer
MFR	Melt flow rate
MGM	Multigrain model
MWD	Molecular weight distribution
MZCR	Multi-zone circulating reactor
ODE	Ordinary differential equation
P	Pressure
PC-SAFT	Perturbed-Chain Statistical Association Fluid Theory
PDI	Polydispersity index
PE	Polyethylene
PE-HD	High density polyethylene
PE-LD	Low density polyethylene
PE-LLD	Linear low density polyethylene
PE-MD	Medium density polyethylene
PET	Polyethylene terephthalate
PFM	Polymeric flow model
PID	Proportional-integral-derivative (controller)
PP	Polypropylene
Prepo	Prepolymerization
PS	Polystyrene
PSD	Particle size distribution
PUR	Polyurethane
PVC	Polyvinyl chloride

Abbreviation	Description
RTD	Residence time distribution
SB	Seed bed (polymerization)
SEM	Scanning electron microscopy
SL	Sanchez-Lacombe
T	Temperature
TEA	Triethylaluminum
WAXS	Wide angle X-ray scattering
XRD	X-ray diffraction
ZN	Ziegler-Natta

Capital letters	Description	Unit
A	Catalyst activity	kg <sub>PP</sub> /g <sub>Cat</sub> /h
$\bar{A}$	Average activity	kg <sub>PP</sub> /g <sub>Cat</sub> /h
A <sub>am</sub>	Integration area of amorphous WAXS spectrum	-
A <sub>exp</sub>	Experimental catalyst activity	kg <sub>PP</sub> /g <sub>Cat</sub> /h
A <sub>int</sub>	Intrinsic catalyst activity	kg <sub>PP</sub> /g <sub>Cat</sub> /h
A <sub>sample</sub>	Integration area of sample WAXS spectrum	-
B <sub>i</sub>	i'th bulk moment	mol/L
[CoCat]	Cocatalyst concentration	mol/L
D	Diffusion coefficient	m/s <sup>2</sup>
D <sub>eff</sub>	Effective diffusion coefficient	m/s <sup>2</sup>
D <sub>i</sub>	i'th moment of dead polymer chains	mol/L
[D <sub>n</sub> ]	Concentration of dead polymer chains	mol/L
[H <sub>2</sub> ]	Hydrogen concentration	mol/L
ΔH <sub>f</sub>	Heat of fusion	J/g
ΔH <sub>f,100 %</sub>	Heat of fusion of 100 % crystalline polypropylene	J/g
L <sub>i</sub>	i'th moment of living polymer chains	mol/L
L <sub>i</sub> <sup>dorm</sup>	i'th moment of dormant polymer chains	mol/L
[M]	Monomer concentration	mol/L
M <sub>n</sub>	Number average molecular weight	kg/mol
M <sub>w</sub>	Weight average molecular weight	kg/mol
MW <sub>C3</sub>	Molecular weight of propylene	kg/mol
MW <sub>H2</sub>	Molecular weight of hydrogen	kg/mol
MW <sub>Ti</sub>	Molecular weight of titanium	kg/mol
P	Pressure	bar

Capital letters	Description	Unit
$P^*$	Characteristic pressure	bar
$P_{C3}$	Propylene pressure	bar
PDI	Polydispersity index	-
$[P_n]$	Concentration of living polymer chains	mol/L
$[P_n^{dorm}]$	Concentration of dormant polymer chains	mol/L
$P_{vap}$	Vapor pressure	bar
R	Sphere radius	m
$R_{particle}$	Particle radius	m
S	Solubility	g <sub>C3</sub> /kg <sub>PP</sub>
$[S_a]$	Concentration of active catalyst sites	mol/L
$S_{am}$	Amorphous solubility	g <sub>C3</sub> /kg <sub>PPam</sub>
$S_{am}^{EoS}$	Amorphous solubility calculated by an equation of state	g <sub>C3</sub> /kg <sub>PPam</sub>
$[S_d]$	Concentration of dead catalyst sites	mol/L
$[S_p]$	Concentration of potential catalyst sites	mol/L
T	Temperature	K
$T^*$	Characteristic temperature	K
$T_c$	Critical temperature	K
$T_r$	Reduced temperature	-
$V_{am}$	Amorphous polypropylene volume	m <sup>3</sup>
$V_{am,0}$	Amorphous polypropylene volume at vacuum	m <sup>3</sup>
$V_{con}$	Sample container volume	m <sup>3</sup>
$V_{cr}$	Crystalline polypropylene volume	m <sup>3</sup>
$V_{PP}$	Polypropylene volume	m <sup>3</sup>
$V_{PP,0}$	Polypropylene volume at vacuum	m <sup>3</sup>
$V_R$	Reactor volume	m <sup>3</sup>
$\Delta V_{swell}$	Polypropylene volume increase upon swelling	m <sup>3</sup>

Small letters	Description	Unit
c	Concentration	mol/L
$c_{am}$	Propylene concentration in amorphous polypropylene	mol/L <sub>PPam</sub>
$c_{am,eq}$	Propylene concentration in amorphous PP at equilibrium	mol/L <sub>PPam</sub>
$c_{C3}$	Propylene concentration in polypropylene	mol/L <sub>PP</sub>
$c_{C3,eq}$	Propylene concentration in PP at equilibrium	mol/L <sub>PP</sub>
$c_p^*$	Concentration of all active polymer chains	mol/L
$f_i^{gas}$	Fugacity of component i of the gas phase	Pa

Small letters	Description	Unit
$f_i^{\text{liq}}$	Fugacity of component i of the liquid phase	Pa
k	Binary interaction parameter	-
$k_r$	Rate constant for a simplified first-order reaction	L/mol/s
$k_a$	Rate constant of activation	1/s
$k_{aCo}$	Rate constant of activation by cocatalyst	L/mol/s
$k_{aH}$	Rate constant of activation by hydrogen	L/mol/s
$k_{aM}$	Rate constant of activation by monomer	L/mol/s
$k_{aSp}$	Rate constant of spontaneous activation	1/s
$k_B$	Boltzmann constant	J/K
$k_d$	Rate constant of deactivation	1/s
$k_{dorm}$	Rate constant of dormant chain formation	L/mol/s
$k_{dormi}$	Rate constant of dormant chain initiation	L/mol/s
$k_{dSp}$	Rate constant of spontaneous deactivation	1/s
$k_{dX}$	Rate constant of activation by species X	L/mol/s
$k_H$	Henry's constant	mol/L <sub>PPam</sub> /atm
$k_i$	Rate constant of initiation	L/mol/s
$k_{ij}$	Binary interaction parameter of components i and j	-
$k_p$	Rate constant of propagation	L/mol/s
$k_{re}$	Rate constant of reactivation	1/s
$k_{reH}$	Rate constant of reactivation by hydrogen	L/mol/s
$k_{reM}$	Rate constant of reactivation by monomer	L/mol/s
$k_{tr}$	Rate constant of chain transfer	1/s
$k_{trCo}$	Rate constant of chain transfer by cocatalyst	L/mol/s
$k_{trH}$	Rate constant of chain transfer by hydrogen	L <sup>0.5</sup> /mol <sup>0.5</sup> /s
$k_{trM}$	Rate constant of chain transfer by monomer	L/mol/s
$k_{trSp}$	Rate constant of spontaneous chain transfer	1/s
m	Segment number	-
$m_{am}$	Amorphous polypropylene mass	kg
$m_{bal}$	Balance mass	kg
$m_{C3}$	Propylene mass	kg
$\dot{m}_{C3}$	Propylene mass flow	kg/h
$m_{C3,eq}$	Propylene mass absorbed in polypropylene at equilibrium	kg
$m_{Cat}$	Catalyst mass	g
$m_{con}$	Sample container mass	kg
$m_{corr}$	Buoyancy corrected balance mass	kg
$m_{cr}$	Crystalline polypropylene mass	kg

Small letters	Description	Unit
$m_{H_2}$	Hydrogen mass	kg
$m_{PP}$	Polypropylene mass	kg
$n_{C_3}$	Moles of propylene	mol
$r$	Radius	m
$r_p$	Rate of polymerization	mol/L/s
$t$	Time	s
$t_r$	Reaction time	h
$v^*$	Characteristic volume of the mixture	$m^3/mol$
$v_0$	Coefficient in Tait equation	$cm^3/g$
$v_{cr}$	Crystalline volume fraction	vol%
$v_i^*$	Characteristic volume of component i	$m^3/mol$
$v_{ij}^*$	Characteristic volume of component i and j	$m^3/mol$
$w_{cr}$	Crystalline mass fraction	wt%
$w_{Ti}$	Mass fraction of titanium	wt%
$x_{active}$	Active fraction of titanium	-
$x_{C_3}$	Propylene molar fraction of the liquid phase	-
$y$	Yield	$kg_{PP}/g_{Cat}$
$y_{C_3}$	Propylene molar fraction of the gas phase	-

Greek symbols	Description	Unit
$\alpha_0$	Coefficient in Tait equation	1/K
$\varepsilon$	Segment energy	J
$\varepsilon^*$	Characteristic energy of the mixture	J/mol
$\varepsilon_i^*$	Characteristic energy of component i	J/mol
$\varepsilon_{ij}^*$	Characteristic energy of component i and j	J/mol
$\eta$	Effectiveness factor	-
$\lambda$	Dimensionless radius	-
$\rho^*$	Characteristic density	$kg/m^3$
$\rho_{am}$	Density of amorphous polypropylene	$kg/m^3$
$\rho_{am,0}$	Density of amorphous polypropylene at vacuum	$kg/m^3$
$\rho_{am}^{EoS}$	Density of amorphous PP calculated by an equation of state	$kg/m^3$
$\rho_{cr}$	Density of crystalline polypropylene	$kg/m^3$
$\rho_{C_3}^{liq}$	Liquid density of propylene	$kg/m^3$
$\rho_{gas}$	Gas density of propylene	$kg/m^3$

<b>Greek symbols</b>	<b>Description</b>	<b>Unit</b>
$\rho_{PP}$	Density of polypropylene	kg/m <sup>3</sup>
$\rho_{PP,0}$	Density of polypropylene at vacuum	kg/m <sup>3</sup>
$\sigma$	Segment diameter	Å
$\varphi_{C_3}^{gas}$	Fugacity coefficient of propylene of the gas phase	-
$\varphi_{C_3}^{liq}$	Fugacity coefficient of propylene of the liquid phase	-
$\varphi_{C_3}^{pure}$	Fugacity coefficient of pure propylene	-
$\phi_i$	Volume fraction of component i	-
$\phi_{Thiele}$	Thiele modulus	-
$\psi$	Dimensionless concentration	-

<b>Chemical formula</b>	<b>Description</b>
AlCl <sub>3</sub>	Aluminum trichloride
AlEt <sub>2</sub> Cl	Diethylaluminum chloride
AlR <sub>3</sub>	Trialkylaluminum
CH	Methine group
CH <sub>2</sub>	Methylene group
CH <sub>3</sub>	Methyl group
CO	Carbon monoxide
COS	Carbonyl sulfide
H	Hydrogen atom
H <sub>2</sub>	Hydrogen molecule
H <sub>2</sub> S	Hydrogen sulfide
MgCl <sub>2</sub>	Magnesium chloride
NaCl	Sodium chloride
SiO <sub>2</sub>	Silicon dioxide
Ti	Titanium
TiCl <sub>3</sub>	Titanium(III) chloride
TiCl <sub>4</sub>	Titanium tetrachloride



## 11 References

1. Plastics Europe (2019) Plastics - the Facts 2019. [https://www.plasticseurope.org/application/files/1115/7236/4388/FINAL\\_web\\_version\\_Plastics\\_the\\_facts2019\\_14102019.pdf](https://www.plasticseurope.org/application/files/1115/7236/4388/FINAL_web_version_Plastics_the_facts2019_14102019.pdf). Accessed 20 Nov 2019
2. Alburnia AR, Prades F, Jeremic D (2019) Multimodal Polymers with Supported Catalysts. Springer International Publishing, Cham
3. Ceresana (2019) Market Study: Polypropylene. <https://www.ceresana.com/en/market-studies/plastics/polypropylene/>. Accessed 21 Nov 2019
4. Soares JBP, McKenna TFL (2013) Polyolefin Reaction Engineering. Wiley, Weinheim
5. Domininghaus H, Elsner P, Eyerer P, Hirth T (2008) Kunststoffe: Eigenschaften und Anwendungen, 7., neu bearb. und erw. Aufl. VDI-Buch. Springer, Berlin, Heidelberg
6. Wilks ES (ed) (2001) Polymerization process, synthetic polymers. Industrial polymers handbook, vol 1. WILEY-VCH, Weinheim
7. Moore EP (1996) Polypropylene handbook: Polymerization, characterization, properties, processing, applications. Hanser Publishers; Hanser/Gardner Publications, Munich, New York, Cincinnati
8. Kaiser W (2016) Kunststoffchemie für Ingenieure: Von der Synthese bis zur Anwendung, 4., neu bearbeitete und erweiterte Auflage. Hanser, München
9. Gahleitner M, Tranninger C, Doshev P (2013) Heterophasic copolymers of polypropylene: Development, design principles, and future challenges. *J. Appl. Polym. Sci.* 130(5): 3028–3037
10. LyondellBasell (2019) Licensed Polyolefin Technologies and Services - Spheripol. <https://www.lyondellbasell.com/globalassets/products-technology/technology/spheripol-brochure.pdf>. Accessed 19 Nov 2019
11. McDermott (2019) McDermott Technology - Polypropylene. <https://www.mcdermott.com/MDRSite/media/MDR/Tech%20Sheets/MD-polypropylene-v3.pdf>. Accessed 19 Nov 2019
12. LyondellBasell (2019) Licensed Polyolefin Technologies and Services - Spherizone. <https://www.lyondellbasell.com/globalassets/products-technology/technology/spherizone-brochure.pdf>. Accessed 19 Nov 2019
13. Covezzi M, Mei G (2001) The multizone circulating reactor technology. *Chem. Eng. Sci.* 56(13): 4059–4067
14. Asua JM (2007) Polymer reaction engineering. Blackwell Pub, Oxford, Ames Iowa
15. Kröner S, Eloranta K, Bergstra MF, Bartke M (2007) Kinetic Study of the Copolymerisation of Ethylene with a Single Site Catalyst in Propane Slurry Polymerisation. *Macromol. Symp.* 259(1): 284–294
16. Choi KY, Ray WH (1985) Polymerization of olefins through heterogeneous catalysis. II. Kinetics of gas phase propylene polymerization with Ziegler–Natta catalysts. *J. Appl. Polym. Sci.* 30(3): 1065–1081

17. Han-Adebekun GC, Ray WH (1997) Polymerization of olefins through heterogeneous catalysis. XVII. Experimental study and model interpretation of some aspects of olefin polymerization over a  $\text{TiCl}_4/\text{MgCl}_2$  catalyst. *J. Appl. Polym. Sci.* 65(6): 1037–1052
18. Meier GB, Weickert G, van Swaaij WPM (2001) Comparison of gas- and liquid-phase polymerization of propylene with heterogeneous metallocene catalyst. *J. Appl. Polym. Sci.* 81(5): 1193–1206
19. Meier GB, Weickert G, van Swaaij WPM (2001) Gas-phase polymerization of propylene: Reaction kinetics and molecular weight distribution. *J. Polym. Sci. A Polym. Chem.* 39(4): 500–513
20. Inge Cornelia van Putten (2004) Propylene Polymerization in a Circulating Slugging Fluidized Bed Reactor. Dissertation, University of Twente
21. Patzlaff M (2006) Kinetische Untersuchung der Polymerisation von Propylen mit neuartigen Ziegler-Natta Katalysatoren in Gas- und Flüssigphase. Dissertation, Technische Universität Berlin
22. Kettner J (2019) Kinetic investigation of different supported catalysts for the polymerization of propylene under industrially relevant conditions. Martin-Luther-Universität Halle-Wittenberg, Dissertation. Cuvillier Verlag, Göttingen
23. Kröner T (2014) Mass transport and kinetics in the heterophasic copolymerization of propylene. Martin-Luther-Universität Halle-Wittenberg, Dissertation. Mensch & Buch Verlag, Berlin
24. Tsutsui T, Kashiwa N, Mizuno A (1990) Effect of hydrogen on propene polymerization with ethylenebis(1-indenyl)zirconium dichloride and methylalumoxane catalyst system. *Makromol. Chem., Rapid Commun.* 11(11): 565–570
25. Busico V, Cipullo R, Corradini P (1992) Hydroooligomerization of propene: a “fingerprint” of a Ziegler-Natta catalyst, 1. Preliminary results for  $\text{MgCl}_2$ -supported systems. *Makromol. Chem., Rapid Commun.* 13(1): 15–20
26. Chadwick JC, Miedema A, Sudmeijer O (1994) Hydrogen activation in propene polymerization with  $\text{MgCl}_2$ -supported Ziegler-Natta catalysts: the effect of the external donor. *Macromol. Chem. Phys.* 195(1): 167–172
27. Samson JJC, Bosman PJ, Weickert G, Westerterp KR (1999) Liquid-phase polymerization of propylene with a highly active Ziegler-Natta catalyst. Influence of hydrogen, cocatalyst, and electron donor on the reaction kinetics. *J. Polym. Sci. A Polym. Chem.* 37(2): 219–232
28. Soares JBP, Hamielec AE (1996) Kinetics of propylene polymerization with a non-supported heterogeneous Ziegler-Natta catalyst—effect of hydrogen on rate of polymerization, stereoregularity, and molecular weight distribution. *Polymer* 37(20): 4607–4614
29. Durand DC, Meurice EMJ, Morterol FRM (1999) BP Chemicals Limited: EP 1 112 121 B1
30. Bidell W, Zitzmann J, Lynch J, Oelze J, Gebhart H (2001) Basell Poliolefine Italia S.r.l.: EP 1 320 559 B1
31. Tonti, Maria, Silvia, Oberhoff M, Fraaije V, Bachmann B (2004) Basell Polyolefine GmbH: WO 2005/005495 A2

32. Paulik C, Lehmus P, Tuominen O (2006) Borealis Technology Oy: EP 1 939 226 A1
33. Samson JJC, Weickert G, Heerze AE, Westerterp KR (1998) Liquid-phase polymerization of propylene with a highly active catalyst. *AIChE J.* 44(6): 1424–1437
34. Samson JJC, van Middelkoop B, Weickert G, Westerterp KR (1999) Gas-phase polymerization of propylene with a highly active ziegler-natta catalyst. *AIChE J.* 45(7): 1548–1558
35. Pater JTM, Weickert G, Loos J, van Swaaij WPM (2001) High precision prepolymerization of propylene at extremely low reaction rates—kinetics and morphology. *Chem. Eng. Sci.* 56(13): 4107–4120
36. Pater JTM, Weickert G, van Swaaij WPM (2002) Polymerization of liquid propylene with a 4th generation Ziegler–Natta catalyst—influence of temperature, hydrogen and monomer concentration and prepolymerization method on polymerization kinetics. *Chem. Eng. Sci.* 57(16): 3461–3477
37. Pater JTM, Weickert G, van Swaaij WPM (2003) Propene bulk polymerization kinetics: Role of prepolymerization and hydrogen. *AIChE J.* 49(1): 180–193
38. Pater JTM, Weickert G, van Swaaij WPM (2003) Polymerization of liquid propylene with a fourth-generation Ziegler-Natta catalyst: Influence of temperature, hydrogen, monomer concentration, and prepolymerization method on powder morphology. *J. Appl. Polym. Sci.* 87(9): 1421–1435
39. Debling JA, Ray WH (2001) Morphological development of impact polypropylene produced in gas phase with a  $\text{TiCl}_4/\text{MgCl}_2$  catalyst. *J. Appl. Polym. Sci.* 81(13): 3085–3106
40. Martin C, McKenna TF (2002) Particle morphology and transport phenomena in olefin polymerisation. *Chem. Eng. Sci.* 87(1): 89–99
41. Marx R (2008) Realisierung einer Versuchsanlage zur Olefinpolymerisation. Diploma Thesis, TU Dresden
42. Han-Adebekun GC, Debling JA, Ray WH (1997) Polymerization of olefins through heterogeneous catalysis. XVI. Design and control of a laboratory stirred bed copolymerization reactor. *J. Appl. Polym. Sci.* 64(2): 373–382
43. Bergstra MF, Weickert G (2006) Semi-batch reactor for kinetic measurements of catalyzed olefin co-polymerizations in gas and slurry phase. *Chem. Eng. Sci.* 61(15): 4909–4918
44. Roos P, Meier GB, Samson JJC, Weickert G, Westerterp KR (1997) Gas phase polymerization of ethylene with a silica-supported metallocene catalyst: influence of temperature on deactivation. *Macromol. Rapid Commun.* 18(4): 319–324
45. Piduhn M (1999) Metallocen-katalysierte Polymerisation von Propen und Ethen aus der Gasphase. TU Berlin, Dissertation. Mensch & Buch Verlag, Berlin
46. Zoellner K, Reichert K-H (2001) Gas phase polymerization of butadiene—kinetics, particle size distribution, modeling. *Chem. Eng. Sci.* 56(13): 4099–4106
47. McKenna TF, Dupuy J, Spitz R (1995) Modeling of transfer phenomena on heterogeneous Ziegler catalysts: Differences between theory and experiment in olefin polymerization (an introduction). *J. Appl. Polym. Sci.* 57(3): 371–384

48. McKenna TF, Cokljat D, Wild P (1998) CFD Modelling of heat transfer during gas phase olefin polymerisation. *Comput. Chem. Eng.* 22: S285-S292
49. McKenna TF, Spitz R, Cokljat D (1999) Heat transfer from catalysts with computational fluid dynamics. *AIChE J.* 45(11): 2392–2410
50. Ranz WE, Marshall WR (1952) Evaporation from drops - part II. *Chem. Eng. Prog.*(48): 173–180
51. Floyd S, Choi KY, Taylor TW, Ray WH (1986) Polymerization of olefines through heterogeneous catalysis IV. Modeling of heat and mass transfer resistance in the polymer particle boundary layer. *J. Appl. Polym. Sci.* 31(7): 2231–2265
52. Sliepcevich A, Storti G, Morbidelli M (2000) Measurement of diffusivity and solubility of olefins in polypropylene by gas chromatography. *J. Appl. Polym. Sci.* 78(2): 464–473
53. Sato Y, Tsuboi A, Sorakubo A, Takishima S, Masuoka H, Ishikawa T (2000) Vapor–liquid equilibrium ratios for hexane at infinite dilution in ethylene+impact polypropylene copolymer and propylene+impact polypropylene copolymer. *Fluid Phase Equilib.* 170(1): 49–67
54. Sato Y, Yurugi M, Yamabiki T, Takishima S, Masuoka H (2001) Solubility of propylene in semicrystalline polypropylene. *J. Appl. Polym. Sci.* 79(6): 1134–1143
55. Bartke M, Kröner S, Wittebrock A, Reichert K-H, Illiopoulos I, Dittrich CJ (2007) Sorption and Diffusion of Propylene and Ethylene in Heterophasic Polypropylene Copolymers. *Macromol. Symp.* 259(1): 327–336
56. Bobak M, Gregor T, Bachman B, Kosek J (2008) Estimation of Morphology Characteristics of Porous Poly(propylene) Particles from Degassing Measurements. *Macromol. React. Eng.* 2(2): 176–189
57. Patzlaff M, Wittebrock A, Reichert K-H (2006) Sorption studies of propylene in polypropylene. Diffusivity in polymer particles formed by different polymerization processes. *J. Appl. Polym. Sci.* 100(4): 2642–2648
58. Kröner T, Bartke M (2013) Sorption of Olefins in High Impact Polypropylene - Experimental Determination and Mass Transport Modeling. *Macromol. React. Eng.* 7(9): 453–462
59. Cancelas AJ, Plata MA, Bashir MA, Bartke M, Monteil V, McKenna TFL (2018) Solubility and Diffusivity of Propylene, Ethylene, and Propylene-Ethylene Mixtures in Polypropylene. *Macromol. Chem. Phys.* 219(8): 1700565
60. Kiparissides C, Dimos V, Boulouka T, Anastasiadis A, Chasiotis A (2003) Experimental and theoretical investigation of solubility and diffusion of ethylene in semicrystalline PE at elevated pressures and temperatures. *J. Appl. Polym. Sci.* 87(6): 953–966
61. Novak A, Bobak M, Kosek J, Banaszak BJ, Lo D, Widya T, Ray WH, Pablo JJ de (2006) Ethylene and 1-hexene sorption in LLDPE under typical gas-phase reactor conditions: Experiments. *J. Appl. Polym. Sci.* 100(2): 1124–1136
62. Michaels AS, Bixler HJ (1961) Flow of gases through polyethylene. *J. Polym. Sci.* 50(154): 413–439
63. Rogers CE, Stannett V, Szwarc M (1960) The sorption, diffusion, and permeation of organic vapors in polyethylene. *J. Polym. Sci.* 45(145): 61–82

64. Stern SA, Mullhaupt JT, Gareis PJ (1969) The effect of pressure on the permeation of gases and vapors through polyethylene. Usefulness of the corresponding states principle. *AIChE J.* 15(1): 64–73
65. Hutchinson RA, Ray WH (1990) Polymerization of olefins through heterogeneous catalysis. VIII. Monomer sorption effects. *J. Appl. Polym. Sci.* 41(1-2): 51–81
66. Kakugo M, Sadatoshi H, Yokoyama M, Kojima K (1989) Transmission electron microscopic observation of nascent polypropylene particles using a new staining method. *Macromolecules* 22(2): 547–551
67. Kakugo M, Sadatoshi H, Sakai J, Yokoyama M (1989) Growth of polypropylene particles in heterogeneous Ziegler-Natta polymerization. *Macromolecules* 22(7): 3172–3177
68. Fink G, Steinmetz B, Zechlin J, Przybyla C, Tesche B (2000) Propene Polymerization with Silica-Supported Metallocene/MAO Catalysts. *Chem. Rev.* 100(4): 1377–1390
69. Kittilsen P, McKenna TF (2001) Study of the kinetics, mass transfer, and particle morphology in the production of high-impact polypropylene. *J. Appl. Polym. Sci.* 82(5): 1047–1060
70. Ray WH (1986) Modelling of polymerization phenomena. *Ber. Bunsengesellschaft Phy. Chem.*(90): 947–955
71. Ray WH (1991) Modelling of addition polymerization processes - Free radical, ionic, group transfer, and ziegler-natta kinetics. *Can. J. Chem. Eng.* 69(3): 626–629
72. Touloupidis V (2014) Catalytic Olefin Polymerization Process Modeling: Multi-Scale Approach and Modeling Guidelines for Micro-Scale/Kinetic Modeling. *Macromol. React. Eng.* 8(7): 508–527
73. Shaffer WKA, Ray WH (1997) Polymerization of olefins through heterogeneous catalysis. XVIII. A kinetic explanation for unusual effects. *J. Appl. Polym. Sci.* 65(6): 1053–1080
74. Soares JBP (2001) Mathematical modelling of the microstructure of polyolefins made by coordination polymerization: a review. *Chem. Eng. Sci.* 56(13): 4131–4153
75. Reginato AS, Zacca JJ, Secchi AR (2003) Modeling and simulation of propylene polymerization in nonideal loop reactors. *AIChE J.* 49(10): 2642–2654
76. Zacca JJ, Debling JA, Ray WH (1996) Reactor residence time distribution effects on the multistage polymerization of olefins—I. Basic principles and illustrative examples, polypropylene. *Chem. Eng. Sci.* 51(21): 4859–4886
77. Mattos Neto AG, Pinto JC (2001) Steady-state modeling of slurry and bulk propylene polymerizations. *Chem. Eng. Sci.* 56(13): 4043–4057
78. Dompazis G, Kanellopoulos V, Kiparissides C (2005) A Multi-Scale Modeling Approach for the Prediction of Molecular and Morphological Properties in Multi-Site Catalyst, Olefin Polymerization Reactors. *Macromol. Mater. Eng.* 290(6): 525–536
79. Khare NP, Lucas B, Seavey KC, Liu YA, Sirohi A, Ramanathan S, Lingard S, Song Y, Chen C-C (2004) Steady-State and Dynamic Modeling of Gas-Phase Polypropylene Processes Using Stirred-Bed Reactors. *Ind. Eng. Chem. Res.* 43(4): 884–900
80. Soares JBP, Hamielec AE (1995) Deconvolution of chain-length distributions of linear polymers made by multiple-site-type catalysts. *Polymer* 36(11): 2257–2263

81. Al-haj Ali M, Betlem B, Roffel B, Weickert G (2006) Hydrogen response in liquid propylene polymerization: Towards a generalized model. *AIChE J.* 52(5): 1866–1876
82. Dubé MA, Soares JBP, Penlidis A, Hamielec AE (1997) Mathematical Modeling of Multicomponent Chain-Growth Polymerizations in Batch, Semibatch, and Continuous Reactors: A Review. *Ind. Eng. Chem. Res.* 36(4): 966–1015
83. McKenna TF, Soares JBP (2001) Single particle modelling for olefin polymerization on supported catalysts: A review and proposals for future developments. *Chem. Eng. Sci.* 56(13): 3931–3949
84. Yermakov YI, Mikhaichenko VG, Beskov VS, Grabovskii YP, Emirova IV (1970) The role of transfer processes in gaseous phase polymerization of ethylene. *Plast. Massy*(9): 7–10
85. Crabtree JR, Grimsby FN, Nummelin AJ, Sketchley JM (1973) The role of diffusion in the Ziegler polymerization of ethylene. *J. Appl. Polym. Sci.* 17(3): 959–976
86. Nagel EJ, Kirillov VA, Ray WH (1980) Prediction of Molecular Weight Distributions for High-Density Polyolefins. *Ind. Eng. Chem. Prod. Res. Dev.* 19(3): 372–379
87. Hock CW (1966) How  $TiCl_3$  Catalysts Control the Texture of As-Polymerized Polypropylene. *J. Polym. Sci. A-1 Polym. Chem.* 4(12): 3055–3064
88. Noristi L, Marchetti E, Baruzzi G, Sgarzi P (1994) Investigation on the particle growth mechanism in propylene polymerization with  $MgCl_2$ -supported ziegler–natta catalysts. *J. Polym. Sci. A Polym. Chem.* 32(16): 3047–3059
89. Floyd S, Choi KY, Taylor TW, Ray WH (1986) Polymerization of olefins through heterogeneous catalysis. III. Polymer particle modelling with an analysis of intraparticle heat and mass transfer effects. *J. Appl. Polym. Sci.* 32(1): 2935–2960
90. Hutchinson RA, Ray WH (1987) Polymerization of olefins through heterogeneous catalysis. VII. Particle ignition and extinction phenomena. *J. Appl. Polym. Sci.* 34(2): 657–676
91. Hutchinson RA, Chen CM, Ray WH (1992) Polymerization of olefins through heterogeneous catalysis X: Modeling of particle growth and morphology. *J. Appl. Polym. Sci.* 44(8): 1389–1414
92. Schmeal WR, Street JR (1971) Polymerization in expanding catalyst particles. *AIChE J.* 17(5): 1188–1197
93. Singh D, Merrill RP (1971) Molecular Weight Distribution of Polyethylene Produced by Ziegler-Natta Catalysts. *Macromolecules* 4(5): 599–604
94. Galvan R, Tirrell M (1986) Orthogonal collocation applied to analysis of heterogeneous Ziegler-Natta polymerization. *Comput. Chem. Eng.* 10(1): 77–85
95. Galvan R, Tirrell M (1986) Molecular weight distribution predictions for heterogeneous Ziegler-Natta polymerization using a two-site model. *Chem. Eng. Sci.* 41(9): 2385–2393
96. Bartke M, Reichert K-H (2000) Calculation of Molecular Weight Distributions of Polymerization Reactions Using Standard Simulation Software. *Chem. Eng. Technol.* 23(12): 1062–1065
97. Kittilsen P, Svendsen H, McKenna TF (2001) Modeling of transfer phenomena on heterogeneous Ziegler catalysts. IV. Convection effects in gas phase processes. *Chem. Eng. Sci.* 56(13): 3997–4005

98. Parasu Veera U (2003) Mass transport models for a single particle in gas-phase propylene polymerisation. *Chem. Eng. Sci.* 58(9): 1765–1775
99. Parasu Veera U, McKenna T, Weickert G (2007) Multi-component mass transfer in a single particle during gaseous propylene polymerization. *J. Sci. Ind. Res.* 66(4): 345–351
100. Yiagopoulos A, Yiannoulakis H, Dimos V, Kiparissides C (2001) Heat and mass transfer phenomena during the early growth of a catalyst particle in gas-phase olefin polymerization : the effect of prepolymerization temperature and time. *Chem. Eng. Sci.* 56(13): 3979–3995
101. Hoel EL, Cozewith C, Byrne GD (1994) Effect of diffusion on heterogeneous ethylene propylene copolymerization. *AIChE J.* 40(10): 1669–1684
102. Kanellopoulos V, Dompazis G, Gustafsson B, Kiparissides C (2004) Comprehensive Analysis of Single-Particle Growth in Heterogeneous Olefin Polymerization: The Random-Pore Polymeric Flow Model. *Ind. Eng. Chem. Res.* 43(17): 5166–5180
103. Alizadeh A, Chmelař J, Sharif F, Ebrahimi M, Kosek J, McKenna TFL (2017) Modeling Condensed Mode Operation for Ethylene Polymerization: Part I. Thermodynamics of Sorption. *Ind. Eng. Chem. Res.* 56(5): 1168–1185
104. Krallis A, Kanellopoulos V (2013) Application of Sanchez–Lacombe and Perturbed-Chain Statistical Associating Fluid Theory Equation of State Models in Catalytic Olefins (Co)polymerization Industrial Applications. *Ind. Eng. Chem. Res.* 52(26): 9060–9068
105. Sanchez IC, Lacombe RH (1976) An elementary molecular theory of classical fluids. *Pure fluids. J. Phys. Chem.* 80(21): 2352–2362
106. Sanchez IC, Lacombe RH (1978) Statistical Thermodynamics of Polymer Solutions. *Macromolecules* 11(6): 1145–1156
107. Kanellopoulos V, Mouratides D, Pladis P, Kiparissides C (2006) Prediction of Solubility of  $\alpha$ -Olefins in Polyolefins Using a Combined Equation of State Molecular Dynamics Approach. *Ind. Eng. Chem. Res.* 45(17): 5870–5878
108. Bashir MA, Al-haj Ali M, Kanellopoulos V, Seppälä J (2013) Modelling of multicomponent olefins solubility in polyolefins using Sanchez–Lacombe equation of state. *Fluid Phase Equilib.* 358: 83–90
109. Bashir MA, Kanellopoulos V, Al-haj Ali M, McKenna TFL (2020) Applied Thermodynamics for Process Modeling in Catalytic Gas Phase Olefin Polymerization Reactors. *Macromol. React. Eng.* 14(1): 1900029
110. Gross J, Sadowski G (2001) Perturbed-Chain SAFT: An Equation of State Based on a Perturbation Theory for Chain Molecules. *Ind. Eng. Chem. Res.* 40(4): 1244–1260
111. Gross J, Sadowski G (2002) Modeling Polymer Systems Using the Perturbed-Chain Statistical Associating Fluid Theory Equation of State. *Ind. Eng. Chem. Res.* 41(5): 1084–1093
112. Banaszak BJ, Lo D, Widya T, Ray WH, Pablo JJ de, Novak A, Kosek J (2004) Ethylene and 1-Hexene Sorption in LLDPE under Typical Gas Phase Reactor Conditions: A Priori Simulation and Modeling for Prediction of Experimental Observations. *Macromolecules* 37(24): 9139–9150

113. Chmelař J, Smolná K, Haškovcová K, Podivinská M, Maršálek J, Kosek J (2015) Equilibrium sorption of ethylene in polyethylene: Experimental study and PC-SAFT simulations. *Polymer* 59: 270–277
114. Chmelař J, Haškovcová K, Podivinská M, Kosek J (2017) Equilibrium Sorption of Propane and 1-Hexene in Polyethylene: Experiments and Perturbed-Chain Statistical Associating Fluid Theory Simulations. *Ind. Eng. Chem. Res.* 56(23): 6820–6826
115. Majer V, Svoboda V (1985) Enthalpies of vaporization of organic compounds: A critical review and data compilation. *Chemical data series*, vol 32. Blackwell Scientific Publications, Oxford
116. Brandrup J, Immergut EH, Grulke EA (eds) (1999) *Polymer Handbook*, 4th ed. Wiley, New York
117. Martins AR, Cancelas AJ, McKenna TFL (2017) A Study of the Gas Phase Polymerization of Propylene: The Impact of Catalyst Treatment, Injection Conditions and the Presence of Alkanes on Polymerization and Polymer Properties. *Macromol. React. Eng.* 11(1): 1600011
118. ASTM International (2013) Standard Test Method for Melt Flow Rates of Thermoplastics by Extrusion Plastometer(D1238-13)
119. International Organization for Standardization (2011) *Plastics -- Determination of the melt mass-flow rate (MFR) and melt volume-flow rate (MVR) of thermoplastics -- Part 1: Standard method 83.080.20(1133-1:2011-12)*
120. Paricaud P, Galindo A, Jackson G (2004) Modeling the Cloud Curves and the Solubility of Gases in Amorphous and Semicrystalline Polyethylene with the SAFT-VR Approach and Flory Theory of Crystallization. *Ind. Eng. Chem. Res.* 43(21): 6871–6889
121. Podivinská M, Jindrová K, Chmelař J, Kosek J (2017) Swelling of polyethylene particles and its relation to sorption equilibria under gas-phase polymerization conditions. *J. Appl. Polym. Sci.* 134(27): 45035
122. Klabunde J (2020) *Propylene Equilibrium Solubility and Diffusion in Polypropylene Homopolymers*. Master Thesis, Martin-Luther-Universität Halle-Wittenberg
123. Kong Y, Hay JN (2003) The enthalpy of fusion and degree of crystallinity of polymers as measured by DSC. *Eur. Polym. J.* 39(8): 1721–1727
124. Eaton JW, Bateman D, Hauberg S, Wehbring R (2019) *GNU Octave version 5.1.0 manual: a high-level interactive language for numerical computations*. <https://www.gnu.org/software/octave/doc/v5.1.0/>. Accessed 11 Mar 2020
125. Neau E (2002) A consistent method for phase equilibrium calculation using the Sanchez–Lacombe lattice–fluid equation-of-state. *Fluid Phase Equilib.* 203(1-2): 133–140
126. McHugh MA, Krukonis VJ (1994) *Supercritical Fluid Extraction: Principles and Practice*, 2. ed. Butterworth-Heinemann Publishing, Woburn, MA
127. Bashir MA, Al-haj Ali M, Kanellopoulos V, Seppälä J, Kokko E, Vijay S (2013) The Effect of Pure Component Characteristic Parameters on Sanchez-Lacombe Equation-of-State Predictive Capabilities. *Macromol. React. Eng.* 7(5): 193–204



128. Martín Á, Bermejo MD, Mato FA, Cocero MJ (2011) Teaching advanced equations of state in applied thermodynamics courses using open source programs. *Educ. Chem. Eng.* 6(4): e114–e121
129. Martín Á, Bermejo MD, Mato FA, Cocero MJ (2014) [Open source software] Equations of State. <http://hpp.uva.es/open-source-software-eos/>. Accessed 12 Mar 2020
130. Khare NP (2003) Predictive Modelling of Metal-Catalyzed Polyolefin Processes. Dissertation, Faculty of the Virginia Polytechnic Institute and State University
131. National Institute of Standards and Technology (2020) NIST Chemistry WebBook. <https://webbook.nist.gov/chemistry/fluid/>. Accessed 13 Mar 2020
132. Zoller P (1979) Pressure–volume–temperature relationships of solid and molten polypropylene and poly(butene-1). *J. Appl. Polym. Sci.* 23(4): 1057–1061
133. Sato Y, Yamasaki Y, Takishima S, Masuoka H (1997) Precise measurement of the PVT of polypropylene and polycarbonate up to 330C and 200 MPa. *J. Appl. Polym. Sci.* 66(1): 141–150
134. Crank J (1975) *The mathematics of diffusion*, 2. ed., reprint. Clarendon Press, Oxford
135. Fogler HS (2006) *Elements of chemical reaction engineering*, 4th ed., 3. printing. Pearson international edition. Pearson Education International/Prentice Hall PTR, Upper Saddle River, NJ
136. Levenspiel O (1999) *Chemical reaction engineering*, 3. ed. Wiley, Hoboken, NJ
137. Kittilsen P (2001) *Mass Transport and Kinetic Phenomena in Catalytic Polymerization of Olefins*. Dissertation, Norwegian University of Science and Technology
138. Keii T, Doi Y, Suzuki E, Tamura M, Murata M, Soga K (1984) Propene polymerization with a magnesium chloride-supported Ziegler catalyst, 2. Molecular weight distribution. *Makromol. Chem.* 185(8): 1537–1557
139. Guastalla G, Giannini U (1983) The influence of hydrogen on the polymerization of propylene and ethylene with an MgCl<sub>2</sub> supported catalyst. *Makromol. Chem., Rapid Commun.* 4(8): 519–527
140. Deuflhard P, Wulkow M (1995) Simulationsverfahren für die Polymerchemie. In: Bachem A, Jünger M, Schrader R (eds) *Mathematik in der Praxis: Fallstudien aus Industrie, Wirtschaft, Naturwissenschaften und Medizin*, vol 2. Springer Verlag, Berlin, Heidelberg: 117–136

# Curriculum Vitae

## Personal data

Name: Jorik Hill  
Date and place of birth: 15.02.1990 in Göttingen, Germany  
Gender: Male  
Citizenship: German  
Contact: jorik.hill@chemie.uni-halle.de

## Education

### University

02/2016 – 03/2020 Martin-Luther-University Halle-Wittenberg  
**PhD student in Polymer Reaction Engineering**  
Group of Prof. Dr.-Ing. M. Bartke  
Subject: “Kinetics and Catalyst Overheating in the Gas Phase Polymerization of Propylene”

10/2013 – 11/2015 FU, HU, TU Berlin and University of Potsdam  
**M.Sc. Polymer Science**  
Master thesis: “Solid State Polycondensation of Low Molecular Weight Lactic Acid Oligomers”

10/2010 – 09/2013 Leipzig University, **B.Sc. Chemistry**  
Bachelor thesis: “Synthese und Testung nickelhaltiger Katalysatoren für die Trockenreformierung von Methan mit CO<sub>2</sub>”

### School

06/2009 Abitur, Felix-Klein-Gymnasium, Göttingen

Mannheim, den 15.12.2020

## List of Publications

- Hill J, Klabunde J, Bartke M (in preparation) Solubility of Propylene in Polypropylene Homopolymers
- Ben Mrad A, Sheibat-Othman N, Hill J, Bartke M, McKenna TFL (2020) A Novel Approach for the Estimation of the Sanchez-Lacombe Interaction Parameters for the Solubility of Ternary Polyolefins Systems. Chem. Eng. J. <https://doi.org/10.1016/j.cej.2020.127778>
- Titus J, Kullmann J, Hill J, Enke D, Wilde N, Gläser R (2015) Dry Reforming of Methane over a Ni Spinel with Bimodal Porosity, DGMK-Tagungsbericht 2015-2, ISBN 978-3-941721-56-2

## Erklärung

Hiermit erkläre ich an Eides statt, dass ich meine Dissertation selbständig und ohne fremde Hilfe verfasst habe. Ich habe keine anderen als die von mir angegebenen Quellen und Hilfsmittel benutzt und habe die den benutzten Werken wörtlich oder inhaltlich entnommenen Stellen als solche kenntlich gemacht.

Des Weiteren erkläre ich, dass ich erstmals eine Dissertation einreichte und diese noch bei keiner anderen Institution eingereicht habe. Ich bin nicht vorbestraft und es gibt keine laufenden Ermittlungsverfahren gegen meine Person.

15.12.2020  
Mannheim, den

\_\_\_\_\_  
Jorik Hill